ALMA MATER STUDIORUM
UNIVERSITÀ DI BOLOGNA

DEPARTMENT OF PHYSICS AND ASTRONOMY "A. RIGHI"

SECOND CYCLE DEGREE

PHYSICS

Mass-imbalanced two-dimensional Bose-Fermi mixtures with boson-fermion pairing

Supervisor
Prof. Pierbiagio Pieri

Co-supervisor
Pietro Bovini

Defended by
Cristiano Luigi Kosman Chiarappa

Graduation Session 03/2026

Academic Year 2024/2025

Ringraziamenti

In questo preambolo, vorrei esprimere la mia gratitudine verso tutte le persone che mi sono state vicine in questi mesi di lavoro di tesi magistrale.

Un sentito ringraziamento va al mio supervisore, prof. Pierbiagio Pieri, per avermi seguito costantemente e per avermi dato fiducia nelle mie idee. Grazie anche al mio co-supervisore, Pietro Bovini, per la disponibilità e la gentilezza con cui mi ha spiegato i vari codici necessari per ottenere i risultati numerici.

Grazie a tutti gli amici e tutte le amiche di Bologna, del gruppo *Per fare robe* e dell'aula studio di via Petroni. Un ringraziamento speciale va a Giuseppe e Martino, per avermi sostenuto in questo periodo emotivamente molto complicato. Vi sarò per sempre riconoscente. Un grazie anche a Lorenzo e Sara per il supporto, e per le lunghe serate trascorse insieme a guardare film e cartoni animati.

Infine, grazie ai miei genitori Maria Antonietta e Saverio e a mio fratello Martino, per l'immancabile sostegno nonostante la mia assenza e la mia altalenante intrattabilità.

Abstract

Ultra-cold atomic Bose-Fermi mixtures constitute a versatile platform for studying quantum many-body phenomena, offering tunability over interparticle interactions, dimensionality, and component populations. Similar mixtures also occur in two-dimensional semiconductor nanostructures known as transition metal dichalcogenides, where excitons act as bosons interacting attractively with charge carriers (electrons or holes). Both examples motivate the theoretical study of Bose-Fermi mixtures with boson-fermion pairing and bosons and fermions with unequal masses.

This thesis investigates two-dimensional mass-imbalanced Bose-Fermi mixtures at zero temperature, extending previous analyses of mass-balanced systems. Using a diagrammatic T-matrix approach that has been validated in three dimensions by a recent experiment as well as by Quantum Monte Carlo simulations, we numerically study fundamental thermodynamic quantities as functions of the boson-fermion attraction strength. (Semi-)analytical expressions in the weak- and strong-coupling regimes are also derived. Mass-imbalance effects are systematically analyzed, and numerical results are tested against the (semi-)analytical expressions.

We further introduce formal improvements to the T-matrix method, including fermion-mediated boson-boson interactions in the anomalous boson self-energy and a partial self-consistency scheme in the fermion and boson self-energies. The inclusion of the additional anomalous term is essential to restore the correct weak-coupling expansion within the partially self-consistent T-matrix approach, suggesting the necessity of both improvements for an even more accurate modeling of the system.

Contents

List of Symbols

Coupling parameters, densities and masses

g	boson-fermion coupling parameter
η	boson-boson coupling parameter
n_{B}	boson density
n_{F}	fermion density
n_0	condensate density
n_{CF}	composite fermion density
x	boson concentration $n_{\mathrm{B}}/n_{\mathrm{F}}$
m_{B}	boson mass
m_{F}	fermion mass
γ_{m}	mass ratio $m_{\mathrm{B}}/m_{\mathrm{F}}$
m_{r}	reduced mass $m_{\mathrm{B}}m_{\mathrm{F}}/(m_{\mathrm{B}}+m_{\mathrm{F}})$
M	mass of a boson-fermion dimer $m_{\mathrm{B}}+m_{\mathrm{F}}$

Transition matrices, self-energies and momentum distributions

T_2	two-body transition matrix
Γ	many-body transition matrix
I_{F}	contribution of the fermionic medium to the many-body transition matrix
T	many-body transition matrix with condensate insertions
$\Gamma^{(n)}$	nth order in $1/g$ of the many-body transition matrix
Σ_{F}	fermion self-energy

$\Sigma_{\rm F}^{(n)}$ nth order in $1/g$ of the fermion self-energy

$\Sigma_{\rm BB}^{11}$ normal boson self-energy from boson-boson interactions

$\Sigma_{\rm BF}^{11}$ normal boson self-energy from boson-fermion interactions

$\Sigma_{\rm BF}^{(n)}$ nth order in $1/g$ of the normal boson self-energy from boson-fermion interactions

$\Sigma_{\rm B}^{11}$ total normal boson self-energy $\Sigma_{\rm BB}^{11} + \Sigma_{\rm BF}^{11}$

$\Sigma_{\rm BB}^{12}$ anomalous boson self-energy from boson-boson interactions

$\Sigma_{\rm BF}^{12}$ anomalous boson self-energy from boson-fermion interactions

$\Sigma_{\rm B}^{12}$ total anomalous boson self-energy $\Sigma_{\rm BB}^{12} + \Sigma_{\rm BF}^{12}$

$n_{\rm B}(\mathbf{k})$ boson momentum distribution

$n_{\rm F}(\mathbf{k})$ fermion momentum distribution

$n_{\rm CF}(\mathbf{k})$ composite fermion momentum distribution

Momenta and energies

$k_{\rm F}$ non-interacting Fermi momentum $\sqrt{4\pi n_{\rm F}}$

$\widetilde{k}_{\rm F}$ interacting Fermi step momentum

$P_{\rm T0}$ step momentum of the T-matrix

$E_{\rm F}$ Fermi energy $k_{\rm F}^2/(2m_{\rm F})$

$\varepsilon_{\rm r}^{\rm F}$ reduced Fermi energy $k_{\rm F}^2/(2m_{\rm r})$

ε_0 boson-fermion binding energy

$\mu_{\rm B}$ boson chemical potential

$\mu_{\rm F}$ fermion chemical potential

$\Sigma_{\rm F}^0$ mean-field shift of $\mu_{\rm F}$

$\mu_{\rm F}'$ shifted fermion chemical potential $\mu_{\rm F} - \Sigma_{\rm F}^0$

$\mu_{\rm B}^{(n)}$ nth order in $1/g$ of the boson chemical potential

$\mu_{\rm F}^{(n)}$ nth order in $1/g$ of the fermion chemical potential

$\xi_{\mathbf{k}}^{\rm B}$ shifted free boson dispersion $\mathbf{k}^2/(2m_{\rm B}) - \mu_{\rm B}$

$\xi_{\mathbf{k}}^{\rm F}$ shifted free fermion dispersion $\mathbf{k}^2/(2m_{\rm F}) - \mu_{\rm F}$

$\xi_{\mathbf{k}}^{\mathrm{CM}}$	shifted center of mass dispersion $\mathbf{k}^2/(2M) - \mu_{\mathrm{B}} - \mu_{\mathrm{F}}$
$E_{\mathbf{k}}^{\pm}$	quasi-particle dispersions with weights $u_{\mathbf{k}}, v_{\mathbf{k}}$
μ_{CF}	composite-fermion chemical potential $\mu_{\mathrm{B}} + \mu_{\mathrm{F}} + \varepsilon_0$
Σ_{CF}^0	mean-field repulsion on composite fermions
$\widetilde{\mu}_{\mathrm{CF}}$	renormalized composite-fermion chemical potential $\mu_{\mathrm{B}} + \mu_{\mathrm{F}} + \varepsilon_0 - \Sigma_{\mathrm{CF}}^0$
$\xi_{\mathbf{k}}^{\mathrm{CF}}$	shifted composite fermion dispersion $\mathbf{k}^2/(2M) - \mu_{\mathrm{CF}}$
$\widetilde{\xi}_{\mathbf{k}}^{\mathrm{CF}}$	renormalized shifted composite fermion dispersion $\mathbf{k}^2/(2M) - \widetilde{\mu}_{\mathrm{CF}}$
Δ_0	hybridization energy

Introduction

The study of ultracold quantum gases has its roots in the early twentieth century, when the theoretical foundations of quantum statistics were laid down by Bose and Einstein for integer-spin particles [1–3], and by Fermi and Dirac for half-integer spin particles [4, 5]. The seminal work from Bose and Einstein predicted striking collective phenomena, most notably Bose-Einstein condensation (BEC), the macroscopic occupation of a single quantum state below a critical temperature. However, the experimental realization of these ideas had to wait for the development of advanced cooling techniques in the 1980s [6, 7]. The first experimental observations of BEC in dilute atomic gases of ^{87}Rb and ^{23}Na came in 1995 [8, 9]. Shortly thereafter, the achievement of quantum degeneracy in fermionic species such as ^{40}K and ^{6}Li [10, 11] paved the way for the investigation of strongly correlated Fermi systems and, crucially, Bose-Fermi mixtures.

Since then, ultracold Bose-Fermi (BF) mixtures have been studied extensively both from a theoretical and experimental perspective, as they offer a wide range of possibilities to tune their properties externally. Magnetic or optical traps allow to cool down atomic vapors to the nanokelvin scale, and reach the quantum degenerate regime in which bosons and fermions exhibit their respective quantum statistics [12–15]. The use of Fano-Feshbach resonances between different interaction channels enables access to tunable interparticle interaction parameters. For instance, in a strong attractive interaction regime, this allows control over the formation of bound states of different atomic species. The optical or magnetic trapping determines the density profile of the atoms, making it possible to tune the effective dimensionality of the system. In particular, confinement-induced resonances allow to realize a dimensional crossover from 3D confinement down to (quasi-)2D one, while at the same time tuning the strength of the BF and the boson-boson (BB) interactions [16–18].

Due to their high degree of tunability, ultracold gases constitute a versatile platform for simulating quantum matter. The realization of ultracold atomic BF mixtures has allowed exploration of a wide range of phenomena like phase separation [19], polarons [20–25], dual superfluidity [26–29], collective excitations [30, 31], mediated interactions [32–34], and Feshbach molecules [35–44].

Besides ultracold quantum gases, BF mixtures have also been realized in semiconductor nanostructures known as transition metal dichalcogenides (TMDs). TMDs are layered systems made up of two-dimensional crystalline sheets of transition metals and chalcogenides [45–53]. Newly developed exfoliation techniques have enabled atomically thin structures of few to only a single layer of TMD, where the electrons are effectively confined in two dimensions. A common TMD is molybdenum

disulfide MoS_2, which in its single-layer form possess a direct band gap [50]. The latter facilitates optical excitations across the band gap, creating a (conduction-band) electron and a (valence-band) hole that experience mutual Coulomb attraction. This attraction can lead to the formation of a bound state called exciton. Due to its spatial extension, an exciton (which is a composite boson) can develop an electric dipole moment and interact attractively with an electron or hole (which are of fermionic nature) [45, 47, 52, 53]. Recently, electrically tunable Fano-Feshbach resonances in TMD bilayers have been detected [46, 49]. In this regard, TMDs are similar to ultracold atomic Bose-Fermi mixtures: TMDs can also realize strong coupling yielding an interspecies bound state, not only between electrons and holes but also between excitons and electrons/holes.

In experiments, Bose-Fermi mixtures are trapped in a potential well with a non-trivial profile. Therefore, bosons and fermions exhibit non-trivial density distributions, and a local population imbalance is unavoidable even when the two components contain the same number of atoms. This inhomogeneity can be partially accounted for by considering a global population imbalance; that is, the two components are taken to be homogeneous, but with a density-imbalance between the two. In the case of attraction between bosons and fermions, the assumption of having a homogeneous system requires tuning the BB repulsion to exceed a certain value in order to guarantee the mechanical stability of the BF mixture against collapse [54, 55]. In addition to density-imbalance, any BF mixture, both in ultracold gases and in TMDs, features components with different masses (in atomic mixtures, these can be different atomic species or different isotopes of the same species; in TMDs, these are excitons and charge carriers); consequently, mass-imbalance is also unavoidable. These considerations motivate the theoretical study of a homogeneous BF mixture with BF pairing, BB repulsion, and density-/mass-imbalance.

In particular, in this thesis we investigate effects arising from mass imbalance, generalizing the results obtained in previous works such as [56] for mass-balanced mixtures. Moreover, possible improvements to the theory developed in that same paper, the so-called transition matrix approach (or T-matrix approach), are discussed in detail from a formal point of view. These improvements include the implementation of a partial self-consistency in the T-matrix, a modified scheme that should allow for a more faithful treatment of Fermi atomic excitations. However, this modification alone is found to worsen the agreement of the numerical results with the known analytical expressions in the weak BF-coupling regime. This requires taking into account, in the calculation of the anomalous boson self-energy, the BB interaction mediated by fermions, which yields an additional contribution not considered in [56]. In the weak-coupling limit, this term compensates for a spurious term originating from the partial self-consistent scheme in the perturbative expansion of the boson chemical potential. In addition, the importance of its inclusion is suggested by comparison with a recent theoretical work on mediated interactions in BF mixtures [57], showing that this term plays an important role in the stability of BF mixtures.

The thesis is organized as follows. In Chap. 1, we introduce the general description of Bose-Fermi mixtures, focusing on the techniques used to realize boson-fermion pairing and on some examples of mixtures realized in ultracold gases and TMDs. In Chap. 2, the general diagrammatic theory for

fermions and bosons in the condensed phase is reviewed. In Chap. 3, the diagrammatic theory is applied to two-dimensional Bose-Fermi mixtures, and expressions for the fundamental thermodynamical quantities are derived within the T-matrix approach. Calculations are carried out for different values of the BF coupling parameter, yielding (semi-)analytical results in the weak- and strong-coupling regimes. The modified T-matrix method and the additional anomalous self-energy term are also presented. Chap. 3 is complemented by Appendices A, B, and C. Finally, in Chap. 4 (and Appendix D), the results for the thermodynamical quantities are presented, with a focus on the effects arising from mass-imbalance. Comparisons with the (semi-)analytical expressions obtained in Chap. 3 are also provided.

Chapter 1

Bose-Fermi mixtures

In this chapter, general concepts of the physics of ultracold atomic gases are introduced. Special attention is given to the techniques underlying boson-fermion pairing and the cooling of the mixture to the quantum degenerate regime. The class of solid state transition-metal dichalcogenides is then briefly presented, with particular focus on the similarities to ultracold atomic Bose-Fermi mixtures that allow for a unified description encompassing both systems.

1.1 Fano-Feshbach resonances

In this section we describe what is meant by a *Fano-Feshbach resonance* and explain why these resonances constitute an important tool for controlling atomic interactions in the systems of interest, making it possible to tune both the magnitude and the sign of the effective coupling parameter between particles. Before doing so, we briefly recall a few concepts from scattering theory and introduce the notion of a *channel*.

In the center of mass frame, the condition of energy conservation for two-particle scattering from one energy eigenstate to another reads (for relative distances far larger than the interaction potential range)

$$\frac{\mathbf{k}^2}{2m_\mathrm{r}} + \varepsilon_1 + \varepsilon_2 = \frac{\mathbf{k}'^2}{2m_\mathrm{r}} + \varepsilon_1' + \varepsilon_2', \tag{1.1}$$

where $\mathbf{k}$ is the initial relative momentum, $m_\mathrm{r} = m_1 m_2/(m_1+m_2)$ is the reduced mass, and ε_i denotes the eigenvalue of the hamiltonian describing the internal degrees of freedom of particle i; the prime indicates the corresponding quantities in the final state. Note that here and in the rest of this thesis we choose units such that $\hbar = 1$.
The above equation can be rearranged as

$$\frac{\mathbf{k}'^2}{2m_\mathrm{r}} = \frac{\mathbf{k}^2}{2m_\mathrm{r}} + \varepsilon_1 + \varepsilon_2 - \varepsilon_1' - \varepsilon_2'. \tag{1.2}$$

A channel is defined by the set of quantum numbers specifying the internal states of the two particles.

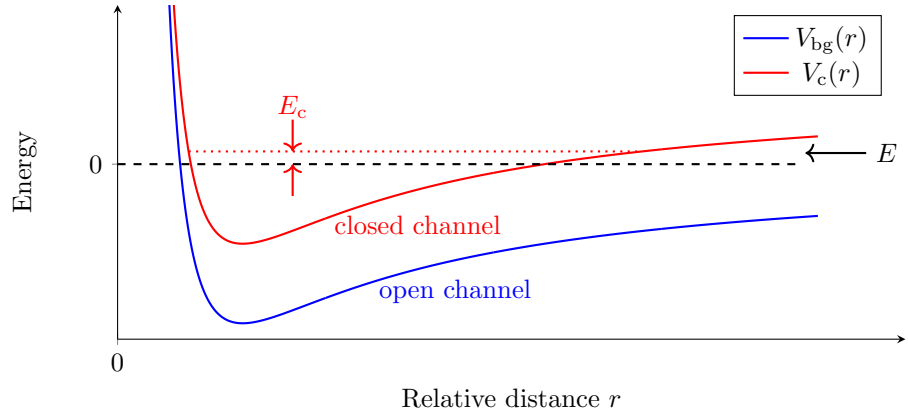

Figure 1.1: Fano-Feshbach resonance model for a two-channel case: two particles scattering at energy E resonantly couple to a molecular bound state with energy $E_{\rm c}$ of the closed channel potential. The separation between the asymptotes of $V_{\rm bg}(r)$ and $V_{\rm c}(r)$ as $r \to \infty$ corresponds the Zeeman energy difference $\Delta\mu\, B$, with $\Delta\mu$ being the difference of the magnetic moments of the two channels.

If $\mathbf{k}'^2/(2m_{\rm r}) > 0$ the final channel is said to be *open*, since the final internal state can be accessed from the initial internal state if the relative momentum varies accordingly. If instead $\mathbf{k}'^2/(2m_{\rm r}) < 0$ the final channel is *closed*, since for that set of internal quantum numbers the process is forbidden by energy conservation.

We speak of a Fano-Feshbach resonance when the energy of a bound state in a closed channel approaches the energy of a scattering state in an open channel [58]. By definition of a closed channel, it is not possible for the two particles to scatter into a final state corresponding to such a bound state; however, due to the bound state's energy being close to that of the allowed scattering state, the overlap between the evolved initial state and the bound state becomes significantly non-zero for times close to the collision time. This means that two particles in an open channel can scatter "virtually" to a bound state in a closed channel, which subsequently decays in one of the open channels.

Fano-Feshbach resonances can be realized in several different ways. For instance, channels can be coupled together by adjusting an external magnetic field (magnetically tunable Fano-Feshbach resonance, see e.g. [59]), or an electric field (electrically tunable Fano-Feshbach resonance, see e.g. [46]) or a laser field (optically tunable Fano-Feshbach resonance, see e.g. [60]).

As a pedagogic example, let us consider a Fano-Feshbach resonance in the isolated resonance approximation, meaning that a single bound state of the closed channel gives a significant contribution to the resonance. Let us further assume that the resonance is magnetically tunable, so that the channels are distinguished by their magnetic moments. For definiteness, let the initial (open) channel be associated with the total magnetic moment $\mu_{\rm bg}$, and the closed channel with the total magnetic moment $\mu_{\rm c}$. If we turn on an external magnetic field B, the interaction energy between particles acquires a dependence on the magnetic moment of the correspondent channel. Let $V_{\rm bg}(r)$ be the potential associated with the initial channel ("background" potential) and $V_{\rm c}(r)$ be the potential associated with the closed channel.

A representative example for $V_{\rm bg}(r)$ and $V_{\rm c}(r)$ is depicted in Fig. 1.1, together with the energy E of the initial scattering state and the energy $E_{\rm c}$ of the closed channel bound state. Under the assumptions of $E \approx E_{\rm c}$ and of small relative momenta $\mathbf{k}$ and $\mathbf{k}'$, it can be shown (see [61]) that the scattering amplitude $f(\mathbf{k}, \mathbf{k}')$ (to be defined in Sec. 2.5.3) for an incoming state with relative momentum $\mathbf{k}$ scattering into a final state with relative momentum $\mathbf{k}'$ is given by

$$f(\mathbf{k}, \mathbf{k}') \propto \frac{1}{E - E_{\rm c}}. \tag{1.3}$$

Denoting the energy of the two scattering particles at vanishing relative kinetic energy and at infinite relative distance by $E_{\rm bg}$, and assuming $E_{\rm c} = E_{\rm c}^0 - \mu_{\rm c}\, B$ and $E_{\rm bg} = E_{\rm bg}^0 - \mu_{\rm bg}\, B$, we can approximate the RHS of equation (1.3) by

$$\frac{1}{E - E_{\rm c}} \approx \frac{1}{(\mu_{\rm c} - \mu_{\rm bg})(B - B_0)}. \tag{1.4}$$

Here, we have defined $B_0 \equiv (E_{\rm c}^0 - E_{\rm bg}^0)/(\mu_{\rm c} - \mu_{\rm bg})$ to be the magnetic field for which the bound state energy $E_{\rm c}$ equals the energy $E_{\rm bg}$, and we have used $|\mathbf{k}| \approx 0$ to approximate $E \approx E_{\rm bg}$. In practice, then, the resonant coupling of the two channels is realized by tuning $E_{\rm c} \approx E_{\rm bg}$.

This simple model shows that we can control the scattering amplitude by tuning the external magnetic field B. We will discuss in Sec. 2.5.3 that $f(\mathbf{k}, \mathbf{k}')$ is closely related to the effective coupling of the interactions in the system of interest for this thesis. By tuning B closer to or further from B_0, the magnitude of the coupling can be made larger or smaller, or change sign.

In current experiments on Bose-Fermi mixtures, Fano-Feshbach resonances can be *broad* or *narrow* [62]. Broad resonances are characterized by the smallness of the effective range parameter of the boson-fermion interaction potential with respect to both the average interparticle distance $l \equiv n^{-d}$ (with d being the dimensionality of the system and n its number density) and the boson-fermion scattering length (to be defined in Sec 2.5.3). Instead, in narrow resonances the range of the interactions is comparable or larger in size than one of the other two lengths.

1.2 Ultracold atomic gases

The term "ultracold gas" is used to describe atoms at low temperature (typically $T \lesssim 1\,\mu$K), that are also assumed to be sufficiently dilute so that the system does not solidify and is indeed a gas.
In this regime, known as *quantum degeneracy*, the quantum statistics of the atomic constituents becomes relevant. In an ideal Bose gas, atoms macroscopically occupy the lowest energy single-particle mode, whereas in an ideal Fermi gas atoms fill up the single-particle modes up to the Fermi energy, forming the so-called Fermi sphere.

The physics of ultracold atomic systems is ruled by three fundamental length scales: the *thermal de Broglie wavelength* $\lambda = \sqrt{2\pi/(m k_{\rm B} T)}$ (with m denoting the mass of the atomic constituents and $k_{\rm B}$ the Boltzmann constant), the average interparticle distance l, and the range of the interaction potential between particles. Quantum degeneracy is realized when $l \lesssim \lambda$.

If the system of ultracold atoms is tuned close to a broad Fano-Feshbach resonance, then the range

of the potential is small compared to all other length scales. In this case interactions between atoms can be described by a single parameter, the scattering length, and the whole spectrum of different values of the coupling can be explored by varying the external parameter that controls the resonance.

For example, a milestone in theoretical quantum many-body physics was achieved in 1957, when the BCS theory was first formulated in [63]. In this framework, electrons with opposite spin and momentum form correlated pairs (known as *Cooper pairs*) which condense below a critical temperature, giving rise to superconductivity. This work provided the first microscopic explanation of conventional superconductivity, a phenomenon discovered in 1911.

The BCS description applies to the weak-coupling regime, where correlations between paired electrons are weak. As the strength of the attractive interaction increases, fermions bind into tightly bound diatomic molecules with bosonic character, which can undergo Bose–Einstein condensation. The excess of fermionic atoms forms instead a background Fermi sea. The continuous evolution between these two regimes, known as the *BCS–BEC crossover*, has been extensively studied over the past decades from both theoretical [64–70] and experimental [71–75] perspectives.

As the interaction strength is increased, Bose-Fermi mixtures with BF pairing undergo a phenomenon similar to the BCS-BEC crossover in Fermi-Fermi systems. In the BF case, bosons and fermions also bind into molecules in the strong-coupling regime; however, these molecules obey Fermi statistics and therefore fill a Fermi sphere instead of forming a Bose-Einstein condensate.

1.2.1 Examples of realized ultracold atomic Bose-Fermi mixtures

The typical procedure to realize an ultracold Bose-Fermi mixture consists of several successive stages of trapping and cooling, until quantum degeneracy of both species is achieved. Once the mixture is prepared, interspecies interactions can be tuned in a controlled way by means of Fano-Feshbach resonances. An example of the specific steps to prepare the mixture may be as follows:

1. both atomic species are captured and laser cooled in a magneto-optical trap (MOT);
2. the mixture is transferred to an optically-plugged magnetic trap (OPT), used to confine the two species;
3. in the OPT, the bosonic species undergoes forced radio-frequency (RF) evaporative cooling while the fermionic species is sympathetically cooled.

The above steps correspond to those of the experiment reported in [13], where the apparatus used for the preparation of a ^{41}K-^{6}Li mixture is described in detail. The outcome is the realization of a degenerate mixture containing 1.4×10^5 ^{41}K atoms with a condensate fraction of 62% and 5.4×10^5 ^{6}Li atoms at $0.25\,T_{\mathrm{F}}$. In the following, we schematically present the trapping and cooling techniques employed in this specific experiment, which are however common to many other experimental realizations of ultracold Bose-Fermi mixtures.

A MOT is an apparatus that employs a spatially varying magnetic field to trap atoms exploiting the Zeeman effect, while at the same time cooling the samples down by absorption and re-emissions of photons [76, 77].

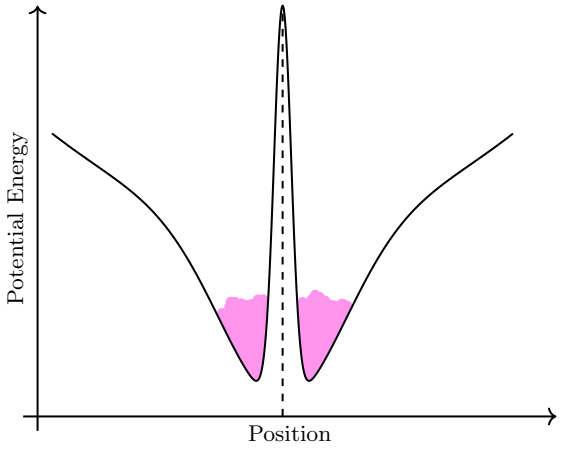

Figure 1.2: Pictorial representation of the potential employed in an optically-plugged magnetic trap. The dashed line locates the peak due to the repulsive light potential, at the position corresponding to the zero of the magnetic field and the center of the trap. Colder atoms are more likely to be detected near the center of the trap, in the potential wells schematically represented by the purple shaded areas. The figure is a 1-dimensional adaptation of Fig. 1 in [9].

An OPT confines atoms through a combination of three potentials: a linear magnetic potential arising from a spatially varying magnetic field, a repulsive light shift potential generated by a laser beam focused onto the point of the trap where the magnetic field vanishes, and a radio-frequency field that enables evaporative cooling [9]. The repulsive potential is used to suppress the trap loss by "plugging the hole" of the magnetic field at the center of the magnetic trap. For a pictorial representation of the potential profile, see Fig. 1.2

RF evaporative cooling is a technique used to reduce the temperature of atoms in a magnetic trap [78]. The atoms with higher kinetic energy spend more time far from the center of the trap, where they experience a stronger magnetic field and therefore a larger Zeeman shift. The chosen frequency defines a surface at which the Zeeman splitting matches the RF photon energy, driving a transition from a trapped state to a non-trapped state and thus removing those atoms from the trap.

Sympathetic cooling is a process in which particles of one type cool particles of another type [79]. In our case, the coolant is made up of the RF cooled bosons, while the temperature of fermion component is reduced by sympathetic cooling.

These trapping and cooling techniques, while reported in [13] for the ^{41}K–^{6}Li experiment, are representative of the methods commonly employed in the preparation of ultracold Bose–Fermi mixtures. In Table 1.1 we report a list of many realized heteronuclear Bose–Fermi mixtures, their mass ratios, and references to the corresponding experimental works.

Mixture (B - F)	m_B/m_F	References
^{87}Rb - ^{171}Yb	0.509	[15]
^{23}Na - ^{40}K	0.575	[23, 31, 37, 40, 41, 44, 59]
^{168}Er - ^{161}Dy	1.043	[12]
^{87}Rb - ^{40}K	2.175	[21, 32, 35, 36, 39, 42]
^{23}Na - ^{6}Li	3.833	[38]
^{41}K - ^{6}Li	6.833	[13, 19, 20, 28, 34, 80]
^{84}Sr - ^{6}Li	14	[14]
^{133}Cs - ^{6}Li	22.167	[30, 33, 43]
^{174}Yb - ^{6}Li	29	[27]

Table 1.1: Examples of realized ultracold heteronuclear Bose-Fermi mixtures, their mass ratios and references to experimental works.

1.3 Transition metal dichalcogenides

The *transition metal chalcogenides* are a group of about 60 materials, most of which are layered structures with weak interlayer van der Waals interactions [81]. Three subsets are identified: the transition metal *monochalcogenides*, with the form of MX (M = Cu, Ag; X = S, Se, Te), the transition metal *dichalcogenides*, with the form of MX_2 (M = W, Mo as semiconductor; V, Nb, Ta as metal), and the (less explored) transition metal *trichalcogenides*, with the form of MX_3 (M = Ti, Zr, Hf, Rf, V, Nb, Ta, Db, and Cr), where X represents chalcogens (S, Se, Te). By using micromechanical cleavage, one can obtain few-layer and monolayer crystals, typically of few to tens of micrometers in lateral dimension [82].

Here, we shall focus on semiconducting TMDs MX_2, with M = Mo, W, which exhibit relevant excitonic properties. In their bulk form, they are *indirect band gap semi-conductors* [45], meaning that the minimal-energy state in the conduction band and the maximal-energy state in the valence band are characterized by a different Bloch momentum. When thinned down to the limit of a single monolayer, the band gap becomes *direct*, meaning that the minimal-energy state in the conduction band and the maximal-energy state in the valence band are characterized by the same Bloch momentum (see Fig. 1.3). This implies that optical excitations across the gap are enhanced, since no Bloch momentum transfer from a photon to an electron is needed to promote the latter from the valence to the conduction band.

Following absorption of a photon with suitable energy, the electron promoted to the conduction band leaves behind a hole in the valence band. In TMD monolayers, the electrons and holes are tightly bound together as *excitons* by the attractive Coulomb interaction.[1] As a result, the fundamental optical properties at both cryogenic and room temperature are determined by strong exciton resonances [45].

[1]The attractive Coulomb interaction is less screened with respect to bulk TMDs, due to the absence of a dielectric environment extending in all directions [48].

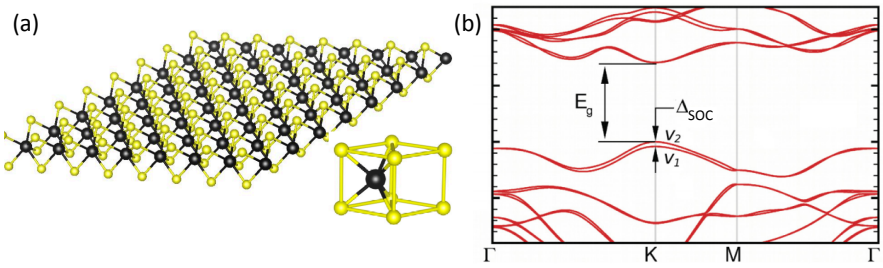

Figure 1.3: (a): Monolayer TMD crystal structure. The transition metal atoms appear in black, the chalcogen atoms in yellow. The hexagonal real-space lattice gives rise to a hexagonal Brillouin zone. (b): Typical band structure of MX_2 TMD monolayers calculated using density functional theory, showing the band gap E_g at the K-points (i.e. the corners of the hexagonal Brillouin zone). The highlighted splitting in the valence band is due to spin-orbit coupling. The figure is reproduced from [45].

1.3.1 Bose-Fermi mixtures in TMDs

In ultracold Bose-Fermi mixtures, bosons do not appear as collective excitations, but they are atoms that can be treated as point-like particles (since the effects originating from the internal degrees of freedom are subleading in collisions at extremely low temperatures) which interact with the fermions by coupling terms that are non-linear in their creation and annihilation operators. In contrast, typical solid state systems concern point-like fermions (electrons) that interact with bosons emerging as collective, low-energy excitations of either the crystal lattice (phonons) or the electronic system itself (e.g. plasmons or magnons). In order to represent pointlike bosons, one faces the challenge to ensure that the fermions remain sufficiently dilute compared to the extent of the bosonic particle, which is characterized, for instance, by its binding energy or internal excitation energies.
Upon doping the semiconductor with charge carriers (either electrons or holes), excitons in bulk semiconductors can form with a binding energy of the order of 10 meV [48, 83], which is roughly of the same order as the Fermi energy that determines the fermion density. This fact invalidates the picture of a "well-defined" Bose-Fermi mixture.
TMD monolayers, on the other hand, exhibit exciton states which are more strongly bound, due to the enhancement of Coulomb attraction between electrons and holes. In particular, the binding energy is of the order of hundreds of meV [48, 84]; as a consequence, it is possible to realize the desired large energy separation where excitons remain well-defined atom-like particles even in the presence of the electronic component.

The analogy with ultracold atomic Bose-Fermi mixtures further involves the following facts:

- excitons are expected to exhibit, at low to intermediate densities, collective phenomena such as Bose-Einstein condensation and superfluidity [85, 86];
- signatures of boson scattering of excitons have been reported ([87] for monolayer WSe_2);
- through inelastic scattering with electrons or holes, an exciton can capture an additional charge

and form a bound three-particle state at intermediate densities, the so-called *trion states*. Since excitons can be considered as composite bosons (at least for not too high carrier densities, as discussed above), trions can be seen as composite fermions made up of a composite boson and an electron or hole, with a mass-imbalance due to the mass of the exciton being roughly two times the mass of the extra charge carrier (in typical TMDs);[2]

- an electrically tunable Fano-Feshbach resonance has recently been realized in a $MoSe_2$ bilayer system, where a perpendicular electric field tunes the interlayer exciton-hole scattering into resonance with the intralayer trion state, enabling precise electrical control over the exciton-hole interaction strength [46]. The emergence of the interlayer Feshbach molecule leaves distinct signatures in the optical excitation spectrum, which can be understood in terms of Fermi polaron formation [49]. This electrical tunability opens a promising route toward the realization of degenerate Bose-Fermi mixtures with fully controllable interactions in a purely 2-dimensional solid-state platform.

[2]However, we should specify that the correlations between trions and the Fermi sea of electrons (or holes) may be relevant [88–90], since the trion's binding energy is typically of the same order of the Fermi energy [48]. This is different from ultracold atomic Bose-Fermi mixtures, for which in the strong-coupling regime the binding energy of the Bose-Fermi molecule is much larger than the Fermi energy.

Chapter 2

Perturbation theory and the transition matrix

In this chapter, we first review the basics of the imaginary-frequency Green's function formalism. Then, we apply it to the case of a Bose-Fermi mixture in the condensed phase, discussing the Feynman rules, Dyson's equations, and the subtleties related to the zero-temperature limit. Finally, we present a class of Feynman diagrams that will be central in the following chapters and discuss their relation to relevant physical quantities from the quantum theory of scattering.

2.1 Imaginary-frequency Green's functions

For the purposes of this work, expectation values of observables are most conveniently evaluated in the grand-canonical ensemble. Therefore, the starting point is writing down the system's grand-canonical hamiltonian

$$K = H - \mu N, \tag{2.1}$$

where μ is the chemical potential. The grand-canonical density matrix ρ_{G} and partition function Z_{G} are defined as

$$\rho_{\mathrm{G}} \equiv \frac{\mathrm{e}^{-\beta K}}{Z_{\mathrm{G}}}, \quad Z_{\mathrm{G}} \equiv \mathrm{tr}\big(\mathrm{e}^{-\beta K}\big), \tag{2.2}$$

where $\beta = 1/(k_{\mathrm{B}}\,T)$ is the inverse temperature. β, μ, and the occupied volume V specify the macrostate of the system. Unless otherwise stated, the system is assumed to live in d-dimensional space.

We define the *single-particle temperature Green's function* as

$$G(\mathbf{r}\tau, \mathbf{r}'\tau') \equiv -\left\langle \mathrm{T}[\psi(\mathbf{r}\tau)\psi^{\dagger}(\mathbf{r}'\tau')]\right\rangle, \tag{2.3}$$

where:

- the time-ordering T[...] orders the operators inside the square brackets according to their value of τ, with the smallest at the right;
- $\langle \ldots \rangle = \mathrm{tr}(\rho_{\mathrm{G}} \ldots)$ and $\mathrm{tr}\,(\ldots) = \sum_{|\chi\rangle} \langle\chi| \ldots |\chi\rangle$ denotes the sum over a complete, orthonormal set of states $\{|\chi\rangle\}$;
- $\psi(\mathbf{r}\tau)$ and its adjoint $\psi^\dagger(\mathbf{r}\tau)$ are the Heisenberg fields (bosonic or fermionic)[1]

$$\psi(\mathbf{r}\tau) = \mathrm{e}^{K\tau}\psi(\mathbf{r})\mathrm{e}^{-K\tau}, \quad \psi^\dagger(\mathbf{r}\tau) = \mathrm{e}^{K\tau}\psi^\dagger(\mathbf{r})\mathrm{e}^{-K\tau}. \tag{2.4}$$

In presence of fermionic fields, T[...] includes the factor $(-1)^P$ with P being the number of permutations of fermionic operators in [...] needed to restore the original ordering.

Green's functions are directly related to equilibrium thermodynamic properties of the system. As a useful example, we show here how to deduce the average number of particles $N(\beta, \mu, V)$: denoting $\tau^+ \equiv \tau + 0^+$

$$\int \mathrm{d}\mathbf{r}\; G(\mathbf{r}\tau, \mathbf{r}\tau^+) = \mp\frac{1}{Z_{\mathrm{G}}} \int \mathrm{d}\mathbf{r}\;\; \mathrm{tr}\big(\mathrm{e}^{-\beta K}\psi^\dagger(\mathbf{r})\psi(\mathbf{r})\big) \tag{2.5}$$

$$= \mp \int \mathrm{d}\mathbf{r}\;\; \langle n(\mathbf{r})\rangle = \mp N(\beta, \mu, V), \tag{2.6}$$

where "−" is for bosons and "+" is for fermions, with this sign difference coming from the time ordering. We have therefore derived the relation

$$n = \mp\frac{1}{V} \int \mathrm{d}\mathbf{r}\; G(\mathbf{r}\tau, \mathbf{r}\tau^+) \tag{2.7}$$

for a homogeneous system's density at given β, μ, V.

If the system of interest is isolated, the Green's functions depend only on the time difference: $G(\mathbf{r}\tau_1, \mathbf{r}'\tau_2) = G(\mathbf{r}, \mathbf{r}'; \tau_1 - \tau_2) \equiv G(\mathbf{r}, \mathbf{r}'; \tau)$. To find a Fourier representation of G in the variable τ, it is important to recall its periodicity properties. In their domain of definition, i.e. $\tau \in (-\beta, \beta)$, the boson Green's functions are periodic in τ with period β, while the fermion Green's functions are anti-periodic with period β (see [91, Sec. 7.25]). Therefore, the following direct and inverse Fourier representations are available:

$$G(\mathbf{r}, \mathbf{r}'; \tau) = \frac{1}{\beta} \sum_{n=-\infty}^{\infty} \mathrm{e}^{-i\omega_n\tau} G(\mathbf{r}, \mathbf{r}'; \omega_n) \tag{2.8}$$

$$G(\mathbf{r}, \mathbf{r}'; \omega_n) = \int_0^\beta \mathrm{d}\tau\; \mathrm{e}^{i\omega_n\tau} G(\mathbf{r}, \mathbf{r}'; \tau) \tag{2.9}$$

[1] Note that since τ is real, the two Heisenberg fields are not actually one the hermitian conjugate of the other. We will nonetheless refer to a field and its "dagger version" as a field and its adjoint. τ is usually called *imaginary time* in the literature, since the operator $\mathrm{e}^{-K\tau}$ is related to the evolution operator e^{-iKt} by the map $t \mapsto -i\tau$.

with

$$\omega_n = \begin{cases} 2n\pi/\beta & \text{for bosons} \\ (2n+1)\pi/\beta & \text{for fermions.} \end{cases} \tag{2.10}$$

We will refer to Green's functions dependent on ω_n as *imaginary frequency Green's functions.*

Assuming the system to be translational invariant, i.e. $G(\mathbf{r}_1, \mathbf{r}_2; \tau) = G(\mathbf{r}_1 - \mathbf{r}_2; \tau) \equiv G(\mathbf{r}, \tau)$, we can employ a Fourier representation of the variable $\mathbf{r}$

$$G(\mathbf{r}, \tau) = \frac{1}{V} \sum_{\mathbf{k}} \mathrm{e}^{i\mathbf{k}\cdot\mathbf{r}}\, G(\mathbf{k}, \tau) \tag{2.11}$$

$$G(\mathbf{k}, \tau) = \int \mathrm{d}\mathbf{r}\ \mathrm{e}^{-i\mathbf{k}\cdot\mathbf{r}}\, G(\mathbf{r}, \tau), \tag{2.12}$$

and thus write the Green's function $G(\mathbf{r}, \tau)$ in terms of the Green's function $G(\mathbf{k}, \omega_n)$ in $(d{+}1)$-momentum space[2]

$$G(\mathbf{r}, \tau) = \frac{1}{\beta V} \sum_{\mathbf{k}} \sum_{\omega_n} \mathrm{e}^{i\mathbf{k}\cdot\mathbf{r} - i\omega_n\tau} G(\mathbf{k}, \omega_n). \tag{2.13}$$

With these definitions, the equation for the density (2.7) can be rewritten as

$$n = \mp \frac{1}{\beta V} \sum_{\mathbf{k}} \sum_{\omega_n} \mathrm{e}^{i\omega_n 0^+} G(\mathbf{k}, \omega_n). \tag{2.14}$$

If we assume periodic boundary conditions on the box of volume V and the thermodynamic limit, $\mathbf{k}$ takes value in a continuum and the sum over the discrete momenta is substituted with an integral: $V^{-1} \sum_{\mathbf{k}} \to \int \mathrm{d}\mathbf{k}/(2\pi)^d$. The density can then written in terms of a d-momentum integral as

$$n = \mp \frac{1}{\beta} \int \frac{\mathrm{d}\mathbf{k}}{(2\pi)^d} \sum_{\omega_n} G(\mathbf{k}, \omega_n) \mathrm{e}^{i\omega_n 0^+}. \tag{2.15}$$

2.1.1 Non-interacting systems

The simplest application of the Green's function formalism is to a non-interacting system, for which

$$K = \int \mathrm{d}\mathbf{r}\ \psi^\dagger(\mathbf{r}) \left(-\frac{\nabla^2}{2m} - \mu \right) \psi(\mathbf{r}), \tag{2.16}$$

and the field operators are conveniently expanded in the free particle's basis, i.e.

$$\psi(\mathbf{r}\tau) = \frac{1}{\sqrt{V}} \sum_{\mathbf{k}} \mathrm{e}^{i\mathbf{k}\cdot\mathbf{r} - \xi_{\mathbf{k}}\tau} a_{\mathbf{k}}, \quad \psi^\dagger(\mathbf{r}\tau) = \frac{1}{\sqrt{V}} \sum_{\mathbf{k}} \mathrm{e}^{-i\mathbf{k}\cdot\mathbf{r} + \xi_{\mathbf{k}}\tau} a^\dagger_{\mathbf{k}}. \tag{2.17}$$

[2] From this point onward, we employ $\sum_{\omega_n}$ as a short-hand notation, with ω_n given by (2.10).

In the case of bosons, few mathematical steps from the definition of the Green's function G^0 yield in imaginary frequency

$$\begin{aligned} G^0(\mathbf{r},\mathbf{r}';\omega_n) &= -\frac{1}{V}\sum_{\mathbf{k}} \mathrm{e}^{i\mathbf{k}\cdot(\mathbf{r}\ -\mathbf{r}')}\int_0^\beta \mathrm{d}\tau\ \mathrm{e}^{i\omega_n\tau}\mathrm{e}^{-\xi_{\mathbf{k}}\tau}(1+n(\mathbf{k})) \\ &= -\frac{1}{V}\sum_{\mathbf{k}} \frac{\mathrm{e}^{i\mathbf{k}\cdot(\mathbf{r}-\mathbf{r}')}(1+n(\mathbf{k}))}{i\omega_n-\xi_{\mathbf{k}}}\left(\exp\left[(i\omega_n-\xi_{\mathbf{k}})\beta\right]-1\right) = \frac{1}{V}\sum_{\mathbf{k}}\frac{\mathrm{e}^{i\mathbf{k}\cdot(\mathbf{r}-\mathbf{r}')}}{i\omega_n-\xi_{\mathbf{k}}}, \end{aligned} \tag{2.18}$$

where $n(\mathbf{k}) = \left\langle a^\dagger_{\mathbf{k}} a_{\mathbf{k}}\right\rangle = (\mathrm{e}^{\beta\xi_{\mathbf{k}}}-1)^{-1}$ and we have used $-(1+n(\mathbf{k}))^{-1} = (\exp(-\beta\xi_{\mathbf{k}}))-1$ together with $\mathrm{e}^{i\omega_n\beta}=1$ to go from the second to the third line.
Taking into consideration the different momentum distribution $n(\mathbf{k}) = (\mathrm{e}^{\beta\xi_{\mathbf{k}}}+1)^{-1}$, expression (2.18) is proven to hold for fermions as well, provided that ω_n is modified according to (2.10).
By looking at the final expression $G^0(\mathbf{r},\mathbf{r}';\omega_n) = V^{-1}\sum_{\mathbf{k}}\mathrm{e}^{i\mathbf{k}\cdot(\mathbf{r}-\mathbf{r}')}/(i\omega_n-\xi_{\mathbf{k}})$ we identify

$$G^0(\mathbf{k},\omega_n) = \frac{1}{i\omega_n-\xi_{\mathbf{k}}} \tag{2.19}$$

to be the non-interacting Green's function in (d+1)-momentum space. From this quantity we define the non-interacting *propagator* in (d+1)-momentum space as $-G^0(\mathbf{k},\omega_n)$, i.e. the Green's function with the opposite sign.

2.1.2 The perturbative expansion

Let us now move to the case of interacting systems. If we split the grand-canonical hamiltonian as $K = K_0 + W$, where K_0 is the non-interacting piece, we can expand the Green's function in perturbation theory [91, Sec. 7.24] as

$$G(\mathbf{r}\tau,\mathbf{r}'\tau') = \frac{\sum_{n=0}^\infty G^{(n)}(\mathbf{r}\tau,\mathbf{r}'\tau')}{\sum_{n=0}^\infty \left\langle S^{(n)}\right\rangle_0}. \tag{2.20}$$

In the above expression

$$G^{(n)}(\mathbf{r}\tau,\mathbf{r}'\tau') = -\left\langle \mathrm{T}[S^{(n)}\psi_{\mathrm{int}}(\mathbf{r}\tau)\psi^\dagger_{\mathrm{int}}(\mathbf{r}'\tau')]\right\rangle_0 \tag{2.21}$$

$$S^{(n)} = \frac{1}{n!}(-1)^n\int_0^\beta \mathrm{d}\tau_1\ldots\int_0^\beta \mathrm{d}\tau_n\ \mathrm{T}[W_{\mathrm{int}}(\tau_1)\ldots W_{\mathrm{int}}(\tau_n)] \tag{2.22}$$

$$\langle\ldots\rangle_0 = \frac{1}{\mathrm{tr}(\mathrm{e}^{-\beta K_0})}\,\mathrm{tr}\left(\mathrm{e}^{-\beta K_0}\ldots\right) \tag{2.23}$$

and the subscript "int" denotes operators in the interaction picture,[3]

$$O_{\mathrm{int}}(\tau) = \mathrm{e}^{K_0\tau}O\mathrm{e}^{-K_0\tau}. \tag{2.24}$$

[3]Note that, as for fields in the Heisenberg picture, ψ_{int} and its adjoint $\psi^\dagger_{\mathrm{int}}$ are not actually one the adjoint of the other.

Clearly, the index n labels the different perturbative orders in the interaction term W.

The general strategy to evaluate the above equations is to apply *Wick's theorem*. It allows to express any correlation function given by the expectation value $\langle \ldots \rangle_0$ of a time-ordered product of fields in the interaction picture as the sum of all products of contractions of two fields. The contraction of two field operators is non-vanishing only if it is between a field and its adjoint. In this case, it yields a non-interacting propagator:

$$\overbrace{\psi_j^\dagger \psi_i} = \overbrace{\psi_i \psi_j^\dagger} \equiv \left\langle \mathrm{T}[\psi_i \psi_j^\dagger] \right\rangle_0 = -G^0(i,j) \text{ for bosons} \tag{2.25}$$

$$-\overbrace{\psi_j^\dagger \psi_i} = \overbrace{\psi_i \psi_j^\dagger} \equiv \left\langle \mathrm{T}[\psi_i \psi_j^\dagger] \right\rangle_0 = -G^0(i,j) \text{ for fermions,} \tag{2.26}$$

using the compact notation $\psi_i = \psi_{\mathrm{int}}(\mathbf{r}_i \tau_i)$, $\psi_i^\dagger = \psi_{\mathrm{int}}^\dagger(\mathbf{r}_i \tau_i)$ and $G^0(i,j) = G^0(\mathbf{r}_i \tau_i, \mathbf{r}_j \tau_j)$.
The sum of products of non-interacting propagators can be pictured as a sum of *Feynman diagrams*. A first consequence of Wick's theorem is that the denominator $\sum_{n=0}^{\infty} \left\langle S^{(n)} \right\rangle_0$ eliminates all disconnected diagrams, leaving us with

$$G(\mathbf{r}\tau, \mathbf{r}'\tau') = \sum_{n=0}^{\infty} G^{(n)}(\mathbf{r}\tau, \mathbf{r}'\tau')\big|_{\mathrm{connected}}. \tag{2.27}$$

Moreover, since each connected graph appears essentially $n!$ times, the factor $1/n!$ in $G^{(n)}$ always simplifies when we sum the diagrams at order n in W_{int} and integrate over all internal variables.

2.2 Perturbation theory for the Bose-Fermi mixture

At this point we have set up the general formalism, and thus the next step is to identify the relevant interactions to include in our theory for the mixture of bosons and fermions. Then, we will formulate a set of Feynman rules to evaluate diagrammatically the perturbative corrections to the Green's functions.

2.2.1 The Bogolyubov substitution

Since we will eventually be working in the limit of vanishing temperature, for sufficiently weak interactions between particles a macroscopic fraction of the bosons forms a Bose-Einstein condensate. In the thermodynamic limit, a way to account for the large number N_0 of bosons that are condensed is through the *Bogolyubov substitution* of the creation and annihilation operators $a_{\mathbf{0}}^\dagger$, $a_{\mathbf{0}}$ with the real number $\sqrt{N_0}$ [91, Sec. 6.18]. Therefore, in terms of the condensate density $n_0 = N_0/V$

$$\frac{1}{\sqrt{V}} a_{\mathbf{0}}^\dagger \to \sqrt{n_0} \tag{2.28}$$

$$\frac{1}{\sqrt{V}} a_{\mathbf{0}} \to \sqrt{n_0}. \tag{2.29}$$

The boson field operator[4] $\psi_{\rm B}(\mathbf{r}) = V^{-1/2}\sum_{\mathbf{k}\neq\mathbf{0}} \mathrm{e}^{i\mathbf{k}\cdot\mathbf{r}}\ a_{\mathbf{k}} + V^{-1/2}a_{\mathbf{0}}$ acquires a non-zero expectation value on the state with all bosons condensed in the $\mathbf{k}=\mathbf{0}$ single-particle mode, while the expectation value of the field $\varphi_{\rm B}(\mathbf{r})$

$$\varphi_{\rm B}(\mathbf{r}) \equiv \sum_{\mathbf{k}\neq\mathbf{0}} \frac{1}{\sqrt{V}} \mathrm{e}^{i\mathbf{k}\cdot\mathbf{r}} a_{\mathbf{k}} \tag{2.30}$$

is vanishing. The resulting expansion $\psi_{\rm B}(\mathbf{r}) = \sqrt{n_0} + \varphi_{\rm B}(\mathbf{r})$ is at the basis of the theory in the broken U(1) symmetry phase. Here, by U(1) symmetry we mean the rigid symmetry associated with the total particle number conservation, which is explicitly broken by the Bogolyubov substitution. This reflects the existence of a condensate that acts as a classical reservoir which non-condensed bosons can enter or leave after a scattering event.
One of the reasons for which it is more convenient to employ the grand-canonical ensemble with control variables $\beta, \mu_{\rm B}, V$ (instead of, for instance, the canonical ensemble, with control variables $\beta, N_{\rm B}, V$) is precisely the possibility of dealing with the variable number of non-condensed bosons.

In its second-quantized form, the grand-canonical hamiltonian that describes the boson component alone reads

$$K_{\rm B} = \int \mathrm{d}\mathbf{r}\ \psi_{\rm B}^\dagger(\mathbf{r}) \left(-\frac{\nabla^2}{2m_{\rm B}} - \mu_{\rm B}\right) \psi_{\rm B}(\mathbf{r}) \tag{2.31}$$

$$+ \frac{1}{2}\int \mathrm{d}\mathbf{r} \int \mathrm{d}\mathbf{r}'\ \psi_{\rm B}^\dagger(\mathbf{r})\psi_{\rm B}^\dagger(\mathbf{r}')U_{\rm BB}(\mathbf{r}-\mathbf{r}')\psi_{\rm B}(\mathbf{r}')\psi_{\rm B}(\mathbf{r}) - \mu_{\rm B}. \tag{2.32}$$

After the Bogolyubov substitution, it becomes

$$K_{\rm B} = E_{\rm B,0} - \mu_{\rm B}N_0 + \sum_{\mathbf{k}\neq 0}\left(\frac{\mathbf{k}^2}{2m_{\rm B}} - \mu_{\rm B}\right) a_{\mathbf{k}}^\dagger a_{\mathbf{k}} + \sum_{j=1}^{5} V_j, \tag{2.33}$$

[4]The subscript "B" indicates that we are referring to the boson component, while we will be using "F" for the fermion component.

with

$$E_{\mathrm{B},0} = \frac{1}{2} n_0^2 \int \mathrm{d}\mathbf{r}\, \mathrm{d}\mathbf{r}'\, U_{\mathrm{BB}}(\mathbf{r}-\mathbf{r}') \tag{2.34}$$

$$V_1 = \frac{1}{2} n_0 \int \mathrm{d}\mathbf{r}\, \mathrm{d}\mathbf{r}'\, U_{\mathrm{BB}}(\mathbf{r}-\mathbf{r}')\, \varphi_{\mathrm{B}}(\mathbf{r}')\varphi_{\mathrm{B}}(\mathbf{r}), \tag{2.35}$$

$$V_2 = \frac{1}{2} n_0 \int \mathrm{d}\mathbf{r}\, \mathrm{d}\mathbf{r}'\, \varphi_{\mathrm{B}}^{\dagger}(\mathbf{r})\varphi_{\mathrm{B}}^{\dagger}(\mathbf{r}')\, U_{\mathrm{BB}}(\mathbf{r}-\mathbf{r}') \tag{2.36}$$

$$V_3 = n_0 \int \mathrm{d}\mathbf{r}\, \mathrm{d}\mathbf{r}'\, \varphi_{\mathrm{B}}^{\dagger}(\mathbf{r})\, U_{\mathrm{BB}}(\mathbf{r}-\mathbf{r}')\, \varphi_{\mathrm{B}}(\mathbf{r}'), \tag{2.37}$$

$$V_4 = n_0 \int \mathrm{d}\mathbf{r}\, \mathrm{d}\mathbf{r}'\, \varphi_{\mathrm{B}}^{\dagger}(\mathbf{r})\, U_{\mathrm{BB}}(\mathbf{r}-\mathbf{r}')\, \varphi_{\mathrm{B}}(\mathbf{r}), \tag{2.38}$$

$$V_5 = \sqrt{n_0} \int \mathrm{d}\mathbf{r}\, \mathrm{d}\mathbf{r}'\, \varphi_{\mathrm{B}}^{\dagger}(\mathbf{r})\, U_{\mathrm{BB}}(\mathbf{r}-\mathbf{r}')\, \varphi_{\mathrm{B}}(\mathbf{r}')\varphi_{\mathrm{B}}(\mathbf{r}), \tag{2.39}$$

$$V_6 = \sqrt{n_0} \int \mathrm{d}\mathbf{r}\, \mathrm{d}\mathbf{r}'\, \varphi_{\mathrm{B}}^{\dagger}(\mathbf{r})\varphi_{\mathrm{B}}^{\dagger}(\mathbf{r}')\, U_{\mathrm{BB}}(\mathbf{r}-\mathbf{r}')\, \varphi_{\mathrm{B}}(\mathbf{r}) \tag{2.40}$$

$$V_7 = \frac{1}{2} \int \mathrm{d}\mathbf{r}\, \mathrm{d}\mathbf{r}'\, \varphi_{\mathrm{B}}^{\dagger}(\mathbf{r})\varphi_{\mathrm{B}}^{\dagger}(\mathbf{r}')\, U_{\mathrm{BB}}(\mathbf{r}-\mathbf{r}')\, \varphi_{\mathrm{B}}(\mathbf{r}')\varphi_{\mathrm{B}}(\mathbf{r}). \tag{2.41}$$

$W_{\mathrm{BB}} \equiv \sum_{i=1}^{7} V_i$ defines the vertices regarding the boson-boson interactions. To include the boson-fermion interactions, we add to the hamiltonian a term

$$W_{\mathrm{BF}} \equiv \int \mathrm{d}\mathbf{r}\, \mathrm{d}\mathbf{r}'\, \psi_{\mathrm{B}}^{\dagger}(\mathbf{r})\psi_{\mathrm{F}}^{\dagger}(\mathbf{r}')U_{\mathrm{BF}}(\mathbf{r}-\mathbf{r}')\psi_{\mathrm{F}}(\mathbf{r}')\psi_{\mathrm{B}}(\mathbf{r}), \tag{2.42}$$

which after performing the Bogolyubov substitution gives rise to four hamiltonian terms $W_{\mathrm{BF}} = \sum_{i=1}^{4} U_i$:

$$U_1 = n_0 \int \mathrm{d}\mathbf{r}\, \mathrm{d}\mathbf{r}'\, \psi_{\mathrm{F}}^{\dagger}(\mathbf{r}')\, U_{\mathrm{BF}}(\mathbf{r}-\mathbf{r}')\, \psi_{\mathrm{F}}(\mathbf{r}') \tag{2.43}$$

$$U_2 = \sqrt{n_0} \int \mathrm{d}\mathbf{r}\, \mathrm{d}\mathbf{r}'\, \psi_{\mathrm{F}}^{\dagger}(\mathbf{r}')\, U_{\mathrm{BF}}(\mathbf{r}-\mathbf{r}')\, \psi_{\mathrm{F}}(\mathbf{r}')\varphi_{\mathrm{B}}(\mathbf{r}) \tag{2.44}$$

$$U_3 = \sqrt{n_0} \int \mathrm{d}\mathbf{r}\, \mathrm{d}\mathbf{r}'\, \varphi_{\mathrm{B}}^{\dagger}(\mathbf{r})\psi_{\mathrm{F}}^{\dagger}(\mathbf{r}')\, U_{\mathrm{BF}}(\mathbf{r}-\mathbf{r}')\, \psi_{\mathrm{F}}(\mathbf{r}') \tag{2.45}$$

$$U_4 = \int \mathrm{d}\mathbf{r}\, \mathrm{d}\mathbf{r}'\, \varphi_{\mathrm{B}}^{\dagger}(\mathbf{r})\psi_{\mathrm{F}}^{\dagger}(\mathbf{r}')\, U_{\mathrm{BF}}(\mathbf{r}-\mathbf{r}')\, \psi_{\mathrm{F}}(\mathbf{r}')\varphi_{\mathrm{B}}(\mathbf{r}). \tag{2.46}$$

Here and in the following, we shall always assume that the interaction potentials U_{BB} and U_{BF} depend only on the modulus of the relative distance $|\mathbf{r}_i - \mathbf{r}_j|$, implying that the Fourier transform

$$U(\mathbf{k}) = \int \mathrm{d}\mathbf{r}\, U(\mathbf{r})\mathrm{e}^{-i\mathbf{k}\cdot\mathbf{r}} \tag{2.47}$$

satisfies $U(\mathbf{k}) = U(-\mathbf{k})$.

2.2.2 Evaluation of the terms at low orders using Wick's theorem

As a pedagogic application of Wick's theorem, we report some of the lowest orders' terms in the Green's function $G'_{\mathrm{B}}(\mathbf{r}\tau, \mathbf{r}'\tau') = -\left\langle \mathrm{T}\left[\varphi_{\mathrm{B}}(\mathbf{r}\tau)\varphi^{\dagger}_{\mathrm{B}}(\mathbf{r}'\tau')\right]\right\rangle$ for non-condensed bosons and in the Green's function $G_{\mathrm{F}}(\mathbf{r}\tau, \mathbf{r}'\tau') = -\left\langle \mathrm{T}\left[\psi_{\mathrm{F}}(\mathbf{r}\tau)\psi^{\dagger}_{\mathrm{F}}(\mathbf{r}'\tau')\right]\right\rangle$ for fermions. The corresponding Feynman diagrams are also presented, but we postpone the discussion of the relation between the graphs and the mathematical expressions to Sec. 2.2.3.

Using the short-hand notation

$$x_i \equiv \mathbf{r}_i\tau_i,\ \ U(i,j) \equiv U(\mathbf{r}_i - \mathbf{r}_j)\delta(\tau_i - \tau_j),\ \ \int \mathrm{d}x_i\, \mathrm{d}x_j \equiv \int \mathrm{d}\mathbf{r}_i \int_0^\beta \mathrm{d}\tau_i \int \mathrm{d}\mathbf{r}_j \int_0^\beta \mathrm{d}\tau_j,$$

the connected diagrams contributing to G'_{B} at first order are written as

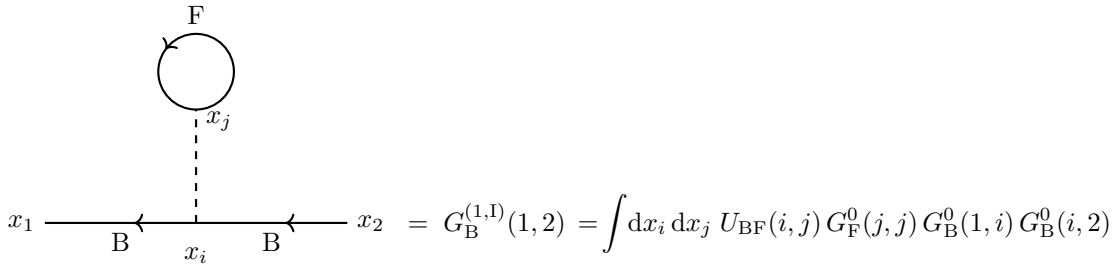

$$= G^{(1,\mathrm{I})}_{\mathrm{B}}(1,2) = \int \mathrm{d}x_i\, \mathrm{d}x_j\, U_{\mathrm{BF}}(i,j)\, G^0_{\mathrm{F}}(j,j)\, G^0_{\mathrm{B}}(1,i)\, G^0_{\mathrm{B}}(i,2)$$

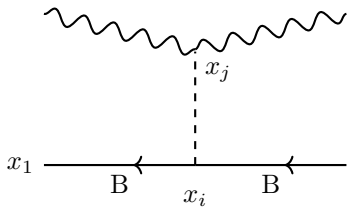

$$= G^{(1,\mathrm{II})}_{\mathrm{B}}(1,2) = n_0 \int \mathrm{d}x_i\, \mathrm{d}x_j\, U_{\mathrm{BB}}(i,j)\, G^0_{\mathrm{B}}(1,i)\, G^0_{\mathrm{B}}(i,2)$$

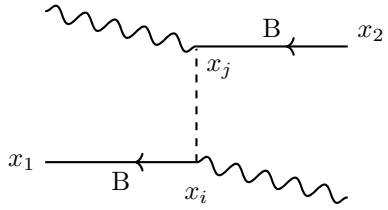

$$= G^{(1,\mathrm{III})}_{\mathrm{B}}(1,2) = n_0 \int \mathrm{d}x_i\, \mathrm{d}x_j\, U_{\mathrm{BB}}(i,j)\, G^0_{\mathrm{B}}(1,i)\, G^0_{\mathrm{B}}(j,2).$$

Moving to G_{F}, there is only one connected diagram at first order:[5]

[5]Note that we are not reporting the first order diagrams featuring a boson loop, which are vanishing in the zero-temperature limit for $\mu_{\mathrm{B}} < 0$.

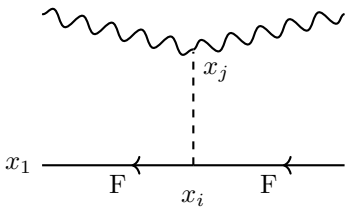

$$= G_{\mathrm{F}}^{(1,\mathrm{I})}(1,2) = n_0 \int \mathrm{d}x_i\, \mathrm{d}x_j\, U_{\mathrm{BF}}(i,j)\, G_{\mathrm{F}}^0(1,i)\, G_{\mathrm{F}}^0(i,2).$$

Using the Fourier form of the Green's functions and the interaction potentials (2.9), (2.18), (2.47) together with the identities

$$\delta(\tau) = \frac{1}{\beta} \sum_{\omega_n = \frac{2\pi n}{\beta}} \mathrm{e}^{-i\omega_n \tau} \quad \text{for } \tau \in (-\beta, \beta) \tag{2.48}$$

$$\frac{1}{\beta} \int_0^\beta \mathrm{d}\tau\, \mathrm{e}^{i\omega_n \tau} = \delta_{n,0}, \tag{2.49}$$

one can derive the following momentum space representations:

$$G_{\mathrm{B}}^{(1,\mathrm{I})}(\mathbf{k}, \omega_n) = n_{\mu_{\mathrm{F}}} U_{\mathrm{BF}}(\mathbf{0})\, G_{\mathrm{B}}^0(\mathbf{k}, \omega_n)^2 \tag{2.50}$$

$$G_{\mathrm{B}}^{(1,\mathrm{II})}(\mathbf{k}, \omega_n) = n_0\, U_{\mathrm{BB}}(\mathbf{0})\, G_{\mathrm{B}}^0(\mathbf{k}, \omega_n)^2 \tag{2.51}$$

$$G_{\mathrm{B}}^{(1,\mathrm{III})}(\mathbf{k}, \omega_n) = n_0\, U_{\mathrm{BB}}(\mathbf{k})\, G_{\mathrm{B}}^0(\mathbf{k}, \omega_n)^2 \tag{2.52}$$

$$G_{\mathrm{F}}^{(1,\mathrm{I})}(\mathbf{k}, \nu_n) = n_0\, U_{\mathrm{BF}}(\mathbf{0})\, G_{\mathrm{F}}^0(\mathbf{k}, \nu_n)^2. \tag{2.53}$$

In the above expressions, ν_n denotes the fermion discrete frequencies and ω_n the boson ones. Moreover, we have replaced the loop integral in $G_{\mathrm{B}}^{(1,\mathrm{I})}$ with the density of the non-interacting Fermi gas

$$n_{\mu_{\mathrm{F}}} = \int \frac{\mathrm{d}\mathbf{k}}{(2\pi)^d} \frac{1}{\beta} \sum_{\nu_n} \mathrm{e}^{i\nu_n 0^+} \frac{1}{i\nu_n - \xi_{\mathbf{k}}^{\mathrm{F}}}. \tag{2.54}$$

Note the presence of the factor $\mathrm{e}^{i\nu_n 0^+}$, due to the contraction $\overbrace{\psi_{\mathrm{F},i} \psi_{\mathrm{F},j}^\dagger}$ with $x_i = \mathbf{r}\tau$ and $x_j = \mathbf{r}\tau^+$ (that corresponds graphically to the fermion loop in the diagram). The positive infinitesimal in $\tau^+ = \tau + 0^+$ has to be added in argument of the adjoint field $\psi^\dagger$ anytime we contract it with a field ψ inside the same interaction term W. The rationale behind this regularization is that in this way the time-ordering in $\langle \mathrm{T}[W_{\mathrm{int}}] \rangle_0$ is well defined and places the adjoint fields to the left of the fields, as they are in W (see [91, Sec. 3.9] for further details).

As a first example of momentum-space Feynman diagrams, we report here that $G_{\mathrm{B}}^{(1,\mathrm{I})}(\mathbf{k}, \omega_n)$ is

assigned the following graph:

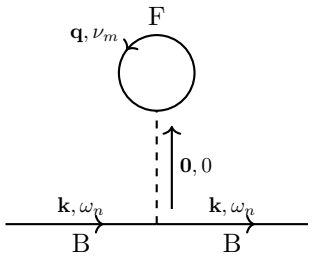

$$= G_{\mathrm{B}}^{(1,\mathrm{I})}(\mathbf{k}, \omega_n) = n_{\mu_{\mathrm{F}}}\, U_{\mathrm{BF}}(\mathbf{0})\, G_{\mathrm{B}}^{0}(\mathbf{k}, \omega_n)^2 .$$

To illustrate the summation of identical $n!$ diagrams mentioned at the end of Sec. 2.1.2, we provide now a perturbative calculation at second order in the interactions. Specifically, we consider the two terms

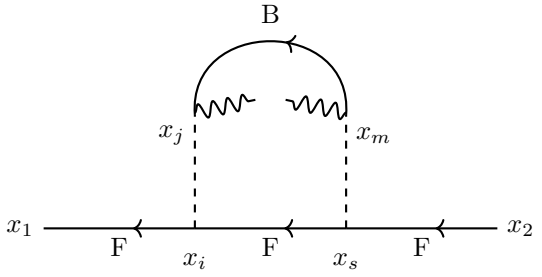

$$\begin{aligned} &= G_{\mathrm{F}}^{(2,\mathrm{I})}(1,2) \\ &= -\frac{1}{2}\, n_0 \int \mathrm{d}x_i\, \mathrm{d}x_j\, \mathrm{d}x_s\, \mathrm{d}x_m \Big(U_{\mathrm{BF}}(i,j)\, U_{\mathrm{BF}}(s,m) \\ &\quad \times G_{\mathrm{F}}^{0}(1,i)\, G_{\mathrm{F}}^{0}(i,s)\, G_{\mathrm{F}}^{0}(s,2)\, G_{\mathrm{B}}^{0}(m,j) \Big) \end{aligned} \tag{2.55}$$

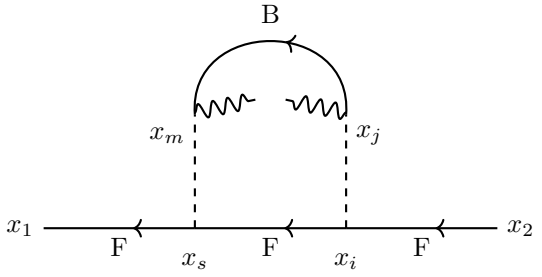

$$\begin{aligned} &= G_{\mathrm{F}}^{(2,\mathrm{II})}(1,2) \\ &= -\frac{1}{2}\, n_0 \int \mathrm{d}x_i\, \mathrm{d}x_j\, \mathrm{d}x_s\, \mathrm{d}x_m \Big(U_{\mathrm{BF}}(i,j)\, U_{\mathrm{BF}}(s,m) \\ &\quad \times G_{\mathrm{F}}^{0}(1,s)\, G_{\mathrm{F}}^{0}(s,i)\, G_{\mathrm{F}}^{0}(i,2)\, G_{\mathrm{B}}^{0}(j,m) \Big). \end{aligned} \tag{2.56}$$

The two contributions arise from two distinct contractions in $G_{\mathrm{F}}^{(2)}(1,2)\big|_{\mathrm{connected}}$, but they are identical after integrating over x_i, x_j, x_s and x_m as seen with the re-labeling of the dummy variables $x_i \leftrightarrow x_s$

and $x_j \leftrightarrow x_m$. Summing the two therefore results in the cancellation of the common factor of $1/2$. In momentum space, the sum reads

$$\begin{aligned} &G_{\mathrm{F}}^{(2,\mathrm{I})}(\mathbf{k},\nu_n) + G_{\mathrm{F}}^{(2,\mathrm{II})}(\mathbf{k},\nu_n) \\ &= -n_0 \left(G_{\mathrm{F}}^0(\mathbf{k},\nu_n)\right)^2 \int \frac{\mathrm{d}\mathbf{q}}{(2\pi)^d} \frac{1}{\beta} \sum_{\omega_m} G_{\mathrm{F}}^0(\mathbf{k}+\mathbf{q},\nu_n+\omega_m) G_{\mathrm{B}}^0(\mathbf{q},\omega_m) U_{\mathrm{BF}}(\mathbf{q})^2, \end{aligned} \tag{2.57}$$

and it corresponds to the following Feynman diagram:

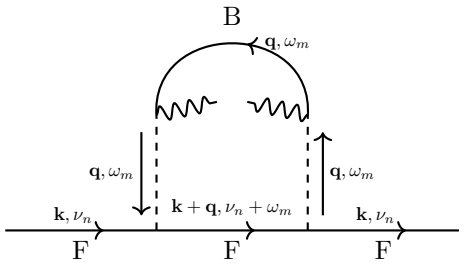

$$\begin{aligned} &= G_{\mathrm{F}}^{(2,\mathrm{I})}(\mathbf{k},\nu_n) + G_{\mathrm{F}}^{(2,\mathrm{II})}(\mathbf{k},\nu_n) \\ &= -n_0 G_{\mathrm{F}}^0(\mathbf{k},\nu_n)^2 \int \frac{\mathrm{d}\mathbf{q}}{(2\pi)^d} \frac{1}{\beta} \sum_{\omega_m} \Big(U_{\mathrm{BF}}(\mathbf{q})^2 \\ &\qquad \times G_{\mathrm{F}}^0(\mathbf{k}+\mathbf{q},\nu_n+\omega_m)\, G_{\mathrm{B}}^0(\mathbf{q},\omega_m) \Big). \end{aligned} \tag{2.58}$$

2.2.3 Feynman rules

We now describe how to relate a momentum space Feynman diagram to its corresponding mathematical expression, starting from particle lines and then moving to interaction vertices. These rules are known as *Feynman rules*.

Focusing on bosons, we consider the correlation function

$$\left\langle \mathrm{T}[\varphi_{\mathrm{B},i_1} \varphi_{\mathrm{B},i_2} \ldots \varphi_{\mathrm{B},j_1}^\dagger \varphi_{\mathrm{B},j_2}^\dagger \ldots] \right\rangle_0 . \tag{2.59}$$

If we include only the boson hamiltonian terms in our theory, it is the most general expectation value that can appear in Eq. (2.21). Because of Wick's theorem, it is non-vanishing only if the number of φ_{B} fields equals the number of $\varphi_{\mathrm{B}}^\dagger$ fields, and in this case it decomposes into a sum of products of $-G_{\mathrm{B}}^0$. Since we can reorder the boson fields inside the time ordering with no sign penalties, there are no relative minus signs between such products. In light of these observations, we assign to the lines of non-condensed bosons the rule

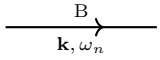

$$= -G_{\mathrm{B}}^0(\mathbf{k},\omega_n). \tag{2.60}$$

This rule is appropriate if we include the boson-fermion vertices too, since a bosonic and a fermionic field commute with each other.

Let us now move to fermions. We have seen that the products of boson fields in Eq. (2.21) decompose into sums of products of free boson propagators. In the full theory with bosons and fermions, any of these products multiplies a fermion correlation function of the kind

$$\left\langle \mathrm{T}\left[\psi^\dagger_{\mathrm{F},i_1}\psi_{\mathrm{F},i_1}\psi^\dagger_{\mathrm{F},i_2}\psi_{\mathrm{F},i_2}\cdots\left(\psi_{\mathrm{F},1}\psi^\dagger_{\mathrm{F},2}\right)^\ell\right]\right\rangle_0, \tag{2.61}$$

where $\ell = 1$ if the field operators at the external points are fermionic and $\ell = 0$ if the field operators at the external points are bosonic. Because of Wick's theorem, the expectation value decomposes into a sum of products of $-G^0_{\mathrm{F}}$. However, we are now dealing with fermionic fields and therefore they anti-commute inside the time ordering, possibly giving rise to relative signs. Specifically, minus signs appear between terms with a different number of fermion loops: for each fermion loop in a diagram we need to multiply the latter by a further factor of (-1). Keeping this additional Feynman rule in mind, we assign to the fermion lines lines a fermion propagator:

$$\overset{\mathrm{F}}{\underset{\mathbf{k},\,\omega_n}{\longrightarrow}} = -G^0_{\mathrm{F}}(\mathbf{k},\omega_n). \tag{2.62}$$

Here we give a short proof of the rule for relative signs. Consider first $\ell = 0$; the pairs $(\psi^\dagger_{\mathrm{F},i}\psi_{\mathrm{F},i})$ inside the sequence $\mathrm{T}[\psi^\dagger_{\mathrm{F},i_1}\psi_{\mathrm{F},i_1}\psi^\dagger_{\mathrm{F},i_2}\psi_{\mathrm{F},i_2}\ldots]$ can be re-ordered with no change in sign. We can think of grouping them in strings of lengths L_1, $L_2, \ldots$

$$\mathrm{T}\left[\left(\psi^\dagger_{\mathrm{F},i_1}\psi_{\mathrm{F},i_1}\psi^\dagger_{\mathrm{F},i_2}\psi_{\mathrm{F},i_2}\cdots\psi^\dagger_{\mathrm{F},i_{L_1}}\psi_{\mathrm{F},i_{L_1}}\right)\left(\psi^\dagger_{\mathrm{F},j_1}\psi_{\mathrm{F},j_1}\psi^\dagger_{\mathrm{F},j_2}\psi_{\mathrm{F},j_2}\cdots\psi^\dagger_{\mathrm{F},j_{L_2}}\psi_{\mathrm{F},j_{L_2}}\right)\ldots\right]. \tag{2.63}$$

An odd number of interchanges is needed to move $\psi_{\mathrm{F},i_{L_1}}$ to the left of $\psi^\dagger_{\mathrm{F},i_1}$, and the same holds for any of the other strings of operators in round brackets. Therefore, if we close any of these strings in a loop, the term acquires a minus sign:

$$\left\langle \mathrm{T}\left[\psi^\dagger_{\mathrm{F},i_1}\psi_{\mathrm{F},i_1}\psi^\dagger_{\mathrm{F},i_2}\psi_{\mathrm{F},i_2}\cdots\psi^\dagger_{\mathrm{F},i_{L_1}}\psi_{\mathrm{F},i_{L_1}}\cdots\right]\right\rangle_0 \tag{2.64}$$

$$= -\left\langle \mathrm{T}\left[\psi_{\mathrm{F},i_{L_1}}\psi^\dagger_{\mathrm{F},i_1}\psi_{\mathrm{F},i_1}\psi^\dagger_{\mathrm{F},i_2}\psi_{\mathrm{F},i_2}\cdots\psi_{\mathrm{F},i_{L_1-1}}\psi^\dagger_{\mathrm{F},i_{L_1}}\cdots\right]\right\rangle_0 \tag{2.65}$$

$$= -\overbrace{\psi_{\mathrm{F},i_{L_1}}\psi^\dagger_{\mathrm{F},i_1}}\overbrace{\psi_{\mathrm{F},i_1}\psi^\dagger_{\mathrm{F},i_2}}\overbrace{\psi_{\mathrm{F},i_2}\psi^\dagger_{\mathrm{F},i_3}}\cdots\overbrace{\psi_{\mathrm{F},i_{L_1-1}}\psi^\dagger_{\mathrm{F},i_{L_1}}}\langle\mathrm{T}[\ldots]\rangle_0 + \text{ other contractions}. \tag{2.66}$$

In the case $\ell = 1$, it is sufficient to note that the two field operators at the external points cannot be part of a string closed to form a loop, and are instead always part of a contracted string like

$$\overbrace{\psi_{\mathrm{F},1}\psi^\dagger_{\mathrm{F},i_1}}\overbrace{\psi_{\mathrm{F},i_1}\psi^\dagger_{\mathrm{F},i_2}}\cdots\overbrace{\psi_{\mathrm{F},i_N}\psi^\dagger_{\mathrm{F},2}}. \tag{2.67}$$

Such a string can be obtained from a re-ordering of the operators with no sign change. For instance:

$$\mathrm{T}\left[\psi^\dagger_{\mathrm{F},i_1}\psi_{\mathrm{F},i_1}\psi^\dagger_{\mathrm{F},i_2}\psi_{\mathrm{F},i_2}\psi_{\mathrm{F},1}\psi^\dagger_{\mathrm{F},2}\right] = \mathrm{T}\left[\psi_{\mathrm{F},1}\psi^\dagger_{\mathrm{F},i_1}\psi_{\mathrm{F},i_1}\psi^\dagger_{\mathrm{F},2}\psi^\dagger_{\mathrm{F},i_2}\psi_{\mathrm{F},i_2}\right] \tag{2.68}$$

$$= \mathrm{T}\left[\psi_{\mathrm{F},1}\psi^\dagger_{\mathrm{F},i_1}\psi_{\mathrm{F},i_1}\psi^\dagger_{\mathrm{F},i_2}\psi_{\mathrm{F},i_2}\psi^\dagger_{\mathrm{F},2}\right]. \tag{2.69}$$

This proof concludes the discussion about particle lines, and we can move to the rules for the vertices.

In the calculation of the low order diagrams of the previous section, only the vertices coming from V_3, V_4, U_1 and U_4 played a role. We assign them the following rules, inserting a wiggly (condensate) line for each factor of $\sqrt{n_0}$ and a dashed line for each factor of U_{BB} or U_{BF}:

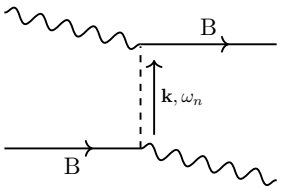

$= -n_0 U_{\mathrm{BB}}(\mathbf{k})$

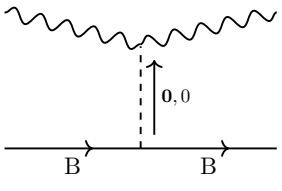

$= -n_0 U_{\mathrm{BB}}(\mathbf{0})$

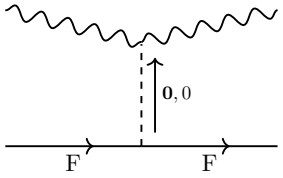

$= -n_0 U_{\mathrm{BF}}(\mathbf{0})$

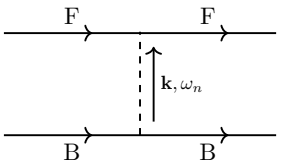

$= -U_{\mathrm{BF}}(\mathbf{k}).$

Including the vertex

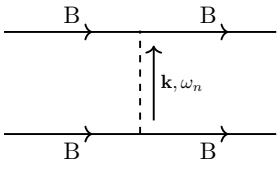

$= -U_{\mathrm{BB}}(\mathbf{k})$

arising from the interaction between non-condensed boson, i.e. the term V_7 in the hamiltonian, we have identified all those interactions that conserve the number of non-condensed bosons and fermions. The *anomalous* interactions, i.e. those that do not conserve the number of non-condensed bosons, arise from the terms V_1, V_2, V_5, V_6, U_2 and U_3 of the hamiltonian. These vertices are assigned the following values:

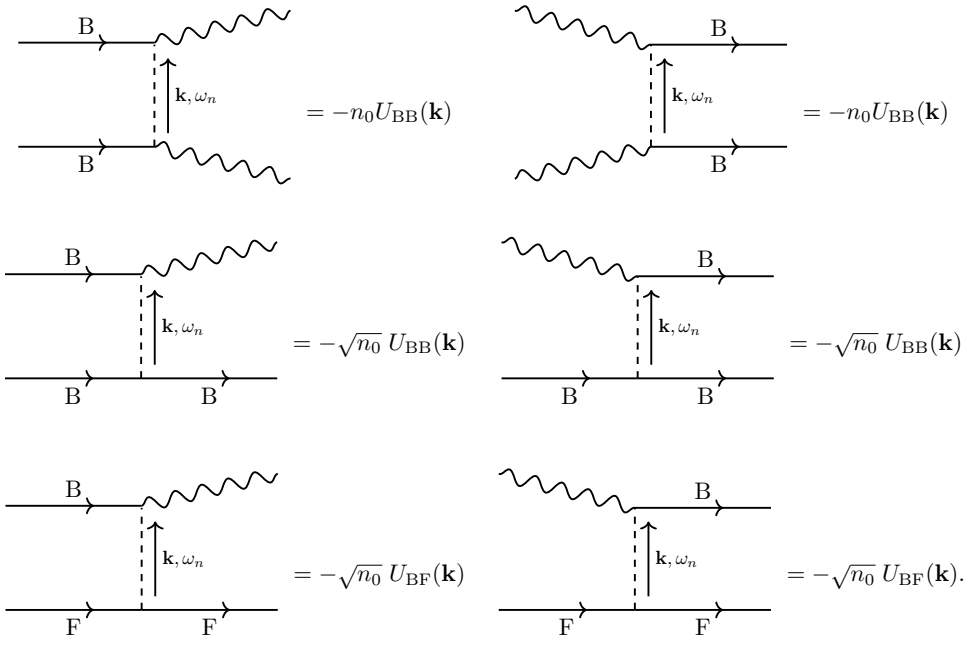

All vertex rules are formally derived from the correlation function

$$\mathcal{V}_i \equiv -\int_0^\beta \mathrm{d}\tau \left\langle \mathrm{T}\left[W_i(\tau) W_i^{(\mathrm{ext})\dagger}\right]\right\rangle_0 \Big|_{\text{connected}}, \tag{2.70}$$

transforming it to Fourier space and amputating its external legs. In the above definition:

- $W_i(\tau)$ denotes the interaction term V_i or U_i (in the interaction picture) for which we want to derive the corresponding vertex rule;
- $W_i^{(\mathrm{ext})\dagger}$ is a product of the adjoint fields of the fields in W_i (in the interaction picture) evaluated at the external points, ensuring that $W_i(\tau)W_i^{(\mathrm{ext})\dagger}$ has a fully connected contraction. The fermion fields in $W_i^{(\mathrm{ext})\dagger}$ have to be ordered with $\psi_{\mathrm{F}}^\dagger$ to the right of ψ_{F} so that the field operators at the external points are contracted as in Eq. (2.67) without introducing further minus signs;
- the number of different external points equals the number of fields in W_i or $W_i^{(\mathrm{ext})\dagger}$;
- the overall minus sign is there because each insertion of an interaction comes with a minus, as indicated by the factor $(-1)^n$ in $S^{(n)}$ (2.22).

In other words, $W_i^{(\mathrm{ext})\dagger}$ is selected so that $-\mathcal{V}_i$ represents the simplest connected correlation function involving exactly the fields of that vertex, and therefore its amputated version yields the vertex factor associated with W_i. For all vertices in our theory, this procedure shows that the vertex rule can simply be identified with minus the product of the interaction potential $U_{\mathrm{BB}}(\mathbf{k})$ or $U_{\mathrm{BF}}(\mathbf{k})$ and the condensate factors $\sqrt{n_0}$ in W_i.

The cases when this fact is somewhat less manifest are those where the integrand of W_i has a symmetry under the exchange of the dummy variables $\mathbf{r}_i$, $\mathbf{r}_j$, and therefore we have to sum terms that arise from different contractions but are identical after integrating over $x_i = \mathbf{r}_i\tau_i$ and $x_j = \mathbf{r}_j\tau_j$. This implies that the factors of $1/2$ in the interactions terms W_i cancel after integration. As an example, consider $W_i = V_1$. $W_i^{(\mathrm{ext})\dagger}$ is given by the adjoint fields

$$W_1^{(\mathrm{ext})\dagger} = \varphi^\dagger_{\mathrm{B,int}}(\mathbf{r}_1\tau_1)\varphi^\dagger_{\mathrm{B,int}}(\mathbf{r}_2\tau_2)$$

and thus

$$\mathcal{V}_1 = -\frac{1}{2}n_0 \int \mathrm{d}x_i\, \mathrm{d}x_j \left\langle \mathrm{T}\left[U_{\mathrm{BB}}(i,j)\varphi_{\mathrm{B},i}\varphi_{\mathrm{B},j}\varphi^\dagger_{\mathrm{B},1}\varphi^\dagger_{\mathrm{B},2}\right]\right\rangle_0\Big|_{\mathrm{connected}} \tag{2.71}$$

$$= -\frac{1}{2}n_0 \int \mathrm{d}x_i\, \mathrm{d}x_j\, U_{\mathrm{BB}}(i,j)\left(-G^0_{\mathrm{B}}(i,1)\right)\left(-G^0_{\mathrm{B}}(j,2)\right) \tag{2.72}$$

$$-\frac{1}{2}n_0 \int \mathrm{d}x_i\, \mathrm{d}x_j\, U_{\mathrm{BB}}(i,j)\left(-G^0_{\mathrm{B}}(j,1)\right)\left(-G^0_{\mathrm{B}}(i,2)\right) \tag{2.73}$$

$$= -n_0 \int \mathrm{d}x_i\, \mathrm{d}x_j\, U_{\mathrm{BB}}(i,j)\left(-G^0_{\mathrm{B}}(i,1)\right)\left(-G^0_{\mathrm{B}}(j,2)\right) \tag{2.74}$$

$$\xrightarrow{\text{F. transfom}} -n_0 U_{\mathrm{BB}}(\mathbf{k})\left(-G^0_{\mathrm{B}}(\mathbf{k},\omega_n)\right)^2 \xrightarrow{\text{amputation}} -n_0 U_{\mathrm{BB}}(\mathbf{k}). \tag{2.75}$$

Here "amputation" means multiplying by $\left(-G^0_{\mathrm{B}}(\mathbf{k},\omega_n)\right)^{-2}$, therefore getting rid of the factors that are taken care of by other Feynman rules.

All in all, one can compute the contribution to a momentum space Green's function $G(\mathbf{k},\omega_n)$ corresponding to a given diagram following these steps:

1. assign a direction to each interaction line;
2. associate a d-momentum $\mathbf{k}$ and a frequency ω_n (in short, a $(d+1)$-momentum) with each line and conserve each quantity at every vertex, considering also that condensate lines carry zero momentum and frequency;
3. assign $-U_{\mathrm{BB}}(\mathbf{k})$ or $-U_{\mathrm{BF}}(\mathbf{k})$ to each interaction line, where $\mathbf{k}$ is the d-momentum associated with that interaction line;
4. assign $-G^0_{\mathrm{B}}(\mathbf{k},\omega_n)$ or $-G^0_{\mathrm{F}}(\mathbf{k},\omega_n)$ to each particle line, where ω_n is given by (2.10), and assign $\sqrt{n_0}$ to each condensate line;
5. sum over all independent internal (d+1)-momenta, performing the operation
$$\int \mathrm{d}^d k/(2\pi)^d \sum_{\omega_n}/\beta;$$
6. multiply by $(-1)(-1)^L$, where the first factor (-1) comes from the global minus in $G^{(n)}$ (2.21), and L is the number of fermion loops; no factors of $1/n!$ are needed, since we implicitly take a momentum space Feynman diagram to contain the sum of all the corresponding position space Feynman diagrams that are related by permutations of identical interaction lines, as done for the diagram (2.58);

7. whenever a particle line either closes on itself or is joined by the same interaction line, insert a convergence factor $\mathrm{e}^{i\omega_n 0^+}$.

Note that, since to order n in perturbation theory for G the total number of particle lines (bosonic or fermionic) is $2n+1-l_0$ where l_0 is the number of condensate densities n_0 in the diagram lines (note that the condensate lines $\sqrt{n_0}$ appear always in pairs in diagrams for G) we can reformulate the above rules by dropping the minus signs in front of G^0_{B} or G^0_{F} in rule 4, and change the overall factor in rule 6 from $(-1)(-1)^L$ to $(-1)^{L+l_0}$.

2.3 Remarks on the zero-temperature limit

The spacing between two consecutive imaginary frequencies (2.10) becomes smaller as β grows. In the zero-temperature limit $\beta \to \infty$, ω_n takes arbitrarily real values, and the sum over discrete frequencies is replaced by an integral:

$$\frac{1}{\beta}\sum_{\omega_n} \to \int \frac{\mathrm{d}\omega}{2\pi}. \tag{2.76}$$

This procedure can be carried out without ambiguities only if the integral and the limit of the sum in the zero-temperature limit are convergent to the same value. Let's consider for instance the free fermion density (2.54): the sum over ω_n yields the Fermi momentum distribution:

$$\frac{1}{\beta}\sum_{\omega_n} \mathrm{e}^{i\omega_n 0^+} \frac{1}{i\omega_n - \xi^{\mathrm{F}}_{\mathbf{k}}} = n_{\mathrm{F}}(\mathbf{k}) \to \Theta(-\xi^{\mathrm{F}}_{\mathbf{k}}) \text{ as } \beta \to \infty. \tag{2.77}$$

This is the same result we would get from the corresponding frequency integral:[6] by closing the contour on the upper complex half-plane

$$\int \frac{\mathrm{d}\omega}{2\pi}\, \mathrm{e}^{i\omega 0^+} \frac{1}{i\omega - \xi^{\mathrm{F}}_{\mathbf{k}}} = \Theta(-\xi^{\mathrm{F}}_{\mathbf{k}}). \tag{2.78}$$

A subtler example, first presented in [92], is given by the following expression:

$$\frac{1}{\beta}\sum_{\omega_n} \mathrm{e}^{i\omega_n 0^+} \frac{1}{(i\omega_n - \xi^{\mathrm{F}}_{\mathbf{k}})^2} = \frac{\partial}{\partial \xi^{\mathrm{F}}_{\mathbf{k}}} \left(\frac{1}{\beta}\sum_{\omega_n} \mathrm{e}^{i\omega_n 0^+} \frac{1}{i\omega_n - \xi^{\mathrm{F}}_{\mathbf{k}}} \right) \tag{2.79}$$

$$= \frac{\partial n_{\mathrm{F}}(\mathbf{k})}{\partial \xi^{\mathrm{F}}_{\mathbf{k}}} \to -\delta(\xi^{\mathrm{F}}_{\mathbf{k}}) \text{ as } \beta \to \infty. \tag{2.80}$$

If the corresponding integral $(2\pi)^{-1}\int \mathrm{d}\omega\ \mathrm{e}^{i\omega 0^+}/(i\omega - \xi^{\mathrm{F}}_{\mathbf{k}})^2$ were evaluated naively, it would appear to be vanishing because the residue at $i\omega = \xi^{\mathrm{F}}_{\mathbf{k}}$ is zero. The origin of this discrepancy lies in the divergence of the frequency integral at $\mathbf{k}^2 = 2m_{\mathrm{F}}\mu_{\mathrm{F}}$. The discrete summation of the finite-temperature theory serves the purpose of defining the value at that point.

[6] Note that the exponential factor $\mathrm{e}^{i\omega_n 0^+}$ coming from rule 7 is important to ensure the convergence of the discrete sum and the integral.

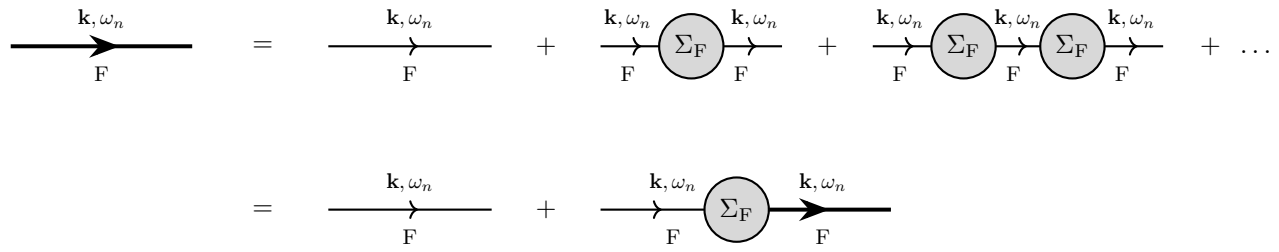

Figure 2.1: Diagrammatic representation of the fermion two-point function $G_{\mathrm{F}}(\mathbf{k}, \omega_n)$, represented by the heavy line. The light lines represents the fermion lines $G^0_{\mathrm{F}}(\mathbf{k}, \omega_n)$. The filled circles represent the fermion self-energy $\Sigma_{\mathrm{F}}(\mathbf{k}, \omega_n)$.

In this thesis, the delicate integrals will be of the kind of the example above, namely

$$\int \frac{\mathrm{d}\omega}{2\pi}\, \mathrm{e}^{i\omega 0^+} \frac{1}{(i\omega - E_{\mathbf{P}})^2} \quad \text{with } E_{\mathbf{P}} \in \mathbb{R}, \tag{2.81}$$

which diverges where $E_{\mathbf{P}} = 0$. For this kind of integrals, another way of making sense of the singular behavior is by splitting the double pole into two simple poles. This is done by introducing an infinitesimal auxiliary momentum $\mathbf{k}$, as follows:

$$\begin{aligned}
&\int \frac{\mathrm{d}\omega}{2\pi} \mathrm{e}^{i\omega 0^+} \frac{1}{(i\omega - E_{\mathbf{P}})^2} \to \lim_{|\mathbf{k}|\to 0} \int \frac{\mathrm{d}\omega}{2\pi}\, \mathrm{e}^{i\omega 0^+} \frac{1}{i\omega - E_{\mathbf{P}}} \frac{1}{i\omega - E_{\mathbf{P}-\mathbf{k}}} \\
&= \lim_{|\mathbf{k}|\to 0} \int \frac{\mathrm{d}\omega}{2\pi}\, \mathrm{e}^{i\omega 0^+} \frac{1}{E_{\mathbf{P}} - E_{\mathbf{P}-\mathbf{k}}} \left(\frac{1}{i\omega - E_{\mathbf{P}}} - \frac{1}{i\omega - E_{\mathbf{P}-\mathbf{k}}} \right) \\
&= \lim_{|\mathbf{k}|\to 0} \frac{\Theta(-E_{\mathbf{P}}) - \Theta(-E_{\mathbf{P}-\mathbf{k}})}{E_{\mathbf{P}} - E_{\mathbf{P}-\mathbf{k}}} = -\delta(E_{\mathbf{P}}).
\end{aligned} \tag{2.82}$$

The take-away of the above discussion is that special care must be reserved for frequency integrals that diverge for certain values of the momentum. One way to define their value is going back to the sums over imaginary frequencies, and then perform the limit of $\beta \to \infty$ afterwards. The pole-splitting prescription is an alternative to the discrete summation, the two being equivalent when dealing with double poles, and it is the one adopted in the following chapters.

2.4 Dyson's equations and Hugenholtz-Pines theorem

We define the *irreducible self-energy*[7] $\Sigma(\mathbf{k}, \omega_n)$ as the sum of all connected (momentum-space) Feynman diagrams which cannot be disconnected by cutting a single particle line. The Green's function (2.27) is obtained as the sum over all irreducible self-energy insertions, each of them connected with the rest of the diagram by two particle lines. To be more specific, we need to separate the cases of fermion and boson self-energies. Starting from fermions, there is only one way to connect a part of a Feynman diagram Σ_{F} with the rest of the diagram with two fermion lines: one line going in Σ_{F} and

[7] Or simply *self-energy* in the following.

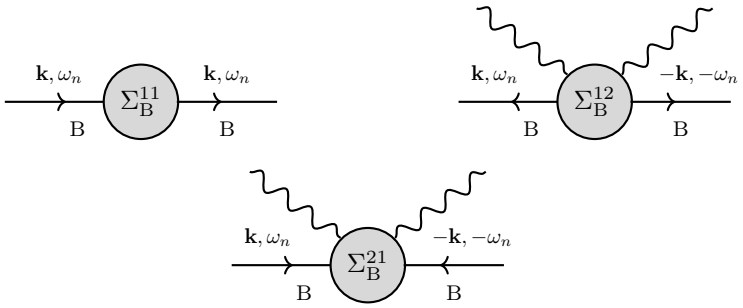

Figure 2.2: Irreducible self-energies for bosons in the condensed phase. The light lines represents the boson lines $G_{\mathrm{B}}^{0}(\mathbf{k}, \omega_n)$. The filled circles represent the boson self-energies $\Sigma_{\mathrm{B}}^{11}(\mathbf{k}, \omega_n)$, $\Sigma_{\mathrm{B}}^{12}(\mathbf{k}, \omega_n)$, $\Sigma_{\mathrm{B}}^{21}(\mathbf{k}, \omega_n)$.

one line going out of Σ_{F}. The sum over all self-energy insertions is then depicted in Fig. 2.1, which corresponds to the fermion *Dyson's equation*

$$G_{\mathrm{F}}(\mathbf{k}, \omega_n) = G_{\mathrm{F}}^{0}(\mathbf{k}, \omega_n)\left(1 + \Sigma_{\mathrm{F}}(\mathbf{k}, \omega_n)\, G_{\mathrm{F}}(\mathbf{k}, \omega_n)\right) \tag{2.83}$$

and is formally solved to yield

$$G_{\mathrm{F}}(\mathbf{k}, \omega_n)^{-1} = G_{\mathrm{F}}^{0}(\mathbf{k}, \omega_n)^{-1} - \Sigma_{\mathrm{F}}(\mathbf{k}, \omega_n). \tag{2.84}$$

The matter is more complicated for bosons, since there are in this case three ways to connect a part of a Feynman diagram with the rest of the diagram with two boson lines. One type of self-energy, Σ_{B}^{11}, has one particle line going in and one coming out. A second type of self-energy, Σ_{B}^{21}, has two lines going in. The last type, Σ_{B}^{12}, has two lines going out (see Fig. 2.2). Σ_{B}^{11} is called *normal* self-energy, while Σ_{B}^{12} and Σ_{B}^{21} are *anomalous* self-energies. Correspondingly, we now deal with a system of three Dyson's equations [93]:

$$G'_{\mathrm{B}}(\mathbf{k}, \omega_n) = G_{\mathrm{B}}^{0}(\mathbf{k}, \omega_n) + G_{\mathrm{B}}^{0}(\mathbf{k}, \omega_n)\Sigma_{\mathrm{B}}^{11}(\mathbf{k}, \omega_n)G'_{\mathrm{B}}(\mathbf{k}, \omega_n) + G_{\mathrm{B}}^{0}(\mathbf{k}, \omega_n)\Sigma_{\mathrm{B}}^{21}(\mathbf{k}, \omega_n)G_{\mathrm{B}}^{21}(\mathbf{k}, \omega_n) \tag{2.85}$$

$$G_{\mathrm{B}}^{12}(\mathbf{k}, \omega_n) = G_{\mathrm{B}}^{0}(\mathbf{k}, \omega_n)\Sigma_{\mathrm{B}}^{12}(\mathbf{k}, \omega_n)G'_{\mathrm{B}}(-\mathbf{k}, -\omega_n) + G_{\mathrm{B}}^{0}(\mathbf{k}, \omega_n)\Sigma_{\mathrm{B}}^{11}(\mathbf{k}, \omega_n)G_{\mathrm{B}}^{12}(\mathbf{k}, \omega_n) \tag{2.86}$$

$$G_{\mathrm{B}}^{21}(\mathbf{k}, \omega_n) = G_{\mathrm{B}}^{0}(-\mathbf{k}, -\omega_n)\Sigma_{\mathrm{B}}^{21}(\mathbf{k}, \omega_n)G'_{\mathrm{B}}(\mathbf{k}, \omega_n) + G_{\mathrm{B}}^{0}(-\mathbf{k}, -\omega_n)\Sigma_{\mathrm{B}}^{11}(-\mathbf{k}, -\omega_n)G_{\mathrm{B}}^{21}(\mathbf{k}, \omega_n), \tag{2.87}$$

where the two anomalous Green's functions G_{B}^{12} and G_{B}^{21} are given by

$$G_{\mathrm{B}}^{12}(\mathbf{r}_1\tau_1, \mathbf{r}_2\tau_2) = -\left\langle \mathrm{T}[\varphi_{\mathrm{B}}(\mathbf{r}_1\tau_1)\varphi_{\mathrm{B}}(\mathbf{r}_2\tau_2)]\right\rangle \tag{2.88}$$

$$G_{\mathrm{B}}^{21}(\mathbf{r}_1\tau_1, \mathbf{r}_2\tau_2) = -\left\langle \mathrm{T}[\varphi_{\mathrm{B}}^{\dagger}(\mathbf{r}_1\tau_1)\varphi_{\mathrm{B}}^{\dagger}(\mathbf{r}_2\tau_2)]\right\rangle \tag{2.89}$$

in position-space.
The self-energies and Green's functions are not all independent: they obey the identities

$$G_{\mathrm{B}}^{12}(\mathbf{k},\omega_n) = G_{\mathrm{B}}^{21}(-\mathbf{k},-\omega_n) \tag{2.90}$$

$$\Sigma_{\mathrm{B}}^{12}(\mathbf{k},\omega_n) = \Sigma_{\mathrm{B}}^{21}(-\mathbf{k},-\omega_n). \tag{2.91}$$

Therefore, the three Dyson's equations are formally solved to give two independent Green's functions

$$G'_{\mathrm{B}}(\mathbf{k},\omega_n)^{-1} = G_{\mathrm{B}}^{0}(\mathbf{k},\omega_n)^{-1} - \Sigma_{\mathrm{B}}^{11}(\mathbf{k},\omega) + \frac{\Sigma_{\mathrm{B}}^{12}(\mathbf{k},\omega_n)^2}{i\omega_n + \xi_{\mathbf{k}}^{\mathrm{B}} + \Sigma_{\mathrm{B}}^{11}(-\mathbf{k},-\omega_n)} \tag{2.92}$$

$$G_{\mathrm{B}}^{12}(\mathbf{k},\omega_n)^{-1} = -G'_{\mathrm{B}}(\mathbf{k},\omega_n)^{-1}\frac{i\omega_n + \xi_{\mathbf{k}}^{\mathrm{B}} + \Sigma_{\mathrm{B}}^{11}(-\mathbf{k},-\omega_n)}{\Sigma_{\mathrm{B}}^{12}(\mathbf{k},\omega_n)}. \tag{2.93}$$

In the limit of $|\mathbf{k}| \to 0$, both of them exhibit a pole at $\omega_n = 0$ if

$$\mu_{\mathrm{B}} = \Sigma_{\mathrm{B}}^{11}(\mathbf{0},0) - \Sigma_{\mathrm{B}}^{12}(\mathbf{0},0), \tag{2.94}$$

a condition which is known as *Hugenholtz-Pines theorem*. If a theory obeys this condition, the energy of single-particle Bose excitations (which are related to the poles of the boson Green's functions) has no gap in the limit of vanishing $\mathbf{k}$. [91, Sec. 6.21] contains a proof at first order in perturbation theory, at zero-temperature. The proof of the theorem at all orders in perturbation theory can be found in the original paper by Hugenholtz and Pines [94], again at zero-temperature. The generalization to finite temperature can instead be found in [95].

2.5 The transition matrices

Dyson's equations provide a way to summarize the various perturbative contributions to a Green's function, in a compact form. As we have seen, the full information contained in the perturbative series (2.27) is encoded in the irreducible Feynman diagrams, i.e., those that cannot be disconnected by cutting a single internal particle line. Clearly, writing out the complete series would still require the evaluation of an infinite number of irreducible diagrams; it is therefore necessary to introduce suitable approximations for the self-energies. In the present work we focus on the irreducible diagrams known as *ladder diagrams*. The sum over all diagrams of this class can be evaluated analytically, and the resulting approximation of the boson and fermion self-energies is able to capture many notable features of the Bose-Fermi mixture, as will be discussed in Sec. 3.2.

In the present section, we introduce the ladder diagrams and discuss how to relate them with physical quantities such as the *scattering length* of the system. From this section onward, we assume the zero-temperature limit.

2.5.1 The two-body transition matrix

Consider the scattering of two particles s_1 and s_2 under the effect of an interparticle potential V, dependent only on the relative distance operator $\mathbf{r} = \mathbf{r}_{s_1} - \mathbf{r}_{s_2}$. After separating the motion of the center of mass, the Schrödinger equation for the wave function of the relative motion reads

$$(H_0 + V)\,|\psi\rangle = \left(\frac{\mathbf{p}^2}{2m_\mathrm{r}} + V\right)|\psi\rangle = E\,|\psi\rangle\,, \tag{2.95}$$

where m_r is the reduced mass of the two-body system. Under the assumptions that

- V is significantly non-vanishing only in a region of space defined by a characteristic relative length $r_{s_1 s_2}$,
- the wave-function in the coordinate basis $\langle\mathbf{r}|\psi\rangle$ is considered at relative distances $|\mathbf{r}| \gg r_{s_1 s_2}$,
- we consider elastic processes,

the scattering states can be labeled by the free-particle energies given by the asymptotic momentum $\mathbf{p}$

$$E = \varepsilon_\mathbf{p} = \frac{\mathbf{p}^2}{2m_\mathrm{r}}. \tag{2.96}$$

The corresponding eigenstates $|\psi_\mathbf{p}\rangle$ are formally given by

$$|\psi_\mathbf{p}\rangle = |\mathbf{p}\rangle + \frac{1}{\varepsilon_\mathbf{p} - H_0 + i0^+} V\,|\psi_\mathbf{p}\rangle\,, \tag{2.97}$$

where the "$+i0^+$ prescription" for choosing the inverse of the operator $\varepsilon_\mathbf{p} - H_0$ accounts for the initial conditions of the problem. Specifically, it could be shown (see Eq. (2.110) for the $d = 2$ case) that in this way $\langle\mathbf{r}|\,(\varepsilon_\mathbf{p} - H_0)^{-1} V\,|\psi_\mathbf{p}\rangle$ is an outgoing wave propagating from the interaction region located around $r = 0$.

Eq. (2.97) is known as *Lippmann-Schwinger equation*. After acting with V on both sides and introducing the *two-body transition matrix* T_2, defined by

$$T_2\,|\mathbf{p}\rangle = V\,|\psi_\mathbf{p}\rangle\,, \tag{2.98}$$

Eq. (2.97) implies

$$T_2\,|\mathbf{p}\rangle = V\,|\mathbf{p}\rangle + V\frac{1}{\varepsilon_\mathbf{p} - H_0 + i0^+} T_2\,|\mathbf{p}\rangle\,. \tag{2.99}$$

By taking the scalar product with another state of definite asymptotic momentum $|\mathbf{p}'\rangle$ and introducing a completeness relation $\mathbb{1} = (2\pi)^{-d}\int \mathrm{d}\mathbf{k}\ |\mathbf{k}\rangle\langle\mathbf{k}|$, we obtain an integral equation for the two-body T_2-matrix element $T_2(\mathbf{p}', \mathbf{p}) \equiv \langle\mathbf{p}'|\,T_2\,|\mathbf{p}\rangle$

$$T_2(\mathbf{p}', \mathbf{p}) = V(\mathbf{p}' - \mathbf{p}) + \int \frac{\mathrm{d}\mathbf{k}}{(2\pi)^d}\ \frac{V(\mathbf{p}' - \mathbf{k})}{\varepsilon_\mathbf{p} - \varepsilon_\mathbf{k} + i0^+} T_2(\mathbf{k}, \mathbf{p}). \tag{2.100}$$

2.5.2 The many-body transition matrix

The *many-body transition matrix* is a generalization of the two-body T_2 that takes into account the interaction of the two scattering particles with the medium of other particles. It is determined digrammatically by

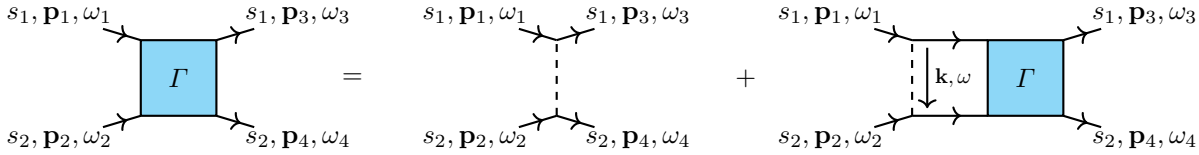

with no external propagators intended. The diagrammatic expression represents the sum over the ladder diagrams of all orders in the interaction. It could be proven that in the limit of vanishing density of the medium, the integral equation corresponding to the above diagrams reduces to Eq. (2.100) with $\mathbf{p} = (\mathbf{p}_1 - \mathbf{p}_2)/2$ and $\mathbf{p}' = (\mathbf{p}_3 - \mathbf{p}_4)/2$, and with $\varepsilon_{\mathbf{p}}$ replaced by the center of mass energy.[8]

For the purposes of this work, it is sufficient to focus on $p_1 = (\mathbf{p}_1, \omega_1) = (\mathbf{p}_3, \omega_3)$, $p_2 = (\mathbf{p}_2, \omega_2) = (\mathbf{p}_4, \omega_4)$. In terms of the center of mass $(d{+}1)$-momentum $p_1 + p_2 = P = (\mathbf{P}, \Omega)$ and the loop $(d{+}1)$-momentum $k = (\mathbf{k}, \omega)$, this yields

$$\Gamma\left(P, \frac{p_2 - p_1}{2}\right) = V(\mathbf{0}) - \int \frac{\mathrm{d}\mathbf{k}}{(2\pi)^d} \int \frac{\mathrm{d}\omega}{2\pi}\, V(\mathbf{k})\, \Gamma(P,k) G^0_{s_1}(p_1 - k) G^0_{s_2}(p_2 + k), \tag{2.101}$$

where we have dropped an overall minus sign in the definition of Γ (which comes from Feynman's rules for interaction lines). This implies that we need to attach a factor (-1) for each insertion of a Γ inside a Green's function.

In general, note that the Γ-matrix can depend on both the center of mass $(d+1)$-momentum (first argument of Γ) and the relative $(d+1)$-momentum (second argument of Γ). If the interaction potential is a contact potential $V(\mathbf{k}) = v_0^{s_1 s_2}$, the Γ-matrix depends on the center of mass $(d+1)$-momentum only: $\Gamma(P,k) = \Gamma(P) = \Gamma(\mathbf{P}, \Omega)$. The integral equation (2.101) yields in this case

$$\Gamma(\mathbf{P}, \Omega) = v_0^{s_1 s_2} - \Gamma(\mathbf{P}, \Omega)\, v_0^{s_1 s_2} \int \frac{\mathrm{d}\mathbf{k}}{(2\pi)^d} \frac{1 - \Theta(-\xi^{s_1}_{\mathbf{P}-\mathbf{k}}) - \Theta(-\xi^{s_2}_{\mathbf{k}})}{\xi^{s_1}_{\mathbf{P}-\mathbf{k}} + \xi^{s_2}_{\mathbf{k}} - i\Omega} \tag{2.102}$$

after performing the integral over ω.

2.5.3 Regularization of the potential for $d = 2$

From this section onward, we specialize to $d = 2$. In this case, we see that the integral

$$\int \frac{\mathrm{d}\mathbf{k}}{(2\pi)^2} \int \frac{\mathrm{d}\omega}{2\pi}\, V(\mathbf{k}) \frac{1 - \Theta(-\xi^{s_1}_{\mathbf{P}-\mathbf{k}}) - \Theta(-\xi^{s_2}_{\mathbf{k}})}{\xi^{s_1}_{\mathbf{P}-\mathbf{k}} + \xi^{s_2}_{\mathbf{k}} - i\Omega} \tag{2.103}$$

[8] See e.g. [96, Sec. 10.4] for the case of $d = 3$, or Eqs. (3.11) and (3.15) in Sec. 3.2.1, with $I_{\mathrm{F}}(\mathbf{P}, \Omega) \to 0$, μ_{B}, $\mu_{\mathrm{F}} \to 0$ in the limit of vanishing density, for the Bose-Fermi mixture in $d = 2$.

is UV divergent for the contact potential case of Eq. (2.102). This leads us to the next sections, where we discuss how to replace the interaction potential $V(\mathbf{k})$ in terms of the two-body T_2 and in turn the scattering length $a_{s_1 s_2}$, which is measurable in low-energy scattering experiments in the vacuum.

Replacement of the interaction potential by T_2

From Eq. (2.100) we can define a continuation of the T_2-matrix to complex energies z:

$$T_2(\mathbf{p}', \mathbf{p}; z) \equiv V(\mathbf{p}' - \mathbf{p}) + \int \frac{\mathrm{d}\mathbf{k}}{(2\pi)^2} \frac{V(\mathbf{p}' - \mathbf{k})}{z - \varepsilon_{\mathbf{k}} + i0^+} T_2(\mathbf{k}, \mathbf{p}; z). \tag{2.104}$$

We can regulate the previously encountered UV divergence via a cutoff, replacing the potential according to

$$V(\mathbf{p}' - \mathbf{p}) \to v_0^{s_1 s_2} \Theta(|\mathbf{p}_0| - |\mathbf{p}|)\Theta(|\mathbf{p}_0| - |\mathbf{p}'|). \tag{2.105}$$

Employing an ansatz for T_2 that resembles this form,

$$T_2(\mathbf{p}', \mathbf{p}; z) = T_2(z)\Theta(|\mathbf{p}_0| - |\mathbf{p}|)\Theta(|\mathbf{p}_0| - |\mathbf{p}'|), \tag{2.106}$$

Eq. (2.104) is solved for $T_2(z)$ yielding

$$T_2(z) = \left(\frac{1}{v_0^{s_1 s_2}} - \int \frac{\mathrm{d}\mathbf{k}}{(2\pi)^2} \frac{\Theta(|\mathbf{p}_0| - |\mathbf{k}|)}{z - \varepsilon_{\mathbf{k}}} \right)^{-1}. \tag{2.107}$$

It could be proven:

- for every value of $v_0^{s_1 s_2} < 0$ there exists one and only one solution to $T_2(z)^{-1} = 0$ along the negative real axis;[9]
- the poles of $T_2(z)$ along the negative real axis correspond to the energies of bound states [96, Sec. 10.3].

Denoting $-\varepsilon_0$, with $\varepsilon_0 > 0$, to be this pole, it follows

$$\frac{1}{v_0^{s_1 s_2}} = -\int \frac{\mathrm{d}\mathbf{k}}{(2\pi)^2} \frac{\Theta(|\mathbf{p}_0| - |\mathbf{k}|)}{\varepsilon_0 + \varepsilon_{\mathbf{k}}} \tag{2.108}$$

$$T_2(z) = -\left(\int \frac{\mathrm{d}\mathbf{k}}{(2\pi)^2} \frac{(z + \varepsilon_0)\Theta(|\mathbf{p}_0| - |\mathbf{k}|)}{(z - \varepsilon_{\mathbf{k}})(\varepsilon_0 + \varepsilon_{\mathbf{k}})} \right)^{-1}. \tag{2.109}$$

The next step is to relate $T_2(z)$ to the scattering length $a_{s_1 s_2}$, which in turn relates the latter to ε_0. This way, Eq. (2.108) formally describes how the bare coupling $v_0^{s_1 s_2}$ changes as a function of the cutoff $|\mathbf{p}_0|$ in order to keep the observable $a_{s_1 s_2}$ constant. For a given scattering length, Eq. (2.108) provides the correct prescription to perform the "contact interaction limit" $V(\mathbf{k}) = v_0^{s_1 s_2}$, canceling

[9] See Sec. 2.5.3 and in particular (2.124), analytically continued to complex energies $\mathbf{p}^2/(2m_\mathrm{r}) + i0^+ \to z$. The logarithm $\log(-z/\varepsilon_0)$ at the denominator vanishes only at the point $z = -\varepsilon_0$.

divergencies like the one in Eq. (2.102) and leaving us with finite predictions in terms of physical entities such as $a_{s_1 s_2}$.

Replacement of T_2 by $a_{s_1 s_2}$

We review here a few facts on quantum scattering theory in two dimensions:

- the wave-function (2.97) associated with the elastic scattering state, in the presence of a localized potential, in a region far from where the potential is significantly non-vanishing, is approximated in terms of the *scattering amplitude* $f(\mathbf{k}, \mathbf{k}')$ as (see e.g. [97])

$$\psi_{\mathbf{k}}(\mathbf{r}) = \mathrm{e}^{i\mathbf{k}\cdot\mathbf{r}} + f(\mathbf{k}, \mathbf{k}')\big|_{|\mathbf{k}|=|\mathbf{k}'|} \frac{\mathrm{e}^{i(|\mathbf{k}|r+\pi/4)}}{\sqrt{r}}, \text{ where} \tag{2.110}$$

$$f(\mathbf{k}, \mathbf{k}') = -\frac{m_{\mathrm{r}}}{\sqrt{2\pi|\mathbf{k}|}} \int \mathrm{d}\mathbf{r}' \; \mathrm{e}^{-i\mathbf{k}'\cdot\mathbf{r}'} V(\mathbf{r}') \psi_{\mathbf{k}}(\mathbf{r}'); \tag{2.111}$$

- the *partial wave expansion* of the scattering amplitude in $d = 2$ reads

$$f(\mathbf{k}, \mathbf{k}')\big|_{|\mathbf{k}|=|\mathbf{k}'|} \equiv f(|\mathbf{k}|, \theta) = 2m_{\mathrm{r}} \sqrt{\frac{2}{\pi|\mathbf{k}|}} \sum_{\lambda=-\infty}^{\infty} \mathrm{e}^{i\delta_\lambda} \sin\delta_\lambda \mathrm{e}^{i\lambda\theta}, \tag{2.112}$$

  where the phase shifts δ_λ are $|\mathbf{k}|$-dependent and θ is the angle between $\mathbf{k}$ and $\mathbf{k}'$;

- from the above two points it follows that the representation of $\psi_{\mathbf{k}}(\mathbf{r})$ in terms of a plane wave and phase-shifted circular waves is

$$\psi_{\mathbf{k}}(\mathbf{r}) = \mathrm{e}^{i\mathbf{k}\cdot\mathbf{r}} + \sum_{\lambda=-\infty}^{\infty} \left(2m_{\mathrm{r}} \sqrt{\frac{2}{\pi|\mathbf{k}|}} \sin\delta_\lambda \right) \frac{\exp\left(i(|\mathbf{k}|r + \pi/4 + \lambda\theta + \delta_\lambda)\right)}{\sqrt{r}}; \tag{2.113}$$

- for small momenta the phase shifts δ_λ vanish according to power laws, apart for δ_0 which vanishes logarithmically and is therefore the leading contribution (s-wave contribution) to the scattering amplitude:

$$\delta_0(|\mathbf{k}|) \sim \frac{\pi}{2\ln(|\mathbf{k}|a_{s_1 s_2})}, \;\; |\mathbf{k}| \to 0, \tag{2.114}$$

  where $a_{s_1 s_2} > 0$ is the scattering length (see e.g. [97, 98]).

Eqs (2.112) and (2.114) together show

$$f(\mathbf{k}, \theta) \sim \sqrt{\frac{2}{\pi|\mathbf{k}|}} \frac{\pi}{2\ln(|\mathbf{k}|a_{s_1 s_2}) - i\pi} \text{ as } |\mathbf{k}| \to 0. \tag{2.115}$$

To relate the scattering amplitude and T_2, we go back once again to Eq. (2.97), write it in the

momentum basis as

$$\psi_{\mathbf{k}}(\mathbf{p}) = (2\pi)^2\delta^{(2)}(\mathbf{p}-\mathbf{k}) - \frac{2m_{\mathrm{r}}}{\mathbf{p}^2-\mathbf{k}^2-i0^+}\int\frac{\mathrm{d}\mathbf{q}}{(2\pi)^2}\,V(\mathbf{q})\psi_{\mathbf{k}}(\mathbf{p}-\mathbf{q}) \tag{2.116}$$

and insert it in Eq. (2.111) after expressing the latter with an integral in momentum space as well:

$$\begin{aligned} f(\mathbf{k},\mathbf{k}') &= -\frac{m_{\mathrm{r}}}{\sqrt{2\pi|\mathbf{k}|}}\int\frac{\mathrm{d}\mathbf{q}}{(2\pi)^2}\,V(\mathbf{q})\psi_{\mathbf{k}}(\mathbf{k}'-\mathbf{q}) \\ &= -\frac{m_{\mathrm{r}}}{\sqrt{2\pi|\mathbf{k}|}}V(\mathbf{k}'-\mathbf{k}) + 2m_{\mathrm{r}}\int\frac{\mathrm{d}\mathbf{q}}{(2\pi)^2}\,\frac{V(\mathbf{k}'-\mathbf{q})}{\mathbf{k}^2-\mathbf{q}^2+i0^+}f(\mathbf{q},\mathbf{k}) \qquad (2.117) \\ \Rightarrow -\frac{\sqrt{2\pi|\mathbf{k}|}}{m_{\mathrm{r}}}f(\mathbf{k},\mathbf{k}') &= V(\mathbf{k}'-\mathbf{k}) + 2m_{\mathrm{r}}\int\frac{\mathrm{d}\mathbf{q}}{(2\pi)^2}\,\frac{V(\mathbf{k}'-\mathbf{q})}{\mathbf{k}^2-\mathbf{q}^2+i0^+}\left(-\frac{\sqrt{2\pi|\mathbf{k}|}}{m_{\mathrm{r}}}f(\mathbf{q},\mathbf{k})\right). \qquad (2.118) \end{aligned}$$

By comparing this last equation with Eq. (2.100) and Eq. (2.104), we can identify

$$\begin{aligned} T_2\left(\mathbf{k}',\mathbf{k};\frac{\mathbf{k}^2}{2m_{\mathrm{r}}}+i0^+\right) &= -\frac{\sqrt{2\pi|\mathbf{k}|}}{m_{\mathrm{r}}}f(\mathbf{k}',\mathbf{k}) \qquad (2.119) \\ &= T_2(\mathbf{k}',\mathbf{k}). \ ^{10} \qquad (2.120) \end{aligned}$$

We have thus reached the desired relation: for elastic scatterings at small momentum $|\mathbf{k}|$

$$T_2(\mathbf{k}',\mathbf{k}) = \frac{2\pi}{m_{\mathrm{r}}}\frac{1}{-2\ln(|\mathbf{k}|a_{s_1s_2})+i\pi}, \tag{2.121}$$

dependent only on the incoming relative momentum $\mathbf{k}$.
In the case of the ansatz (2.106), this last equation translates into

$$T_2\left(\frac{\mathbf{p}^2}{2m_{\mathrm{r}}}+i0^+\right)\Theta(|\mathbf{p}_0|-|\mathbf{p}|)\Theta(|\mathbf{p}_0|-|\mathbf{p}'|) = \frac{2\pi}{m_{\mathrm{r}}}\frac{1}{-2\ln(|\mathbf{p}|a_{s_1s_2})+i\pi}. \tag{2.122}$$

Removing the regulator $|\mathbf{p}_0|\to\infty$ yields

$$\begin{aligned} T_2\left(\frac{\mathbf{p}^2}{2m_{\mathrm{r}}}+i0^+\right) &\to \frac{2\pi}{m_{\mathrm{r}}}\frac{1}{-2\ln(|\mathbf{p}|a_{s_1s_2})+i\pi} \qquad (2.123) \\ T_2\left(\frac{\mathbf{p}^2}{2m_{\mathrm{r}}}+i0^+\right) &\to -\left(\int\frac{\mathrm{d}\mathbf{k}}{(2\pi)^2}\,\frac{(\varepsilon_{\mathbf{p}}+\varepsilon_0)}{(\varepsilon_{\mathbf{p}}-\varepsilon_{\mathbf{k}})(\varepsilon_0+\varepsilon_{\mathbf{k}})}\right)^{-1} = -\frac{2\pi}{m_{\mathrm{r}}}\frac{1}{\ln\left(-\mathbf{p}^2/(2m_{\mathrm{r}}\varepsilon_0)\right)}, \qquad (2.124) \end{aligned}$$

where the second equation comes from (2.109). Comparing the two yields the binding energy in terms of the scattering length,

$$\varepsilon_0 = \frac{1}{2m_{\mathrm{r}}a_{s_1s_2}^2}. \tag{2.125}$$

[10] This shows that the two-body T_2-matrix is closely related to the scattering amplitude $f(\mathbf{k},\mathbf{k}')$, i.e. the probability amplitude for the incoming wave with momentum $\mathbf{k}$ to scatter into the outgoing wave with momentum $\mathbf{k}'$, in the vacuum; the Γ-matrix can be seen as a generalized scattering amplitude that takes into account the presence of a medium.

Chapter 3

The transition matrix approach for the Bose-Fermi mixture

In this chapter we present the T-matrix formalism applied to a 2-dimensional Bose-Fermi mixture at zero temperature. The self-energies, momentum distribution and densities are introduced within this framework, and are used to set up a system of equations which can be numerically solved to deduce crucial physical quantities such as the chemical potentials and the condensate density. We show that the ladder diagrams yield the perturbative corrections to the chemical potentials up to second order in the relevant small parameter of the theory. The comparison with the perturbative expansions in [99] motivates the need for (partial) self-consistency in the T-matrix. We also present semi-analytical expressions in the opposite regime of large parameter values, generalizing results for mass-balanced Bose–Fermi mixtures to the mass-imbalanced case.

3.1 The system

We consider a homogeneous mixture of bosons and spin-polarized fermions in $2d$ space. We consider the boson density n_{B} not to be larger than the fermion density n_{F}, so that a full competition between pairing and condensation is possible. $x = n_{\mathrm{B}}/n_{\mathrm{F}}$ denotes the boson concentration, and therefore we restrict to the case $x \leq 1$ in the present work. We consider the gas to be diluted, in the sense that the average interparticle distance is large compared to the range of interactions; using the notation introduced in Sec. 2.5.1 for the range of interactions, now with $s = \mathrm{B}$ (boson) or F (fermion):

$$n_{\mathrm{B}} r_{\mathrm{BB}}^2 \ll 1 \tag{3.1}$$

$$n_{\mathrm{F}} r_{\mathrm{BF}}^2 \ll 1. \tag{3.2}$$

Regarding the masses of the two species, m_{B} and m_{F}, we focus on values of the mass ratio $\gamma_{\mathrm{m}} = m_{\mathrm{B}}/m_{\mathrm{F}}$ close to those in Tab. 1.1.

As for interactions, we consider repulsion between bosons and attraction between the two species; we neglect the interaction between fermions in light of the Pauli exclusion principle, which forbids s-wave scattering. In the repulsive interaction case, the scattering length is positive and typically of the same order as, or smaller than, the range of the interaction potential. This implies $n_{\mathrm{B}} a_{\mathrm{BB}}^2 \ll 1$, justifying the Bogolyubov approximation of the boson-boson interaction U_{BB}. In this framework, the effective coupling parameter parameter for Bose-Bose interaction is $\eta \equiv -1/\ln\left(n_{\mathrm{B}} a_{\mathrm{BB}}^2\right) \ll 1$ (see [100] for the original development of the effective interaction).
The experimental conditions[1] relevant for the system of interest are such that the range r_{BF} of the interactions between bosons and fermions is small compared to the scattering length a_{BF} and the average interparticle distance. This justifies the adoption of a contact potential for the boson-fermion interaction; therefore, we consider the grand-canonical hamiltonian

$$K = \sum_{s=\mathrm{B,F}} \int \mathrm{d}\mathbf{r}\, \psi_s^\dagger(\mathbf{r}) \left(-\frac{\nabla^2}{2m_s} - \mu_s \right) \psi_s(\mathbf{r}) + v_0^{\mathrm{BF}} \int \mathrm{d}\mathbf{r}\, \psi_{\mathrm{B}}^\dagger(\mathbf{r}) \psi_{\mathrm{F}}^\dagger(\mathbf{r}) \psi_{\mathrm{F}}(\mathbf{r}) \psi_{\mathrm{B}}(\mathbf{r})$$
$$+ \frac{1}{2} \int \mathrm{d}\mathbf{r} \int \mathrm{d}\mathbf{r}'\, \psi_{\mathrm{B}}^\dagger(\mathbf{r}) \psi_{\mathrm{B}}^\dagger(\mathbf{r}') U_{\mathrm{BB}}(\mathbf{r}-\mathbf{r}') \psi_{\mathrm{B}}(\mathbf{r}') \psi_{\mathrm{B}}(\mathbf{r}). \tag{3.3}$$

For the Bose-Fermi interaction, we introduce an effective coupling and a Fermi momentum

$$g \equiv -\ln(k_{\mathrm{F}} a_{\mathrm{BF}}), \tag{3.4}$$
$$k_{\mathrm{F}} \equiv \sqrt{4\pi n_{\mathrm{F}}}. \tag{3.5}$$

We define also a Fermi energy E_{F} as $E_{\mathrm{F}} = k_{\mathrm{F}}^2/(2m_{\mathrm{F}})$. Since the interaction between bosons and fermions is attractive, the scattering length a_{BF} is set by the radius of the bound state of a boson and a fermion.[2]
The weak and strong BF couplings are identified by the regimes $-g \gg 1$ and $g \gg 1$ respectively. The former corresponds to a weakly bound state with a large radius compared to the average interparticle distance, and for practical calculations we may consider to be in this situation whenever $g \lesssim -2$. The latter is the regime of strong coupling, and for practical calculations we may consider to be in this situation whenever $g \gtrsim 2$. $g \to \infty$ is the molecular limit, where almost all bosons are expelled out of the condensate and fill up the Fermi sphere of composite fermions.

3.2 Transition matrices for the Bose-Fermi mixture

We can now apply the techniques developed in the previous chapter to set up the computation of the equilibrium thermodynamic observables of the mixture. We adopt the diagrammatic approach of the non-self-consistent T-matrix approximation in the zero-temperature limit, based on the summation of the ladder diagrams introduced in Sec. 2.5.2. This method has proved to have many virtues in a wide variety of situations. Here, we list a few of them, among those that will be discussed in more

[1] Specifically, the broad Fano-Feshbach resonance [62].
[2] Recall from Sec. 2.5.3 that in the 2-dimensional case a bound state always exists.

detail throughout this thesis:

- in the weak coupling limit the lowest order contributions in $1/g$ originate from the ladder diagrams, a fact that has been tested against fixed-node diffusion Quantum Monte Carlo calculations [99];

- the Γ-matrix in the strong-coupling limit takes the form of a molecular propagator, reflecting the boson-fermion binding into fermionic molecules if the attraction is sufficiently strong;

- the transition matrix approach predicts a universal behavior of the condensate fraction with respect to the boson concentration x as the coupling parameter g is varied, an outcome that was recently confirmed in an experiment on $3d$ BF mixtures [41].

3.2.1 The Γ-matrix

Before evaluating the many-body Γ-matrix analytically, it is convenient to recall Eqs. (2.108) and (2.109) for the vacuum T_2-matrix, in the limit $|\mathbf{p}_0| \to \infty$. Setting $s_1 = \mathrm{F}$ and $s_2 = \mathrm{B}$, we have

$$\frac{1}{v_0^{\mathrm{BF}}} = -\int \frac{\mathrm{d}\mathbf{k}}{(2\pi)^2} \frac{1}{\varepsilon_0 + \mathbf{k}^2/(2m_{\mathrm{r}})} \tag{3.6}$$

$$T_2(z) = -\left(\int \frac{\mathrm{d}\mathbf{k}}{(2\pi)^2} \, \frac{(z+\varepsilon_0)}{(z - \mathbf{k}^2/(2m_{\mathrm{r}}))(\varepsilon_0 + \mathbf{k}^2/(2m_{\mathrm{r}}))} \right)^{-1} = -\frac{2\pi}{m_{\mathrm{r}}} \frac{1}{\ln\big(-z/\varepsilon_0\big)}. \tag{3.7}$$

Moving to the Γ, Eq. (2.102) with $s_1 = \mathrm{F}$ and $s_2 = \mathrm{B}$ (note that boson lines represent non-condensed bosons) yields

$$\Gamma(\mathbf{P},\Omega)^{-1} = \frac{1}{v_0^{\mathrm{BF}}} + \int \frac{\mathrm{d}\mathbf{k}}{(2\pi)^2} \, \frac{1 - \Theta(-\xi^{\mathrm{F}}_{\mathbf{P}-\mathbf{k}}) - \Theta(-\xi^{\mathrm{B}}_{\mathbf{k}})}{\xi^{\mathrm{F}}_{\mathbf{P}-\mathbf{k}} + \xi^{\mathrm{B}}_{\mathbf{k}} - i\Omega} \tag{3.8}$$

$$= \int \frac{\mathrm{d}\mathbf{k}}{(2\pi)^2} \left(\frac{1}{\xi^{\mathrm{F}}_{\mathbf{P}-\mathbf{k}} + \xi^{\mathrm{B}}_{\mathbf{k}} - i\Omega} - \frac{1}{\mathbf{k}^2/(2m_{\mathrm{r}}) + \varepsilon_0} \right) - \int \frac{\mathrm{d}\mathbf{k}}{(2\pi)^2} \, \frac{\Theta(-\xi^{\mathrm{F}}_{\mathbf{P}-\mathbf{k}}) + \Theta(-\xi^{\mathrm{B}}_{\mathbf{k}})}{\xi^{\mathrm{F}}_{\mathbf{P}-\mathbf{k}} + \xi^{\mathrm{B}}_{\mathbf{k}} - i\Omega}, \tag{3.9}$$

where we have used (3.6). Observe that $\int \mathrm{d}\mathbf{k}/(2\pi)^2 \; 1/\left(\mathbf{k}^2/(2m_{\mathrm{r}}) + \varepsilon_0\right)$ acts as a counter-term that cancels the divergence of $\int \mathrm{d}\mathbf{k}/(2\pi)^2 \; 1/\big(\xi^{\mathrm{F}}_{\mathbf{P}-\mathbf{k}} + \xi^{\mathrm{B}}_{\mathbf{k}} - i\Omega\big)$.
The first integral of the RHS of (3.9) yields (with $\Omega \neq 0$)

$$\int \frac{\mathrm{d}\mathbf{k}}{(2\pi)^2} \left(\frac{1}{\xi^{\mathrm{F}}_{\mathbf{P}-\mathbf{k}} + \xi^{\mathrm{B}}_{\mathbf{k}} - i\Omega} - \frac{1}{\mathbf{k}^2/(2m_{\mathrm{r}}) + \varepsilon_0} \right) = -\frac{m_{\mathrm{r}}}{2\pi} \ln \frac{\mathbf{P}^2/(2M) - \mu_{\mathrm{F}} - \mu_{\mathrm{B}} - i\Omega}{\varepsilon_0} \tag{3.10}$$

$$= T_2\left(z = -\frac{\mathbf{P}^2}{2M} + \mu_{\mathrm{F}} + \mu_{\mathrm{B}} + i\Omega \right)^{-1} \equiv T_2(\mathbf{P},\Omega)^{-1}, \tag{3.11}$$

recalling (3.7).
The second integral reads

$$\begin{aligned} I_{\mathrm{F}}(\mathbf{P},\Omega) &\equiv \int \frac{\mathrm{d}\mathbf{k}}{(2\pi)^2}\, \frac{\Theta(-\xi^{\mathrm{F}}_{\mathbf{P}-\mathbf{k}}) + \Theta(-\xi^{\mathrm{B}}_{\mathbf{k}})}{\xi^{\mathrm{F}}_{\mathbf{P}-\mathbf{k}} + \xi^{\mathrm{B}}_{\mathbf{k}} - i\Omega} \\ &= \frac{m_{\mathrm{r}}}{2\pi}\left(\ln \mathcal{A}(\mathbf{P},\Omega) - \ln\left(-\frac{\mathbf{P}^2}{2M} + \mu_{\mathrm{F}} + \mu_{\mathrm{B}} + i\Omega\right)\right), \end{aligned} \tag{3.12}$$

where

$$\mathcal{A}(\mathbf{P},\Omega) = \frac{z(\mathbf{P},\Omega)}{2} + \frac{\mathbf{P}^2}{2M\gamma_{\mathrm{m}}} + \mathrm{sgn}\big(\mathrm{Re}(z(\mathbf{P},\Omega))\big)\sqrt{\left(\frac{z(\mathbf{P},\Omega)}{2}\right)^2 - \frac{\mathbf{P}^2}{2m_{\mathrm{B}}\gamma_{\mathrm{m}}}\,\mu_{\mathrm{F}}}, \tag{3.13}$$

and

$$z(\mathbf{P},\Omega) = \mu_{\mathrm{B}} - \frac{\mu_{\mathrm{F}}}{\gamma_{\mathrm{m}}} - \frac{\mathbf{P}^2}{2m_{\mathrm{B}}} + i\Omega, \tag{3.14}$$

assuming $\mu_{\mathrm{B}} < 0, \mu_{\mathrm{F}} > 0$. A negative μ_{F} results in a vanishing $I_{\mathrm{F}}(\mathbf{P},\Omega)$; we thus see that the latter stems from the presence of a degenerate component of fermionic atoms.

All in all, using Eqs. (3.11) and (3.12) we can write the Γ-matrix as

$$\Gamma(\mathbf{P},\Omega) = \big(T_2(\mathbf{P},\Omega)^{-1} - I_{\mathrm{F}}(\mathbf{P},\Omega)\big)^{-1}, \tag{3.15}$$

which for $\mu_{\mathrm{F}} > 0$, $\mu_{\mathrm{B}} < 0$, $\mathrm{Re}\,\Omega \neq 0$ simplifies to

$$\Gamma(\mathbf{P},\Omega) = \frac{2\pi}{m_{\mathrm{r}}}\left(\ln\frac{\varepsilon_0}{\mathcal{A}(\mathbf{P},\Omega)} + i\pi\,\mathrm{sgn}\,(\mathrm{Re}\,\Omega)\right)^{-1} \tag{3.16}$$

after inserting the analytic expressions for T_2 and I_{F}.

3.2.2 The T-matrix

In the definition of the Γ-matrix, we did not take into account the presence of the condensate. Specifically, it is necessary to include the repeated interactions of the fermions with the condensed bosons, besides the non-condensed ones. Diagrammatically, we thus need to include all possible insertions of condensate lines. To construct such modified transition matrix, the T-matrix, we proceed by drawing a progressively larger number of condensate lines, as shown in the diagrammatic expression in Figure 3.1. It corresponds to the equation

$$T(\mathbf{P},\Omega) = \Gamma(\mathbf{P},\Omega) + n_0\Gamma(\mathbf{P},\Omega)G^0_{\mathrm{F}}(\mathbf{P},\Omega)T(\mathbf{P},\Omega), \tag{3.17}$$

which yields when formally solved for T

$$T(\mathbf{P},\Omega) = \frac{1}{\Gamma(\mathbf{P},\Omega)^{-1} - n_0 G^0_{\mathrm{F}}(\mathbf{P},\Omega)}. \tag{3.18}$$

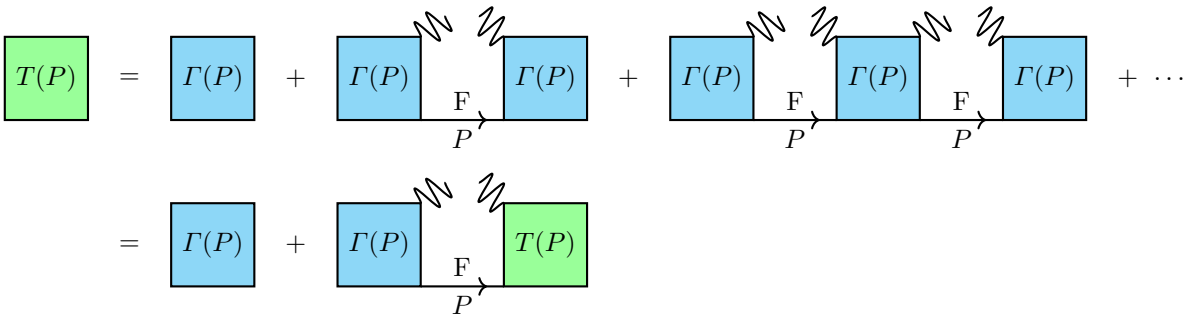

Figure 3.1: Feynman's diagrams for the T-matrix. Wiggly lines corresponds to condensed bosons insertions and give the usual condensate factor of $\sqrt{n_0}$ each. P represents the (2+1)-momentum $P = (\mathbf{P}, \Omega)$.

For the same reason discussed for the Γ, the insertion of a T-matrix inside a Green's function carries a factor of (-1), since we have dropped an overall minus sign in its definition.

Dispersion relations of the poles of T-matrix

We define the *retarded* T-matrix, denoted by $T^{\mathrm{R}}(\mathbf{P}, \Omega)$, as the analytic continuation of the T-matrix to real frequencies via the replacement $i\Omega \to \Omega + i0^+$. The dispersion relations of poles of the T-matrix are found as the solutions $E_{\mathbf{P}}$ to the equation

$$\mathrm{Re}\, T^{\mathrm{R}}(\mathbf{P}, E_{\mathbf{P}})^{-1} = 0 \tag{3.19}$$

when, simultaneously,

$$\mathrm{Im}\, T^{\mathrm{R}}(\mathbf{P}, E_{\mathbf{P}})^{-1} = 0. \tag{3.20}$$

In particular, these conditions yield two dispersion relations $E^{\pm}_{\mathbf{P}}$, which will be discussed thoroughly in Sec. 3.6.1 for the strong coupling regime. Here we simply mention that only one of the two dispersions, say $E^{-}_{\mathbf{P}}$, crosses zero, and this happens at all considered values of the concentration x, the mass ratio γ_{m} and the coupling parameters g and η. The momentum $|\mathbf{P}|$ for which $E^{-}_{\mathbf{P}}$ vanishes is identified by solving

$$\mathrm{Re}\, T(\mathbf{P}, 0^+)^{-1} = 0 \tag{3.21}$$

and is labeled as P_{T0}. P_{T0} plays a crucial role in analytical and numerical calculations, because it represents one of the momenta where the frequency integrals of the kind $\int \mathrm{d}\Omega\ \mathrm{e}^{i\Omega 0^+} T(\mathbf{P}, \Omega)(\ldots)$ may present a step discontinuity. This happens when the Laurent expansion of the integrand around $i\Omega = E^{-}_{\mathbf{P}}$ contains a term $\propto 1/(i\Omega - E^{-}_{\mathbf{P}})$, i.e. when the residue at $i\Omega = E^{-}_{\mathbf{P}}$ is non-vanishing. In this case, the integral over Ω contains a term $\propto \Theta(-E^{-}_{\mathbf{P}})$ that gives a step at P_{T0}.

3.3 Physical quantities

3.3.1 Normal self-energies

The normal boson self-energy Σ_{B}^{11} of our theory is a sum of two terms, $\Sigma_{\mathrm{B}}^{11}(\mathbf{k},\omega) = \Sigma_{\mathrm{BF}}^{11}(\mathbf{k},\omega) + \Sigma_{\mathrm{BB}}^{11}$: the first term $\Sigma_{\mathrm{BF}}^{11}$ stems from the interactions of bosons with fermions, while the second terms $\Sigma_{\mathrm{BB}}^{11}$ stems from the interactions of bosons with other bosons. $\Sigma_{\mathrm{BF}}^{11}$ is determined diagrammatically by Fig. 3.2(b) (with no external propagators intended), and reads

$$\Sigma_{\mathrm{BF}}^{11}(\mathbf{k},\omega) = \int \frac{\mathrm{d}\mathbf{P}}{(2\pi)^2} \int \frac{\mathrm{d}\Omega}{2\pi}\, T(\mathbf{P},\Omega) G_{\mathrm{F}}^{0}(\mathbf{P}-\mathbf{k},\Omega-\omega)\mathrm{e}^{i\Omega 0^+}. \tag{3.22}$$

$\Sigma_{\mathrm{BB}}^{11}$ is computed within the Bogolyubov approximation for weak boson-boson interactions [100, 101], and reads

$$\Sigma_{\mathrm{BB}}^{11} = \frac{8\pi\, n_0\, \eta}{m_{\mathrm{B}}}. \tag{3.23}$$

The fermion self-energy Σ_{F} is determined diagrammatically by Fig. 3.2(a) (with no external propagators intended), and reads

$$\Sigma_{\mathrm{F}}(\mathbf{k},\omega) = n_0 \Gamma(\mathbf{k},\omega) - \int \frac{\mathrm{d}\mathbf{P}}{(2\pi)^2} \int \frac{\mathrm{d}\Omega}{2\pi}\, T(\mathbf{P},\Omega) G_{\mathrm{B}}^{0}(\mathbf{P}-\mathbf{k},\Omega-\omega)\mathrm{e}^{i\Omega 0^+}. \tag{3.24}$$

3.3.2 Anomalous self-energies

The anomalous boson self-energy Σ_{B}^{12} is a sum of two terms as well, $\Sigma_{\mathrm{B}}^{12}(\mathbf{k},\omega) = \Sigma_{\mathrm{BB}}^{12} + \Sigma_{\mathrm{BF}}^{12}(\mathbf{k},\omega)$. As for the normal self-energy, the first term $\Sigma_{\mathrm{BF}}^{12}$ stems from the interactions of bosons with fermions, while the second terms $\Sigma_{\mathrm{BB}}^{12}$ stems from the interactions of bosons with other bosons.

$\Sigma_{\mathrm{BF}}^{12}$ is determined diagrammatically by Fig. 3.3 (with no external propagators intended), and reads

$$\Sigma_{\mathrm{BF}}^{12}(\mathbf{k},\omega) = n_0 \int \frac{\mathrm{d}\mathbf{P}}{(2\pi)^2} \int \frac{\mathrm{d}\Omega}{2\pi}\, T(\mathbf{P}-\mathbf{k},\Omega-\omega) T(\mathbf{P},\Omega) G_{\mathrm{F}}^{0}(\mathbf{P}-\mathbf{k},\Omega-\omega) G_{\mathrm{F}}^{0}(\mathbf{P},\Omega). \tag{3.25}$$

$\Sigma_{\mathrm{BB}}^{12}$ is computed within the Bogolyubov approximation for weak boson-boson interactions, and reads

$$\Sigma_{\mathrm{BB}}^{12} = \frac{4\pi\, n_0\, \eta}{m_{\mathrm{B}}}. \tag{3.26}$$

Many interesting properties of $\Sigma_{\mathrm{BF}}^{12}$ are discussed in Sec. A.2 in relation to the optimization of the numerical program. Here, we note at zero (2+1)-momentum $(\mathbf{k},\omega) = (\mathbf{0},0)$ the integral over Ω is singular at $|\mathbf{P}| = P_{\mathrm{T0}}$; therefore, this is one of the cases where the zero-temperature limit has to be handled as prescribed in Sec. 2.3. The limit as $|\mathbf{k}| \to 0$ yields a Dirac delta, depicted in Fig. 3.4 for the weak-coupling example.

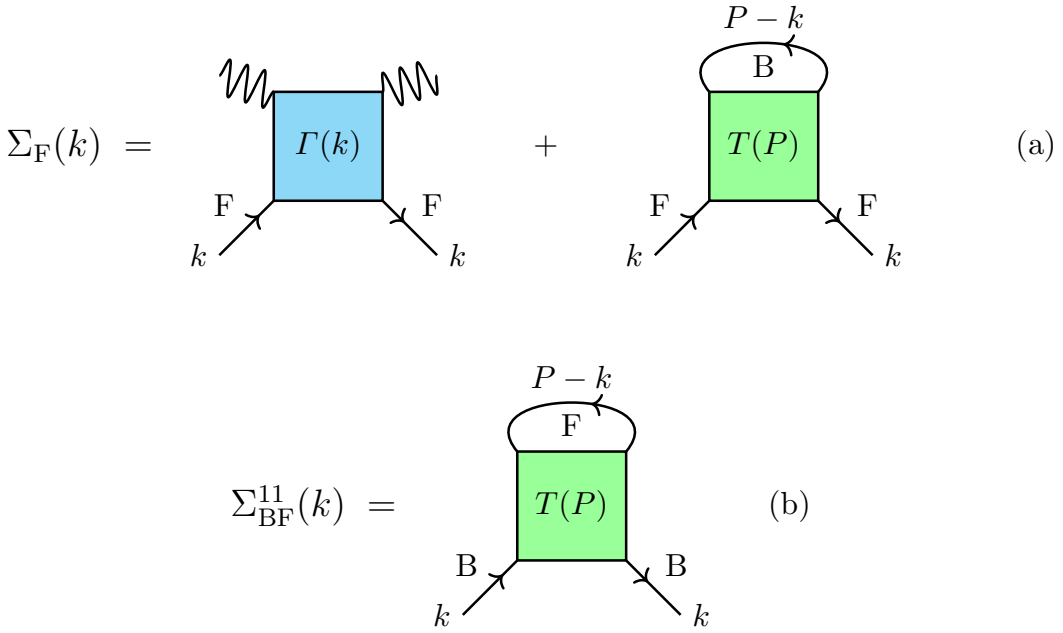

Figure 3.2: Feynman diagrams for: (a) the fermion self-energy $\Sigma_{\rm F}$; (b) $\Sigma^{11}_{\rm BF}$, i.e. the contribution to the normal boson self-energy $\Sigma^{11}_{\rm B}$ arising from the interactions of bosons with fermions. P and k denote (2+1)-momenta: $P=(\mathbf{P},\Omega)$, $k=(\mathbf{k},\omega)$.

After solving the equation $\mathrm{Re}\,T(\mathbf{P},0^+)^{-1}=0$ that determines $P_{\rm T0}$, it is possible to evaluate the contribution of the Dirac delta as follows. Let us consider $|\mathbf{P}|\sim P_{\rm T0}$ and $|\mathbf{k}|\sim 0$; the Laurent expansion of the T-matrix around $i\Omega=E^-_{\mathbf{P}}$ reads

$$\begin{aligned} T(\mathbf{P},\Omega) &= \frac{i}{i\Omega-E^-_{\mathbf{P}}}\mathrm{Res}\left(T(\mathbf{P},\Omega),\Omega=-iE^-_{\mathbf{P}}\right)+\ \text{regular at } i\Omega=E^-_{\mathbf{P}} \\ &\equiv \frac{Z(P)}{i\Omega-E^-_{\mathbf{P}}},\ \text{with} \qquad (3.27) \\ Z(P) &= \lim_{i\Omega\to E^-_{\mathbf{P}}} T(\mathbf{P},\Omega)(i\Omega-E^-_{\mathbf{P}}) \qquad (3.28) \end{aligned}$$

and analogously for $T(\mathbf{P}-\mathbf{k},\Omega)$. $T(\mathbf{P},\Omega)$ and $T(\mathbf{P}-\mathbf{k},\Omega)$ can be approximated as

$$T(\mathbf{P},\Omega)\sim\frac{Z(P_{\rm T0})}{i\Omega-E^-_{\mathbf{P}}},\quad T(\mathbf{P}-\mathbf{k},\Omega)\sim\frac{Z(P_{\rm T0})}{i\Omega-E^-_{\mathbf{P}-\mathbf{k}}},\ \text{with} \qquad (3.29)$$

$$Z(P_{\rm T0})=\lim_{i\Omega\to 0}\Big(i\Omega\,T(P_{\rm T0},\Omega)\Big). \qquad (3.30)$$

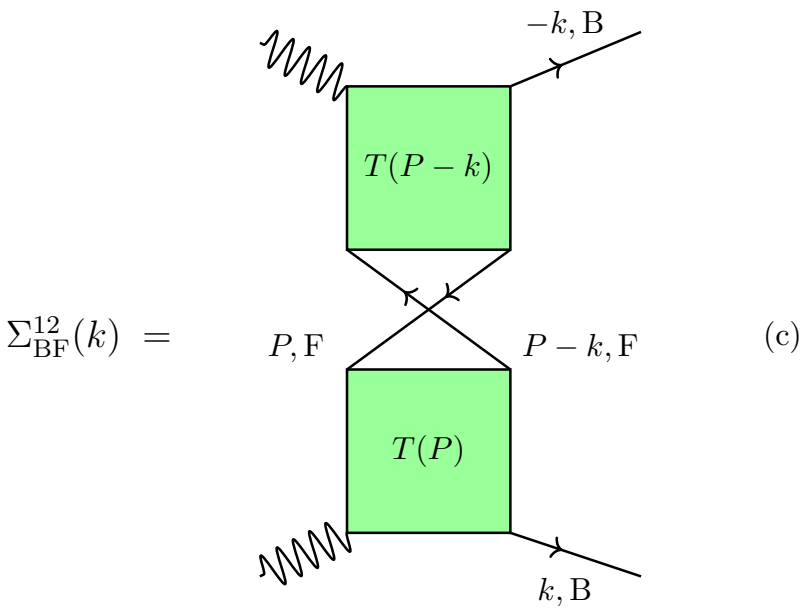

Figure 3.3: Feynman diagram for the contribution to the anomalous boson self-energy Σ^{12}_{B} arising from the interactions of bosons with fermions. P and k denote (2+1)-momenta: $P = (\mathbf{P}, \Omega)$, $k = (\mathbf{k}, \omega)$.

Therefore,

$$\lim_{|\mathbf{k}|\to 0} \int \frac{\mathrm{d}\Omega}{2\pi}\, T(\mathbf{P}-\mathbf{k},\Omega) T(\mathbf{P},\Omega) G^0_{\mathrm{F}}(\mathbf{P},\Omega) G^0_{\mathrm{F}}(\mathbf{P}-\mathbf{k},\Omega)$$
$$\sim -\delta\left(-E^-_{\mathbf{P}}\right) \left(\frac{1}{E^-_{\mathbf{P}} - \mathbf{P}^2/(2m_{\mathrm{F}}) + \mu_{\mathrm{F}}} \right)^2 Z(P_{\mathrm{T}0})^2. \tag{3.31}$$

We postulate the simplest expansion of $E^-_{\mathbf{P}}$ around $P_{\mathrm{T}0}$:

$$E^-_{\mathbf{P}} = v_{\mathrm{CF}}(|\mathbf{P}| - P_{\mathrm{T}0}) + \mathrm{O}\left((|\mathbf{P}| - P_{\mathrm{T}0})^2\right). \tag{3.32}$$

If we have already computed the residue $Z(P_{\mathrm{T}0})$, the slope v_{CF} can be evaluated as[3]

$$\frac{1}{v_{\mathrm{CF}}} = -\lim_{P\to P_{\mathrm{T}0}} \frac{T(P, 0^+)(P - P_{\mathrm{T}0})}{Z(P_{\mathrm{T}0})}. \tag{3.33}$$

[3]With $P = |\mathbf{P}|$. In what follows, we use the symbol P both for the (2+1)-momentum $P = (\mathbf{P}, \Omega)$ and for the magnitude $|\mathbf{P}|$; this should not cause confusion, as the intended meaning will be clear from the context.

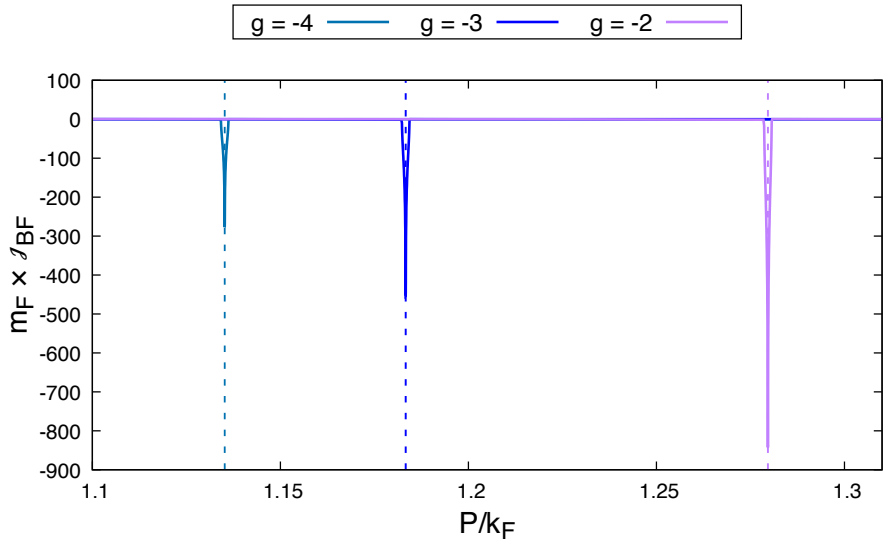

Figure 3.4: Plot of $\mathscr{I}_{\rm BF} \equiv n_0(2\pi)^{-2}\int \mathrm{d}\Omega \int_0^{2\pi} \mathrm{d}\theta\; T(\mathbf{P}-\mathbf{k},\Omega)T(\mathbf{P},\Omega)G^0_{\rm F}(\mathbf{P}-\mathbf{k},\Omega)G^0_{\rm F}(\mathbf{P},\Omega)$ in units of $1/m_{\rm F}$, as a function of $|\mathbf{P}|/k_{\rm F}$. The magnitude of the external momentum is set to the small value $|\mathbf{k}| = 0.001\, k_{\rm F}$. θ denotes the angle between $\mathbf{P}$ and $\mathbf{k}$. The boson concentration is $x = 1$ and the mass ratio is $\gamma_{\rm m} = 1$. Different values of the BF coupling g are reported, while the BB coupling is set to $\eta = 0$. The chemical potentials are set to $\mu_{\rm B} = -0.01\, E_{\rm F}$, $\mu_{\rm F} = E_{\rm F}$ and the condensate density to $n_0 = 0.999\, n_{\rm F}$. The dashed lines correspond to the different values of $P_{\rm T0}$, which are evaluated numerically by solving $\mathrm{Re}\, T(\mathbf{P},0^+)^{-1} = 0$ at the given g. The program used to compute $\mathscr{I}_{\rm BF}$ is described in Sec. A.2.

Integrating over a small interval I around $P_{\rm T0}$ yields

$$\begin{aligned}
&-\int_I \frac{\mathrm{d}P}{2\pi}\; P\;\delta\left(E_P^-\right)\left(\frac{1}{E_P^- - P^2/(2m_{\rm F}) + \mu_{\rm F}}\right)^2 Z(P_{\rm T0})^2 \\
&= -\frac{P_{\rm T0}}{2\pi\,|v_{\rm CF}|}\left(\frac{1}{P_{\rm T0}^2/(2m_{\rm F}) - \mu_{\rm F}}\right)^2 Z(P_{\rm T0})^2 \\
&= \frac{P_{\rm T0}}{2\pi}\left(\frac{1}{P_{\rm T0}^2/(2m_{\rm F}) - \mu_{\rm F}}\right)^2 Z(P_{\rm T0}) \lim_{P\to P_{\rm T0}} \left(T(P,0^+)(P-P_{\rm T0})\right), \qquad (3.34)
\end{aligned}$$

assuming $v_{\rm CF}$ to be positive.

All in all, we have reached the following estimate for the contribution of the Dirac delta to $\Sigma^{12}_{\rm BF}(\mathbf{0},0)$:

$$\begin{aligned}
A^{\delta}_{\rm BF} &\equiv n_0 \int_I \frac{\mathrm{d}\mathbf{P}}{(2\pi)^2} \lim_{|\mathbf{k}|\to 0} \int \frac{\mathrm{d}\Omega}{2\pi}\; T(\mathbf{P}-\mathbf{k},\Omega-\omega)T(\mathbf{P},\Omega)G^0_{\rm F}(\mathbf{P}-\mathbf{k},\Omega-\omega)G^0_{\rm F}(\mathbf{P},\Omega) \\
&= n_0\,\frac{P_{\rm T0}}{2\pi}\left(\frac{1}{P_{\rm T0}^2/(2m_{\rm F}) - \mu_{\rm F}}\right)^2 Z(P_{\rm T0}) \lim_{P\to P_{\rm T0}} \left(T(P,0^+)(P-P_{\rm T0})\right). \qquad (3.35)
\end{aligned}$$

Therefore, recalling Eq. (3.25), $\Sigma^{12}_{\rm BF}(\mathbf{0},0)$ can be evaluated as

$$\Sigma^{12}_{\rm BF}(\mathbf{0},0) = n_0 \int' \frac{\mathrm{d}\mathbf{P}}{(2\pi)^2} \int \frac{\mathrm{d}\Omega}{2\pi}\, T(\mathbf{P},\Omega)^2 G^0_{\rm F}(\mathbf{P},\Omega)^2 + A^{\delta}_{\rm BF}, \tag{3.36}$$

where the notation $\int' \mathrm{d}\mathbf{P}(\ldots)$ means that we exclude the interval I from the integration over $|\mathbf{P}|$.

$\Sigma^{12}_{\rm BF}$ was not considered in recent theoretical papers such as [56], but there are several reasons for including it. In Sec. 3.5, we will discuss the importance of $\Sigma^{12}_{\rm BF}$ in the weak-coupling limit, in the case where a partial dressing of the fermion bare Green's functions inside the self-energy is implemented. In addition, $\Sigma^{12}_{\rm BF}$ is expected to play a role in discussing the stability of the Bose-Fermi mixture. For example, another recent work [57] developed a strong-coupling theory for the stability of a 3-dimensional Bose-Fermi mixture, based on a T-matrix approach similar to that of [56], but including the anomalous $\Sigma^{12}_{\rm BF}$ term. In particular, the authors considered a BEC immersed in a large Fermi gas acting as a reservoir for the fermions inside the mixture, with BF pairing interactions and BB repulsion (the latter treated within Bogolyubov theory). The fundamental conditions for studying the stability of the system in this setting are $\mu_{\rm F} = \mu^{\rm res}_{\rm F}$ (i.e., the chemical potential of the fermion reservoir) and $\partial\mu_{\rm B}/\partial n_{\rm B}\big|_{\mu_{\rm F}} \geq 0$. The first equation places a constraint on the fermion density inside the mixture, while the second condition ensures that the mixture is stable against collapse. In that paper, it is shown that (outside the phase-separation region)

$$\left.\frac{\partial\mu_{\rm B}}{\partial n_{\rm B}}\right|_{\mu_{\rm F}} = \frac{4\pi}{m_{\rm B}}\left(a_{\rm BB} + a_{\rm eff}\right), \tag{3.37}$$

where the effective scattering length $a_{\rm eff}$ stems from fermion-mediated interactions between bosons and reads

$$\frac{4\pi}{m_{\rm B}}\, a_{\rm eff} = \int \frac{\mathrm{d}\mathbf{k}}{(2\pi)^3} \frac{1}{\beta} \sum_{\omega_n} G^0_{\rm F}(\mathbf{k},\omega_n)^2 \Gamma(\mathbf{k},\omega_n)^2. \tag{3.38}$$

This quantity is identical to the momentum integral in $\Sigma^{12}_{\rm BF}(\mathbf{0},0)$, upon replacing Γ with T.
The authors proved that $a_{\rm eff}$ is negative[4] and hence that the mediated BF interaction is attractive, undermining the stability of the system. This fact requires to tune $a_{\rm BB}$ to a sufficiently large value to avoid the collapse of the system.
Similarly, for all boson concentrations, mass ratios, and coupling parameters considered in this thesis, $\Sigma^{12}_{\rm BF}(\mathbf{0},0)$ is found to be negative,[5] and therefore, also in our case, the contribution of fermion-mediated interactions between bosons to the anomalous self-energy is expected to be important. This study remains a subject for future work.

[4] Even though with a magnitude $|a_{\rm eff}|$ which is smaller than the expectation from perturbation theory, in agreement with the outcomes of recent experiments [30] on sound propagation and stability of a ^{133}Cs-^{6}Li mixture that questioned the validity of the perturbative calculations.

[5] In the weak-coupling case, this fact can be understood from the dominant contribution of the Dirac delta, reported in Fig. 3.4 and discussed in Sec. 3.4.3. See also Sec. A.2 for further numerical results.

3.3.3 Green's functions, momentum distributions and densities

The dressed fermion Green's function $G_{\rm F}(\mathbf{k},\omega)$ is obtained by inserting the irreducible graphs of Fig. 3.2(a) in Dyson's Eq. (2.84), which we report here for convenience

$$G_{\rm F}(\mathbf{k},\omega)^{-1} = G^0_{\rm F}(\mathbf{k},\omega)^{-1} - \Sigma_{\rm F}(\mathbf{k},\omega). \tag{3.39}$$

Similarly, the dressed boson Green's function is given by (2.92)

$$G'_{\rm B}(\mathbf{k},\omega)^{-1} = G^0_{\rm B}(\mathbf{k},\omega)^{-1} - \Sigma^{11}_{\rm B}(\mathbf{k},\omega) + \frac{\Sigma^{12}_{\rm BF}(\mathbf{k},\omega)^2}{i\omega + \xi^{\rm B}_{\mathbf{k}} + \Sigma^{11}_{\rm B}(-\mathbf{k},-\omega)}, \tag{3.40}$$

with the self-energies discussed in the previous section.

With the Green's functions at hand, the momentum distributions for fermions and out-of-condensate bosons are given by

$$n_{\rm F}(\mathbf{k}) = \int \frac{{\rm d}\omega}{2\pi}\, G_{\rm F}(\mathbf{k},\omega){\rm e}^{i\omega 0^+} \tag{3.41}$$

$$n_{\rm B}(\mathbf{k}) = -\int \frac{{\rm d}\omega}{2\pi}\, G'_{\rm B}(\mathbf{k},\omega){\rm e}^{i\omega 0^+}. \tag{3.42}$$

Finally, integrating over $\mathbf{k}$ yields the densities $n_{\rm F}$ and $n_{\rm B}$ of the two components.

3.3.4 Equations for $\mu_{\rm B}$, $\mu_{\rm F}$, n_0

The set of equations

$$\mu_{\rm B} = \Sigma^{11}_{\rm B}(\mathbf{0},0) - \Sigma^{12}_{\rm B}(\mathbf{0},0) \tag{3.43}$$

$$n_{\rm F} = \int \frac{{\rm d}\mathbf{k}}{(2\pi)^2}\, n_{\rm F}(\mathbf{k}) \tag{3.44}$$

$$n_{\rm B} = n_0 + \int \frac{{\rm d}\mathbf{k}}{(2\pi)^2}\, n_{\rm B}(\mathbf{k}). \tag{3.45}$$

allows to numerically evaluate $\mu_{\rm B}$, $\mu_{\rm F}$ and n_0, for given boson concentration x, mass ratio $\gamma_{\rm m}$, and coupling parameters g and η. The workflow of the numerical implementation in *Fortran 90* is as follows. First, a solution is found for $\mu_{\rm B}$ from Eq. (3.43) with a standard bisections method assuming a suitable ansatz for $\mu_{\rm F}$ and n_0. Then, we consider the 2×2 system of the remaining Eqs. (3.44) and (3.45) as functions of $\mu_{\rm F}$ and n_0 and apply a two-dimensional secant (quasi-Newton) method whereby the approximate jacobian matrix (which corresponds to the approximate hessian of the total energy) is updated according to a symmetric rank 1 algorithm, which is a generalization of the secant method to multidimensional problems.

All numerical integrations are performed employing the Gauss-Legendre quadrature method. In Appendix A the strategy for the evaluation of the boson and fermion self-energies, momentum distributions and densities is briefly discussed, mostly following [56]. However, note that in [56] the

anomalous term stemming from BF interactions was not taken into account. Therefore, in Sec. A.2 special attention is devoted to the inclusion of $\Sigma_{\rm BF}^{12}$.

3.4 Perturbative expansions in the weak-coupling limit

At this point, we have established the general formalism and the resulting system of equations to study in a fully numerical manner the equilibrium thermodynamic properties of the mixture. This numerical implementation is necessary in the regime of "intermediate" coupling values $-2 \lesssim g \lesssim 2$, while for $g \gtrsim 2$ and $g \lesssim -2$ the numerical results are expected to approach the analytical expressions available for these extremal regimes.

The goal of this section is to derive analytical expressions for the chemical potentials $\mu_{\rm B}$ and $\mu_{\rm F}$, valid in the weak-coupling limit up to second order in $1/g$. A similar calculation has already been carried out in [99], although with some differences in the setup. In particular, in [99] the perturbative expansions are performed within the *real*-frequency formalism, as opposed to our choice of *imaginary* frequencies. Moreover, fermions are treated in the *canonical* ensemble, while imaginary-frequency Green's functions are typically used in the *grand-canonical*. The choice of ensemble is particularly important here and leads to a discrepancy between the boson chemical potential reported in [99] and that derived in this thesis.

In this section we focus on $\eta = 0$, implying $\mu_{\rm B} < 0$.

3.4.1 The Γ-matrix

Defining the shifted center of mass energy $\xi_{\mathbf{P}}^{\rm CM} \equiv \mathbf{P}^2/(2M) - \mu_{\rm F} - \mu_{\rm B}$ and the energy $\varepsilon_{\rm r}^{\rm F} \equiv k_{\rm F}^2/(2m_{\rm r})$, the two-body T_2 (3.11)

$$T_2(\mathbf{P},\Omega)^{-1} = -\frac{m_{\rm r}}{2\pi} \ln \frac{\xi_{\mathbf{P}}^{\rm CM} - i\Omega}{\varepsilon_0} \tag{3.46}$$

can be written as (recalling $\varepsilon_0 = (2m_{\rm r}a_{\rm BF}^2)^{-1} = (k_{\rm F}a_{\rm BF})^{-2}\ \varepsilon_{\rm r}^{\rm F}$)

$$T_2(\mathbf{P},\Omega)^{-1} = -\frac{m_{\rm r}}{\pi} \ln(k_{\rm F}a_{\rm BF}) - \frac{m_{\rm r}}{2\pi} \ln \frac{\xi_{\mathbf{P}}^{\rm CM} - i\Omega}{\varepsilon_{\rm r}^{\rm F}}. \tag{3.47}$$

We can proceed to expand T_2 and Γ in orders of $1/g = -1/\ln(k_{\rm F}a_{\rm BF})$:

$$\begin{aligned}
\Gamma(\mathbf{P},\Omega) &= \left(-\frac{m_{\rm r}}{\pi}\ln(k_{\rm F}a_{\rm BF}) - \frac{m_{\rm r}}{2\pi}\ln\frac{\xi^{\rm CM}_{\mathbf{P}} - i\Omega}{\varepsilon^{\rm F}_{\rm r}} - I_{\rm F}(\mathbf{P},\Omega)\right)^{-1} \\
&= \left(-\frac{m_{\rm r}}{\pi}\ln(k_{\rm F}a_{\rm BF})\right)^{-1}\left(1 + \frac{1}{\ln(k_{\rm F}a_{\rm BF})}\left(\frac{1}{2}\ln\frac{\xi^{\rm CM}_{\mathbf{P}} - i\Omega}{\varepsilon^{\rm F}_{\rm r}} + \frac{\pi}{m_{\rm r}}I_{\rm F}(\mathbf{P},\Omega)\right)\right)^{-1} \\
&= -\frac{\pi}{m_{\rm r}\ln(k_{\rm F}a_{\rm BF})}\left(1 - \frac{1}{\ln(k_{\rm F}a_{\rm BF})}\left(\frac{1}{2}\ln\frac{\xi^{\rm CM}_{\mathbf{P}} - i\Omega}{\varepsilon^{\rm F}_{\rm r}} + \frac{\pi}{m_{\rm r}}I_{\rm F}(\mathbf{P},\Omega)\right)\right) + \dots \\
&= \frac{\pi}{m_{\rm r}}\left(\frac{1}{g} + \frac{1}{g^2}\left(\frac{1}{2}\ln\frac{\xi^{\rm CM}_{\mathbf{P}} - i\Omega}{\varepsilon^{\rm F}_{\rm r}} + \frac{\pi}{m_{\rm r}}I_{\rm F}(\mathbf{P},\Omega)\right)\right) + \mathrm{O}\left(\frac{1}{g^3}\right),
\end{aligned} \tag{3.48}$$

and identify the following perturbative orders $\Gamma(\mathbf{P},\Omega) = \Gamma^{(1)} + \Gamma^{(2)}(\mathbf{P},\Omega) + \dots$

$$\Gamma^{(1)} = \frac{1}{g}\frac{\pi}{m_{\rm r}} \tag{3.49}$$

$$\begin{aligned}
\Gamma^{(2)}(\mathbf{P},\Omega) &= \frac{1}{g^2}\frac{\pi}{m_{\rm r}}\left(\frac{1}{2}\ln\frac{\xi^{\rm CM}_{\mathbf{P}} - i\Omega}{\varepsilon^{\rm F}_{\rm r}} + \frac{\pi}{m_{\rm r}}I_{\rm F}(\mathbf{P},\Omega)\right) \\
&= \frac{1}{g^2}\frac{\pi}{2m_{\rm r}}\left(\ln\left(\frac{\mathcal{A}(\mathbf{P},\Omega)}{\varepsilon^{\rm F}_{\rm r}}\right) - i\pi\,\mathrm{sgn}\left(\mathrm{Re}\,\Omega\right)\right).
\end{aligned} \tag{3.50}$$

In the next sections, it will sometimes be convenient to express $\Gamma^{(2)}$ in integral form as (recalling Eqs. (3.11) and (3.12))

$$\Gamma^{(2)}(\mathbf{P},\Omega) = \frac{1}{g^2}\frac{\pi^2}{m_{\rm r}^2}\int\frac{\mathrm{d}\mathbf{q}}{(2\pi)^2}\left(\frac{\Theta(-\xi^{\rm F}_{\mathbf{P}-\mathbf{q}}) - 1}{\xi^{\rm F}_{\mathbf{P}-\mathbf{q}} + \xi^{\rm B}_{\mathbf{q}} - i\Omega} + \frac{1}{\mathbf{q}^2/(2m_{\rm r}) + \varepsilon^{\rm F}_{\rm r}}\right). \tag{3.51}$$

In the last equation we have used $\mu_{\rm B} < 0$ to set $\Theta(-\xi^{\rm B}_{\mathbf{k}}) = 0$ in $I_{\rm F}(\mathbf{P},\Omega)$.
Observe that $\int \mathrm{d}\mathbf{q}/(2\pi)^2\ 1/\left(\mathbf{q}^2/(2m_{\rm r}) + \varepsilon^{\rm F}_{\rm r}\right)$ acts as a counter-term to cancel the divergence of $\int \mathrm{d}\mathbf{q}/(2\pi)^2\left(\Theta(-\xi^{\rm F}_{\mathbf{P}-\mathbf{q}}) - 1\right)/\left(\xi^{\rm F}_{\mathbf{P}-\mathbf{q}} + \xi^{\rm B}_{\mathbf{q}} - i\Omega\right)$.

In this way, we have expanded the Γ-matrix at fixed chemical potentials. For clarity, it can be useful to highlight this parametric dependence on $\mu_{\rm F}$ and $\mu_{\rm B}$, employing the notation

$$\Gamma(\mathbf{P},\Omega\,|\,\mu_{\rm F},\mu_{\rm B}) = \Gamma^{(1)} + \Gamma^{(2)}(\mathbf{P},\Omega\,|\,\mu_{\rm F},\mu_{\rm B}) + \dots \tag{3.52}$$

Similarly, for the self-energies

$$\Sigma(\mathbf{k},\omega\,|\,\mu_{\rm F},\mu_{\rm B}) = \Sigma^{(1)}(\mathbf{k},\omega\,|\,\mu_{\rm F},\mu_{\rm B}) + \Sigma^{(2)}(\mathbf{k},\omega\,|\,\mu_{\rm F},\mu_{\rm B}) + \dots \tag{3.53}$$

It is important to note that the chemical potentials should also be seen as functions of g, as they are determined after solving Eqs. (3.43), (3.44) and (3.45) at given coupling parameters, boson concen-

tration and mass ratio. Therefore, they are also expanded in powers of $1/g$

$$\mu_{\rm F} = E_{\rm F} + \mu_{\rm F}^{(1)} + \mu_{\rm F}^{(2)} + \dots \tag{3.54}$$

$$\mu_{\rm B} = \mu_{\rm B}^{(1)} + \mu_{\rm B}^{(2)} + \dots \tag{3.55}$$

resulting in the following series for the self-energies:

$$\Sigma(\mathbf{k},\omega\,|\,\mu_{\rm F},\mu_{\rm B}) = \Sigma^{(1)}(\mathbf{k},\omega\,|\,E_{\rm F},0) + \Sigma^{(2)}(\mathbf{k},\omega\,|\,E_{\rm F},0) + \left.\frac{\partial\Sigma^{(1)}(\mathbf{k},\omega\,|\,\mu_{\rm F},\mu_{\rm B})}{\partial\mu_{\rm F}}\right|_{\substack{\mu_{\rm F}=E_{\rm F}\\ \mu_{\rm B}=0}} \mu_{\rm F}^{(1)} + \left.\frac{\partial\Sigma^{(1)}(\mathbf{k},\omega\,|\,\mu_{\rm F},\mu_{\rm B})}{\partial\mu_{\rm B}}\right|_{\substack{\mu_{\rm F}=E_{\rm F}\\ \mu_{\rm B}=0}} \mu_{\rm B}^{(1)} + \dots \tag{3.56}$$

3.4.2 The fermion chemical potential

We will use the self-energy expansion above to derive the series (3.54) and (3.55) for the chemical potentials. For the boson chemical potential, the relation between $\mu_{\rm B}$ and $\Sigma_{\rm B}$ is established by the Hugenholtz-Pines theorem (3.43). To evaluate $\mu_{\rm F}$, however, we must first relate it to $\Sigma_{\rm F}$ in a similar fashion.

Luttinger's theorem

We start from rewriting Dyson's equation as

$$\begin{aligned} G_{\rm F}(\mathbf{k},\omega)^{-1} &= G_{\rm F}^0(\mathbf{k},\omega)^{-1} - {\rm Re}\Sigma_{\rm F}\left(\widetilde{k}_{\rm F},0^+\right) - \Sigma_{\rm F}(\mathbf{k},\omega) + {\rm Re}\Sigma_{\rm F}\left(\widetilde{k}_{\rm F},0^+\right) \\ &\equiv \widetilde{G}_{\rm F}^0(\mathbf{k},\omega)^{-1} - \widetilde{\Sigma}_{\rm F}(\mathbf{k},\omega). \end{aligned} \tag{3.57}$$

We have defined

$$\widetilde{G}_{\rm F}^0(\mathbf{k},\omega)^{-1} \equiv G_{\rm F}^0(\mathbf{k},\omega)^{-1} - {\rm Re}\Sigma_{\rm F}\left(\widetilde{k}_{\rm F},0^+\right) \tag{3.58}$$

$$\widetilde{\Sigma}_{\rm F}(\mathbf{k},\omega) \equiv \Sigma_{\rm F}(\mathbf{k},\omega) - {\rm Re}\Sigma_{\rm F}\left(\widetilde{k}_{\rm F},0^+\right) \tag{3.59}$$

with $\widetilde{k}_{\rm F}$ being the solution of the equation (note that $\Sigma_{\rm F}$ depends on $\mathbf{k}$ only through its magnitude $k \equiv |\mathbf{k}|$)

$$\frac{k^2}{2m_{\rm F}} - \mu_{\rm F} + {\rm Re}\Sigma_{\rm F}(k,0^+) = 0 \tag{3.60}$$

that identifies the position of the Fermi step of the momentum distribution of the interacting fermions.

Eq. (3.60) is solved by $\widetilde{k}_{\rm F} = k_{\rm F}$ if

$$\mu_{\rm F} = E_{\rm F} + {\rm Re}\Sigma_{\rm F}(k_{\rm F},0^+), \tag{3.61}$$

a condition which is known as *Luttinger's theorem*. The statement is that the volume of the Fermi

sphere of fermions does not depend on interactions, and thus coincides with the volume of the Fermi sphere of the corresponding non-interacting Fermi gas [92]. It was originally proved for Fermi liquids, with its validity later extended to density-imbalanced two-component Fermi gases [102] and, within a two-channel model, to BF mixtures [103].

Let us go back to Dyson's equation (3.57). In the second part of this section, we will show that $\Sigma_{\rm F}(\mathbf{k},\omega) = \mathrm{O}(1/g)$, with the leading order being independent of $(\mathbf{k},\omega)$. Therefore, $\widetilde{\Sigma}_{\rm F}(\mathbf{k},\omega) = \mathrm{O}(1/g^2)$ and having introduced the shifted $\widetilde{G}^0_{\rm F}(\mathbf{k},\omega)$ and $\widetilde{\Sigma}_{\rm F}(\mathbf{k},\omega)$ from $G^0_{\rm F}(\mathbf{k},\omega)$ and $\Sigma_{\rm F}(\mathbf{k},\omega)$ accelerates the convergence of the expansion

$$G_{\rm F}(\mathbf{k},\omega) = \widetilde{G}^0_{\rm F}(\mathbf{k},\omega) + \left(\widetilde{G}^0_{\rm F}(\mathbf{k},\omega)\right)^2 \widetilde{\Sigma}_{\rm F}(\mathbf{k},\omega) + \dots \tag{3.62}$$

By performing the operation $\int \mathrm{d}\mathbf{k}/(2\pi)^2 \int \mathrm{d}\omega/(2\pi)\ \mathrm{e}^{i\omega 0^+}(\dots)$ on both sides of Eq. (3.62) and using

$$\int \frac{\mathrm{d}\mathbf{k}}{(2\pi)^2} \int \frac{\mathrm{d}\omega}{2\pi}\, G_{\rm F}(\mathbf{k},\omega)\, \mathrm{e}^{i\omega 0^+} = n_{\rm F} \tag{3.63}$$

$$\int \frac{\mathrm{d}\mathbf{k}}{(2\pi)^2} \int \frac{\mathrm{d}\omega}{2\pi}\, \widetilde{G}^0_{\rm F}(\mathbf{k},\omega)\, \mathrm{e}^{i\omega 0^+} = \frac{m_{\rm F}}{2\pi}\left(\mu_{\rm F} - \mathrm{Re}\Sigma_{\rm F}\left(\widetilde{k}_{\rm F}, 0^+\right)\right), \tag{3.64}$$

we obtain the equation (neglecting orders higher than $\mathrm{O}(1/g^2)$)

$$\begin{aligned}\mu_{\rm F} = {} & E_{\rm F} + \mathrm{Re}\Sigma_{\rm F}\left(k_{\rm F}, 0^+\right) \\ & + \mathrm{Re}\Sigma_{\rm F}\left(\widetilde{k}_{\rm F}, 0^+\right) - \mathrm{Re}\Sigma_{\rm F}\left(k_{\rm F}, 0^+\right) - \frac{2\pi}{m_{\rm F}}\,\mathrm{tr}\left(\left(\widetilde{G}^0_{\rm F}(\mathbf{k},\omega)\right)^2 \widetilde{\Sigma}_{\rm F}(\mathbf{k},\omega)\right),\end{aligned} \tag{3.65}$$

where we have summed and subtracted $\mathrm{Re}\Sigma_{\rm F}\left(k_{\rm F}, 0^+\right)$.

The validity of Luttinger's theorem in the weak-coupling limit for our system is discussed in detail in Sec. B.2, where it is proven that the terms in Eq. (3.65) that are "spurious" with respect to (3.61) contribute only beyond $\mathrm{O}(1/g^2)$. Therefore, in what follows, we neglect the additional terms in (3.65) and compute $\mu_{\rm F}$ perturbatively within this framework.

Perturbative expansion of $\Sigma_{\rm F}(k_{\rm F}, 0^+ \,|\, \mu_{\rm F}, \mu_{\rm B})$

At this point, we have all the tools needed to compute $\mu_{\rm F}$ at $\mathrm{O}(1/g^2)$. By noting that in the RHS of Fig. 3.1 we can replace the T-matrix in the second diagram with the Γ-matrix up to $\mathrm{O}(1/g^3)$ corrections, we can identify the orders up to $\mathrm{O}(1/g^2)$ of the self-energy from the following diagrammatic expression (with no external fermion propagators intended)

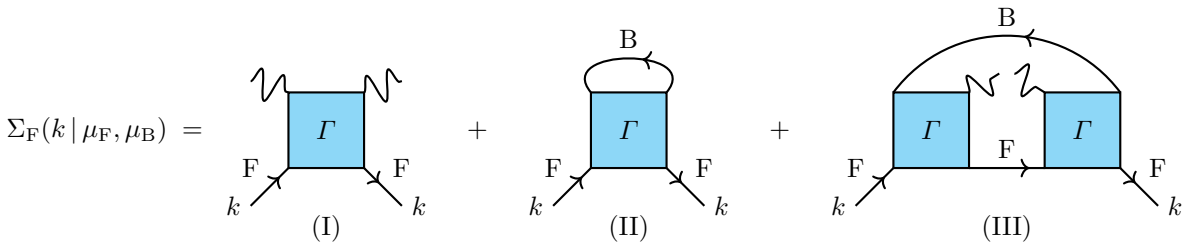

The first order $\Sigma_{\mathrm{F}}^{(1)}(\mathbf{k},\omega\,|\,\mu_{\mathrm{F}},\mu_{\mathrm{B}})$ comes from diagrams (I) and (II), yielding

$$\begin{aligned}\Sigma_{\mathrm{F}}^{(1)}(\mathbf{k},\omega\,|\,\mu_{\mathrm{F}},\mu_{\mathrm{B}}) &= n_0\Gamma^{(1)} - \Gamma^{(1)}\int\frac{\mathrm{d}\mathbf{P}}{(2\pi)^2}\int\frac{\mathrm{d}\Omega}{2\pi}\,\frac{1}{i(\Omega-\omega)-\xi^{\mathrm{B}}_{\mathbf{P}-\mathbf{k}}}\mathrm{e}^{i\Omega 0^+}\\ &= n_0\Gamma^{(1)}\end{aligned} \tag{3.66}$$

as the pole $\Omega = -i\xi^{\mathrm{B}}_{\mathbf{P}-\mathbf{k}}$ lies on the negative imaginary axis. Since $\Gamma^{(1)}$ is already of first order in $1/g$, $\mu_{\mathrm{F}}^{(1)}$ is obtained by setting $n_0 = n_{\mathrm{B}}$:[6]

$$\mu_{\mathrm{F}}^{(1)} = x\frac{\gamma_{\mathrm{m}}+1}{2\gamma_{\mathrm{m}}}\frac{1}{g}\,E_{\mathrm{F}}. \tag{3.67}$$

Let us now move to $\Sigma_{\mathrm{F}}^{(2)}(k_{\mathrm{F}},0^+\,|\,\mu_{\mathrm{F}},\mu_{\mathrm{B}})$, to which all of the above diagrams can in principle contribute:

$$\Sigma_{\mathrm{F}}^{(2)}(k_{\mathrm{F}},0^+\,|\,\mu_{\mathrm{F}},\mu_{\mathrm{B}}) = n_{\mathrm{B}}\Gamma^{(2)}(k_{\mathrm{F}},0^+\,|\,\mu_{\mathrm{F}},\mu_{\mathrm{B}}) \tag{3.68}$$

$$-\int\frac{\mathrm{d}\mathbf{P}}{(2\pi)^2}\int\frac{\mathrm{d}\Omega}{2\pi}\,\Gamma^{(2)}(\mathbf{P},\Omega\,|\,\mu_{\mathrm{F}},\mu_{\mathrm{B}})\frac{1}{i\Omega-\xi^{\mathrm{B}}_{\mathbf{P}-\mathbf{k}_{\mathrm{F}}}}\mathrm{e}^{i\Omega 0^+} \tag{3.69}$$

$$-n_{\mathrm{B}}\big(\Gamma^{(1)}\big)^2\int\frac{\mathrm{d}\mathbf{P}}{(2\pi)^2}\int\frac{\mathrm{d}\Omega}{2\pi}\,\frac{1}{i\Omega-\xi^{\mathrm{F}}_{\mathbf{P}}}\frac{1}{i\Omega-\xi^{\mathrm{B}}_{\mathbf{P}-\mathbf{k}_{\mathrm{F}}}}\mathrm{e}^{i\Omega 0^+}, \tag{3.70}$$

where (3.68), (3.69) and (3.70) come from (I), (II) and (III) respectively.
We focus on $\mu_{\mathrm{F}} = E_{\mathrm{F}} - \Delta\mu_{\mathrm{F}}$ with $0 \le \Delta\mu_{\mathrm{F}} < E_{\mathrm{F}}$, and $\mu_{\mathrm{B}} = -\Delta\mu_{\mathrm{B}}$ with $0 \le \Delta\mu_{\mathrm{B}} < E_{\mathrm{F}}$. For notational convenience, we define $\eta_{\mathrm{F}} \equiv \Delta\mu_{\mathrm{F}}/E_{\mathrm{F}}$, $\eta_{\mathrm{B}} \equiv \Delta\mu_{\mathrm{B}}/E_{\mathrm{F}}$ and $\eta \equiv \eta_{\mathrm{F}} - \eta_{\mathrm{B}}$. To compute (3.68), we note that with this parametrization of the chemical potentials $\mathcal{A}(k_{\mathrm{F}},0^+)$ (3.13) reads

$$\mathcal{A}(k_{\mathrm{F}},0^+\,|\,\eta_{\mathrm{F}},\eta_{\mathrm{B}}) = -\frac{E_{\mathrm{F}}}{1+\gamma_{\mathrm{m}}} + i0^+ + \frac{E_{\mathrm{F}}}{2}\left(\frac{\eta_{\mathrm{F}}}{\gamma_{\mathrm{m}}} - \eta_{\mathrm{B}}\right) - E_{\mathrm{F}}\sqrt{\frac{1}{4}\left(\frac{\eta_{\mathrm{F}}}{\gamma_{\mathrm{m}}} - \eta_{\mathrm{B}}\right)^2 + \frac{\eta_{\mathrm{B}}}{\gamma_{\mathrm{m}}}} \tag{3.71}$$

[6] Moreover, since the leading perturbative order of n_0 turns out to be $\mathrm{O}(1/g^2)$ [104], the product $n_0\Gamma^{(1)}$ does not yield a contribution to the second order either.

and therefore

$$\frac{\mathcal{A}(k_{\mathrm{F}},0^{+}\,|\,\eta_{\mathrm{F}},\eta_{\mathrm{B}})}{\varepsilon_{\mathrm{r}}^{\mathrm{F}}} = -\frac{\gamma_{\mathrm{m}}}{(1+\gamma_{\mathrm{m}})^{2}} + \frac{\gamma_{\mathrm{m}}}{1+\gamma_{\mathrm{m}}}\left(\frac{1}{2}\left(\frac{\eta_{\mathrm{F}}}{\gamma_{\mathrm{m}}}-\eta_{\mathrm{B}}\right)-\sqrt{\frac{1}{4}\left(\frac{\eta_{\mathrm{F}}}{\gamma_{\mathrm{m}}}-\eta_{\mathrm{B}}\right)^{2}+\frac{\eta_{\mathrm{B}}}{\gamma_{\mathrm{m}}}}\right)+i0^{+}. \tag{3.72}$$

Keeping the parametric dependence on η_{F} and η_{B} explicit while making implicit the dependence on the external 3-momentum $(k_{\mathrm{F}},0^{+})$, we define $\Sigma_{\mathrm{F}}^{[\mathrm{I}]}(\eta_{\mathrm{F}},\eta_{\mathrm{B}})$ to be the contribution to $\Sigma_{\mathrm{F}}^{(2)}(k_{\mathrm{F}},0^{+}\,|\,\mu_{\mathrm{F}},\mu_{\mathrm{B}})$ arising from diagram (I). Recalling the right pre-factors from (3.50), it reads

$$\begin{aligned}\Sigma_{\mathrm{F}}^{[\mathrm{I}]}(\eta_{\mathrm{F}},\eta_{\mathrm{B}}) &= n_{\mathrm{B}}\frac{\pi}{2m_{\mathrm{r}}}\left(\ln\Bigg(-\frac{\gamma_{\mathrm{m}}}{(1+\gamma_{\mathrm{m}})^{2}}\right.\\ &\quad\left.+\frac{\gamma_{\mathrm{m}}}{1+\gamma_{\mathrm{m}}}\left(\frac{1}{2}\left(\frac{\eta_{\mathrm{F}}}{\gamma_{\mathrm{m}}}-\eta_{\mathrm{B}}\right)-\sqrt{\frac{1}{4}\left(\frac{\eta_{\mathrm{F}}}{\gamma_{\mathrm{m}}}-\eta_{\mathrm{B}}\right)^{2}+\frac{\eta_{\mathrm{B}}}{\gamma_{\mathrm{m}}}}\right)+i0^{+}\Bigg)-i\pi\right)\frac{1}{g^{2}}\\ &= n_{\mathrm{B}}\frac{\pi}{2m_{\mathrm{r}}}\left(\ln\frac{\gamma_{\mathrm{m}}}{(1+\gamma_{\mathrm{m}})^{2}}+\frac{1+\gamma_{\mathrm{m}}}{\sqrt{\gamma_{\mathrm{m}}}}\sqrt{\eta_{\mathrm{B}}}\right)\frac{1}{g^{2}}+\mathrm{O}\left(\frac{\eta_{\mathrm{F}}}{g^{2}}\right)+\mathrm{O}\left(\frac{\eta_{\mathrm{B}}}{g^{2}}\right).\end{aligned} \tag{3.73}$$

The expansion in the last line is performed as a single variable series expansion in the small parameter $1/g$, to which both η_{F} and η_{B} are assumed to be proportional.

The integral (3.69) gives no contribution, as seen by writing $\Gamma^{(2)}$ in the integral form (3.51). Indeed, the counter-term is independent of Ω and thus its frequency integral is vanishing due to $\mu_{\mathrm{B}}<0$; regarding the other term,

$$\begin{aligned}&(\Theta(-\xi^{\mathrm{F}}_{\mathbf{P}-\mathbf{k}})-1)\int\frac{\mathrm{d}\Omega}{2\pi}\,\frac{1}{\xi^{\mathrm{F}}_{\mathbf{P}-\mathbf{k}}+\xi^{\mathrm{B}}_{\mathbf{k}}-i\Omega}\frac{1}{i\Omega-\xi^{\mathrm{B}}_{\mathbf{P}-\mathbf{k}_{\mathrm{F}}}}\mathrm{e}^{i\Omega 0^{+}}\\ &=(1-\Theta(-\xi^{\mathrm{F}}_{\mathbf{P}-\mathbf{k}}))\frac{\Theta(-\xi^{\mathrm{F}}_{\mathbf{P}-\mathbf{k}}-\xi^{\mathrm{B}}_{\mathbf{k}})}{\xi^{\mathrm{F}}_{\mathbf{P}-\mathbf{k}}+\xi^{\mathrm{B}}_{\mathbf{k}}-\xi^{\mathrm{B}}_{\mathbf{P}-\mathbf{k}_{\mathrm{F}}}}=0\end{aligned} \tag{3.74}$$

since $\Theta(-\xi^{\mathrm{F}}_{\mathbf{P}-\mathbf{k}})\Theta(-\xi^{\mathrm{F}}_{\mathbf{P}-\mathbf{k}}-\xi^{\mathrm{B}}_{\mathbf{k}})=\Theta(-\xi^{\mathrm{F}}_{\mathbf{P}-\mathbf{k}}-\xi^{\mathrm{B}}_{\mathbf{k}})$.

The frequency integral of (3.70) reads

$$\begin{aligned}&\int\frac{\mathrm{d}\Omega}{2\pi}\,\frac{1}{i\Omega-\xi^{\mathrm{F}}_{\mathbf{P}}}\frac{1}{i\Omega-\xi^{\mathrm{B}}_{\mathbf{P}-\mathbf{k}_{\mathrm{F}}}}\mathrm{e}^{i\Omega 0^{+}}\\ &\qquad=\Theta(k_{\mu_{\mathrm{F}}}-P)\frac{m_{\mathrm{B}}}{Pk_{\mathrm{F}}}\left(\cos\theta+\frac{P}{2k_{\mathrm{F}}}(\gamma_{\mathrm{m}}-1)-\frac{k_{\mathrm{F}}}{2P}\left(\gamma_{\mathrm{m}}\left(1-\eta\right)+1\right)\right)^{-1},\end{aligned} \tag{3.75}$$

with $k_{\mu_{\mathrm{F}}}=\sqrt{2m_{\mathrm{F}}(E_{\mathrm{F}}-\Delta\mu_{\mathrm{F}})}=\sqrt{1-\eta_{\mathrm{F}}}\;k_{\mathrm{F}}$. Integrating over the angle θ yields (using dimensionless

variables $\widetilde{P} \equiv |\mathbf{P}|/k_{\mathrm{F}}$ and $u = 1/\widetilde{P}$)

$$\int \frac{\mathrm{d}\mathbf{P}}{(2\pi)^2} \frac{\Theta(-\xi^{\mathrm{F}}_{\mathbf{P}})}{\xi^{\mathrm{F}}_{\mathbf{P}} - \xi^{\mathrm{B}}_{\mathbf{P}-\mathbf{k}_{\mathrm{F}}}} = -\frac{m_{\mathrm{B}}}{\pi} \int_0^{\sqrt{1-\eta_{\mathrm{F}}}} \mathrm{d}\widetilde{P}\, \frac{1}{\sqrt{\alpha \widetilde{P}^2 + \beta(\eta)/\widetilde{P}^2 + \delta(\eta)}} \tag{3.76}$$

$$= -\frac{m_{\mathrm{B}}}{2\pi} \int_0^{1-\eta_{\mathrm{F}}} \mathrm{d}u\, \frac{1}{\sqrt{\alpha u^2 + \delta(\eta) u + \beta(\eta)}} \tag{3.77}$$

with

$$\alpha = (1-\gamma_{\mathrm{m}})^2,$$

$$\beta(\eta) \;=\; (1+(1-\eta)\,\gamma_{\mathrm{m}})^2\,, \;\; \delta(\eta) \;=\; -2\left(1+\eta\gamma_{\mathrm{m}}+(1-\eta)\,\gamma_{\mathrm{m}}^2\right).$$

Recalling the right pre-factors from (3.70) and (3.49), it follows that the contribution $\Sigma_{\mathrm{F}}^{[\mathrm{III}]}(\eta_{\mathrm{F}}, \eta_{\mathrm{B}})$ to $\Sigma_{\mathrm{F}}^{(2)}(k_{\mathrm{F}}, 0^+ \,|\, \mu_{\mathrm{F}}, \mu_{\mathrm{B}})$ from diagram (III) reads

$$\begin{aligned}
\Sigma_{\mathrm{F}}^{[\mathrm{III}]}(\eta_{\mathrm{F}}, \eta_{\mathrm{B}}) &= -n_{\mathrm{B}} \frac{\pi}{2m_{\mathrm{r}}} (1+\gamma_{\mathrm{m}}) \\
&\quad \times (-1) \int_0^{1-\eta_{\mathrm{F}}} \mathrm{d}u\, \frac{1}{\sqrt{\alpha u^2 + \delta(\eta_{\mathrm{F}}-\eta_{\mathrm{B}}) u + \beta(\eta_{\mathrm{F}}-\eta_{\mathrm{B}})}} \frac{1}{g^2} \\
&= n_{\mathrm{B}} \frac{\pi}{2m_{\mathrm{r}}} (1+\gamma_{\mathrm{m}}) \left(\frac{1}{\gamma_{\mathrm{m}}-1} \ln \gamma_{\mathrm{m}} - \frac{1}{\sqrt{\gamma_{\mathrm{m}}}} \sqrt{\eta_{\mathrm{B}}} \right) \frac{1}{g^2} + \mathrm{O}\left(\frac{\eta_{\mathrm{F}}}{g^2}\right) + \mathrm{O}\left(\frac{\eta_{\mathrm{B}}}{g^2}\right),
\end{aligned} \tag{3.78}$$

where the expansion in the last line is performed after the integral and with the same method mentioned for $\Sigma_{\mathrm{F}}^{[\mathrm{I}]}$.

Taking η_{F} and η_{B} to be of first order in $1/g$, the second-order contribution is identified after summing the contributions from the two diagrams:

$$\Sigma_{\mathrm{F}}^{[\mathrm{I}]}(\eta_{\mathrm{F}}, \eta_{\mathrm{B}}) + \Sigma_{\mathrm{F}}^{[\mathrm{III}]}(\eta_{\mathrm{F}}, \eta_{\mathrm{B}}) = n_{\mathrm{B}} \frac{\pi}{2m_{\mathrm{r}}} \left(\ln\left(\frac{\gamma_{\mathrm{m}}}{(1+\gamma_{\mathrm{m}})^2} \right) + \frac{\gamma_{\mathrm{m}}+1}{\gamma_{\mathrm{m}}-1} \ln \gamma_{\mathrm{m}} \right) \frac{1}{g^2} + \mathrm{O}\left(\frac{1}{g^3}\right). \tag{3.79}$$

Note that the two terms of order $1/|g|^{5/2}$ cancel each other, and that the term of order $1/g^2$ is independent of η_{F} and η_{B}.

Since we have shown that $\Sigma_{\mathrm{F}}^{(1)}(\mathbf{k}, \omega \,|\, \mu_{\mathrm{F}}, \mu_{\mathrm{B}})$ is independent of μ_{F} and μ_{B}, its derivatives with respect to the chemical potentials do not contribute to the second order of $\Sigma_{\mathrm{F}}(\mathbf{k}, \omega \,|\, \mu_{\mathrm{F}}, \mu_{\mathrm{B}})$; therefore, from (3.79) we can read off $\mu_{\mathrm{F}}^{(2)}$:

$$\mu_{\mathrm{F}}^{(2)} = x \frac{\gamma_{\mathrm{m}}+1}{4\,\gamma_{\mathrm{m}}} \left(\ln\left(\frac{\gamma_{\mathrm{m}}}{(1+\gamma_{\mathrm{m}})^2} \right) + \frac{\gamma_{\mathrm{m}}+1}{\gamma_{\mathrm{m}}-1} \ln \gamma_{\mathrm{m}} \right) \frac{1}{g^2}\, E_{\mathrm{F}}. \tag{3.80}$$

All in all Eqs. (3.61), (3.67) and (3.80) yield the following expression for μ_{F}, valid up to $\mathrm{O}(1/g^3)$:

$$\mu_{\mathrm{F}} = E_{\mathrm{F}} + E_{\mathrm{F}}\, x \frac{\gamma_{\mathrm{m}}+1}{2\,\gamma_{\mathrm{m}}} \frac{1}{g} + E_{\mathrm{F}}\, x \frac{\gamma_{\mathrm{m}}+1}{4\,\gamma_{\mathrm{m}}} \left(\ln\left(\frac{\gamma_{\mathrm{m}}}{(1+\gamma_{\mathrm{m}})^2} \right) + \frac{\gamma_{\mathrm{m}}+1}{\gamma_{\mathrm{m}}-1} \ln \gamma_{\mathrm{m}} \right) \frac{1}{g^2}. \tag{3.81}$$

3.4.3 The boson chemical potential

To compute the boson chemical potential we rely on the Hugenholtz-Pines theorem at zero repulsion between bosons,

$$\mu_{\rm B} = \Sigma^{11}_{\rm BF}(\mathbf{0},0) - \Sigma^{12}_{\rm BF}(\mathbf{0},0), \tag{3.82}$$

evaluating the normal term first and then moving to the anomalous.

Normal self-energy

By noting that in the RHS of Fig. 3.1 we can replace the T-matrix in the second diagram with the Γ-matrix up to $\mathrm{O}(1/g^3)$ corrections, we can identify the orders up to $\mathrm{O}(1/g^2)$ in the self-energy $\Sigma^{11}_{\rm BF}(\mathbf{0},0)$ from the following diagrammatic expansion (with no external bosonic propagators intended)

$\Sigma^{11}_{\rm BF}(k\,|\,\mu_{\rm F},\mu_{\rm B}) \;=$

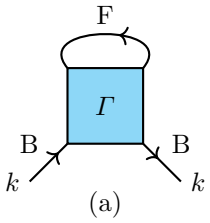

(a)

$+$

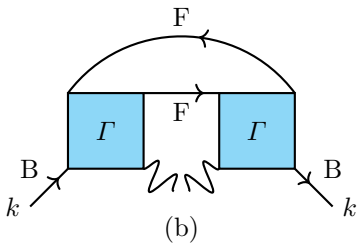

(b)

This time the analogous of diagram (II), i.e. diagram (a), does give a contribution since the density of free fermions at zero temperature is non vanishing: the first order $\Sigma^{(1)}_{\rm BF}(\mathbf{k},\omega\,|\,\mu_{\rm F},\mu_{\rm B})$ reads

$$\begin{aligned}\Sigma^{(1)}_{\rm BF}(\mathbf{k},\omega\,|\,\mu_{\rm F},\mu_{\rm B}) &= \Gamma^{(1)}\int\frac{\mathrm{d}\mathbf{P}}{(2\pi)^2}\int\frac{\mathrm{d}\Omega}{2\pi}\,\frac{1}{i(\Omega-\omega)-\xi^{\rm F}_{\mathbf{P}-\mathbf{k}}}\mathrm{e}^{i\Omega 0^+}\\ &= \Gamma^{(1)}\frac{k^2_{\mu_{\rm F}}}{4\pi},\end{aligned} \tag{3.83}$$

where $k_{\mu_{\rm F}} = \sqrt{2m_{\rm F}\mu_{\rm F}}$. To zeroth order $\mu_{\rm F} = E_{\rm F}$ and we have

$$\mu^{(1)}_{\rm B} = \frac{\gamma_{\rm m}+1}{2\gamma_{\rm m}}\frac{1}{g}\,E_{\rm F}. \tag{3.84}$$

However, differently from the perturbative calculation in Sec. 3.4.2, this time there is a second order contribution to $\mu_{\rm B}$ stemming from the first order in $\mu_{\rm F} = E_{\rm F}+\mu^{(1)}_{\rm F}$, as a consequence of the dependence of $\Sigma^{(1)}_{\rm BF}(\mathbf{0},0\,|\,\mu_{\rm F},\mu_{\rm B})$ on the fermion chemical potential. Indeed

$$\begin{aligned}\Sigma^{(1)}_{\rm BF}(\mathbf{0},0\,|\,\mu_{\rm F},\mu_{\rm B}) &= E_{\rm F}\frac{\gamma_{\rm m}+1}{2\gamma_{\rm m}}\frac{1}{g} + \frac{\gamma_{\rm m}+1}{2\gamma_{\rm m}}\frac{\mu^{(1)}_{\rm F}}{g} + \mathrm{O}\left(\frac{1}{g^3}\right)\\ &= E_{\rm F}\left(\frac{\gamma_{\rm m}+1}{2\gamma_{\rm m}}\frac{1}{g} + x\left(\frac{\gamma_{\rm m}+1}{2\,\gamma_{\rm m}}\right)^2\frac{1}{g^2}\right) + \mathrm{O}\left(\frac{1}{g^3}\right).\end{aligned} \tag{3.85}$$

Going back to the diagrammatic expression for $\Sigma^{11}_{\rm BF}$, further second order terms in $\mu_{\rm B}$ are given by

$$\Sigma^{(2)}_{\rm BF}(\mathbf{0},0\,|\,E_{\rm F},0) = \int \frac{{\rm d}\mathbf{P}}{(2\pi)^2}\int\frac{{\rm d}\Omega}{2\pi}\,\Gamma^{(2)}(\mathbf{P},\Omega\,|\,E_{\rm F},0)\frac{1}{i\Omega-\xi^{\rm F}_{\mathbf{P}}}{\rm e}^{i\Omega 0^+} \tag{3.86}$$

$$+\,n_{\rm B}\left(\Gamma^{(1)}\right)^2\int\frac{{\rm d}\mathbf{P}}{(2\pi)^2}\int\frac{{\rm d}\Omega}{2\pi}\,\left(\frac{1}{i\Omega-\xi^{\rm F}_{\mathbf{P}}}\right)^2, \tag{3.87}$$

where (3.86) and (3.87) come from (a) and (b) respectively. Note that we have already set $\mu_{\rm F} = E_{\rm F}$ and $\mu_{\rm B} = 0^-$ in all diagrams for $\Sigma^{(2)}_{\rm BF}$. This is because, as we have verified explicitly in Sec. 3.4.2 by keeping $\mu_{\rm F} = (1-\eta_{\rm F})\,E_{\rm F}$ and $\mu_{\rm B} = -\eta_{\rm B}\,E_{\rm F}$ in the analogous second order contribution $\Sigma^{(2)}_{\rm F}(k_{\rm F},0^+\,|\,\mu_{\rm F},\mu_{\rm B})$, the higher order corrections $\eta_{\rm F}$ and $\eta_{\rm B}$ play a role only beyond $\mathrm{O}(1/g^2)$.

Let us focus on (3.86), denoted by $\Sigma^{[a]}_{\rm BF}$. Recalling (3.51), the frequency integral can be separated into two terms: one of them is proportional to $\int{\rm d}\Omega/(2\pi)\,\left(1/(i\Omega-\xi^{\rm F}_{\mathbf{P}})\right){\rm e}^{i\Omega 0^+} = \Theta(-\xi^{\rm F}_{\mathbf{P}})$; the other one is proportional to

$$(\Theta(-\xi^{\rm F}_{\mathbf{P}-\mathbf{q}})-1)\int\frac{{\rm d}\Omega}{2\pi}\,\frac{1}{\xi^{\rm F}_{\mathbf{P}-\mathbf{q}}+\xi^{\rm B}_{\mathbf{q}}-i\Omega}\frac{1}{i\Omega-\xi^{\rm F}_{\mathbf{P}}} = \Theta(k_{\rm F}-|\mathbf{P}|)\frac{\Theta(-\xi^{\rm F}_{\mathbf{P}-\mathbf{q}})-1}{\xi^{\rm F}_{\mathbf{P}-\mathbf{q}}+\xi^{\rm B}_{\mathbf{q}}-\xi^{\rm F}_{\mathbf{P}}}. \tag{3.88}$$

Note that only the pole of $1/(i\Omega-\xi^{\rm F}_{\mathbf{P}})$ contributes in Eq. (3.88), and therefore the integral over Ω in (3.86) yields $\Gamma^{(2)}$ evaluated at $i\Omega=\xi^{\rm F}_{\mathbf{P}}$:

$$\begin{aligned}\Sigma^{[a]}_{\rm BF} &= \int\frac{{\rm d}\mathbf{P}}{(2\pi)^2}\,\Theta(k_{\rm F}-|\mathbf{P}|)\lim_{i\Omega\to\xi^{\rm F}_{\mathbf{P}}+i0^+}\Gamma^{(2)}\left(\mathbf{P},\Omega\,|\,E_{\rm F},0\right)\\ &= \frac{1}{g^2}\frac{\pi}{2m_{\rm r}}\int\frac{{\rm d}\mathbf{P}}{(2\pi)^2}\,\Theta(k_{\rm F}-|\mathbf{P}|)\,\ln\left(-\frac{\mathcal{A}(\mathbf{P},-i\xi^{\rm F}_{\mathbf{P}}\,|\,E_{\rm F},0)}{\varepsilon^{\rm F}_{\rm r}}\right),\end{aligned} \tag{3.89}$$

using (3.50) to go from the first to the second line.

Integrating over the angle and expressing everything in terms of the dimensionless quantities

$$\widetilde{P} = |\mathbf{P}|/k_{\rm F} \tag{3.90}$$

$$\widetilde{z}\left(\widetilde{P}\right) = \frac{1}{\gamma_{\rm m}}\left(\gamma_{\rm m}(\widetilde{P}^2-1)-1-\widetilde{P}^2\right), \tag{3.91}$$

we arrive at

$$\begin{aligned}\Sigma^{[a]}_{\rm BF} &= E_{\rm F}\frac{\gamma_{\rm m}+1}{2\gamma_{\rm m}}\int_0^1{\rm d}\widetilde{P}\,\widetilde{P}\,\ln\left(\frac{\gamma_{\rm m}}{\gamma_{\rm m}+1}\left(-\frac{\widetilde{z}\left(\widetilde{P}\right)}{2}-\frac{\widetilde{P}^2}{\gamma_{\rm m}(\gamma_{\rm m}+1)}+\sqrt{\frac{\widetilde{z}^2\left(\widetilde{P}\right)}{4}-\frac{\widetilde{P}^2}{\gamma_{\rm m}^2}}\right)\right)\frac{1}{g^2}\\ &= E_{\rm F}\frac{\gamma_{\rm m}+1}{2\gamma_{\rm m}}\left(-\frac{1}{2}+\frac{\gamma_{\rm m}\ln\gamma_{\rm m}}{\gamma_{\rm m}-1}-\ln(\gamma_{\rm m}+1)\right)\frac{1}{g^2}.\end{aligned} \tag{3.92}$$

Let us now move to (3.87), denoted by $\Sigma^{[b]}_{\rm BF}$. Observe that the frequency integral is of the type that needs to be interpreted as a limit for $\mathbf{k}\to\mathbf{0}$, splitting the double pole as described in Sec. 2.3.

In particular:

$$\int \frac{\mathrm{d}\mathbf{P}}{(2\pi)^2} \lim_{|\mathbf{k}|\to 0} \int \frac{\mathrm{d}\Omega}{2\pi} \frac{1}{i\Omega - \xi^{\mathrm{F}}_{\mathbf{P}}} \frac{1}{i\Omega - \xi^{\mathrm{F}}_{\mathbf{P}-\mathbf{k}}} = -\frac{1}{2\pi} \int_0^\infty \mathrm{d}P\, P\, \delta(P^2/(2m_{\mathrm{F}}) - E_{\mathrm{F}}) = -\frac{m_{\mathrm{F}}}{2\pi}. \tag{3.93}$$

Therefore, collecting the right pre-factors

$$\Sigma^{[b]}_{\mathrm{BF}} = -x \left(\frac{\gamma_{\mathrm{m}}+1}{2\,\gamma_{\mathrm{m}}}\right)^2 \frac{1}{g^2}\, E_{\mathrm{F}}. \tag{3.94}$$

Note that $\Sigma^{[b]}_{\mathrm{BF}}$ precisely cancels the concentration-dependent term in (3.85), resulting in $\Sigma^{11}_{\mathrm{BF}}(\mathbf{0}, 0 \,|\, \mu_{\mathrm{F}}, \mu_{\mathrm{B}})$ being independent of the boson density.

All in all, the sum of $\Sigma^{(1)}_{\mathrm{BF}}(\mathbf{0}, 0 \,|\, \mu_{\mathrm{F}}, \mu_{\mathrm{B}})$ and $\Sigma^{(2)}_{\mathrm{BF}}(\mathbf{0}, 0 \,|\, E_{\mathrm{F}}, 0)$ yields, truncating at the second order in $1/g$:

$$\Sigma^{11}_{\mathrm{BF}}(\mathbf{0}, 0 \,|\, \mu_{\mathrm{F}}, \mu_{\mathrm{B}}) = E_{\mathrm{F}}\, \frac{1}{2} \frac{\gamma_{\mathrm{m}}+1}{\gamma_{\mathrm{m}}\, g} \left(1 + \frac{1}{2g} \left(\frac{\gamma_{\mathrm{m}} \ln\!\left(\gamma_{\mathrm{m}}^2\right)}{\gamma_{\mathrm{m}}-1} - \ln\!\left((\gamma_{\mathrm{m}}+1)^2\right) - 1\right)\right). \tag{3.95}$$

Anomalous self-energy

As for the anomalous term, it easy to see from (3.25) that its leading order has to be $\mathrm{O}(1/g^2)$ since the T-matrix is of order $1/g$. By replacing the T-matrix with $\Gamma^{(1)}$, the $\mathrm{O}(1/g^2)$ term in $\Sigma^{12}_{\mathrm{BF}}(\mathbf{0}, 0 \,|\, E_{\mathrm{F}}, 0)$ is found to be identical to (3.94):

$$\Sigma^{12}_{\mathrm{BF}}(\mathbf{0}, 0 \,|\, E_{\mathrm{F}}, 0) = -x \left(\frac{\gamma_{\mathrm{m}}+1}{2\,\gamma_{\mathrm{m}}}\right)^2 \frac{1}{g^2}\, E_{\mathrm{F}} \tag{3.96}$$

up to orders higher than $\mathrm{O}(1/g^2)$.

Including the anomalous contribution in $\mu_{\mathrm{B}} = \Sigma^{11}_{\mathrm{BF}}(\mathbf{0}, 0) - \Sigma^{12}_{\mathrm{BF}}(\mathbf{0}, 0)$, one reaches the following expression for the boson chemical potential, valid up to orders beyond $1/g^2$:

$$\mu_{\mathrm{B}} = E_{\mathrm{F}}\, \frac{1}{2} \frac{\gamma_{\mathrm{m}}+1}{\gamma_{\mathrm{m}}\, g} \left(1 + \frac{1}{2g} \left(x\, \frac{\gamma_{\mathrm{m}}+1}{\gamma_{\mathrm{m}}} + \frac{\gamma_{\mathrm{m}} \ln\!\left(\gamma_{\mathrm{m}}^2\right)}{\gamma_{\mathrm{m}}-1} - \ln\!\left((\gamma_{\mathrm{m}}+1)^2\right) - 1\right)\right). \tag{3.97}$$

3.4.4 Remarks on the convergence of infinite series

In the previous sections, we avoided addressing the details about the convergence of infinite sums. In particular, the T-matrix (3.18) was defined as the *formal* sum of an infinite series of terms involving Γ-matrices. Approximating it by the first few terms of this series, as we did when computing the lowest order contributions to $\Sigma_{\mathrm{F}}(k_{\mathrm{F}}, 0^+)$, $\Sigma^{11}_{\mathrm{BF}}(\mathbf{0}, 0)$ and $\Sigma^{12}_{\mathrm{BF}}(\mathbf{0}, 0)$, is justified only if the series is convergent.

The same issue arises in Dyson's equations. For instance, in the case of G_{F}, (2.84) represents the formal sum of an infinite series involving Σ_{F}. Truncating this series at some finite order in Σ_{F} may

or may not yield physical results, depending on its convergence properties. The sum-and-subtraction scheme used in (3.57) served the purpose of solving this difficulty, but we have not yet specified where and why the convergence of the series fails in quantitative terms.

The detailed discussion about all these aspects is found in Appendix B.

3.5 Mean-field shift of the fermion chemical potential

By comparing expression (3.97) with Eq. (23) in [99], we note that the two differ by the concentration-dependent term at second order, $E_{\mathrm{F}}\,(\gamma_{\mathrm{m}}+1)^2/(2\gamma_{\mathrm{m}}\,g)^2\,x$. Hence, the perturbative expansion in this thesis appears to disagree with the expansion in [99], which has been tested against an independent Quantum Monte Carlo study (in the repulsive case) and is believed to be the correct perturbative series that describes the mixture in the limit where the coupling parameter $1/g$ is small.

The origin of the discrepancy can be traced back to the μ_{F}-dependence of $\Sigma^{(1)}_{\mathrm{BF}}(\mathbf{0},0\,|\,\mu_{\mathrm{F}},\mu_{\mathrm{B}})$ (3.85), which is peculiar to our treatment of the fermion component by using Green's functions in the grand-canonical ensemble. If $\Sigma^{(1)}_{\mathrm{BF}}(\mathbf{0},0\,|\,\mu_{\mathrm{F}},\mu_{\mathrm{B}})$ did not yield the term proportional to $\mu^{(1)}_{\mathrm{F}}$, the contributions in Eqs. (3.94) and (3.96) would cancel each other, leaving no dependence on x.

This evidence suggests that, to recover the correct perturbative expansion, it is necessary to introduce an modified T-matrix method featuring a *partial self-consistency*. By (full) "self-consistency" we mean the replacement of the non-interacting Green's functions inside the self-energies by the dressed Green's functions given by Dyson's Eqs. (3.39) and (3.40). While the implementation of full self-consistency in BF mixtures at zero temperature remains an open problem, in our case partial self-consistency is sufficient. That is, we dress the bare Green's function with a constant mean-field approximation to the self-energies.

Similar approaches were studied in [105, 106] for Fermi-Fermi mixtures, and more recently in [107, 108] for Bose-Fermi mixtures. Here we focus on [107, 108], where the subject of the study is a $3d$ BF mixture with a paring interaction, at temperature greater than or equal to the Bose-Einstein condensation temperature T_{BEC}. The authors propose the replacement of the non-interacting boson Green's functions in the self-energies by the modified boson Green's functions

$$\begin{aligned}&\widetilde{G}^{0}_{\mathrm{B}}(\mathbf{k},\omega)=\frac{1}{i\omega-\mathbf{k}^2/(2m_{\mathrm{B}})+\mu'_{\mathrm{B}}}\ \text{with}\\&\mu'_{\mathrm{B}}=\mu_{\mathrm{B}}-\Sigma^{11}_{\mathrm{B}}\left(\mathbf{0},0\,|\,\mu_{\mathrm{F}},\mu'_{\mathrm{B}}\right).\end{aligned}\tag{3.98}$$

The rationale behind this replacement is as follows. The fully dressed boson Green's function has gapless excitations at T_{BEC}, as ensured by the Hughenholtz-Pines condition $\mu_{\mathrm{B}}=\Sigma^{11}_{\mathrm{B}}(\mathbf{0},0)$; the non-interacting boson Green's function, on the other hand, does not (with the energy gap $E_{\mathrm{gap}}=-\Sigma^{11}_{\mathrm{B}}(\mathbf{0},0)$), so that the low-energy Bose-atomic excitations are underestimated in the ordinary T-matrix self-energies. The replacement in Eq. (3.98) restores the Hughenholtz-Pines condition in the boson Green's functions within the self-energies, and in turn enhances the low-energy Bose atomic excitations.

One of the benefits of this modification is that, at T_{BEC} and for $n_{\mathrm{F}} = n_{\mathrm{B}}$, by increasing the BF coupling from weak to strong attraction the fermion chemical potential decreases and becomes negative. This is not verified within the ordinary T-matrix approach, where μ_{F} stays positive suggesting that a Fermi sphere of unpaired Fermi atoms survives.

Following a similar principle, we are lead to replace the non-interacting fermion Green's functions (while not touching the boson Green's functions) in the boson and fermion self-energies by

$$\widetilde{G}^0_{\mathrm{F}}(\mathbf{k},\omega) = \frac{1}{i\omega - \mathbf{k}^2/(2m_{\mathrm{F}}) + \mu'_{\mathrm{F}}} \text{ with} \tag{3.99}$$

$$\mu'_{\mathrm{F}} = \mu_{\mathrm{F}} - \Sigma_{\mathrm{F}}\left(\widetilde{k}_{\mathrm{F}}, 0^+ \,\middle|\, \mu'_{\mathrm{F}}, \mu_{\mathrm{B}}\right), \tag{3.100}$$

where $\widetilde{k}_{\mathrm{F}}$ as usual is the Fermi step momentum of the interacting fermions momentum distribution, determined by the equation

$$\widetilde{k}_{\mathrm{F}} = \sqrt{2m_{\mathrm{F}}\left(\mu_{\mathrm{F}} - \Sigma_{\mathrm{F}}\left(\widetilde{k}_{\mathrm{F}}, 0^+ \,\middle|\, \mu'_{\mathrm{F}}, \mu_{\mathrm{B}}\right)\right)}. \tag{3.101}$$

$\Sigma_{\mathrm{F}}\left(\widetilde{k}_{\mathrm{F}}, 0^+ \,\middle|\, \mu'_{\mathrm{F}}, \mu_{\mathrm{B}}\right)$ is real and we denote it by Σ^0_{F} in the following.
This modification can be seen as a mean-field shift of the fermion chemical potential $\mu_{\mathrm{F}} \mapsto \mu'_{\mathrm{F}}$ in the self-energies (represented in Fig. 3.5), while in Dyson's equation for the dressed fermion Green's function we maintain the "real" fermion chemical potential[7] $\mu_{\mathrm{F}} = \mu'_{\mathrm{F}} + \Sigma^0_{\mathrm{F}}$ inside $G^0_{\mathrm{F}}(\mathbf{k},\omega)^{-1}$, that is

$$G_{\mathrm{F}}(\mathbf{k},\omega)^{-1} = i\omega - \frac{\mathbf{k}^2}{2m_{\mathrm{F}}} + \mu'_{\mathrm{F}} + \Sigma^0_{\mathrm{F}} - \Sigma_{\mathrm{F}}\left(\mathbf{k},\omega \,|\, \mu'_{\mathrm{F}}, \mu_{\mathrm{B}}\right). \tag{3.102}$$

Since at first order $\Sigma^0_{\mathrm{F}} = x/(2g)\,(\gamma_{\mathrm{m}}+1)/\gamma_{\mathrm{m}}$, the transformation $\mu_{\mathrm{F}} \mapsto \mu_{\mathrm{F}} - \Sigma^0_{\mathrm{F}}$ exactly compensates the term proportional to x in Eq. (3.85) for μ_{B}, which originates from the anomalous self-energy $\Sigma^{12}_{\mathrm{BF}}$. The remaining terms in the perturbative expansion for μ_{F} and μ_{B} are unaltered, thus recovering the correct result of [99].

Note that, somehow accidentally, the correct second-order weak-coupling expansion of the chemical potentials is also recovered by the theory in which the anomalous term and the mean-field shift are simultaneously dropped. This is the theory that was used in the recent work [56] for equal masses and it is the theory that we will numerically study in the next chapter for different masses.

Finally, observe that shifting μ_{F} by Σ^0_{F} implies that $\widetilde{G}^0_{\mathrm{F}}(\mathbf{k},0^+)$ shares the same pole at $|\mathbf{k}| = \widetilde{k}_{\mathrm{F}}$ as the fully dressed Green's function $G_{\mathrm{F}}(\mathbf{k},0^+)$.[8] Therefore, in this way we expect to take into account the Fermi-atomic excitations more faithfully; however, the shortcoming is that we are still ignoring many-body effects described by the dynamical part of the self-energy.

A discussion on the numerical implementation of this modified T-matrix method can be found in Appendix C, where numerical results are reported in various regimes for the BF coupling. In the

[7] In [105, 106] this shift of μ_{F} was performed in a very similar manner.

[8] This is in analogy with [107, 108] for boson Green's functions: at T_{BEC}, $\widetilde{G}^0_{\mathrm{B}}(\mathbf{k},0^+)$ and $G_{\mathrm{B}}(\mathbf{k},0^+)$ share the pole at $|\mathbf{k}| = 0$.

remaining sections of the main text we will instead stick to the ordinary T-matrix with no mean field shift of μ_{F}.

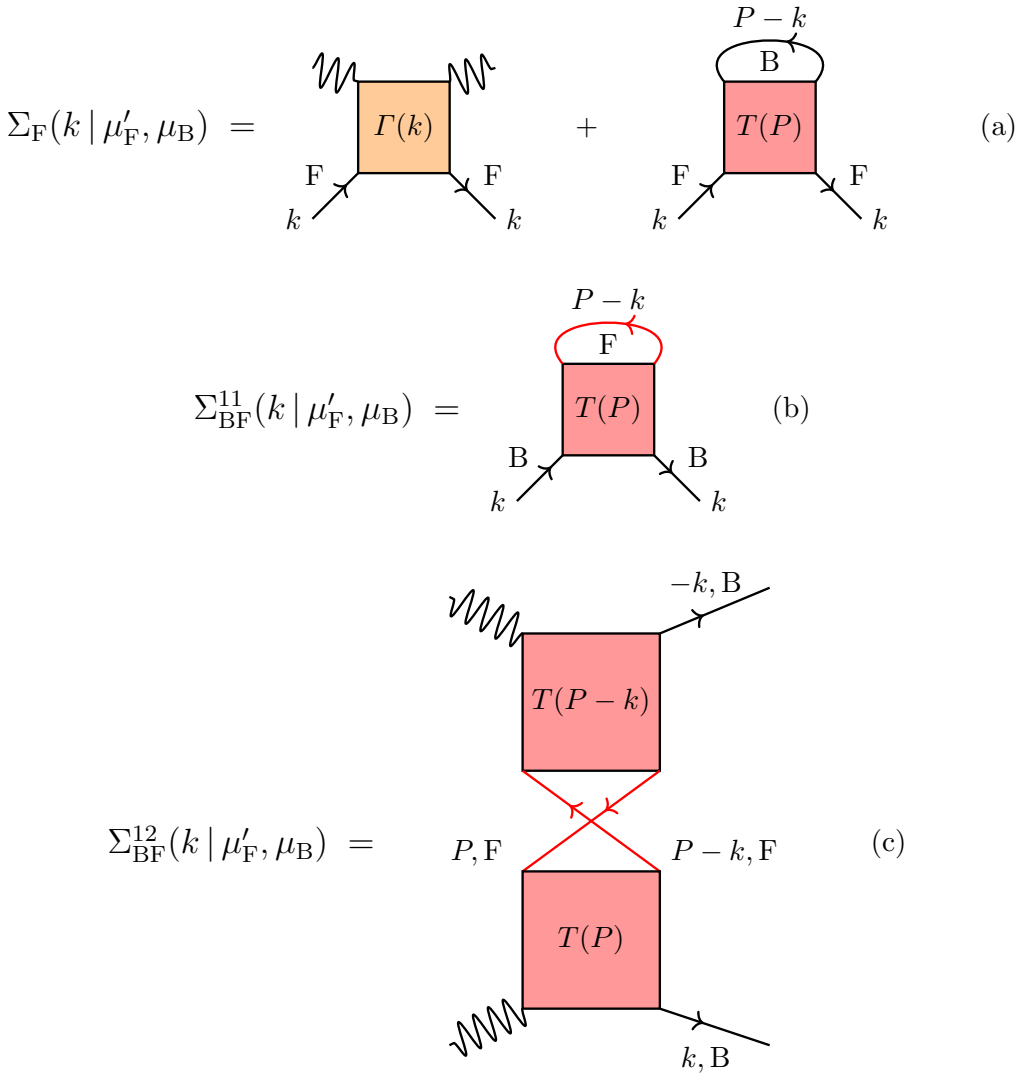

Figure 3.5: Feynman diagrams for: (a) the fermion self-energy Σ_{F}; (b) $\Sigma^{11}_{\mathrm{BF}}$, i.e. the contribution to the normal boson self-energy Σ^{11}_{B} arising from the interactions of bosons with fermions; (c) $\Sigma^{12}_{\mathrm{BF}}$, i.e. the contribution to the anomalous boson self-energy Σ^{12}_{B} arising from the interactions of bosons with fermions. All self-energy diagrams feature the mean-field shift of μ_{F}, with the red lines indicating the modified fermion lines $\widetilde{G}^{0}_{\mathrm{F}}$. Fermion lines inside Γ and T are also modified.

3.6 Strong-coupling regime

We now move to the strong-coupling limit $g \gg 1$, that is, the limit opposite to the case $-g \ll 1$ of the previous sections. Similarly to the weak-coupling regime, in the strong-coupling regime it is

possible to derive analytical expressions for many relevant physical quantities. In particular, the system of Eqs. (3.43), (3.44), (3.45) is replaced by a simpler one, for which a semi-analytical solution is available.

We will follow the treatment of the strong BF interaction found in [56]; however, in that paper the reported closed forms for the composite fermion density, the fermion density and the boson chemical potential are specific to the mass-balanced case $m_{\rm F} = m_{\rm B}$, while here we present the expressions for the general mass-imbalanced case $m_{\rm F} \neq m_{\rm B}$.

The BB interaction set by η is expected to produce only minor effects in this regime, and therefore we neglect it altogether. Moreover, we do not take into account the anomalous term from BF interactions (3.25).

3.6.1 The T-matrix

In the limit $\varepsilon_0 \gg E_{\rm F}$, T_2 (3.11) and $I_{\rm F}$ (3.12) become the simpler expressions

$$T_2(\mathbf{P}, \Omega) = \frac{2\pi\varepsilon_0}{m_{\rm r}} \frac{1}{i\Omega - \mathbf{P}^2/(2M) + \mu_{\rm CF}} \tag{3.103}$$

$$I_{\rm F}(\mathbf{P}, \Omega) = \frac{m_{\rm F}\mu_{\rm F}\Theta(\mu_{\rm F})}{2\pi\,\varepsilon_0}, \tag{3.104}$$

with $\mu_{\rm CF} = \mu_{\rm B} + \mu_{\rm F} + \varepsilon_0$. Defining the effective self-energy term

$$\Sigma^0_{\rm CF} \equiv \frac{m_{\rm F}\,\mu_{\rm F}}{m_{\rm r}}\Theta(\mu_{\rm F}), \tag{3.105}$$

the Γ-matrix takes the strong coupling form

$$\Gamma_{\rm SC}(\mathbf{P}, \Omega) = \frac{2\pi\varepsilon_0}{m_{\rm r}} \frac{1}{i\Omega - \mathbf{P}^2/(2M) + \mu_{\rm CF} - \Sigma^0_{\rm CF}}. \tag{3.106}$$

Note that $\Sigma^0_{\rm CF} > 0$ if $\mu_{\rm F} > 0$, and it vanishes otherwise; therefore, it is interpreted as an effective repulsion field generated by the medium of atomic fermions onto the molecular fermions.
Being a constant mean-field shift, $\Sigma^0_{\rm CF}$ can be re-absorbed into a redefinition of the chemical potential $\widetilde{\mu}_{\rm CF} \equiv \mu_{\rm CF} - \Sigma^0_{\rm CF}$, which yields Γ in the form

$$\Gamma_{\rm SC}(\mathbf{P}, \Omega) = \frac{2\pi\varepsilon_0}{m_{\rm r}} \widetilde{G}^0_{\rm CF}(\mathbf{P}, \Omega), \text{ with} \tag{3.107}$$

$$\widetilde{G}^0_{\rm CF}(\mathbf{P}, \Omega) = \frac{1}{i\Omega - \mathbf{P}^2/(2M) + \widetilde{\mu}_{\rm CF}}. \tag{3.108}$$

$\widetilde{G}^0_{\rm CF}(\mathbf{P}, \Omega)$ is a bare-like fermion Green's function of a particle of mass M and chemical potential $\widetilde{\mu}_{\rm CF}$; the latter is the chemical potential of a molecule made up of a boson and an atomic fermion, renormalized by the mean-field shift $\Sigma^0_{\rm CF}$ that is due to the interaction of the molecules with the atomic medium.

All in all, Γ in the strong coupling regime takes the form of a molecular Green's function, with a constant of proportionality $2\pi\varepsilon_0/m_{\rm r}$ that can also be justified by the composite nature of the molecules (see [56]).

Inserting the strong coupling form of the Γ-matrix inside the definition of the T-matrix (3.18), we obtain

$$\begin{aligned} T_{\rm SC}(\mathbf{P},\Omega)^{-1} &= \frac{m_{\rm r}}{2\pi\varepsilon_0}\left(i\Omega - \frac{\mathbf{P}^2}{2M} + \widetilde{\mu}_{\rm CF} - \frac{2\pi\varepsilon_0 n_0/m_{\rm r}}{i\Omega - \mathbf{P}^2/(2m_{\rm F}) + \mu_{\rm F}}\right) \\ &\equiv \frac{m_{\rm r}}{2\pi\varepsilon_0} G_{\rm CF}(\mathbf{P},\Omega)^{-1}. \end{aligned} \tag{3.109}$$

$G_{\rm CF}$ can be interpreted as a dressed composite fermion Green's function, resulting from the hybridization between a molecular bound state and an unpaired state made of a fermionic atom and a boson belonging to the condensate. This hybridization is controlled by the quantity $\Delta_0^2 \equiv 2\pi\varepsilon_0 n_0/m_{\rm r}$.[9]

By solving the equation $E_{\mathbf{P}} - \widetilde{\xi}^{\rm CF}_{\mathbf{P}} - \Delta_0^2/(E_{\mathbf{P}} - \xi^{\rm F}_{\mathbf{P}}) = 0$, the dispersion relations $E^{\pm}_{\mathbf{P}}$ of the poles of the T-matrix in the strong coupling regime are found to be

$$E^{\pm}_{\mathbf{P}} = \frac{\widetilde{\xi}^{\rm CF}_{\mathbf{P}} + \xi^{\rm F}_{\mathbf{P}} \pm \sqrt{\left(\widetilde{\xi}^{\rm CF}_{\mathbf{P}} - \xi^{\rm F}_{\mathbf{P}}\right)^2 + 4\Delta_0^2}}{2}. \tag{3.110}$$

Here, we have defined the renormalized molecule dispersion $\widetilde{\xi}^{\rm CF}_{\mathbf{P}} \equiv \mathbf{P}^2/(2M) - \widetilde{\mu}_{\rm CF}$. $E^{\pm}_{\mathbf{P}}$ are the energies of the quasi-particle excitations, and their structure reflects the hybrization of a molecule with dispersion $\widetilde{\xi}^{\rm CF}_{\mathbf{P}}$ with an unpaired atom with dispersion $\xi^{\rm F}_{\mathbf{P}}$.

The composite fermion propagator $G_{\rm CF}$ con be expressed in the Bogolyubov two-fraction form in terms of the quasi-particle energies $E^{\pm}_{\mathbf{P}}$ and the weights $u^2_{\mathbf{P}}$ and $v^2_{\mathbf{P}}$,

$$G_{\rm CF}(\mathbf{P},\Omega) = \frac{u^2_{\mathbf{P}}}{i\Omega - E^{+}_{\mathbf{P}}} + \frac{v^2_{\mathbf{P}}}{i\Omega - E^{-}_{\mathbf{P}}}, \tag{3.111}$$

with

$$u^2_{\mathbf{P}} = \frac{1}{2}\left(1 + \frac{\widetilde{\xi}^{\rm CF}_{\mathbf{P}} - \xi^{\rm F}_{\mathbf{P}}}{\sqrt{\left(\widetilde{\xi}^{\rm CF}_{\mathbf{P}} - \xi^{\rm F}_{\mathbf{P}}\right)^2 + 4\Delta_0^2}}\right) \tag{3.112}$$

$$v^2_{\mathbf{P}} = 1 - u^2_{\mathbf{P}}. \tag{3.113}$$

[9] This fact can be qualitatively understood in terms of the creation and annihilation operators. If we denote the operator that creates a molecular bound state when acting on the vacuum by $\psi^{\dagger}_{\rm CF}$, the undressed molecular Green's function $\langle {\rm T}[\psi_{\rm CF}\psi^{\dagger}_{\rm CF}]\rangle$ is given by $\widetilde{G}^0_{\rm CF}$ (3.108). If we then add to the hamiltonian a hybridization term $\Delta_0\,\psi^{\dagger}_{\rm F}\psi_{\rm CF} + {\rm h.c.}$ with $\psi^{\dagger}_{\rm F}$ being the creation operator of atomic fermions, the reciprocal of the dressed Green's function of the composite fermions is given by $\left(\widetilde{G}^0_{\rm CF}\right)^{-1} - \Delta_0^2\langle {\rm T}[\psi_{\rm F}\psi^{\dagger}_{\rm F}]\rangle$, i.e. $G^{-1}_{\rm CF}$ in (3.109).

The density of composite fermions n_{CF} is obtained as

$$\begin{aligned} n_{\mathrm{CF}} &= \int \frac{\mathrm{d}\mathbf{P}}{(2\pi)^2} \int \frac{\mathrm{d}\Omega}{2\pi}\, G_{\mathrm{CF}}(\mathbf{P},\Omega)\mathrm{e}^{i\Omega 0^+} \\ &= \int \frac{\mathrm{d}\mathbf{P}}{(2\pi)^2} \left(u_{\mathbf{P}}^2 \Theta(-E_{\mathbf{P}}^+) + v_{\mathbf{P}}^2 \Theta(-E_{\mathbf{P}}^-)\right), \end{aligned} \tag{3.114}$$

with the integrand in (3.114) interpreted as the composite fermion momentum distribution $n_{\mathrm{CF}}(\mathbf{P})$. In practice, only the term containing $v_{\mathbf{P}}^2$ contributes to (3.114) since $E_{\mathbf{P}}^+$ turns out to be always positive for the concentrations, couplings and mass ratios considered in this thesis.
The integration over $\mathbf{P}$ in (3.114) can be performed in a closed form, yielding

$$\begin{aligned} \frac{n_{\mathrm{CF}}}{n_{\mathrm{F}}} &= \int_0^{y_-} \mathrm{d}y\, v_y^2 \\ &= \frac{1}{4}\Bigg\{ \overline{\widetilde{\mu}}_{\mathrm{CF}}(1+\gamma_{\mathrm{m}}) + \overline{\mu}_{\mathrm{F}} + \overline{\mathcal{K}} - 2\frac{1+\gamma_{\mathrm{m}}}{\gamma_{\mathrm{m}}} \Bigg[\sqrt{4\overline{\Delta}_0^2 + \left(\overline{\widetilde{\mu}}_{\mathrm{CF}} - \overline{\mu}_{\mathrm{F}}\right)^2} \\ &\qquad - \sqrt{\left(4\overline{\Delta}_0^2 + \frac{1}{4(1+\gamma_{\mathrm{m}})^2}\overline{\mathcal{J}}^2\right)} \Bigg] \Bigg\}, \end{aligned} \tag{3.115}$$

with

$$\overline{\mathcal{K}} \equiv \sqrt{4\overline{\Delta}_0^2(1+\gamma_{\mathrm{m}}) + \left(\overline{\widetilde{\mu}}_{\mathrm{CF}}(1+\gamma_{\mathrm{m}}) - \overline{\mu}_{\mathrm{F}}\right)^2}, \tag{3.116}$$

$$\overline{\mathcal{J}} \equiv \overline{\widetilde{\mu}}_{\mathrm{CF}}(\gamma_{\mathrm{m}}^2 + 3\gamma_{\mathrm{m}} + 2) - \overline{\mu}_{\mathrm{F}}(2+\gamma_{\mathrm{m}}) + \gamma_{\mathrm{m}}\overline{\mathcal{K}} \tag{3.117}$$

and where all barred quantities are in units of E_{F}. The integration variable y is defined as $y = \mathbf{P}^2/k_{\mathrm{F}}^2$ and $y_- = (1/2)\left(\overline{\widetilde{\mu}}_{\mathrm{CF}}(1+\gamma_{\mathrm{m}}) + \overline{\mu}_{\mathrm{F}} + \overline{\mathcal{K}}\right)$ is one of the solutions $y_\pm$ of the equation

$$\overline{\widetilde{\xi}}_y^{\mathrm{CF}} + \overline{\xi}_y^{\mathrm{F}} - \sqrt{4\Delta_0^2 + \left(\overline{\widetilde{\xi}}_y^{\mathrm{CF}} - \overline{\xi}_y^{\mathrm{F}}\right)^2} = 0 \tag{3.118}$$

that identifies the zeros of $E_{\mathbf{P}}^-$. The other solution y_+ is negative and therefore not interesting since y is positive by its definition. E_y^- is negative for $y \in (0, y_-)$ and positive for $y > y_-$; hence, the integral in (3.115) is restricted to $(0, y_-)$.

3.6.2 Fermion self-energy and momentum distribution

Let us now discuss the fermion self-energy in the strong coupling limit, i.e. (3.24) with Γ replaced by Γ_{SC} and T replaced by T_{SC}. The frequency integral is evaluated as always by contour integration, yielding

$$\Sigma_{\mathrm{F}}(\mathbf{k},\omega) = \frac{\Delta_0^2}{i\omega - \widetilde{\xi}_{\mathbf{k}}^{\mathrm{CF}}} + \frac{2\pi\varepsilon_0}{m_{\mathrm{r}}} \int \frac{\mathrm{d}\mathbf{P}}{(2\pi)^2} \left(\frac{u_{\mathbf{P}}^2 \Theta(-E_{\mathbf{P}}^+)}{i\omega + \xi_{\mathbf{P}-\mathbf{k}}^{\mathrm{B}} - E_{\mathbf{P}}^+} + \frac{v_{\mathbf{P}}^2 \Theta(-E_{\mathbf{P}}^-)}{i\omega + \xi_{\mathbf{P}-\mathbf{k}}^{\mathrm{B}} - E_{\mathbf{P}}^-} \right). \tag{3.119}$$

In the strong-coupling limit, for $x \leq 1$, the boson chemical potential $\mu_{\rm B} \sim -\varepsilon_0$ is the dominant energy scale. One is then allowed to take $\mathbf{P} = \mathbf{0}$ in the denominators of the integrand and neglect $E^{\pm}_{\mathbf{0}}$, thus obtaining

$$\Sigma_{\rm F}(\mathbf{k},\omega) = \frac{\Delta_0^2}{i\omega - \widetilde{\xi}^{\rm CF}_{\mathbf{k}}} + \frac{\Delta^2_{\rm CF}}{i\omega + \xi^{\rm B}_{\mathbf{k}}}, \tag{3.120}$$

with $\Delta^2_{\rm CF} \equiv 2\pi\varepsilon_0 n_{\rm CF}/m_{\rm r}$.

With the self-energy at hand, one immediately obtains the fermion Green's function

$$G_{\rm F}(\mathbf{k},\omega)^{-1} = i\omega - \xi^{\rm F}_{\mathbf{k}} - \frac{\Delta_0^2}{i\omega - \widetilde{\xi}^{\rm CF}_{\mathbf{k}}} - \frac{\Delta^2_{\rm CF}}{i\omega + \xi^{\rm B}_{\mathbf{k}}}, \tag{3.121}$$

and in turn the fermion momentum distribution, after integrating over ω

$$n_{\rm F}(\mathbf{k}) = \sum_{i=1}^{3} \lim_{z\to z_i} \frac{z - z_i}{z - \xi^{\rm F}_{\mathbf{k}} - \Delta_0^2/\left(z - \widetilde{\xi}^{\rm CF}_{\mathbf{k}}\right) - \Delta^2_{\rm CF}/\left(z - \xi^{\rm B}_{\mathbf{k}}\right)} \Theta(-z_i). \tag{3.122}$$

In the above equation, z_i are the three different real roots of the cubic equation

$$z - \xi^{\rm F}_{\mathbf{k}} - \frac{\Delta_0^2}{i\omega - \widetilde{\xi}^{\rm CF}_{\mathbf{k}}} - \frac{\Delta^2_{\rm CF}}{i\omega + \xi^{\rm B}_{\mathbf{k}}} = 0. \tag{3.123}$$

3.6.3 Hugenholtz-Pines condition

In the strong-coupling limit, the boson self-energy (3.22) acquires the form

$$\Sigma^{11}_{\rm BF}(\mathbf{k},\omega) = \frac{2\pi\varepsilon_0}{m_{\rm r}} \int \frac{{\rm d}\mathbf{P}}{(2\pi)^2} \left(u^2_{\mathbf{P}} \frac{\Theta(-E^+_{\mathbf{P}}) - \Theta(-\xi^{\rm F}_{\mathbf{P}-\mathbf{k}})}{E^+_{\mathbf{P}} - \xi^{\rm F}_{\mathbf{P}-\mathbf{k}} - i\omega} + v^2_{\mathbf{P}} \frac{\Theta(-E^-_{\mathbf{P}}) - \Theta(-\xi^{\rm F}_{\mathbf{P}-\mathbf{k}})}{E^-_{\mathbf{P}} - \xi^{\rm F}_{\mathbf{P}-\mathbf{k}} - i\omega} \right). \tag{3.124}$$

The Hugenholtz-Pines condition requires to evaluate the above expression at vanishing (2+1)-momentum: in absence of the boson-boson repulsion and the anomalous term $\Sigma^{12}_{\rm BF}$, we get

$$\mu_{\rm B} = \Sigma^{11}_{\rm BF}(\mathbf{0},0) = \frac{2\pi\varepsilon_0}{m_{\rm r}} \int \frac{{\rm d}\mathbf{P}}{(2\pi)^2} \left(u^2_{\mathbf{P}} \frac{\Theta(-E^+_{\mathbf{P}})}{E^+_{\mathbf{P}} - \xi^{\rm F}_{\mathbf{P}}} + v^2_{\mathbf{P}} \frac{\Theta(-E^-_{\mathbf{P}})}{E^-_{\mathbf{P}} - \xi^{\rm F}_{\mathbf{P}}} \right).$$

This integral can be evaluated in closed form:

$$\begin{aligned}
\mu_{\rm B} &= \varepsilon_0 \frac{1+\gamma_{\rm m}}{\gamma_{\rm m}} \int_0^{y_-} {\rm d}y \, \frac{v_y^2}{\overline{E}^-_y - \overline{\xi}^{\rm F}_y} \\
&= -\varepsilon_0 \left(\frac{1+\gamma_{\rm m}}{\gamma_{\rm m}} \right)^2 \left(\ln\left(2(1+\gamma_{\rm m})\right) + \ln\left(\overline{\mu}_{\rm F} - \overline{\widetilde{\mu}}_{\rm CF} + \sqrt{4\overline{\Delta}_0^2 + \left(\overline{\widetilde{\mu}}_{\rm CF} - \overline{\mu}_{\rm F}\right)^2} \right) \right. \\
&\left. - \ln\left(2\sqrt{4\overline{\Delta}_0^2(1+\gamma_{\rm m})^2 + \frac{1}{4}\overline{\mathcal{J}}^2} - \overline{\mathcal{J}} \right) \right).
\end{aligned} \tag{3.125}$$

3.6.4 Complete set of equations for semi-analytical calculations

All in all, the system of Eqs. (3.43), (3.44), (3.45) becomes analytically tractable in the strong-coupling limit. Indeed, Eq. (3.43) is given in closed form in (3.125); the fermion momentum distribution is given in closed form in (3.122); finally, Eq. (3.45) can be dealt with by observing that for large g all non-condensed bosons are expected to bind with fermions into molecules (we recall that $n_{\rm B} \leq n_{\rm F}$). One can then trade (3.45) for the density (3.115) of composite fermions, since $n_{\rm B} - n_0 \sim n_{\rm CF}$. As a consequence, one obtains the following set of equations for the unknowns $\mu_{\rm F}, \mu_{\rm B}$ and n_0 (and implicitly $\mu_{\rm CF} \equiv \mu_{\rm F} + \mu_{\rm B} + \varepsilon_0$):

- fermion number equation
$$n_{\rm F} = \int \frac{{\rm d}\mathbf{k}}{(2\pi)^2}\, n_{\rm F}(\mathbf{k}), \tag{3.126}$$
with $n_{\rm F}(\mathbf{k})$ given by (3.122);

- composite-fermion number
$$n_{\rm B} - n_0 = \int \frac{{\rm d}\mathbf{P}}{(2\pi)^2}\, \left(u^2_{\mathbf{P}}\Theta(-E^+_{\mathbf{P}}) + v^2_{\mathbf{P}}\Theta(-E^-_{\mathbf{P}})\right), \tag{3.127}$$
whose analytic form is given in (3.115);

- Hugenholtz-Pines condition
$$\mu_{\rm B} = \Sigma^{11}_{\rm BF}(\mathbf{0},0) = \frac{2\pi\varepsilon_0}{m_{\rm r}} \int \frac{{\rm d}\mathbf{P}}{(2\pi)^2} \left(\frac{u^2_{\mathbf{P}}}{E^+_{\mathbf{P}} - \xi^{\rm F}_{\mathbf{P}}}\Theta(-E^+_{\mathbf{P}}) + \frac{v^2_{\mathbf{P}}}{E^-_{\mathbf{P}} - \xi^{\rm F}_{\mathbf{P}}}\Theta(-E^-_{\mathbf{P}}) \right), \tag{3.128}$$
whose analytic expression is given in (3.125).

This simple system of equations can be solved for $\mu_{\rm F}, \mu_{\rm B}$, and n_0 with a standard root finder, and no particular care has to be taken when performing the momentum integral in Eq. (3.126). These operations are performed using *Wolfram Mathematica* code.

3.7 Overview of the results

In this section, we present a summary of the (semi-)analytical results obtained so far and recap their dependence on the choice of parameters and Feynman diagrams.

In Sec. 3.4 we treated the weak-BF coupling limit, $-g \gg 1$. In this regime, we obtained analytical results for $\mu_{\rm F}$ and $\mu_{\rm B}$, valid up to second order in $1/g$. These expressions cover the cases of density-imbalanced mixtures ($x \neq 1$) and mass-imbalanced mixtures ($\gamma_{\rm m} \neq 1$). We discussed how to account for the anomalous contribution $\Sigma^{12}_{\rm BF}(\mathbf{0},0)$ to the boson chemical potential, and in Sec. 3.5 we presented how the perturbative series should be modified if the fermion chemical potential $\mu_{\rm F}$ is replaced by the shifted $\mu_{\rm F} - \Sigma^0_{\rm F}$ inside the self-energies.
What we did not take into account is the effect on $\mu_{\rm B}$ of a finite BB repulsion, $\eta \neq 0$. If η is sufficiently small, namely $4\pi n_{\rm B}\eta/m_{\rm B} < -E_{\rm F}(\gamma_{\rm m}+1)/(g\,\gamma_{\rm m})$, the boson chemical potential is small and

negative even in the presence of the repulsion. As a consequence, the derivation of the perturbative expansions in Sec. 3.4 remains applicable, with the only difference being the mean-field Bogolyubov term $\Sigma^{11}_{\mathrm{BB}} - \Sigma^{12}_{\mathrm{BB}} = 4\pi n_{\mathrm{B}}\eta/m_{\mathrm{B}}$ that needs to be added to μ_{B} in Eq. (3.97). However, if the repulsion is strong enough to render μ_{B} positive, our calculations in Sec. 3.4 are no longer valid.

In Sec. 3.6 we treated the strong-BF coupling limit, $g \gg 1$. In this regime, we obtained the system of Eqs. (3.126), (3.122), (3.115) that can be solved to yield μ_{B}, μ_{F} and n_0. These expressions cover the cases of density-imbalanced mixtures ($x \neq 1$) and mass-imbalanced mixtures ($\gamma_{\mathrm{m}} \neq 1$). In Sec. C.2 we describe how to modify these equations if the fermion chemical potential μ_{F} is replaced by the shifted $\mu_{\mathrm{F}} - \Sigma^0_{\mathrm{F}}$ inside the self-energies. In the strong coupling regime, the effect on $\mu_{\mathrm{B}}, \mu_{\mathrm{F}}$ and n_0 of a finite BB repulsion is expected to be negligible, and therefore the expressions we have derived are applicable also when $\eta \neq 0$.
What we did not take into account is the effect of the anomalous contribution $\Sigma^{12}_{\mathrm{BF}}$, which remains as our future problem.

	Density-imb.	Mass-imb.	BB repulsion	Anomalous $\Sigma^{12}_{\mathrm{BF}}$	MF shift of μ_{F}
Weak-coupling	✓	✓	✗	✓	✓
Strong-coupling	✓	✓	irrelevant	✗	✓

Table 3.1: Summary of the different effects considered in this thesis, for the analytical calculations in the weak-BF coupling limit and the semi-analytical calculations in strong-BF coupling limit.

In Tab. 3.1, we summarize the different contributions included in our semi-analytical derivations. In principle, the fully numerical calculation based on Eqs. (3.43), (3.44), and (3.45) could be implemented to include all of the above effects on the thermodynamics of the system.

In [56], the authors report numerical results for a density-imbalanced but mass-balanced mixture, with and without BB repulsion. The anomalous contribution $\Sigma^{12}_{\mathrm{BF}}$ is not included, nor are the modifications due to a mean-field shift of μ_{F}.
In Chap. 4, we report numerical results for a density- and mass-imbalanced mixture. The effects of BB repulsion and of the anomalous contribution $\Sigma^{12}_{\mathrm{BF}}$ are not included, nor are the modifications due to a mean-field shift of μ_{F}.
In Sec. C.1, we present preliminary results for a density- and mass-balanced mixture, including the mean-field shift of μ_{F} in the self-energies. The effects of BB repulsion and of the anomalous contribution $\Sigma^{12}_{\mathrm{BF}}$ are not included.
The determination of the contribution of $\Sigma^{12}_{\mathrm{BF}}$ in the numerical evaluation of μ_{B}, μ_{F}, and n_0 remains as a problem for future work.

Chapter 4

Numerical results for mass-imbalanced mixtures

In this chapter, we present the numerical results obtained by solving Eqs. (3.43)*,* (3.44)*, and* (3.45) *for the unknowns* μ_{B}*,* μ_{F}*, and* n_0*. The calculations are performed within the non-self-consistent* T*-matrix approach, without the anomalous self-energy* $\Sigma^{12}_{\mathrm{BF}}$*, and at zero boson-boson repulsion* $\eta = 0$*. Effects of mass-imbalance are identified, both in the density-balanced and in the density-imbalanced cases. A comparison between the numerical results and the (semi-)analytical expressions in the weak- and strong-BF coupling regimes is also carried out.*

4.1 Results for $n_{\mathrm{B}} = n_{\mathrm{F}}$

In this section, we study the thermodynamics of a density-balanced but mass-imbalanced mixture: therefore, we consider the boson concentration to be $x = 1$ and different values for the mass ratio γ_{m}, close to those in Tab. 1.1. We do not include the anomalous self-energy $\Sigma^{12}_{\mathrm{BF}}$ in the calculations, nor do we treat the interaction between bosons (therefore $\eta = 0$ in the following) or the mean-field shift of the chemical potential $\mu_{\mathrm{F}} \mapsto \mu_{\mathrm{F}} - \Sigma^0_{\mathrm{F}}$. The treatment of the system is therefore the same as in the recent work [56]. Note that the analogous theory in $3d$ space, studied e.g. in [109, 110], was recently tested experimentally on a ^{23}Na–^{40}K mixture [41].

4.1.1 Boson and fermion momentum distributions

Fig. 4.1 shows the boson momentum distribution, for unitary concentration of bosons $x = 1$, for different values of the mass ratio γ_{m} and the BF coupling g. A feature that was already identified in [56] in the case of $\gamma_{\mathrm{m}} = 1$ is the presence of a peak for small but non-zero momentum, depending on the coupling g. In Fig. 4.1 the case of $\gamma_{\mathrm{m}} = 1$ is reported in panel (b), and the mentioned peak is visible in the curve for $g = -4$.

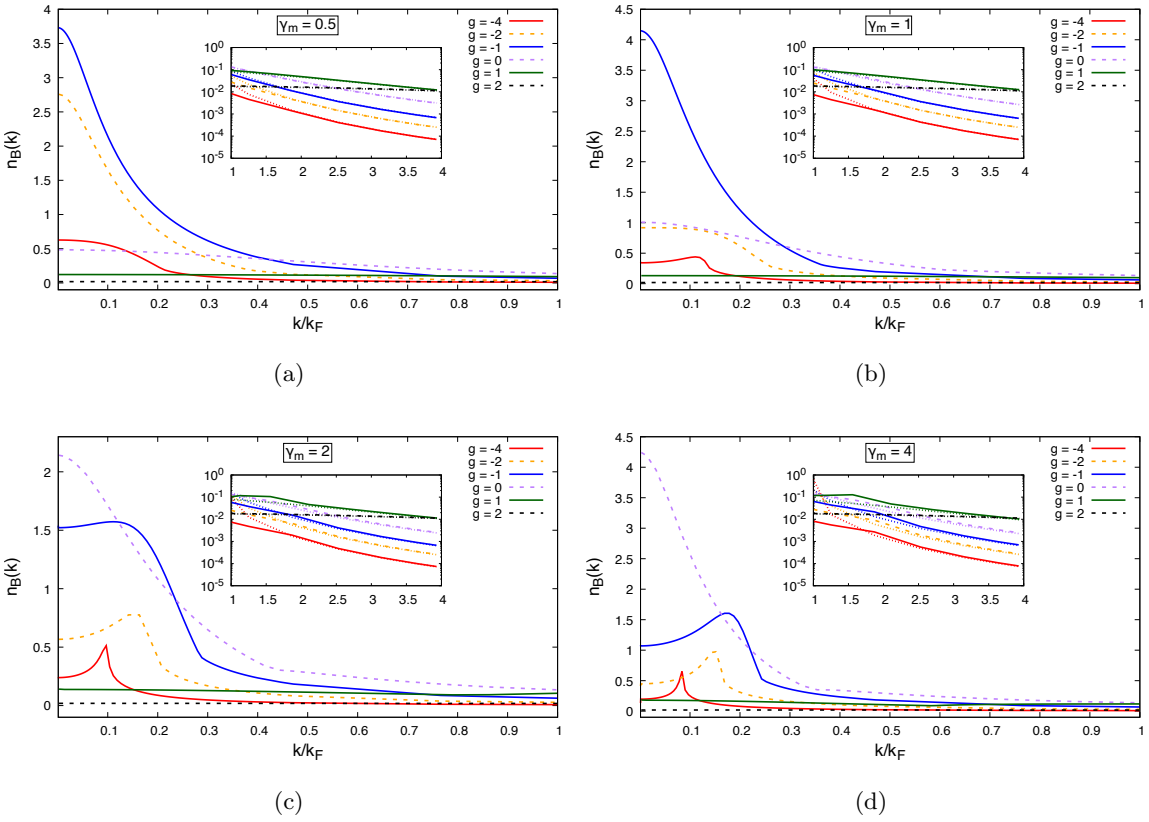

Figure 4.1: Boson momentum distribution $n_{\mathrm{B}}(\mathbf{k})$ as a function of k/k_{F}, for different values of the BF coupling g, and boson concentration $x = 1$. Different values of the mass ratio γ_{m} are reported: (a) $\gamma_{\mathrm{m}} = 0.5$ (b) $\gamma_{\mathrm{m}} = 1$ (c) $\gamma_{\mathrm{m}} = 2$ (d) $\gamma_{\mathrm{m}} = 4$. Inset: comparison between numerical results and large momentum behavior described by equation (A.16) (dotted lines).

Panel (a) shows that this feature is lost in the case of $\gamma_{\mathrm{m}} = 0.5$. On the other hand, panels (c) and (d) reveal that the peak is preserved in the case where $\gamma_{\mathrm{m}} > 1$, where it appears also for larger couplings $g > -4$.

In Fig. 4.2 is reported the momentum distribution $n_{\mathrm{B}}(\mathbf{k})$ at $g = -4$ for $\gamma_{\mathrm{m}} = 0.5$, $\gamma_{\mathrm{m}} = 1$, $\gamma_{\mathrm{m}} = 2$, $\gamma_{\mathrm{m}} = 4$, $\gamma_{\mathrm{m}} = 7$, $\gamma_{\mathrm{m}} = 14$, $\gamma_{\mathrm{m}} = 22$, to better illustrate how the position, width and height of the peak vary as functions of the boson mass.

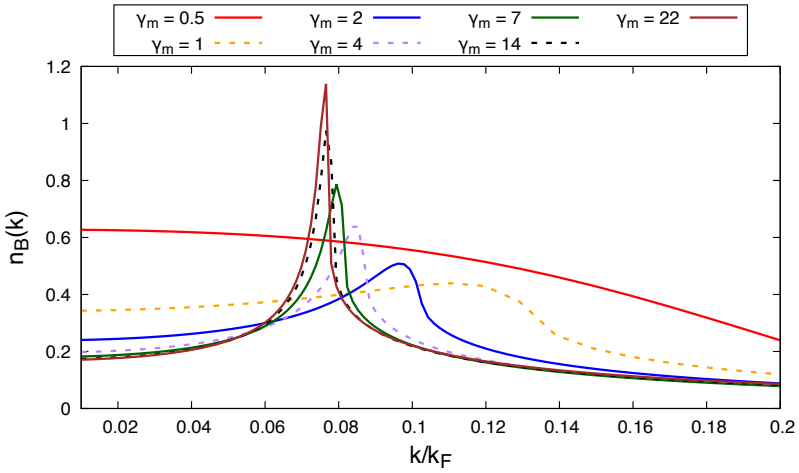

Figure 4.2: Zoom on the peak of $n_{\rm B}(\mathbf{k})$ at $g = -4$, $x = 1$, for several different mass ratios.

The Fermi momentum distributions are reported in Fig. 4.3, at unitary concentration of bosons $x = 1$, for different values of the mass ratio $\gamma_{\rm m}$ and the coupling g. We note that, from weak to strong coupling, the position of the Fermi step varies the most in the case $\gamma_{\rm m} = 0.5$, while it does not change significantly for larger mass ratios.

4.1.2 Chemical potentials and condensate density

Fig. 4.4 presents the plots the boson chemical potential $\mu_{\rm B}$, the fermion chemical potential $\mu_{\rm F}$ and the condensate fraction $n_0/n_{\rm B}$ in the range $-4 \leq g \leq 4$ for $x = 1$.

Fig. 4.4(a) reports the quantity $\mu_{\rm B} + \varepsilon_0$, to remove from the boson chemical potential the leading strong coupling contribution, given by $-\varepsilon_0 = -E_{\rm F}\, {\rm e}^{2g}(\gamma_{\rm m} + 1)/\gamma_{\rm m}$. The inset on the other hand avoids the subtraction and illustrate on a logarithmic scale that, in the strong coupling limit, the boson chemical (with a minus sign) approaches the binding energy. In particular, the "relative difference" $|\mu_{\rm B} + \varepsilon_0|/\varepsilon_0$ goes below 5% at $g \simeq 1$ for the mass ratios $\gamma_{\rm m} = 1$, $\gamma_{\rm m} = 2$, $\gamma_{\rm m} = 4$ and at a slightly bigger coupling $g \simeq 1.2$ for $\gamma_{\rm m} = 0.5$ (see Fig. 4.5).

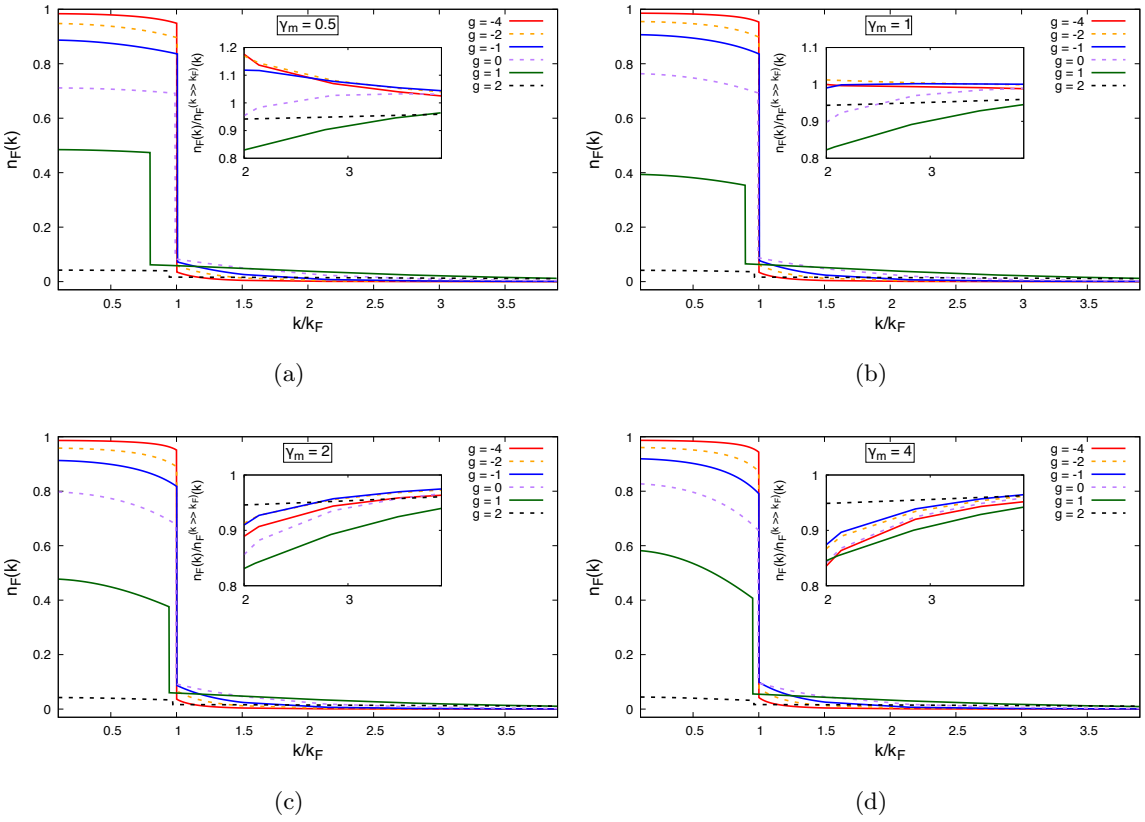

Figure 4.3: Fermion momentum distribution $n_{\mathrm{F}}(\mathbf{k})$ as a function of k/k_{F}, for different values of the BF coupling g and for the boson concentration $x = 1$. Different values of the mass ratio γ_{m} are reported: (a) $\gamma_{\mathrm{m}} = 0.5$ (b) $\gamma_{\mathrm{m}} = 1$ (c) $\gamma_{\mathrm{m}} = 2$ (d) $\gamma_{\mathrm{m}} = 4$. Insets: ratio of $n_{\mathrm{F}}(\mathbf{k})$ to its large momentum behavior given by (A.15). In the large momentum limit, the ratio is expected to approach one.

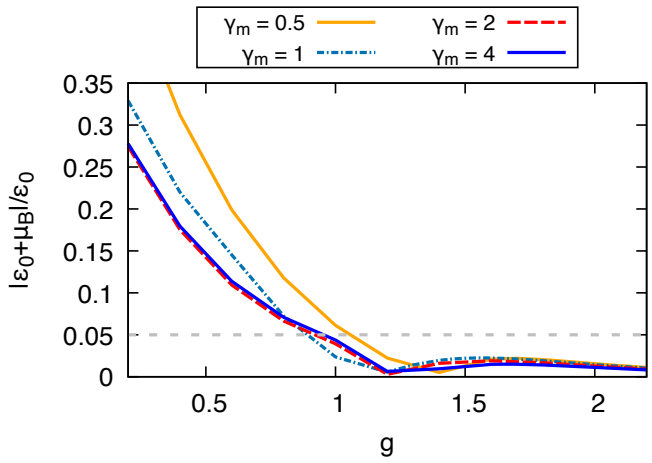

Figure 4.5: Relative difference $|\mu_{\mathrm{B}} + \varepsilon_0|/\varepsilon_0$ compared to 0.05 (dashed gray line), as a function of g and for the boson concentration $x = 1$.

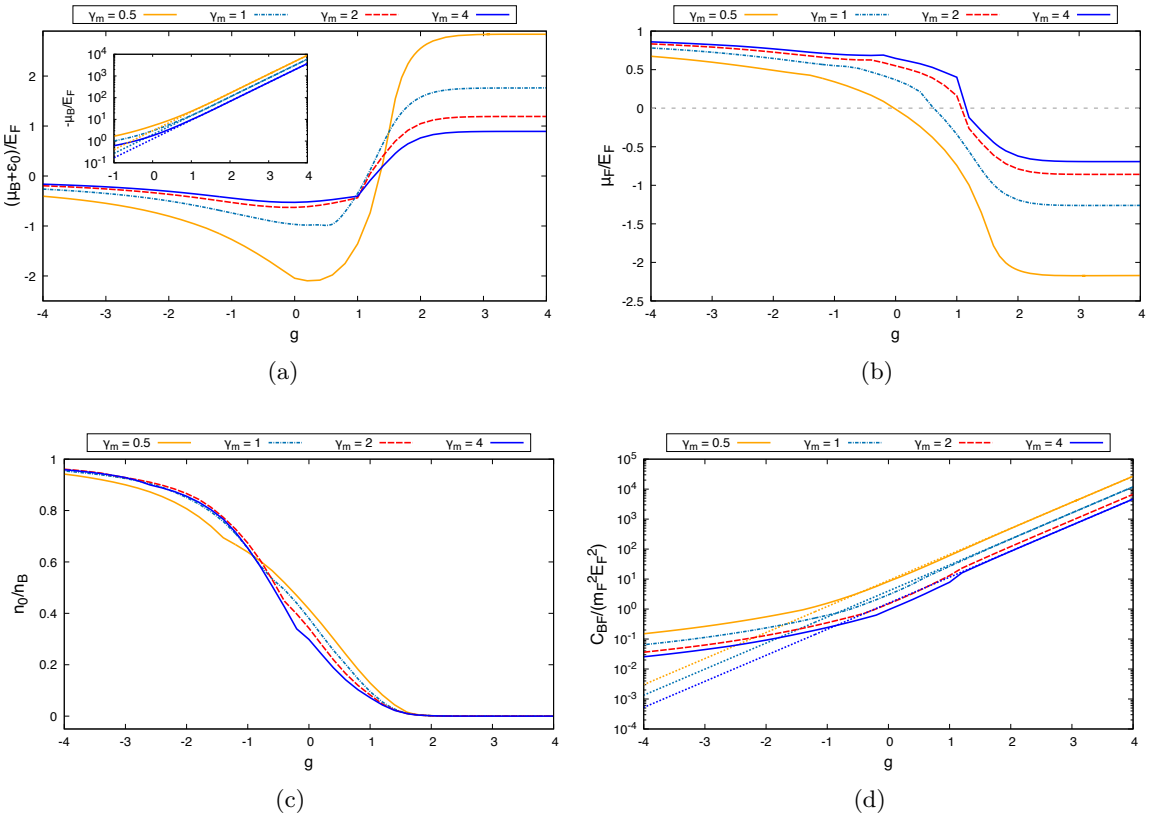

Figure 4.4: (a): boson chemical potential μ_B (shifted by the binding energy ε_0), in units of E_F, as a function of the BF coupling g, for different values of the mass ratio γ_m, for the boson concentration $x = 1$. Inset: comparison between $-\mu_B$ and the binding energy ε_0 (dotted lines, reported for clarity only for $\gamma_m = 0.5$, $\gamma_m = 1$ and $\gamma_m = 4$). (b): corresponding fermion chemical potential μ_F in units of E_F. (c): corresponding boson condensate fraction. (d): dimensionless Tan's contact parameter $C_{BF}/(m_F^2 E_F^2)$. Dotted lines: quantity $(x\,\varepsilon_0\,(\gamma_m + 1)/\gamma_m)\,/E_F$, reported for clarity only for $\gamma_m = 0.5$, $\gamma_m = 1$, $\gamma_m = 4$.

Fig. 4.4(b) reports the fermion chemical potential as a function of the BF coupling. The figure illustrates that $\mu_{\rm F}$ crosses zero (dashed gray line) for all considered mass ratios, with the value of g at which the sign change occurs becoming larger with $\gamma_{\rm m}$.

4.1.3 Tan's contact parameter

For large momenta, the fermion and boson distributions have asymptotic behaviors given by Eqs. (A.15) and (A.15).
We define the *Tan's contact parameter* $C_{\rm BF}$ as the coefficient of the leading order term of expressions (A.16) and (A.15) (proportional to k^{-4}):

$$\int \frac{\mathrm{d}^2 P}{(2\pi)^2} \int \frac{\mathrm{d}\Omega}{2\pi}\, T(\mathbf{P},\Omega)\mathrm{e}^{i\Omega 0^+} \equiv \frac{C_{\rm BF}}{4m_{\rm r}^2}, \tag{4.1}$$

Tan's contact parameter is reported in Fig. 4.4(d), from weak to strong coupling for the usual values of the mass ratio $\gamma_{\rm m}$.

As shown in [56], for $\gamma_{\rm m} = 1$ the dimensionless Tan's contact parameter $C_{\rm BF}/(m_{\rm F}^2 E_{\rm F}^2)$ scales as $2x\,\varepsilon_0/E_{\rm F}$ in the strong coupling limit. The same exponential behavior is found in the mass-imbalanced case, upon the replacement

$$2\frac{\varepsilon_0}{E_{\rm F}} \to \frac{\gamma_{\rm m}+1}{\gamma_{\rm m}}\frac{\varepsilon_0}{E_{\rm F}} = \left(\frac{\gamma_{\rm m}+1}{\gamma_{\rm m}}\right)^2 \mathrm{e}^{2g} \tag{4.2}$$

(dotted lines in Fig. 4.4(d)).

4.2 Numerical results for $n_{\rm B} < n_{\rm F}$

In this section we study the thermodynamics of a density- and mass-imbalanced mixture: therefore, we consider the boson concentration to be $x < 1$, specifically $x = 0.5$, $x = 0.175$ and $x = 0.1$, and different values for the mass ratio $\gamma_{\rm m}$, close to those in Tab. 1.1. We do not include the anomalous self-energy $\Sigma^{12}_{\rm BF}$ in the calculations, nor do we treat the interaction between bosons (therefore $\eta = 0$ in the following) or the mean-field shift of the chemical potential $\mu_{\rm F} \mapsto \mu_{\rm F} - \Sigma^0_{\rm F}$.

4.2.1 Boson momentum distributions

Figures D.1 and D.2 in Appendix D.1 report the boson momentum distributions for $x = 0.5$ and $x = 0.1$, for several different values of the mass ratio and the BF coupling. Here we present only the case of $x = 0.1$, $\gamma_{\rm m} = 0.5$, in Fig. 4.6, to illustrate that the peak at small momentum missing for $g = -4$, $x = 1$ instead appears at lower boson concentrations.

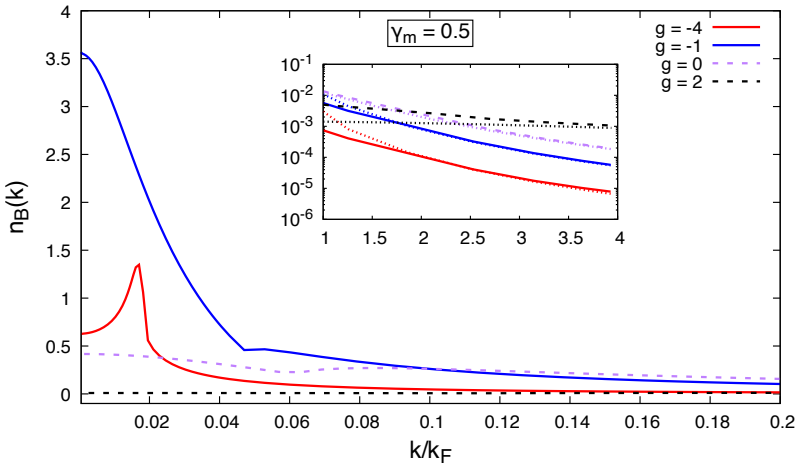

Figure 4.6: Boson momentum distribution $n_B(\mathbf{k})$ as a function of k/k_F, for different values of the BF coupling g, boson concentration $x = 0.1$, and mass ration $\gamma_m = 0.5$. Inset: comparison between numerical results and large momentum behavior described by equation (A.16) (dotted lines).

4.2.2 Chemical potentials

Concerning the the boson chemical potential (Figures D.3(a), D.4(a) and D.5(a) in Appendix D.2), we note that $-\mu_B$ approaches the leading contribution ε_0 in the strong coupling regime as expected. In Appendix D.2, Fig. D.6 we report the plot of the relative difference $|\mu_B + \varepsilon_0|/\varepsilon_0$ for $x = 0.5$, $x = 0.175$, $x = 0.1$, while here we present only the case of $x = 0.1$, in Fig. 4.7.

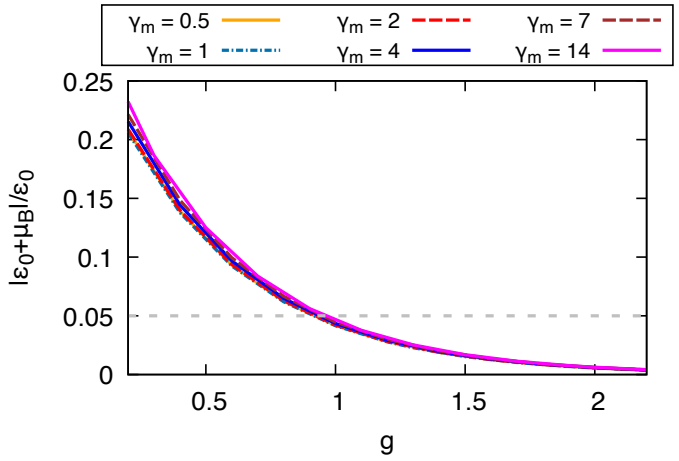

Figure 4.7: Relative difference $|\mu_B + \varepsilon_0|/\varepsilon_0$ compared to 0.05 (dashed gray line), as a function of g and for the boson concentration $x = 0.1$.

These plots show that for all values of the boson concentration $x < 1$ and the mass ratio γ_m, the difference is below 5% for $g \gtrsim 1$.

Figures D.3(b), D.4(b) and D.5(b) in Appendix 4.5 reports the results for the fermion chemical potential. As for the mass-balanced case, μ_{F} is progressively less affected by the increase of g as the boson concentration x decreases. This behavior is better illustrated in Fig. 4.8.

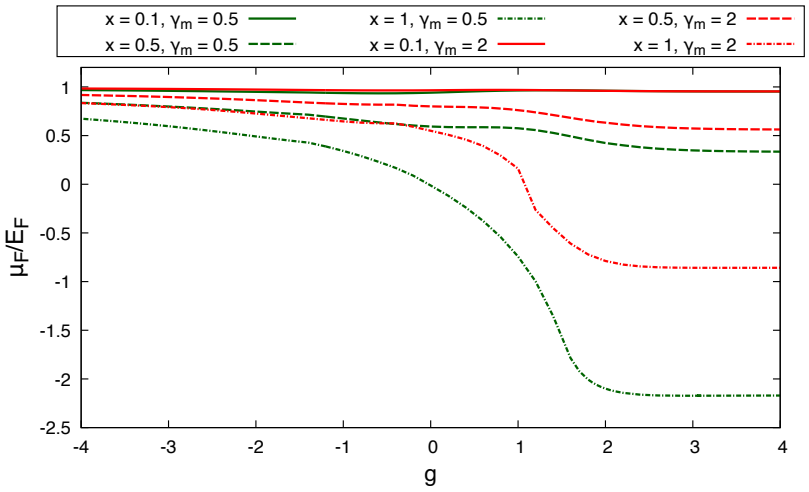

Figure 4.8: Fermion chemical potential μ_{F} in units of E_{F}, as a function of the BF coupling g, for several different choices of the combination of the boson concentration x and the mass ratio γ_{m}.

4.2.3 Universality of the boson condensate density

Fig. 4.10 reports the value of the condensate fraction as a function of the BF coupling, for different boson concentrations and mass ratios. In [56], the authors discussed the approximately universal behavior of n_0 with respect to concentration, in the case $\gamma_{\mathrm{m}} = 1$ (which we have reproduced in Fig. 4.9). From Fig. 4.10, we find that this universality holds with even greater accuracy for $\gamma_{\mathrm{m}} > 1$, whereas for $\gamma_{\mathrm{m}} = 0.5$ the curves corresponding to different concentrations separate visibly in the region $-1 \lesssim g \lesssim 2$.

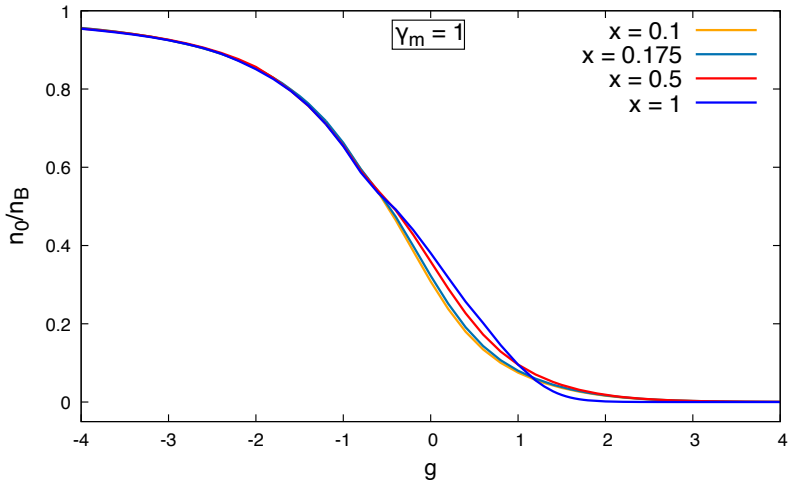

Figure 4.9: Boson condensate fraction n_0/n_B as a function of the BF coupling parameter g for different values of the boson concentration x and $\gamma_\mathrm{m} = 1$.

4.3 Weak-coupling limit

4.3.1 Fermion chemical potential

As discussed in Sec. 3.4, we can expand μ_F and μ_B in powers of $1/g$ in the weak-coupling limit $-g \gg 0$.

For clarity, we report here the result for the fermion chemical potential

$$\mu_\mathrm{F} = E_\mathrm{F} + E_\mathrm{F}\,\frac{x}{2}\,\frac{\gamma_\mathrm{m}+1}{\gamma_\mathrm{m}\,g}\left(1+\frac{1}{2g}\left(\ln\left(\frac{\gamma_\mathrm{m}}{(1+\gamma_\mathrm{m})^2}\right)+\frac{\gamma_\mathrm{m}+1}{\gamma_\mathrm{m}-1}\ln\gamma_\mathrm{m}\right)\right), \tag{4.3}$$

valid up to higher orders in $1/g$. In [56] formula (4.3) was shown to hold in the mass-balanced case $\gamma_\mathrm{m} = 1$, while in this work we verify it in the mass-imbalanced case as well.

Fig. 4.11(a) shows that, in the weak coupling regime $g \lesssim -2$, the numerical curve for the fermion chemical potential approach the asymptotic limit given by (4.3). The figure reports the case of $x = 1$, while the plots for $x < 1$ are presented in Appendix D.3. To make the comparison more stringent, we subtract from the fermion chemical potential the zeroth and first perturbative orders in $1/g$, i.e. $E_\mathrm{F} + E_\mathrm{F}x(\gamma_\mathrm{m}+1)/(2\gamma_\mathrm{m}g)$, multiply the result of the subtraction by g^2, and perform a curve fit to the model $f(g) = A + B/g$. These steps are carried out in the very weak BF coupling regime, namely $g \leq -15$. Fig. 4.11(b) shows the optimal curve, for $x = 1$ and several different mass ratios. The results of the fit procedure are listed in Tab. 4.1, and reveal an excellent agreement between numerical data and the asymptote expected from the perturbative expansion (4.3).

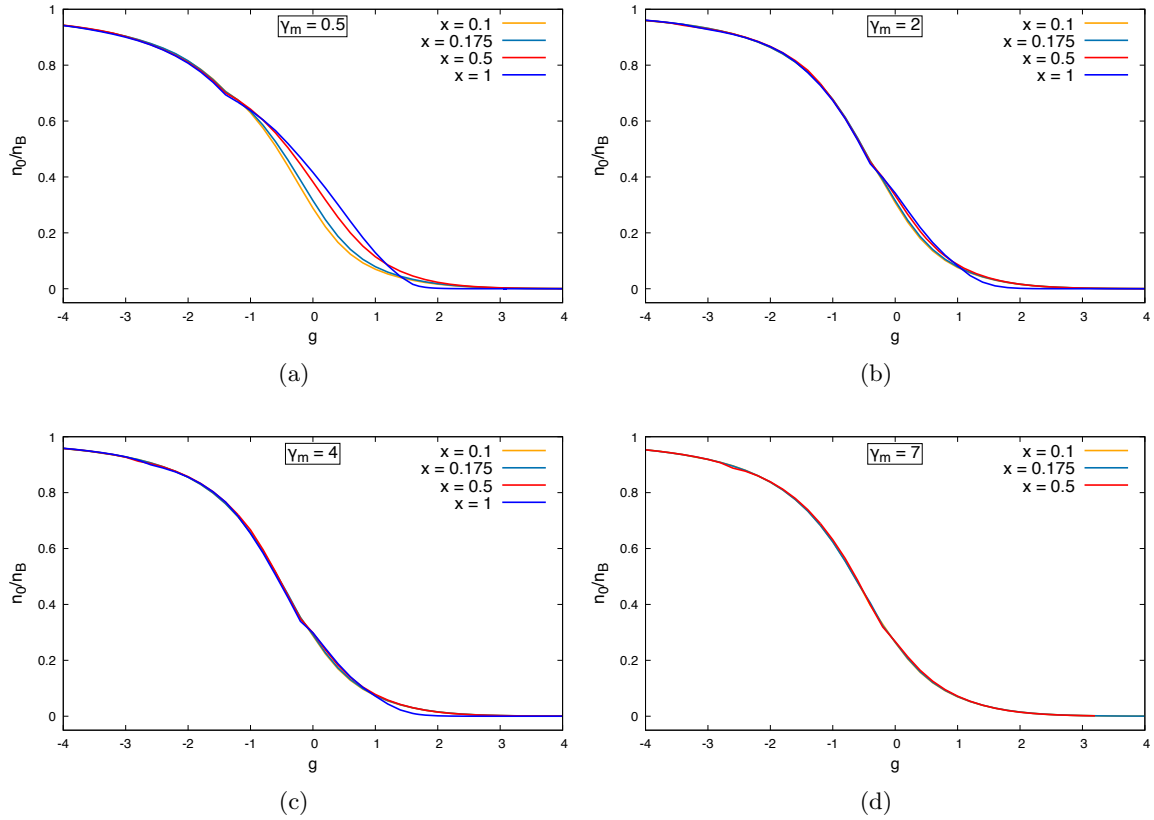

Figure 4.10: Boson condensate fraction n_0/n_B as a function of the BF coupling parameter g for different values of the boson concentration x and mass ratio γ_m: (a) $\gamma_\mathrm{m} = 0.5$, (b) $\gamma_\mathrm{m} = 2$, (c) $\gamma_\mathrm{m} = 4$, (d) $\gamma_\mathrm{m} = 7$.

4.3.2 Boson chemical potential

The perturbative result for the boson chemical potential reads (for $\eta = 0$ and without the anomalous term $\Sigma^{12}_{\mathrm{BF}}$)

$$\mu_\mathrm{B} = E_\mathrm{F}\,\frac{1}{2}\,\frac{\gamma_\mathrm{m}+1}{\gamma_\mathrm{m}\,g}\left(1+\frac{1}{2g}\left(\frac{\gamma_\mathrm{m}\ln\!\left(\gamma_\mathrm{m}^2\right)}{\gamma_\mathrm{m}-1}-\ln\!\left((\gamma_\mathrm{m}+1)^2\right)-1\right)\right), \tag{4.4}$$

valid up to higher orders in $1/g$.

Formula (4.4) in the weak-coupling limit is verified to hold in the mass-imbalanced case, by the same tests we have carried out for the fermion chemical potential. Fig. 4.12 shows that the numerical curve for the boson chemical potential approaches the asymptotic limit given by (4.4) (both shifted by ε_0). The figure reports the case of $x = 1$, while the plots for $x < 1$ are presented in Appendix D.3.

$\gamma_{\rm m}$	$\mu_{\rm F}^{(2)} g^2/E_{\rm F}$	A	B
0.5	0.432	0.431	−1.497
1	0.307	0.311	−0.765
2	0.216	0.218	−0.542
22	0.054	0.054	−0.589

Table 4.1: Results of the fit with points $(\mu_{\rm F} - E_{\rm F} - \mu_{\rm F}^{(1)})g^2/E_{\rm F}$ and model $f(g) = A + B/g$, for $x = 1$. $\mu_{\rm F}^{(1)}$ is computed in perturbation theory as the $\mathrm{O}(1/g)$ term in the expansion $\mu_{\rm F} = E_{\rm F} + \mu_{\rm F}^{(1)} + \mu_{\rm F}^{(2)}$ (4.3). The second column of the table is useful for comparing A with the coupling independent, perturbative result $\mu_{\rm F}^{(2)} g^2$.

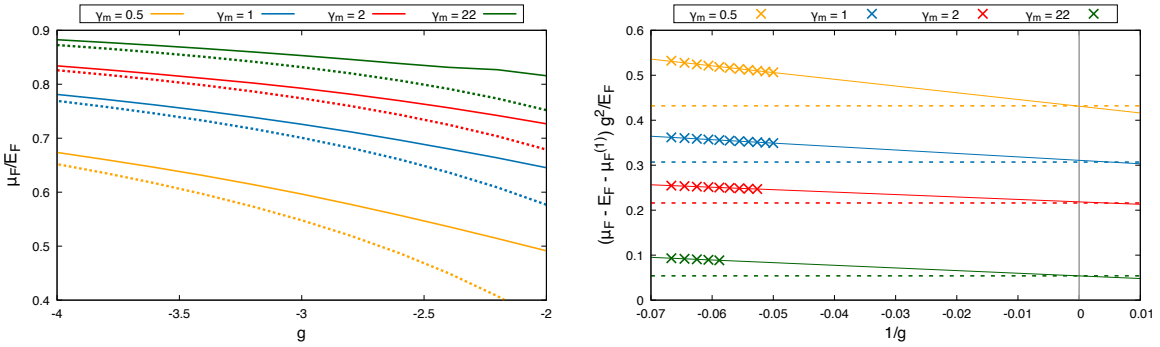

(a) (b)

Figure 4.11: Plots in the weak coupling regime for $x = 1$ and several different values of $\gamma_{\rm m}$. (a): fermion chemical potential $\mu_{\rm F}$, in units of $E_{\rm F}$, as a function of the BF coupling g. The dotted lines represent the weak-coupling result (4.3). (b): the crosses represent the quantity $(\mu_{\rm F} - E_{\rm F} - \mu_{\rm F}^{(1)})g^2/E_{\rm F}$, as a function of $1/g$; the full lines represent the fit to the model $f(g) = A + B/g$; the dashed lines represent the expected asymptotic value $\mu_{\rm F}^{(2)} g^2$ of the fitting curve in the limit $1/g \to 0^-$.

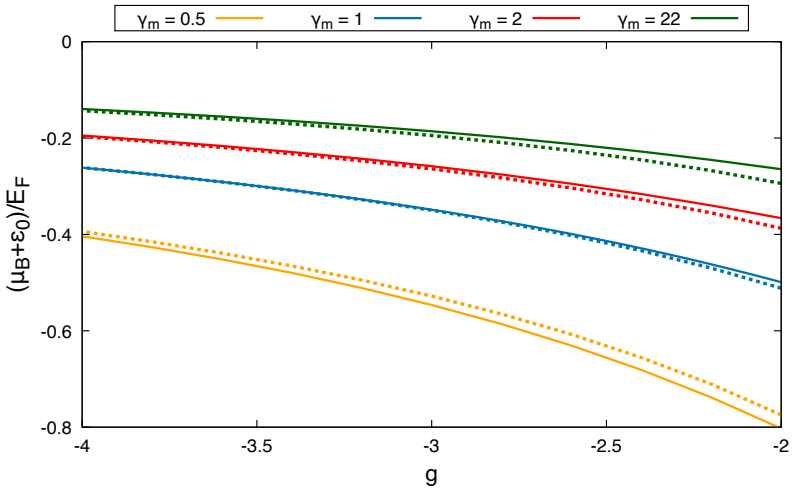

Figure 4.12: Boson chemical potential $\mu_{\rm B}$, in units of $E_{\rm F}$, as a function of the BF coupling g, for $x = 1$ and different values of the mass ratio. The dotted lines represent the weak-coupling result (4.4).

Note that the convergence of the curve of numerical data to the curve corresponding to the analytic expression (4.4) occurs in a universal way, i.e. independently of the boson concentration x.

4.4 Strong-coupling limit

Let us now turn to the strong-BF coupling limit, and discuss the numerical solutions of the system of Eqs. (3.126), (3.127) and (3.128).

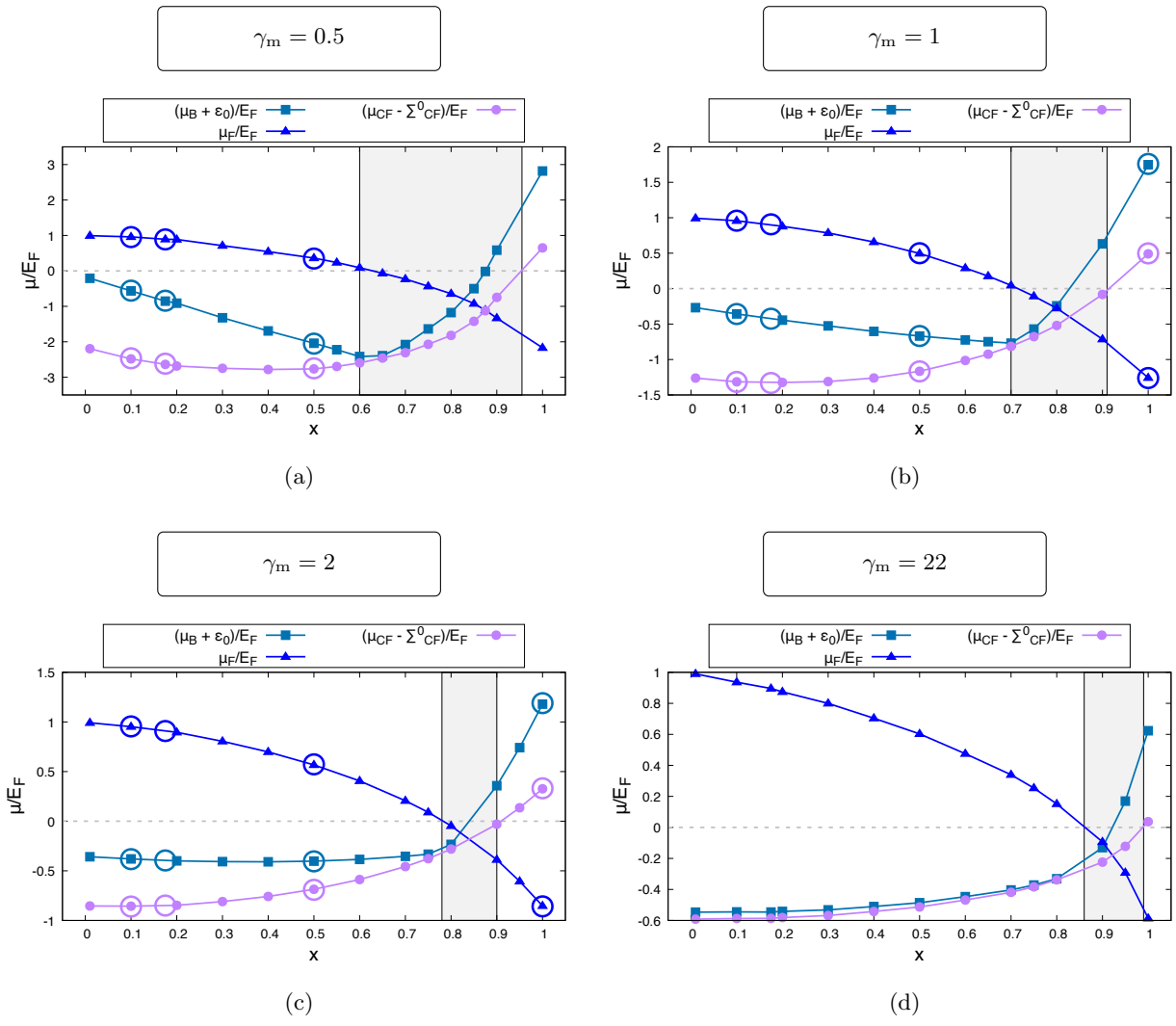

Figure 4.13: Chemical potentials $\mu_{\rm F}$, $\mu_{\rm B}+\varepsilon_0$ and $\widetilde{\mu}_{\rm CF}=\mu_{\rm CF}-\Sigma^0_{\rm CF}$ (in units of $E_{\rm F}$) as functions of the boson concentration x, for strong BF attraction $g=3$ and different mass ratios: (a) $\gamma_{\rm m}=0.5$, (b) $\gamma_{\rm m}=1$, (c) $\gamma_{\rm m}=2$, (d) $\gamma_{\rm m}=22$. The circles represent the chemical potentials computed using the fully numerical implementation in Fortran 90, and reveal a good agreement between $\mu_{\rm B}$, $\mu_{\rm F}$ evaluated with the strong-coupling expressions in Mathematica and $\mu_{\rm B}$, $\mu_{\rm F}$ evaluated with the Fortran 90 code.

In Fig. 4.13 we report the chemical potentials $\mu_{\rm B}$ (once subtracted the leading term $-\varepsilon_0$), $\mu_{\rm F}$ and $\widetilde{\mu}_{\rm CF} = \mu_{\rm CF} - \Sigma^0_{\rm CF}$ as functions of the boson concentration x, for different values of the mass ratio $\gamma_{\rm m}$.

The boson chemical potential $\mu_{\rm B}$ follows the dominant energy scale $-\varepsilon_0$, meaning that as soon as boson is expelled out of the condensate it binds with a fermion (in agreement with $n_{\rm CF} = n_{\rm B} - n_0$). Therefore, the out-of-condensate component of the system can be regarded as a mixture of atomic and composite fermions, with the effect of the repulsion of the former on the latter encoded in $\Sigma^0_{\rm CF}$ and the hybridization between the two encoded in Δ_0^2.

The fermion chemical potential $\mu_{\rm F}$ approaches the non-interacting value $\mu_{\rm F} = E_{\rm F}$ as $x \to 0$, reflecting the fact that in this regime the effects of interactions on atomic fermions are mild.
As $x \to 1$, on the other hand, $\mu_{\rm F}$ becomes negative, reflecting the disappearance of the Fermi sphere of unpaired atomic fermions. Note also that $\Sigma^0_{\rm CF} = 0$, indicating that the effective repulsive field of atomic fermions on the composite fermions is not present.

The shifted composite fermion chemical potential $\widetilde{\mu}_{\rm CF}$ varies as function of the boson concentration x in the opposite way as $\mu_{\rm F}$. When $x \to 0$, $\widetilde{\mu}_{\rm CF}$ is negative and the presence of a non-vanishing component of composite fermions is due to their momentum distribution $n_{\rm CF}(\mathbf{P})$ being different from the Fermi sphere $\Theta(-\widetilde{\xi}^{\rm CF}_{\mathbf{P}})$ (see Fig. 4.14). This indicates that the composite fermions are strongly affected by interactions.
As $x \to 1$, $\widetilde{\mu}_{\rm CF}$ approaches the value $E_{\rm F}/(1+\gamma_{\rm m})$, which is expected for a non-interacting gas of fermions with mass $m_{\rm F} + m_{\rm B}$.

The shaded areas in Fig. 4.13 indicate the crossover regions in which the two chemical potentials $\widetilde{\mu}_{\rm CF}$ and $\mu_{\rm F}$ cross and change their sign. For concentrations below the lower bound of one such region, the system is in a regime dominated by Fermi atoms interacting weakly and Fermi molecules experiencing strong interaction effects, whereas for concentrations above the upper bound, it is dominated by weakly interacting Fermi molecules.
Note that the crossover region shifts towards higher concentrations for larger mass ratios. One might think this is due to a decrease in the number of composite fermions associated with the increase in the mass ratio at fixed boson concentration. However, the dependence of n_0 on $\gamma_{\rm m}$ is mild (see Fig. D.7 and the insets of Fig. 4.15), and consequently the same is true for $n_{\rm CF}$, assuming that $n_{\rm CF} = n_{\rm B} - n_0$ holds independently of $\gamma_{\rm m}$. Furthermore, the condensate density n_0 slightly decreases as the mass ratio $\gamma_{\rm m}$ increases, which leads to an increase (rather than the expected decrease) in the composite-fermion density $n_{\rm CF}$.
Therefore the shift of the crossover region indicates that, if we increase the boson mass, it is necessary to simultaneously increase the boson concentration x (thus forming more composite fermions) to attenuate the influence of the atomic fermion component on the molecules. This fact is illustrated in Fig. 4.14, reporting the composite-fermion momentum distribution $n_{\rm CF}(\mathbf{P})$ for different values of the boson concentration and the mass ratio. Note that $n_{\rm CF}(\mathbf{P})$ approaches the non-interacting result $\Theta(-\widetilde{\xi}^{\rm CF}_{\mathbf{P}})$ as $x \to 1$, but in the large-$\gamma_{\rm m}$ case the upward bending at momenta lower than the step momentum persists even at concentrations close to $x = 1$ (see, e.g., $x = 0.9$ and $x = 0.95$). This peculiar behavior is due to interaction effects that remain relevant at large boson concentrations.

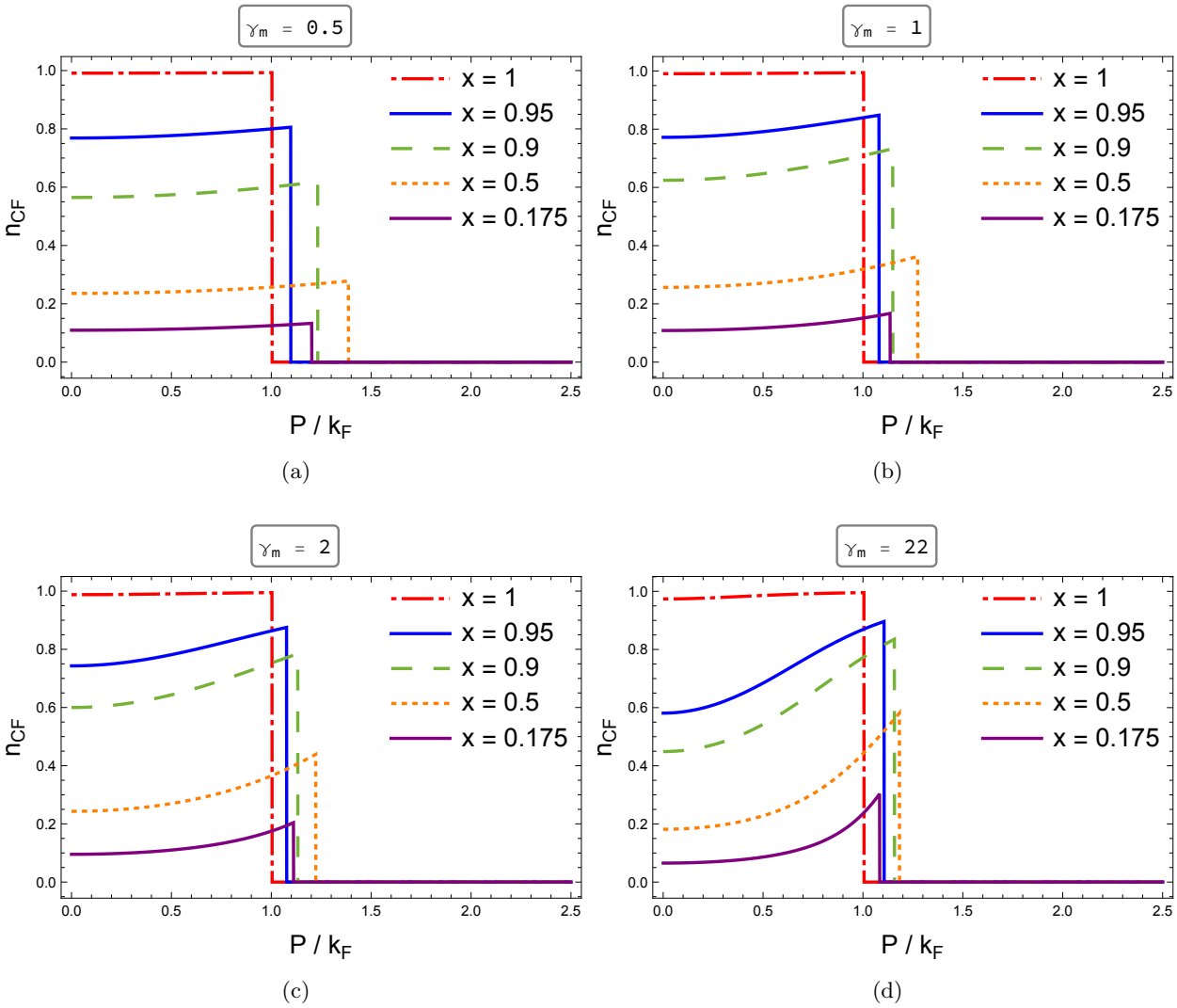

Figure 4.14: Composite-fermion momentum distribution $n_{\rm CF}(\mathbf{P}) = v^2_{\mathbf{P}}\Theta(-E^-_{\mathbf{P}})$ as a function of $P/k_{\rm F}$, for strong BF attraction $g = 3$ and different boson concentrations and mass ratios: (a) $\gamma_{\rm m} = 0.5$, (b) $\gamma_{\rm m} = 1$, (c) $\gamma_{\rm m} = 2$, (d) $\gamma_{\rm m} = 22$.

Let us now analyze in detail the effect of the hybridization between atoms and molecules.

The square of the hybridization energy Δ_0^2 is reported in Fig. 4.15, together with the condensate density n_0 (in the insets' upper panels) and the condensate fraction $n_0/n_{\rm B}$ (in the insets' lower panels). n_0 is exponentially suppressed for strong coupling; however, this exponentially small value is compensated by the exponentially large binding energy in the expression of Δ_0^2, yielding the sizable values of Δ_0^2 shown in the main panels of Fig. 4.15.

To better understand the role of Δ_0^2, it is useful to analyze the molecular quasi-particle energies $E^{\pm}_{\mathbf{P}}$, which are reported in Figs. 4.16, 4.17 and 4.18 for several different boson concentrations and

mass ratios. The hybridized dispersions $E^{\pm}_{\mathbf{P}}$ are compared with the unhybridized molecular $\widetilde{\xi}^{\mathrm{CF}}_{\mathbf{P}}$ and atomic $\xi^{\mathrm{F}}_{\mathbf{P}}$ dispersions.

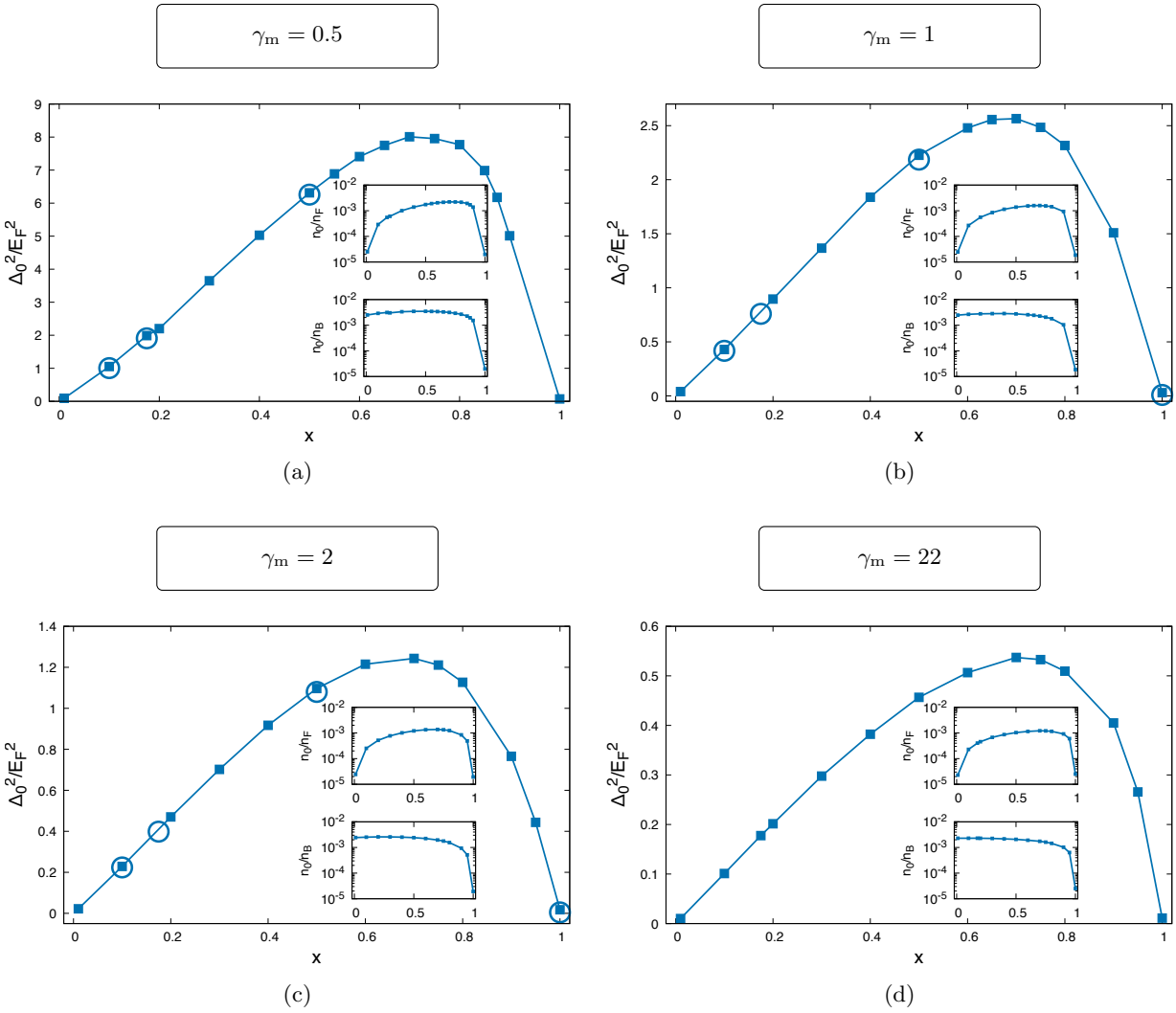

Figure 4.15: Square of the hybridization energy $\Delta_0^2 = 2\pi\varepsilon_0 n_0/m_{\mathrm{r}}$ (in units of E_{F}^2) as a function of the boson condensate x, for strong BF attraction $g = 3$ and different mass ratios: (a) $\gamma_{\mathrm{m}} = 0.5$, (b) $\gamma_{\mathrm{m}} = 1$, (c) $\gamma_{\mathrm{m}} = 2$, (d) $\gamma_{\mathrm{m}} = 22$. Insets: condensate density n_0 in units of n_{F} (top) and condensate fraction n_0/n_{B} (bottom) for the same set of parameters. The circles represent Δ_0^2 computed using the fully numerical implementation in Fortran 90, and reveal a good agreement between n_0 evaluated with the strong-coupling expressions in Mathematica and n_0 evaluated with the Fortran 90 code.

At exactly matched densities, all fermions are essentially paired up with all bosons ($n_0 \approx 0$), and the system is effectively made of a gas of non-interacting molecules, with the hybridized dispersions coinciding with the unhybridized since $\Delta_0 \approx 0$.

As soon as the concentration decreases (see the case $x = 0.95$ in Figs. 4.16, 4.17 and 4.18), the hybridization energy scale Δ_0 sharply rises and hybrid quasi-particles form out of the molecular and unpaired Fermi states, resulting in a downward shift of the energy dispersion $E^-_{\mathbf{P}}$ with respect to $\widetilde{\xi}^{\mathrm{CF}}_{\mathbf{P}}$. This shift is especially visible in the case of $\gamma_{\mathrm{m}} = 0.5$ (see Fig. 4.16(b)), which has the largest hybridization energy (see Fig. 4.15(a)).

The bottom panels of Figs. 4.16, 4.17 and 4.18 display the typical level crossing (dotted and dashed lines) and avoided crossing (solid and dot-dashed lines) of a non-hybridized and hybridized two-level system, respectively. The dispersion of the occupied composite fermion states $E^-_{\mathbf{P}}$ approaches the non-interacting molecular dispersion $\widetilde{\xi}^{\mathrm{CF}}_{\mathbf{P}}$ for large x; as x is reduced below the crossover concentration $x \approx 0.7$ (where the hybridization energy is maximal, see Fig. 4.15), the character of the occupied composite fermion states changes from molecular to mostly atomic and eventually approaches the non-interacting atomic dispersion $\xi^{\mathrm{F}}_{\mathbf{P}}$, albeit with a small quasi particle weight $v^2_{\mathbf{P}}$ (see panels (d) of Figs. 4.16, 4.17 and 4.18, and Fig. 4.14).

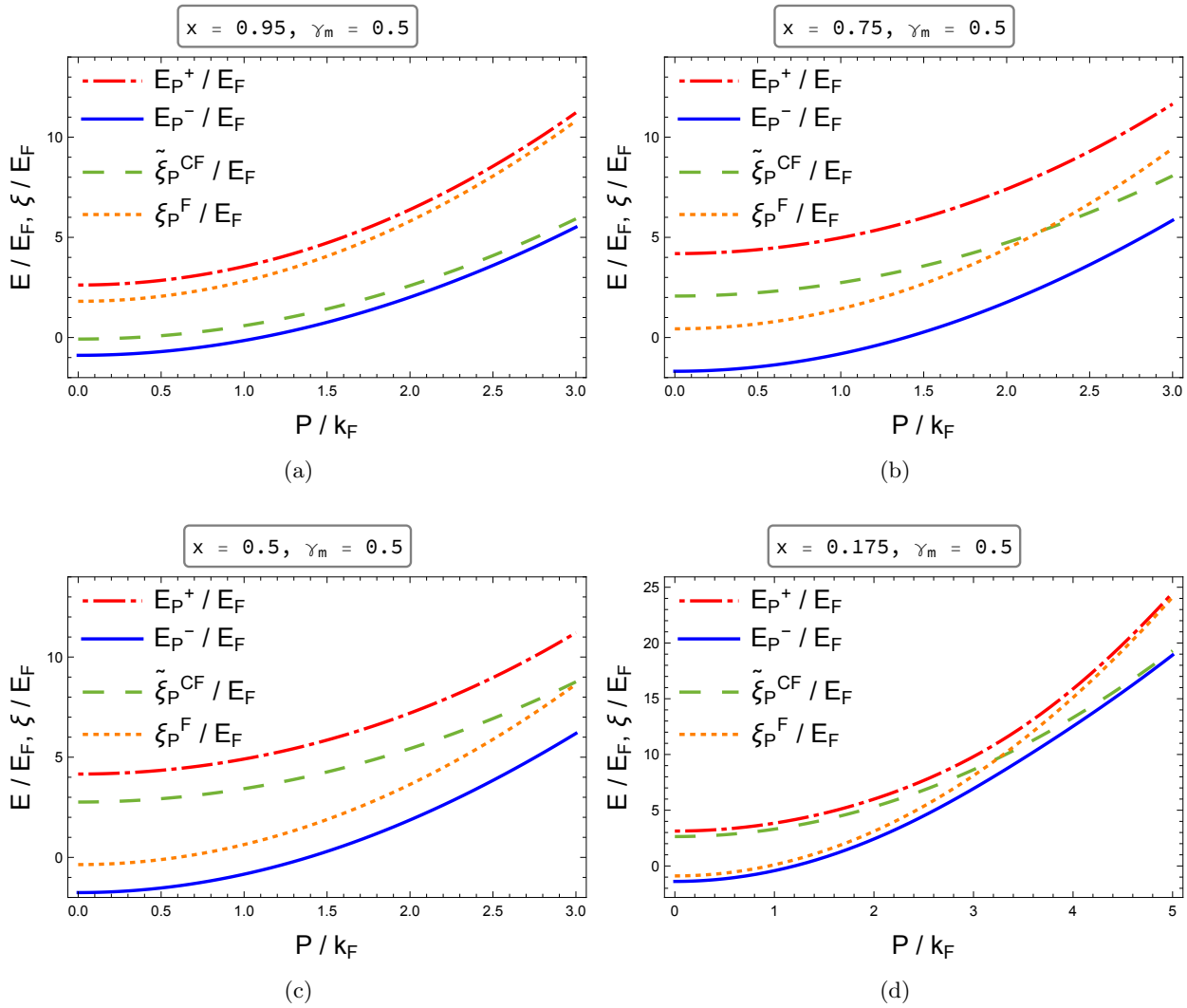

Figure 4.16: Hybridized dispersions $E^{\pm}_{\mathbf{P}}$ of the poles of the strong coupling limit of the T-matrix $T_{\rm SC}(\mathbf{P},\Omega)$ and unhybridized molecular and atomic dispersions $\widetilde{\xi}^{\rm CF}_{\mathbf{P}}$ and $\xi^{\rm F}_{\mathbf{P}}$ (in units of $E_{\rm F}$) as functions of $P/k_{\rm F}$. All data are obtained for strong BF attraction $g = 3$ and mass ratio $\gamma_{\rm m} = 0.5$. Different boson concentration are considered: (a) $x = 0.95$, (b) $x = 0.75$, (c) $x = 0.5$, (d) $x = 0.175$.

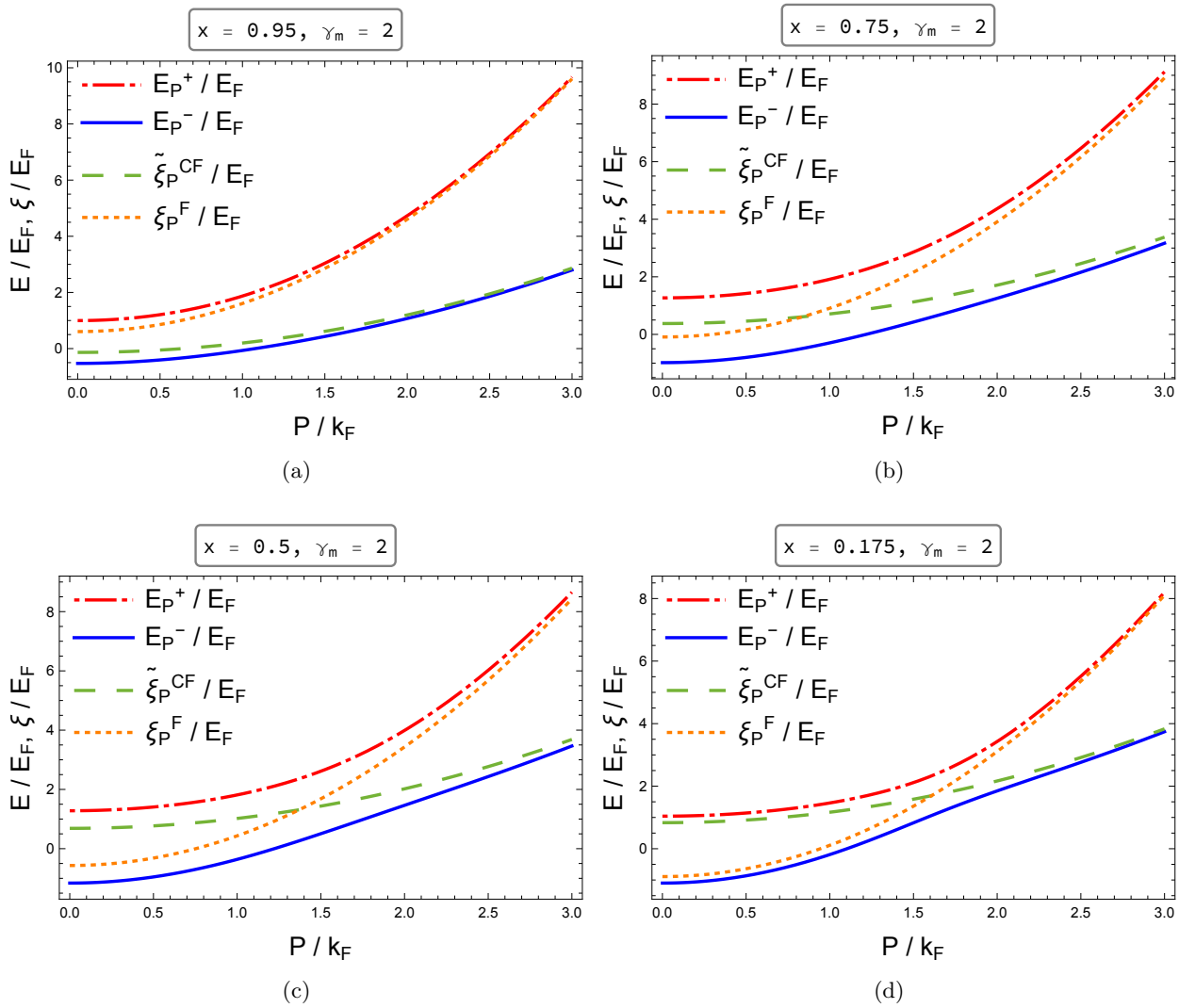

Figure 4.17: Hybridized dispersions $E^{\pm}_{\mathbf{P}}$ of the poles of the strong coupling limit of the T-matrix $T_{\rm SC}(\mathbf{P},\Omega)$ and unhybridized molecular and atomic dispersions $\widetilde{\xi}^{\rm CF}_{\mathbf{P}}$ and $\xi^{\rm F}_{\mathbf{P}}$ (in units of $E_{\rm F}$) as functions of $P/k_{\rm F}$. All data are obtained for strong BF attraction $g = 3$ and mass ratio $\gamma_{\rm m} = 2$. Different boson concentration are considered: (a) $x = 0.95$, (b) $x = 0.75$, (c) $x = 0.5$, (d) $x = 0.175$.

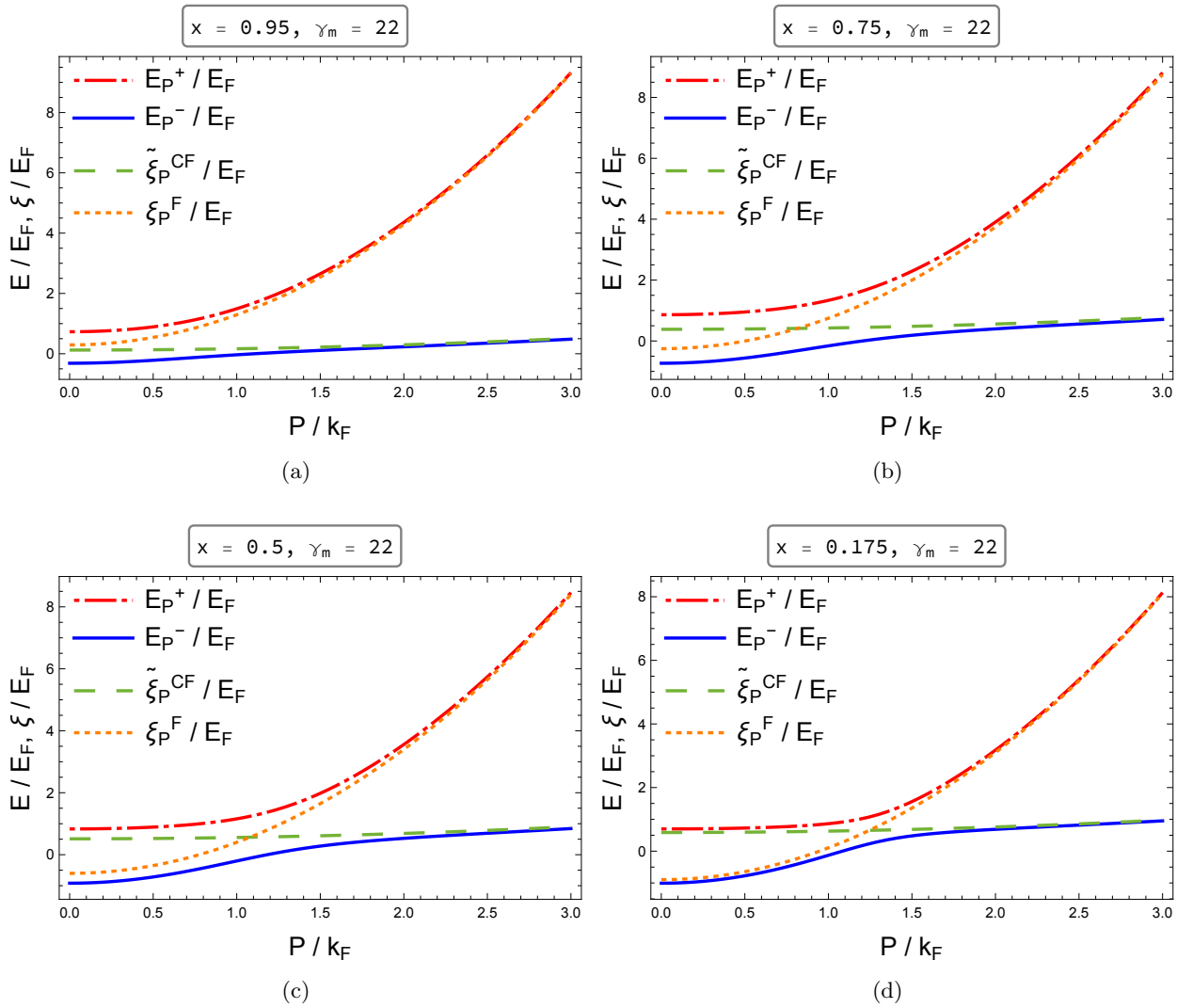

Figure 4.18: Hybridized dispersions $E^{\pm}_{\mathbf{P}}$ of the poles of the strong coupling limit of the T-matrix $T_{\rm SC}(\mathbf{P},\Omega)$ and unhybridized molecular and atomic dispersions $\widetilde{\xi}^{\rm CF}_{\mathbf{P}}$ and $\xi^{\rm F}_{\mathbf{P}}$ (in units of $E_{\rm F}$) as functions of $P/k_{\rm F}$. All data are obtained for strong BF attraction $g = 3$ and mass ratio $\gamma_{\rm m} = 22$. Different boson concentration are considered: (a) $x = 0.95$, (b) $x = 0.75$, (c) $x = 0.5$, (d) $x = 0.175$.

Conclusions and perspectives

In this thesis, we studied 2-dimensional Bose-Fermi mixtures at zero temperature with BF pairing and mass imbalance between the bosons and fermions. We chose realistic values for the mass imbalance from BF mixtures realized in experiments, as summarized in Tab. 1.1. The equilibrium thermodynamic quantities were evaluated within the T-matrix approach adopted in [56], employing a a numerical code (written in Fortran 90) that solves the system given by the Hugenholtz-Pines theorem and the density equations to determine the unknowns μ_{B}, μ_{F}, and n_0 for given boson concentration, mass ratio, and coupling parameters. Two interesting results found using this fully numerical implementation are:

- The boson momentum distribution $n_{\mathrm{B}}(\mathbf{k})$ presents a peak at small but non-zero momentum in the BF coupling regime $g \lesssim -4$. In the density-balanced example, this feature for $g = -4$ is lost in the case $\gamma_{\mathrm{m}} = 0.5$, while for $\gamma_{\mathrm{m}} > 1$ the peak persists also for larger BF couplings $g > -4$. However, when the boson concentration n_{B} is sufficiently lowered, the peak for $g = -4$ appears in the case $\gamma_{\mathrm{m}} = 0.5$ as well.

- The approximately universal behavior of n_0 with respect to the boson concentration holds with greater accuracy when the boson mass is increased.

Overall, most of the qualitative features identified in the numerical study of [56] for mass-balanced mixtures are present in the mass-imbalanced case as well.

The results from the fully numerical calculation of μ_{B} and μ_{F} were compared with the corresponding analytical expressions in the weak-BF coupling regime $g \lesssim -2$, showing agreement to second order in the parameter $1/g$.

The results from the fully numerical calculation of μ_{B}, μ_{F}, and n_0 were compared with the corresponding semi-analytical calculations in the strong-BF coupling regime $g \gtrsim 2$, showing agreement in this case as well. The semi-analytical expressions, computed numerically using a Mathematica program which is a generalization to mass-imbalanced mixtures of the Mathematica code employed in [56], allow for a simpler and faster evaluation of the thermodynamic quantities compared to the Fortran 90 program. In this way, we characterized in detail the interaction effects on the fermionic molecules that form from the binding of atomic bosons and fermions. In this context, by studying the dependence on the boson concentration of the atomic and molecular chemical potentials and of the molecular momentum distribution, we found that when the boson mass is increased, it is necessary to

simultaneously increase the boson concentration x in order to attenuate the influence of the atomic fermion component on the molecules.

Two possible improvements to the above T-matrix theory were proposed: the inclusion of an additional anomalous boson self-energy, originating from fermion-mediated interactions, and the implementation of a partially self-consistent modified T-matrix approach. The latter boils down to a mean-field shift of the fermion chemical potential in the bare fermion propagators inside the self-energies.

Part of the work of this thesis involved writing a program to compute μ_{B}, μ_{F}, and n_0 with these two improvements. A Fortran 90 code and a Mathematica code (the latter valid in the strong-BF coupling regime) to implement the mean-field shift in absence of the additional anomalous term have been written and were used in this thesis to obtain preliminary results in the density- and mass-balanced case. An interesting result is the achievement of a more physical momentum distribution of the interacting atomic fermions in the strong-coupling regime, compared to that of the previous T-matrix method of [56]. Concerning the additional term in the anomalous boson self-energy, a Fortran 90 code has been written and tested against the expected value of this term computed in perturbation theory in the weak-BF coupling regime.

Analytical expressions for μ_{B} and μ_{F} were derived in the weak-coupling limit up to second order in $1/g$, taking into account the two improvements to the T-matrix described above. We found that the inclusion of the additional anomalous term is crucial for recovering the correct weak-coupling expansion within the partially self-consistent T-matrix approach, suggesting that both improvements are necessary for a more accurate and reliable modeling of the BF mixture.

This thesis work could be extended in several directions:

- To identify and understand the origin of the peak in $n_{\mathrm{B}}(\mathbf{k})$ in the weak-coupling regime, it would be helpful to study the bosonic spectral weight function of the mixture.
- The effects of the mean-field shift of μ_{F} inside the self-energies on the thermodynamic properties of the mixture still need to be studied systematically. In particular, extending the analysis to density-imbalanced mixtures could be important for discussing the Fermi liquid features of the mixture in the strong-BF coupling regime in more detail.
- The effects of the anomalous BF term on the thermodynamic properties of the mixture also remain to be investigated. In particular, it is important to understand the consequences for the stability of the mixture. Developing a simplified model for the anomalous BF term in the strong-BF coupling regime is another problem for future work.
- The T-matrix approach adopted in [56] and in the numerical analysis of this thesis misses the polaron-to-molecule transition (which is instead found in $3d$ within the same T-matrix method [55, 110] and in $2d$ using more sophisticated approaches that go beyond the ladder diagram approximation [111, 112]). It is important to investigate whether introducing the partially self-consistent scheme and the additional anomalous self-energy term moves in the direction of recovering this transition.

Appendix A

Numerical methods

A.1 Calculation of the normal self-energies

The numerical evaluation of the normal boson and fermion self-energies requires special care when dealing with the slow convergence of the frequency convolutions appearing in Eq. (3.22) and (3.24), owing to the low dimensionality of the problem at hand. In order to speed up the convergence, the integrand of the convolution is added and subtracted by an auxiliary function with the same asymptotic behavior yet analytically integrable. As a result, the numerical integration is truncated by applying a large frequency cutoff, which we fix at $\Omega_{\rm c} = \pm 50000\ E_{\rm F}$. For $|\Omega| > \Omega_{\rm c}$ integration is done by making use of asymptotic expressions. The strategy is inherited unchanged from [56, 109].

Starting from the self-energy for bosons, we recast it as follows

$$\begin{aligned}\Sigma^{11}_{\rm BF}(\mathbf{k},\omega) = &\int \frac{{\rm d}\mathbf{P}}{(2\pi)^2}\int\frac{{\rm d}\Omega}{2\pi}\left(T(\mathbf{P},\Omega)G^0_{\rm F}(\mathbf{P}-\mathbf{k},\Omega-\omega) - T_2(\mathbf{P},\Omega)G^{00}_{\rm F}(\mathbf{P}-\mathbf{k},\Omega-\omega)\right)\\ &+\int\frac{{\rm d}\mathbf{P}}{(2\pi)^2}\int\frac{{\rm d}\Omega}{2\pi}\,T_2(\mathbf{P},\Omega)G^{00}_{\rm F}(\mathbf{P}-\mathbf{k},\Omega-\omega){\rm e}^{i\Omega 0^+},\end{aligned} \tag{A.1}$$

where $G^{00}_{\rm F}$ is a bare fermion Green's function with $\xi^{\rm F}_{\mathbf{k}} = \mathbf{k}^2/(2m_{\rm F}) + 0^+$, and T_2 is given by Eq. (3.11). The frequency integral at the second line is evaluated analytically by contour integration closing on the left-hand side and contributing with a pole and a branch cut when they fall in this region. Instead, the first frequency integration is split into three regions: $(-\infty,-\Omega_{\rm c})\cup[-\Omega_{\rm c},\Omega_{\rm c}]\cup(\Omega_{\rm c},\infty)$. The intermediate frequency range is treated numerically. The integrals over the external ranges $|\Omega|>\Omega_{\rm c}$ are instead computed analytically, exploiting the improved convergence:

$$\begin{aligned}&T(\mathbf{P},\Omega)G^0_{\rm F}(\mathbf{P}-\mathbf{k},\Omega-\omega) - T_2(\mathbf{P},\Omega)G^{00}_{\rm F}(\mathbf{P}-\mathbf{k},\Omega-\omega)\\ &\quad\sim\left(\frac{2\pi}{m_{\rm r}}\right)^2\frac{n_0 - k^2_{\mu_{\rm F}}/(4\pi)}{\ln^2(-i\Omega/\varepsilon_0)}\frac{1}{(i\Omega)^2} + \frac{2\pi}{m_{\rm r}}\frac{1}{\ln(-i\Omega/\varepsilon_0)}\frac{\mu_{\rm F}-0^+}{(i\Omega)^2}\quad\text{for large }\Omega.\end{aligned} \tag{A.2}$$

Here $k_{\mu_{\rm F}} = \sqrt{2m_{\rm F}\mu_{\rm F}}$ if $\mu_{\rm F}\geq 0$, and $k_{\mu_{\rm F}} = 0$ otherwise.

Regarding integration in momentum space, the angular integral can be carried out analytically, since the dependence on the angle appears only in the bare Green's function. Finally, radial integrals are evaluated numerically up to a natural cut-off given by the position of the largest momentum corresponding to a non-differentiable point in the integrand function. In particular, we find one step due to the pole of the T-matrix and up to two kinks coming from the poles of the angular integral of the fermion bare Green's function $\int_0^{2\pi} \mathrm{d}\theta\, G_{\mathrm{F}}^0(\mathbf{P}-\mathbf{k}, \Omega-\omega)$.

The calculations for the fermion self-energy Σ_{F} follow the same approach as above provided that G_{F}^{00} and G_{F}^0 are replaced with G_{B}^0. Since the boson bare Green's function $G_{\mathrm{B}}^0(\mathbf{P}-\mathbf{k}, \Omega-\omega)$ does not have a pole, the final momentum integration is carried out simply over a single finite interval, up to the step in the integrand coming from the pole $P_{\mathrm{T}0}$ of the T-matrix.

In the Fortan program, the fully numerical calculation of the self-energies is carried out only for small frequencies ω. In particular, for $\omega > 100\, E_{\mathrm{F}}$, the following asymptotic expressions are used:

$$\Sigma_{\mathrm{F}}(\mathbf{k}, \omega) \sim n_0 \Gamma(\mathbf{k}, \omega) - G_{\mathrm{B}}^0(\mathbf{k}, -\omega) \int \frac{\mathrm{d}\mathbf{P}}{(2\pi)^2} \int \frac{\mathrm{d}\Omega}{2\pi}\, T(\mathbf{P}, \Omega) \mathrm{e}^{i\Omega 0^+} \tag{A.3}$$

$$\Sigma_{\mathrm{B}}^{11}(\mathbf{k}, \omega) \sim \Sigma_{\mathrm{BB}}^{11} + \frac{k_{\mu_{\mathrm{F}}}^2}{4\pi} T(\mathbf{k}, \omega) - G_{\mathrm{F}}^0(\mathbf{k}, -\omega) \int \frac{\mathrm{d}\mathbf{P}}{(2\pi)^2} \int \frac{\mathrm{d}\Omega}{2\pi}\, T(\mathbf{P}, \Omega) \mathrm{e}^{i\Omega 0^+}. \tag{A.4}$$

A.2 Calculation of the anomalous self-energy

Let us now move to the evaluation of $\Sigma_{\mathrm{BF}}^{12}$. The high-frequency approximation of the integrand reads in this case

$$T(\mathbf{P}-\mathbf{k}, \Omega-\omega) T(\mathbf{P}, \Omega) G_{\mathrm{F}}^0(\mathbf{P}-\mathbf{k}, \Omega-\omega) G_{\mathrm{F}}^0(\mathbf{P}, \Omega) \sim \left(\frac{2\pi}{m_{\mathrm{r}}}\right)^2 \frac{1}{(i\Omega)^2 \ln^2(-i\Omega/\varepsilon_0)}, \tag{A.5}$$

and therefore there is no need to add and subtract an auxiliary function to accelerate the convergence of the frequency convolution. The frequency interval is split into three sets: $(-\infty, -\Omega_{\tilde{\mathrm{c}}}) \cup [-\Omega_{\tilde{\mathrm{c}}}, \Omega_{\tilde{\mathrm{c}}}] \cup (\Omega_{\tilde{\mathrm{c}}}, \infty)$ with $\Omega_{\tilde{\mathrm{c}}} = 5000\, E_{\mathrm{F}}$, and the asymptotic form (A.5) is exploited in the outer regions.

The angular integral cannot be performed analytically because of the dependence of $T(\mathbf{P}-\mathbf{k}, \Omega-\omega)$ on $\mathbf{k}$; therefore, it is evaluated numerically by performing the change of variable $\theta \mapsto \cos\theta$ and sampling $[-1, 1]$ with 30 points. This step is carried out prior to the integration over the frequency. The double integral over the frequency and the angle reads

$$\begin{aligned}
&\int_0^{2\pi} \frac{\mathrm{d}\theta}{2\pi} \int \frac{\mathrm{d}\Omega}{2\pi}\, T(\mathbf{P}-\mathbf{k}, \Omega-\omega) T(\mathbf{P}, \Omega) G_{\mathrm{F}}^0(\mathbf{P}-\mathbf{k}, \Omega-\omega) G_{\mathrm{F}}^0(\mathbf{P}, \Omega) \\
&= \int_{-\Omega_{\tilde{\mathrm{c}}}}^{\Omega_{\tilde{\mathrm{c}}}} \frac{\mathrm{d}\Omega}{2\pi} \left(\int_{-1}^{1} \frac{\mathrm{d}(\cos\theta)}{\pi}\, \frac{T(\mathbf{P}-\mathbf{k}, \Omega-\omega) G_{\mathrm{F}}^0(\mathbf{P}-\mathbf{k}, \Omega-\omega)}{\sqrt{1-\cos^2\theta}} \right) T(\mathbf{P}, \Omega) G_{\mathrm{F}}^0(\mathbf{P}, \Omega) \\
&- 2\mathrm{Re} \int_0^{1/\Omega_{\tilde{\mathrm{c}}}} \mathrm{d}y\, \frac{2\pi}{m_{\mathrm{r}}^2}\, \frac{1}{\ln^2(-i/(\varepsilon_0\, y))}.
\end{aligned} \tag{A.6}$$

Before discussing the integral over $[-\Omega_{\tilde{\mathrm{c}}}, \Omega_{\tilde{\mathrm{c}}}]$, note that, for the evaluation of the boson momentum

distribution, we can focus on positive ω (see (A.12)); depending on the values of $\omega > 0$ and $|\mathbf{k}| > 0$, the integral over Ω is performed in slightly different ways. If $0 < \omega < 0.1\, E_\mathrm{F}$ then $[-\Omega_{\tilde{c}}, \Omega_{\tilde{c}}]$ is split as

$$[-\Omega_{\tilde{c}}, \Omega_{\tilde{c}}] = [-\Omega_{\tilde{c}}, -b] \cup (-b, -a) \cup [-a, a] \cup (a, b) \cup [b, \Omega_{\tilde{c}}]. \tag{A.7}$$

The sub-intervals are sampled with, respectively, (going in order from left to right in (A.7)) $N_{\Omega 1}$, $N_{\Omega 2}$, $N_{\Omega 3}$, $N_{\Omega 2}$, $N_{\Omega 1}$ points. Otherwise, if $\omega > 0.1\, E_\mathrm{F}$, $[-\Omega_{\tilde{c}}, \Omega_{\tilde{c}}]$ is split as

$$\begin{aligned}[-\Omega_{\tilde{c}}, \Omega_{\tilde{c}}] = {} & [-\Omega_{\tilde{c}}, -b] \cup (-b, -a/5) \\ & \cup [-a/5, a/5] \cup (a/5, \omega - a/5) \cup [\omega - a/5, \omega + a/5] \cup (\omega + a/5, b) \cup [b, \Omega_{\tilde{c}}]\end{aligned} \tag{A.8}$$

(note that $\omega < b$, since an asymptotic expression (A.10) is employed for $\omega > 50\, E_\mathrm{F}$). The sub-intervals are sampled with, respectively, (going in order from left to right in (A.8)) $N_{\Omega 1}$, $N_{\Omega 2}$, $N_{\Omega 3}$, $N_{\Omega 2}$, $N_{\Omega 3}$, $N_{\Omega 2}$, $N_{\Omega 1}$ points. The parameters a, b, $N_{\Omega i}$ are reported in Tab. A.1.

Finally, the contribution from the tail is computed numerically sampling $[0, 1/\Omega_{\tilde{c}}]$ with 100 points. At this point, we are left to perform the integral over $|\mathbf{P}|$. The T-matrix can introduce steps and

a	$0.25\, E_\mathrm{F}$
b	$200\, E_\mathrm{F}$
$N_{\Omega 1}$	50
$N_{\Omega 2}$	100
$N_{\Omega 3}$	800 if $\omega < 0.01\, E_\mathrm{F}$ and $\lvert\mathbf{k}\rvert < 0.05\, k_\mathrm{F}$, 200 otherwise

Table A.1: Parameters used for constructing the grid in Ω for the numerical integration in $[-\Omega_{\tilde{c}}, \Omega_{\tilde{c}}]$.

kinks; therefore, the grid is conveniently divided into sub-intervals delimited by pairs of these sensitive momenta. Specifically, these points are found to be

$$P_{\mathrm{T}0}, \quad P_{\mathrm{T}0} + k, \quad |P_{\mathrm{T}0} - k|; \tag{A.9}$$

therefore $[0, P_{\mathrm{T}0} + k]$ is divided in three sub-intervals, each sampled with 10 points. Note that the momenta k_{μ_F}, $k_{\mu_\mathrm{F}} + k$, $|k_{\mu_\mathrm{F}} - k|$ do not play any role in the optimization of the Fortran program, since the divergence of $G^0_\mathrm{F}(\mathbf{P}, 0^+)$ at $|\mathbf{P}| = k_{\mu_\mathrm{F}}$ is canceled by the vanishing of $T(\mathbf{P}, 0^+)$ at the same point (and analogously for $G^0_\mathrm{F}(\mathbf{P} - \mathbf{k}, 0^+)$ and $T(\mathbf{P} - \mathbf{k}, 0^+)$ at $k_{\mu_\mathrm{F}} + k$ and $|k_{\mu_\mathrm{F}} - k|$).
The case $(\mathbf{k}, \omega) = (\mathbf{0}, 0)$ requires special attention due to the singularity at $|\mathbf{P}| = P_{\mathrm{T}0}$. Since the contribution of the Dirac delta is known from A^δ_BF in Eq. (3.35), the numerical momentum integral is evaluated over $[0, P^-_{\mathrm{T}0}]$, with $P^-_{\mathrm{T}0} = P_{\mathrm{T}0} - 10^{-6}\, k_\mathrm{F}$; then, A^δ_BF is added to it.[1]

The fully numerical calculation of the anomalous self-energy is carried out only for small frequen-

[1] The number $10^{-6}\, k_\mathrm{F}$ is chosen since the tolerance with which we find $P_{\mathrm{T}0}$ by the bisection method is $10^{-7}\, k_\mathrm{F}$, and we want the grid cutoff to lie safely below the singularity by an amount larger than the numerical uncertainty on $P_{\mathrm{T}0}$ itself.

cies ω. In particular, for $\omega > 50\,E_{\rm F}$, the following asymptotic expression is used:

$$\Sigma^{12}_{\rm BF}(\mathbf{k},\omega) \sim 2\,n_0\,\Sigma^{11}_{\rm BF}(\mathbf{0},0)\,{\rm Re}\left(T(\mathbf{k},\omega)G^0_{\rm F}(\mathbf{k},\omega)\right). \tag{A.10}$$

Focusing on large ω, Fig. A.1 illustrates the convergence of (A.10) toward the fully numerical data for various $|\mathbf{k}|$ and BF coupling parameters g, for $x = 0.5$ and $\gamma_{\rm m} = 1$.

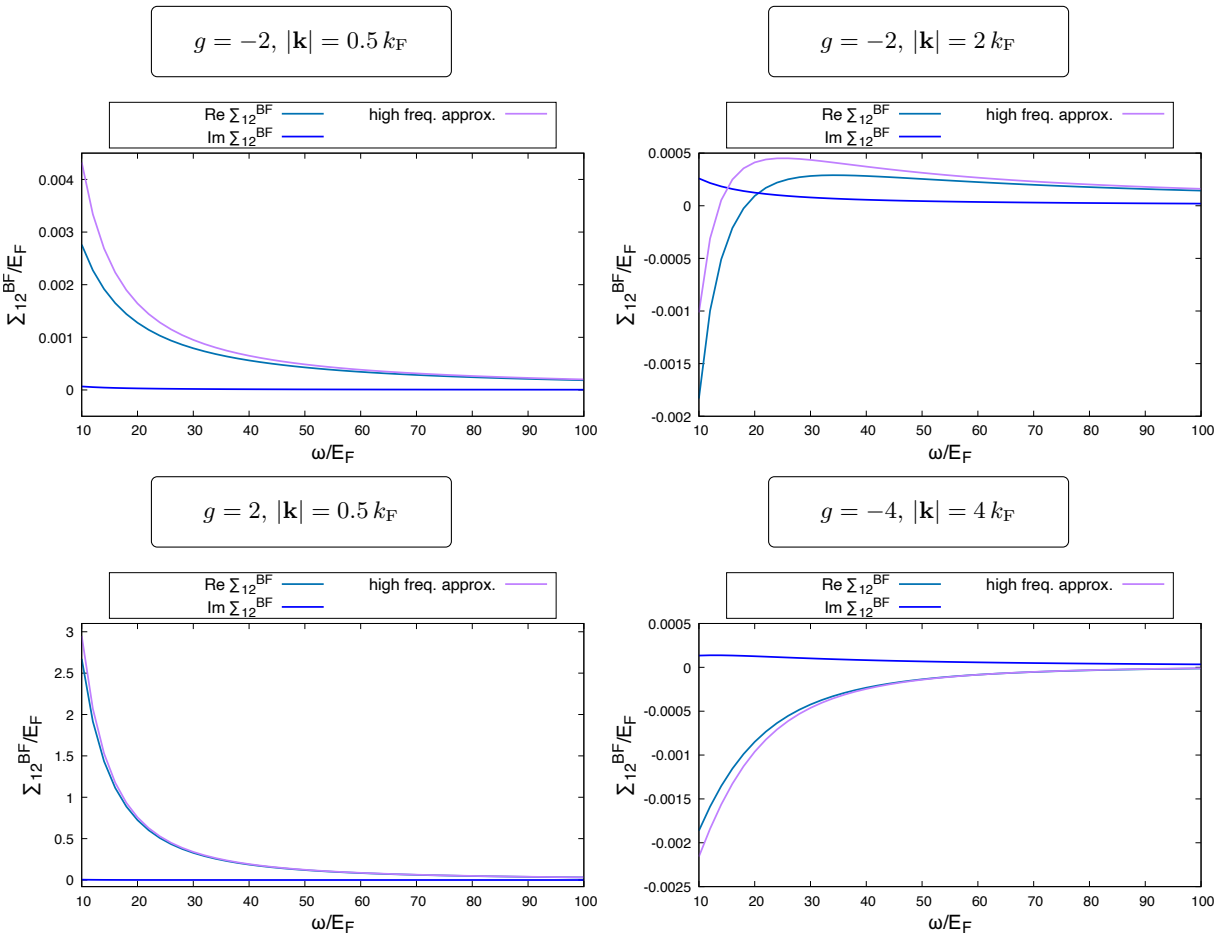

Figure A.1: Anomalous self-energy $\Sigma^{12}_{\rm BF}(\mathbf{k},\omega)$ as function of ω for different choices of k and g, for $x = 0.5$ and $\gamma_{\rm m} = 1$. The plots report the comparison with the expression (A.10). Input parameters for $g = -2$: $\mu_{\rm B} = -0.5\,E_{\rm F}$, $\mu_{\rm F} = 0.8\,E_{\rm F}, n_0 = 0.4\,n_{\rm F}$. Input parameters for $g = 2$: $\mu_{\rm B} = -110\,E_{\rm F}$, $\mu_{\rm F} = 0.6\,E_{\rm F}, n_0 = 7\times10^{-3}\,n_{\rm F}$. Input parameters for $g = -4$: $\mu_{\rm B} = -0.26\,E_{\rm F}$, $\mu_{\rm F} = 0.89\,E_{\rm F}, n_0 = 0.48\,n_{\rm F}$.

Focusing on small ω, Fig. A.2 reports $\Sigma^{12}_{\rm BF}(\mathbf{k},\omega)$ for $|\mathbf{k}| = 0.01\,k_{\rm F}$, $x = 0.5$, $\gamma_{\rm m} = 1$, and various BF coupling parameters g; in particular, we observe that $\lim_{\omega\to0}\Sigma^{12}_{\rm BF}(\mathbf{k},\omega)$ approaches the expression given by Eq. (3.96). We are currently investigating the origin of the feature at $\omega \approx 0.08\,E_{\rm F}$ in Fig. A.2. Finally, the lower panels of Fig. A.2 report $\Sigma^{12}_{\rm BF}(\mathbf{k},\omega)$ (multiplied by g^2) evaluated at exactly $\mathbf{k} = \mathbf{0}$

and $\omega = 0$, using Eq. (3.36); we consider here extremely weak coupling values, to show agreement with the perturbative result (3.96) at order $\mathrm{O}(1/g^2)$.

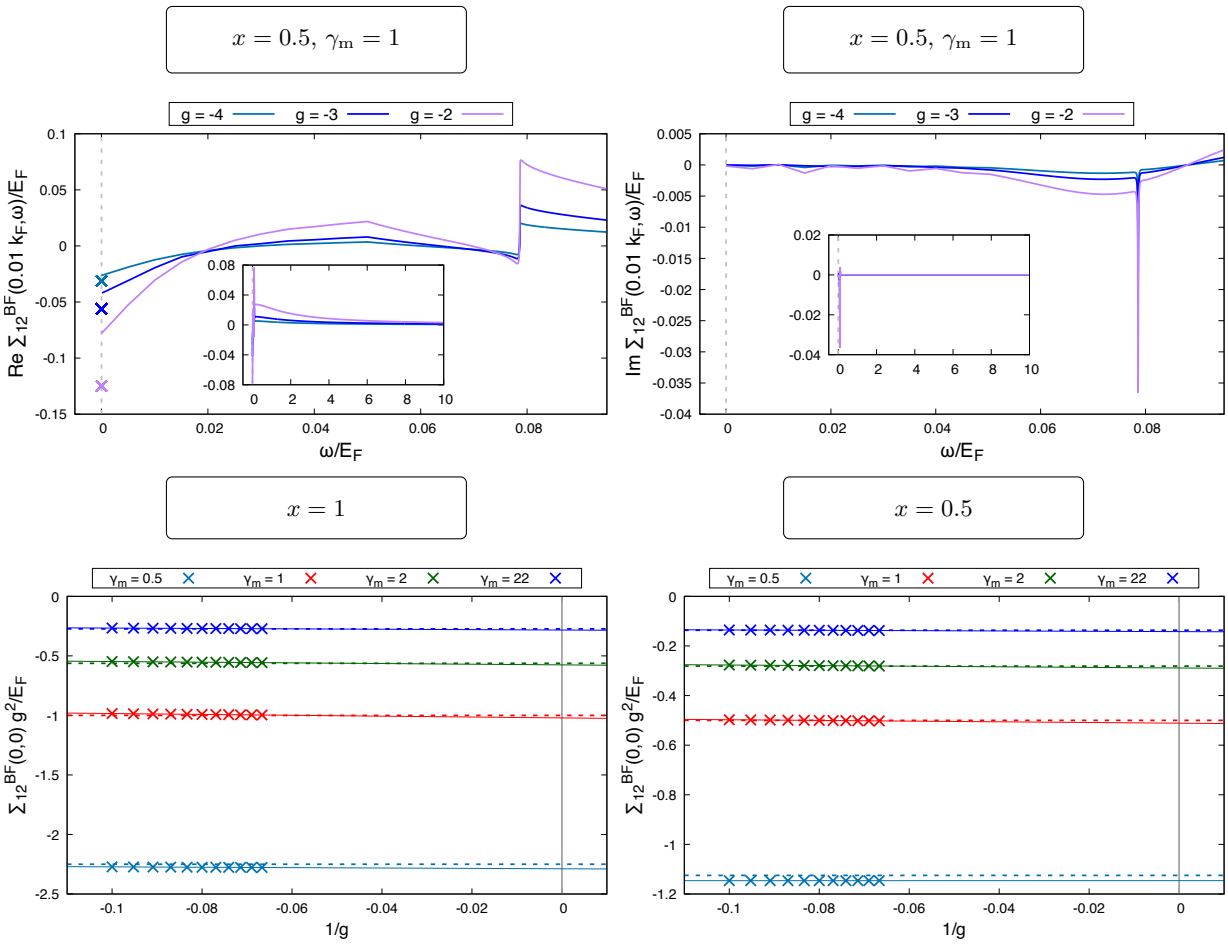

Figure A.2: Upper panels: anomalous self-energy $\Sigma^{12}_{\mathrm{BF}}(\mathbf{k},\omega)$ as function of ω for $|\mathbf{k}| = 0.01\,k_{\mathrm{F}}$, $x = 0.5$ and $\gamma_{\mathrm{m}} = 1$. Different values of the BF coupling g are considered. The plots report the comparison between $\lim_{\omega\to 0}\Sigma^{12}_{\mathrm{BF}}(\mathbf{k},\omega)$ and the expression (3.96) (crosses). Insets: anomalous self-energy $\Sigma^{12}_{\mathrm{BF}}(\mathbf{k},\omega)$ as function of ω, plotted in the wider range $0 < \omega < 10\,E_{\mathrm{F}}$, for the same $|\mathbf{k}|$, x and γ_{m}. Input parameters for $g = -4$: $\mu_{\mathrm{B}} = -0.26\,E_{\mathrm{F}}$, $\mu_{\mathrm{F}} = 0.89\,E_{\mathrm{F}}, n_0 = 0.48\,n_{\mathrm{F}}$. Input parameters fo $g = -3$: $\mu_{\mathrm{B}} = -0.35\,E_{\mathrm{F}}$, $\mu_{\mathrm{F}} = 0.86\,E_{\mathrm{F}}, n_0 = 0.46\,n_{\mathrm{F}}$. Input parameters for $g = -2$: $\mu_{\mathrm{B}} = -0.5\,E_{\mathrm{F}}$, $\mu_{\mathrm{F}} = 0.8\,E_{\mathrm{F}}, n_0 = 0.4\,n_{\mathrm{F}}$. Lower panels: crosses represent the quantity $\Sigma^{12}_{\mathrm{BF}}(\mathbf{0},0)\,g^2/E_{\mathrm{F}}$, as a function of $1/g$, in the extreme weak-coupling range $g \in [-15,-10]$, for several values of the boson concentration x and the mass ratio γ_{m}; the full lines represent the fit to the model $f(g) = A + B/g$; the dashed lines represent the expected asymptotic value of the fitting curve in the limit $1/g \to 0^-$, given by the perturbative result (3.96) (multiplied by g^2). Input parameters: $\mu_{\mathrm{B}} = -0.01\,E_{\mathrm{F}}$, $\mu_{\mathrm{F}} = 0.999\,E_{\mathrm{F}}$, $n_0 = 0.999\,n_{\mathrm{F}}$ (for $x = 1$) or $0.499\,n_{\mathrm{F}}$ (for $x = 0.5$).

A.3 Calculation of the momentum distributions and the densities

The momentum distributions Eqs. (3.41) and (3.42) are treated introducing an addition/subtraction scheme as well (as for the normal self-energies, the strategy is inherited unchanged from [56, 109]):

$$\begin{aligned} n_{\mathrm{F}}(\mathbf{k}) &= \int \frac{\mathrm{d}\omega}{2\pi}\left(G_{\mathrm{F}}(\mathbf{k},\omega) - G^0_{\mathrm{F}}(\mathbf{k},\omega)\right) + \int \frac{\mathrm{d}\omega}{2\pi} G^0_{\mathrm{F}}(\mathbf{k},\omega)\mathrm{e}^{i\omega 0^+} \\ &= 2\mathrm{Re}\int_0^\infty \frac{\mathrm{d}\omega}{2\pi}\left(G_{\mathrm{F}}(\mathbf{k},\omega) - G^0_{\mathrm{F}}(\mathbf{k},\omega)\right) + \Theta(-\xi^{\mathrm{F}}_{\mathbf{k}}) \qquad \text{(A.11)} \\ n_{\mathrm{B}}(\mathbf{k}) &= -\int \frac{\mathrm{d}\omega}{2\pi}\left(G'_{\mathrm{B}}(\mathbf{k},\omega) - G^{0'}_{\mathrm{B}}(\mathbf{k},\omega)\right) - \int \frac{\mathrm{d}\omega}{2\pi} G^{0'}_{\mathrm{B}}(\mathbf{k},\omega)\mathrm{e}^{i\omega 0^+} \\ &= -2\mathrm{Re}\int_0^\infty \frac{\mathrm{d}\omega}{2\pi}\left(G'_{\mathrm{B}}(\mathbf{k},\omega) - G^{0'}_{\mathrm{B}}(\mathbf{k},\omega)\right) - \frac{1}{2}\left(\frac{\xi^{\mathrm{B}}_{\mathbf{k}} + \Sigma^{11}_{\mathrm{BB}}}{\sqrt{(\xi^{\mathrm{B}}_{\mathbf{k}} + \Sigma^{11}_{\mathrm{BB}})^2 - \left(\Sigma^{12}_{\mathrm{BB}}\right)^2}} - 1\right). \qquad \text{(A.12)} \end{aligned}$$

Here,

$$G^{0'}_{\mathrm{B}}(\mathbf{k},\omega)^{-1} \equiv G^0_{\mathrm{B}}(\mathbf{k},\omega)^{-1} - \Sigma^{11}_{\mathrm{BB}} + \frac{\left(\Sigma^{12}_{\mathrm{BB}}\right)^2}{i\omega + \xi^{\mathrm{B}}_{\mathbf{k}} + \Sigma^{11}_{\mathrm{BB}}}. \qquad \text{(A.13)}$$

The remaining integral is computed numerically up to a chosen cutoff ω_{c}, exploiting the improved convergence: for instance, in the fermionic case

$$G_{\mathrm{F}}(\mathbf{k},\omega) - G^0_{\mathrm{F}}(\mathbf{k},\omega) \sim \frac{1}{(i\omega)^2}\left(n_0\Gamma(\mathbf{k},\omega) - G^0_{\mathrm{B}}(\mathbf{k},-\omega)\int\frac{\mathrm{d}\mathbf{P}}{(2\pi)^2}\int\frac{\mathrm{d}\Omega}{2\pi}\,T(\mathbf{P},\Omega)\mathrm{e}^{i\Omega 0^+}\right) \qquad \text{(A.14)}$$

for large ω, and therefore decreases as $1/(\omega^2 \ln\omega)$. Note that we have used the asymptotic formula (A.3) for the self-energy at large ω. The frequency cutoff ω_{c} is set to 50000 E_{F} so to make the contributions of the integrands negligible for $\omega > \omega_{\mathrm{c}}$. In the range 100 $E_{\mathrm{F}} < \omega < \omega_{\mathrm{c}}$ the asymptotic expressions for the normal self-energies (A.3) and (A.4) are exploited, whereas the asymptotic expression for the anomalous self-energy (A.10) is employed in the range 50 $E_{\mathrm{F}} < \omega < \omega_{\mathrm{c}}$.

Finally, the densities are obtained integrating over the momentum $\mathbf{k}$. The integral over $|\mathbf{k}|$ is separated in two ranges $[0, k_{\mathrm{c}}] \cup (k_{\mathrm{c}}, \infty)$. The cutoff k_{c} is chosen in such a way that in the large-momentum range (k_{c}, ∞) one can use the asymptotic expressions

$$n^{(k\gg k_{\mathrm{F}})}_{\mathrm{F}}(\mathbf{k}) = \frac{1}{(\mathbf{k}^2/(2m_{\mathrm{r}}) - \mu_{\mathrm{B}} - \mu_{\mathrm{F}})^2}\int\frac{\mathrm{d}\mathbf{P}}{(2\pi)^2}\int\frac{\mathrm{d}\Omega}{2\pi}\,T(\mathbf{P},\Omega)\mathrm{e}^{i\Omega 0^+} \qquad \text{(A.15)}$$

$$n^{(k\gg k_{\mathrm{F}})}_{\mathrm{B}}(\mathbf{k}) = \frac{1}{(\mathbf{k}^2/(2m_{\mathrm{r}}) - \mu_{\mathrm{B}} - \mu_{\mathrm{F}})^2}\int\frac{\mathrm{d}\mathbf{P}}{(2\pi)^2}\int\frac{\mathrm{d}\Omega}{2\pi}\,T(\mathbf{P},\Omega)\mathrm{e}^{i\Omega 0^+} + \frac{\left(\Sigma^{12}_{\mathrm{BB}}\right)^2}{4(\mathbf{k}^2/(2m_{\mathrm{B}}) - \mu_{\mathrm{B}})^2}. \qquad \text{(A.16)}$$

In particular, we set $k_{\mathrm{c}} = 4\,k_{\mathrm{F}}$.

Appendix B

Series expansions under the integral sign

This appendix discusses series expansions within (2+1)-momentum integrals. In particular, we examine the conditions under which the T-matrix and the fermion Green's function can be represented as convergent geometric series. The goal is to rigorously justify the expressions (3.80) and (3.95), which were obtained by expanding the T and the $G_{\rm F}$ without explicitly addressing the convergence of the resulting series.

B.1 Boson chemical potential

We are interested in computing

$$\Sigma^{11}_{\rm BF}(\mathbf{0},0) = \int^{P_{\rm T0}} \frac{{\rm d}\mathbf{P}}{(2\pi)^2} \int \frac{{\rm d}\Omega}{2\pi}\, T(\mathbf{P},\Omega) G^0_{\rm F}(\mathbf{P},\Omega) {\rm e}^{i\Omega 0^+}, \tag{B.1}$$

the notation $\int^{P_{\rm T0}} {\rm d}\mathbf{P}\,(\ldots)$ means that the integral over $|\mathbf{P}|$ is performed over the sphere $|\mathbf{P}| < P_{\rm T0}$.

At a given frequency Ω, a sufficient condition to grant the convergence of the geometric series

$$S(\mathbf{P},\Omega) = \mathit{\Gamma}(\mathbf{P},\Omega) \sum_{n=0}^{\infty} \left(n_0 G^0_{\rm F}(\mathbf{P},\Omega)\, \mathit{\Gamma}(\mathbf{P},\Omega)\right)^n \tag{B.2}$$

is given by

$$0 < |\mathbf{P}| < \sqrt{2m_{\rm F}\left(\mu_{\rm F} - n_0 |\mathit{\Gamma}(\mathbf{P},\Omega)|\right)}, \tag{B.3}$$

since in this case $(\mathbf{P},\Omega)$ is out of the set

$$\{(\mathbf{P},\Omega) : |i\Omega - \xi^{\rm F}_{\mathbf{P}}| \leq n_0 |\mathit{\Gamma}(\mathbf{P},\Omega)|\} \tag{B.4}$$

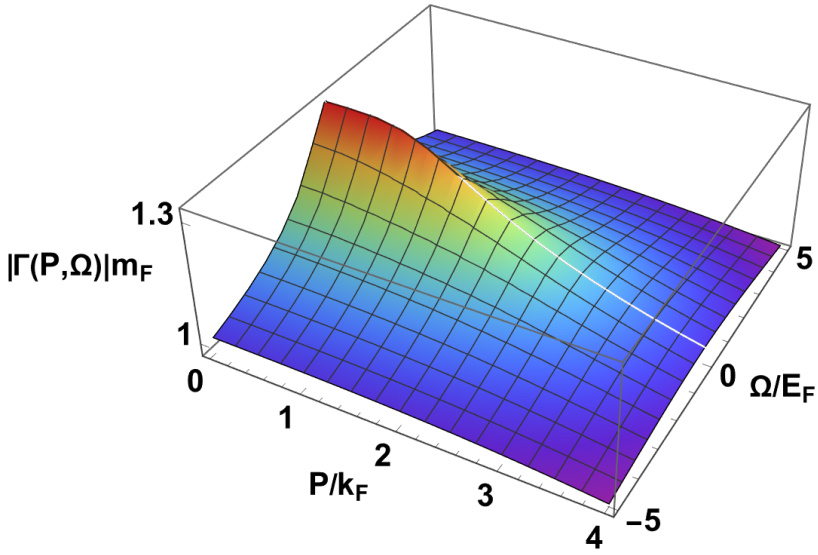

Figure B.1: Plot of $|\Gamma(P,\Omega)|$ in units of $1/m_{\rm F}$ as a function of $(P/k_{\rm F}, \Omega/E_{\rm F})$, in the case of $x = 1$, $\gamma_{\rm m} = 2$, $g = -4$. Input parameters: $\mu_{\rm B} = -0.20\, E_{\rm F}$, $\mu_{\rm F} = 0.83\, E_{\rm F}$, $n_0 = 0.96\, n_{\rm F}$.

where the series diverges. At the points $(\mathbf{P}, \Omega)$ where $S(\mathbf{P}, \Omega)$ is convergent, $S(\mathbf{P}, \Omega)$ coincides with $T(\mathbf{P}, \Omega)$. Therefore, for such points $T(\mathbf{P}, \Omega)$ can be approximated in perturbation theory by a finite number of terms of (B.2).

Since $|\Gamma(\mathbf{P}, \Omega)|$ is even in Ω and decreasing in $|\Omega|$ (see for instance Fig. B.1), inequality (B.3) implies that

$$0 < |\mathbf{P}| < \sqrt{2m_{\rm F}\left(\mu_{\rm F} - n_0 |\Gamma(\mathbf{P}, 0^+)|\right)} \tag{B.5}$$

is another sufficient condition on $\mathbf{P}$ for $T(\mathbf{P}, \Omega)$ to be expanded perturbatively, now independent of Ω. We define $P_{\rm gs}$ to be the solution to the equation

$$|\mathbf{P}| - \sqrt{2m_{\rm F}\left(\mu_{\rm F} - n_0 |\Gamma(\mathbf{P}, 0^+)|\right)} = 0. \tag{B.6}$$

In the range $[P_{\rm gs}, P_{\rm T0}]$ we are not allowed to expand the T-matrix for all momenta and frequencies. To order $1/g$

$$P_{\rm gs} = \sqrt{2m_{\rm F}\left(\mu_{\rm F} + \mu_{\rm F}^{(1)}\right)} \tag{B.7}$$

$$P_{\rm T0} = \sqrt{2m_{\rm F}\left(\mu_{\rm F} - \mu_{\rm F}^{(1)}\right)}, \tag{B.8}$$

as shown in Fig. B.2 for $\gamma_{\rm m} = 2$ and several values for the boson concentration x.

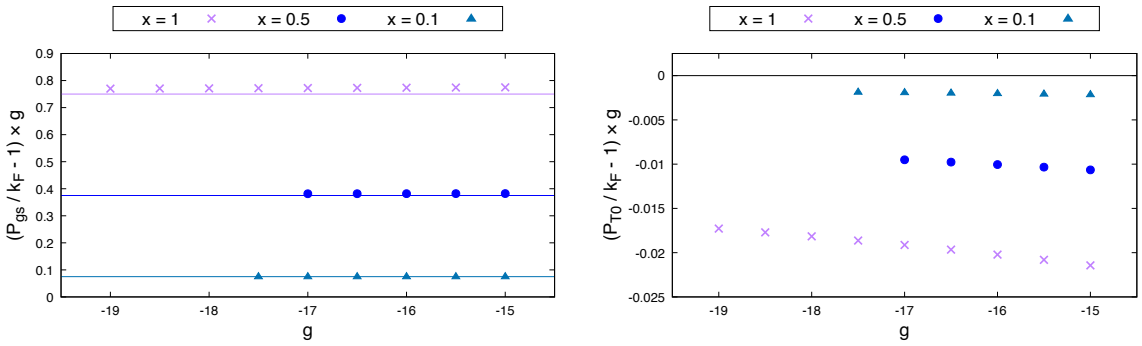

(a) (b)

Figure B.2: Points represent the momenta $P_{\rm gs}/k_{\rm F}$ (a) and $P_{\rm T0}/k_{\rm F}$ (b) as functions of the BF coupling g, after subtracting the leading order contribution and multiplying by g. The data are obtained for the mass ratio $\gamma_{\rm m} = 2$. The colored lines in (a) represent the expected values $a_{P_{\rm gs}}$ for $(P_{\rm gs}/k_{\rm F} - 1)g$ in the limit $g \to -\infty$, i.e. $a_{P_{\rm gs}} = (\mu_{\rm F}^{(1)} g)/E_{\rm F}$. The black line in (b) represents the expected value $a_{P_{\rm T0}}$ for $(P_{\rm T0}/k_{\rm F} - 1)g$ in the limit $g \to -\infty$, i.e. $a_{P_{\rm T0}} = 0$. The asymptotes $a_{P_{\rm gs}}$ and $a_{P_{\rm T0}}$ are easily read off from (B.7) and (B.8) respectively.

The momentum integral from 0 to $P_{\rm gs}$ can be performed following the same steps discussed in Sec. 3.4.3, and yields[1]

$$\int^{P_{\rm gs}} \frac{{\rm d}\mathbf{P}}{(2\pi)^2} \int \frac{{\rm d}\Omega}{2\pi}\, T(\mathbf{P},\Omega) G_{\rm F}^0(\mathbf{P},\Omega) {\rm e}^{i\Omega 0^+}$$
$$= E_{\rm F}\, \frac{1}{2}\frac{\gamma_{\rm m}+1}{\gamma_{\rm m}\, g}\left(1 + \frac{1}{2g}\left(2x\,\frac{\gamma_{\rm m}+1}{\gamma_{\rm m}} + \frac{\gamma_{\rm m}\ln\left(\gamma_{\rm m}^2\right)}{\gamma_{\rm m}-1} - \ln\left((\gamma_{\rm m}+1)^2\right) - 1\right)\right) + \text{ higher orders.} \quad \text{(B.9)}$$

The integral from $P_{\rm gs}$ to $P_{\rm T0}$ is instead given by

$$I \equiv \int_{P_{\rm gs}}^{P_{\rm T0}} \frac{{\rm d}P}{2\pi} \int \frac{{\rm d}\Omega}{2\pi}\, P\, \frac{\Gamma(P,\Omega)}{i\Omega - P^2/(2m_{\rm F}) + \mu_{\rm F} - n_0\Gamma(P,\Omega)} {\rm e}^{i\Omega 0^+}$$
$$= -\,E_{\rm F}\frac{x}{2}\left(\frac{\gamma_{\rm m}+1}{\gamma_{\rm m}}\right)^2 \frac{1}{g^2} + \text{ higher orders,} \quad \text{(B.10)}$$

employing the notation $P \equiv |\mathbf{P}|$.
To show that (B.10) holds, it is sufficient to approximate n_0 with $n_{\rm B}$ and $\Gamma(P,\Omega)$ with the first order term $\Gamma^{(1)} = \pi/(m_{\rm r}\, g)$. The reason is the following:

- when $|\Omega|$ is large, namely

$$|\Omega| > |P^2/(2m_{\rm F}) - \mu_{\rm F} + n_0\Gamma(P,\Omega)|,$$

[1] Note that, since $P_{\rm gs} < k_{\mu_{\rm F}}$, $\int {\rm d}\Omega\, (1/(i\Omega - \xi_{\mathbf{P}}^{\rm F}))^2 = 0$ and there is no need to introduce an infinitesimal momentum $\mathbf{k}$ to make sense of its singular behavior.

the leading term in the denominator is $i\Omega$:

$$\frac{1}{i\Omega - P^2/(2m_{\rm F}) + \mu_{\rm F} - n_0\Gamma(P,\Omega)} = \frac{1}{i\Omega}\left(1 + \frac{P^2/(2m_{\rm F}) - \mu_{\rm F} + n_0\Gamma(P,\Omega)}{i\Omega} + \dots\right) = \frac{1}{i\Omega} + \mathrm{O}\left(\frac{1}{g}\right). \tag{B.11}$$

As a consequence, the lowest order in $1/g$ of the integral is set by the product of the Γ at the numerator of $\Gamma(P,\Omega)/\big(i\Omega - P^2/(2m_{\rm F}) + \mu_{\rm F} - n_0\Gamma(P,\Omega)\big)$ with the variation, in the integration domain, of the momentum squared $\Delta\left(P^2\right) = \left(P_{\rm T0}\right)^2 - \left(P_{\rm gs}\right)^2$. That is, $\Delta\left(P^2\right)\Gamma(P,\Omega) = \mathrm{O}(1/g^2)$, already with $\Gamma(P,\Omega) = \Gamma^{(1)}$. In symbols

$$I\big|_{\text{large }|\Omega|} \approx \frac{1}{4\pi}\Delta\left(P^2\right)\Gamma^{(1)}\int_{\text{large }|\Omega|}\frac{\mathrm{d}\Omega}{2\pi}\left(\frac{1}{i\Omega} + \dots\right) + \text{higher orders.} \tag{B.12}$$

- When $|\Omega|$ is small, namely

$$|\Omega| \le |P^2/(2m_{\rm F}) - \mu_{\rm F} + n_0\Gamma(P,\Omega)| = \mathrm{O}\left(1/g\right), \tag{B.13}$$

the denominator $i\Omega - P^2/(2m_{\rm F}) + \mu_{\rm F} - n_0\Gamma(P,\Omega)$ is of order $1/g$. The inequality (B.13) implicitly determines the extrema of the restricted domain for the frequency integral, and we denote the difference between the upper and the lower extrema by $\Delta\Omega$. Note that the leading order of the frequency integral is a constant in $1/g$ already with n_0 set to $n_{\rm B}$ and $\Gamma(P,\Omega)$ set to $\Gamma^{(1)}$. Indeed, both $\Delta\Omega$ and $i\Omega - P^2/(2m_{\rm F}) + \mu_{\rm F} - n_{\rm B}\Gamma^{(1)}$ are of order $\mathrm{O}(1/g)$, and the two are divided one by the other. Therefore, the lowest order in $1/g$ again comes from $\Delta\left(P^2\right)\Gamma^{(1)} = \mathrm{O}(1/g^2)$. In symbols (with P and Ω now representing suitable points chosen in the integration domain)

$$I\big|_{\text{small }|\Omega|} \approx \frac{1}{8\pi^2}\Delta\left(P^2\right)\Gamma^{(1)}\frac{\Delta\Omega}{i\Omega - P^2/(2m_{\rm F}) + \mu_{\rm F} - n_{\rm B}\Gamma^{(1)}} + \text{higher orders.} \tag{B.14}$$

Evidently, the same argument shows that to calculate I at $\mathrm{O}(1/g^2)$ it is sufficient to evaluate $\Delta\left(P^2\right)$ at $\mathrm{O}(1/g)$, which amounts to approximate the extrema of the momentum integration by (B.7) and (B.8).

All in all, up to higher orders:

$$I = \frac{\mu_{\rm F}^{(1)}}{n_{\rm B}}\int_{\sqrt{2m_{\rm F}\left(\mu_{\rm F}+\mu_{\rm F}^{(1)}\right)}}^{\sqrt{2m_{\rm F}\left(\mu_{\rm F}-\mu_{\rm F}^{(1)}\right)}}\frac{\mathrm{d}P}{2\pi}\,P\,\Theta\left(\sqrt{2m_{\rm F}\left(\mu_{\rm F}-\mu_{\rm F}^{(1)}\right)} - P\right)$$
$$= \frac{1}{g}\frac{\pi}{m_{\rm F}}\frac{\gamma_{\rm m}+1}{\gamma_{\rm m}}\,k_{\rm F}^2\int_{\sqrt{\left(\mu_{\rm F}+\mu_{\rm F}^{(1)}\right)/E_{\rm F}}}^{\sqrt{\left(\mu_{\rm F}-\mu_{\rm F}^{(1)}\right)/E_{\rm F}}}\frac{\mathrm{d}\widetilde{P}}{2\pi}\,\widetilde{P} = \frac{\gamma_{\rm m}+1}{2\gamma_{\rm m}}\left(-2\mu_{\rm F}^{(1)}\right)\frac{1}{g} = -E_{\rm F}\frac{x}{2}\left(\frac{\gamma_{\rm m}+1}{\gamma_{\rm m}}\right)^2\frac{1}{g^2}. \tag{B.15}$$

Note that when we sum I and (B.9) the concentration dependent terms cancel exactly, as it happened in our previous calculation in Sec. 3.4.3. Therefore the final take-away is that, up to orders higher than $\mathrm{O}(1/g^2)$, evaluating $\Sigma^{11}_{\mathrm{BF}}(\mathbf{0},0)$ as in (B.1) is equivalent to evaluating the same momentum integral but expanding the T-matrix as a geometric series in the whole (2+1)-momentum space, provided that we keep $\mathbf{k}$ finite throughout the calculation and take the limit $\mathbf{k}\to\mathbf{0}$ at the very end. In symbols (as always, up to orders higher than $\mathrm{O}(1/g^2)$)

$$\int \frac{\mathrm{d}\mathbf{P}}{(2\pi)^2}\int\frac{\mathrm{d}\Omega}{2\pi}\,T(\mathbf{P},\Omega)G^0_{\mathrm{F}}(\mathbf{P},\Omega)\mathrm{e}^{i\Omega 0^+} = \int\frac{\mathrm{d}\mathbf{P}}{(2\pi)^2}\left(\lim_{\mathbf{k}\to\mathbf{0}}\int\frac{\mathrm{d}\Omega}{2\pi}\,\left(\Gamma(\mathbf{P},\Omega)+n_0\Gamma(\mathbf{P},\Omega)^2G^0_{\mathrm{F}}(\mathbf{P},\Omega)\right)G^0_{\mathrm{F}}(\mathbf{P}-\mathbf{k},\Omega)\mathrm{e}^{i\Omega 0^+}\right). \tag{B.16}$$

A numerical check of the above argument can be found in Fig. B.3, for $\gamma_{\mathrm{m}}=2$ and several values for the boson concentration x. In particular, we report the quantities

$$\Sigma^1_{\mathrm{B}} \equiv \left(\int_0^{P_{\mathrm{gs}}}\frac{\mathrm{d}P}{2\pi}\int\frac{\mathrm{d}\Omega}{2\pi}\,P\,T(P,\Omega)G^0_{\mathrm{F}}(P,\Omega)\mathrm{e}^{i\Omega 0^+} - E_{\mathrm{F}}\frac{1}{2}\frac{\gamma_{\mathrm{m}}+1}{\gamma_{\mathrm{m}}\,g}\right)g^2 - E_{\mathrm{F}}\frac{1}{2}\frac{\gamma_{\mathrm{m}}+1}{\gamma_{\mathrm{m}}}\left(\frac{\gamma_{\mathrm{m}}\ln\left(\gamma_{\mathrm{m}}^2\right)}{\gamma_{\mathrm{m}}-1}-\ln\left((\gamma_{\mathrm{m}}+1)^2\right)-1\right), \tag{B.17}$$

i.e. the coefficient of the $\mathrm{O}(1/g^2)$, concentration-dependent term of (B.9), and

$$\Sigma^2_{\mathrm{B}} \equiv \left(\int_{P_{\mathrm{gs}}}^{P_{\mathrm{T0}}}\frac{\mathrm{d}P}{2\pi}\int\frac{\mathrm{d}\Omega}{2\pi}\,P\,T(P,\Omega)G^0_{\mathrm{F}}(P,\Omega)\mathrm{e}^{i\Omega 0^+}\right)g^2, \tag{B.18}$$

i.e. the integral $I\,g^2$. The integrals in Σ^1_{B} and Σ^2_{B} are performed numerically by Gauss-Legendre integration. In agreement with our analytical calculation, Fig. B.3 shows that $\Sigma^1_{\mathrm{B}}\approx-\Sigma^2_{\mathrm{B}}$.

B.2 Luttinger theorem and fermion chemical potential

Expansion of $\Sigma_{\mathrm{F}}(\mathbf{k},\omega)$

Let us now adapt the arguments developed for the boson chemical potential to the fermion case. In particular, we are interested in the fermion self-energy

$$\Sigma_{\mathrm{F}}(\mathbf{k},\omega) = -\int\frac{\mathrm{d}\mathbf{P}}{(2\pi)^2}\int\frac{\mathrm{d}\Omega}{2\pi}\,T(\mathbf{P},\Omega)G^0_{\mathrm{B}}(\mathbf{P}-\mathbf{k},\Omega-\omega)\mathrm{e}^{i\Omega 0^+}, \tag{B.19}$$

where we have dropped the term $n_0\Gamma(\mathbf{k},\omega)$ since here we want to focus on the expansion of the T-matrix.

The main difference with respect to the boson case is the replacement of the fermion Green's function with the boson Green's function $G^0_{\mathrm{B}}(\mathbf{P}-\mathbf{k},\Omega-\omega)$ in the convolution with the T-matrix.

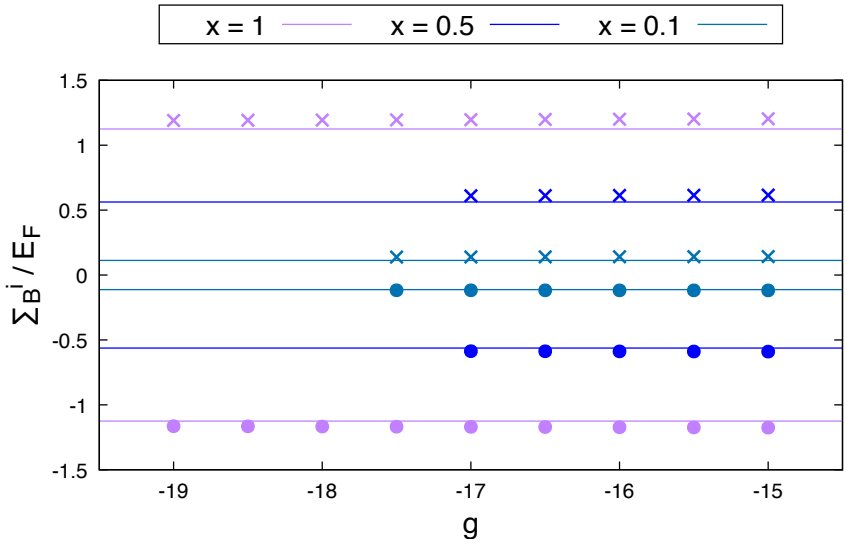

Figure B.3: The crosses represent $\Sigma^1_{\rm B}/E_{\rm F}$, while the circles $\Sigma^2_{\rm B}/E_{\rm F}$, for different values of the BF coupling g and the boson concentration x, and $\gamma_{\rm m}=2$. The lines represent the quantities $\pm((\gamma_{\rm m}+1)/\gamma_{\rm m})^2\, x/2$, i.e. the expected values in the $g\to-\infty$ limit for $\Sigma^1_{\rm B}/E_{\rm F}$ and $\Sigma^2_{\rm B}/E_{\rm F}$ respectively.

Carrying out the steps that we have discussed in the previous section, one deduces the contribution to $\Sigma_{\rm F}(\mathbf{k},\omega)$ from the momentum interval where the convergence of the geometric series is spoiled:

$$-\int_{P_{\rm gs}}^{P_{\rm T0}}\frac{{\rm d}P}{2\pi}\,P\int_0^{2\pi}\frac{{\rm d}\theta}{2\pi}\int\frac{{\rm d}\Omega}{2\pi}\,\frac{\mathit{\Gamma}(\mathbf{P},\Omega)}{i\Omega-\xi^{\rm F}_{\mathbf{P}}-n_0\mathit{\Gamma}(\mathbf{P},\Omega)}\,\frac{i\Omega-\xi^{\rm F}_{\mathbf{P}}}{i(\Omega-\omega)-\xi^{\rm B}_{\mathbf{P}-\mathbf{k}}}{\rm e}^{i\Omega 0^+}. \tag{B.20}$$

Observe that only the factor $\mathit{\Gamma}(\mathbf{P},\Omega)/\big(i\Omega-\xi^{\rm F}_{\mathbf{P}}-n_0\mathit{\Gamma}(\mathbf{P},\Omega)\big)$ exhibits a pole in the upper half of the complex plane, since the boson chemical potential in the denominator of the second factor is assumed negative.

The same argument that allowed us to replace $\mathit{\Gamma}(\mathbf{P},\Omega)$ with $\mathit{\Gamma}^{(1)}$ and n_0 with $n_{\rm B}$ in Sec. B.1 can be applied here, yielding

$$\begin{aligned}\int\frac{{\rm d}\Omega}{2\pi}\,\frac{\mathit{\Gamma}^{(1)}}{i\Omega-\xi^{\rm F}_{\mathbf{P}}-n_{\rm B}\mathit{\Gamma}^{(1)}}\,\frac{i\Omega-\xi^{\rm F}_{\mathbf{P}}}{i(\Omega-\omega)-\xi^{\rm B}_{\mathbf{P}-\mathbf{k}}}{\rm e}^{i\Omega 0^+}&\\ =\Theta\left(|\mathbf{P}|-P_{\rm T0}\right)\,\frac{n_{\rm B}\left(\mathit{\Gamma}^{(1)}\right)^2}{\xi^{\rm F}_{\mathbf{P}}-n_{\rm B}\mathit{\Gamma}^{(1)}-\xi^{\rm B}_{\mathbf{P}-\mathbf{k}}-i\omega}&=\mathrm{O}\left(\frac{1}{g^2}\right).\end{aligned} \tag{B.21}$$

This implies that the integral over the momentum interval $[P_{\rm gs},P_{\rm T0}]$ is of order higher than $\mathrm{O}(1/g^2)$, since $[P_{\rm gs},P_{\rm T0}]$ has width of order $1/g$. Hence, the contribution (B.20) is sub-leading in the fermion self-energy, which can therefore be evaluated treating the T-matrix as a convergent geometric series independently of the internal (2+1)-momentum $(\mathbf{P},\Omega)$. The perturbative approximation for $\Sigma_{\rm F}$ that

one obtains by inserting the T-matrix expanded at second order,[2]

$$\Sigma_{\rm F}(\mathbf{k},\omega) = \Sigma_{\rm F}^{(1)} + \Sigma_{\rm F}^{(2)}(\mathbf{k},\omega), \tag{B.22}$$

is valid irrespective of the external $(2+1)$-momentum $(\mathbf{k},\omega)$. We shall now use this result to prove the validity of Luttinger's theorem at $\mathrm{O}(1/g^2)$.

Luttinger's theorem

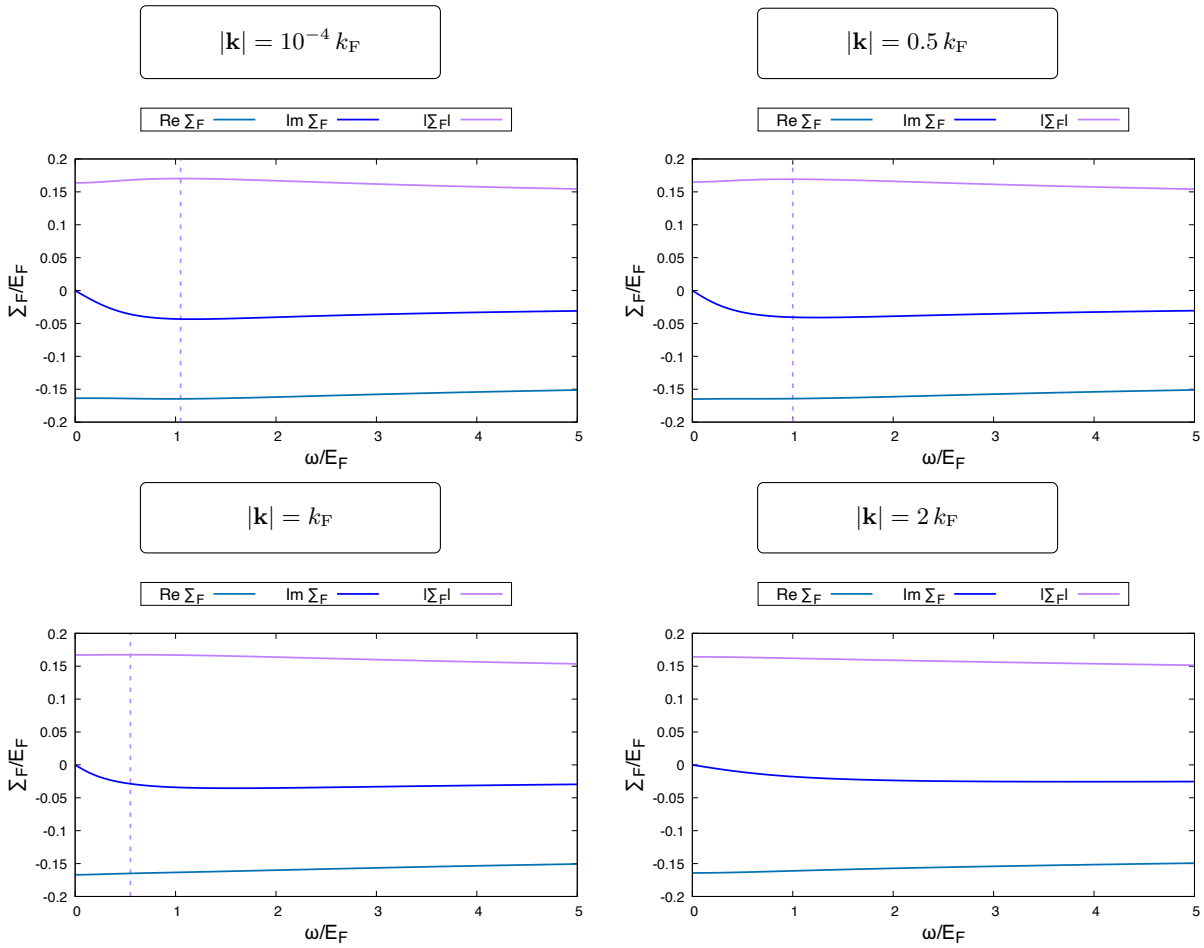

Figure B.4: Fermion self-energy in units of $E_{\rm F}$ as a function of $\omega/E_{\rm F}$, in the case of $x = 1$, $\gamma_{\rm m} = 2$, $g = -4$. The dashed line represent the frequency for which $|\Sigma_{\rm F}(\mathbf{k},\omega)|$ is at its maximum. Input parameters: $\mu_{\rm B} = -0.20\,E_{\rm F}$, $\mu_{\rm F} = 0.83\,E_{\rm F}, n_0 = 0.96\,n_{\rm F}$.

[2] Using the notation of the main text, (B.22) would be written as $\Sigma_{\rm F}(\mathbf{k},\omega\,|\,\mu_{\rm F},\mu_{\rm B}) = \Sigma_{\rm F}^{(1)} + \Sigma_{\rm F}^{(2)}(\mathbf{k},\omega\,|\,E_{\rm F},0)$.

Let us start from Dyson's equation for the fermion Green's function,

$$G_{\mathrm{F}}(\mathbf{k},\omega)=\frac{1}{i\omega-\xi^{\mathrm{F}}_{\mathbf{k}}}\frac{1}{1-\Sigma_{\mathrm{F}}(\mathbf{k},\omega)/(i\omega-\xi^{\mathrm{F}}_{\mathbf{k}})}. \tag{B.23}$$

At a given ω, a sufficient condition on $\mathbf{k}$ for $1/\big(1-\Sigma_{\mathrm{F}}(\mathbf{k},\omega)/(i\omega-\xi^{\mathrm{F}}_{\mathbf{k}})\big)$ to be expanded as a convergent geometric series is

$$\left|\frac{\mathbf{k}^2}{2m_{\mathrm{F}}}-\mu_{\mathrm{F}}\right|>|\Sigma_{\mathrm{F}}(\mathbf{k},\omega)|, \tag{B.24}$$

which implies the following:

$$|\mathbf{k}|<\sqrt{2m_{\mathrm{F}}(\mu_{\mathrm{F}}-|\Sigma_{\mathrm{F}}(\mathbf{k},\omega)|)}\ \text{ if } |\mathbf{k}|<k_{\mu_{\mathrm{F}}} \tag{B.25}$$

$$|\mathbf{k}|>\sqrt{2m_{\mathrm{F}}(\mu_{\mathrm{F}}+|\Sigma_{\mathrm{F}}(\mathbf{k},\omega)|)}\ \text{ if } |\mathbf{k}|>k_{\mu_{\mathrm{F}}}. \tag{B.26}$$

$|\Sigma_{\mathrm{F}}(\mathbf{k},\omega)|$ is even in ω and for sufficiently large $|\mathbf{k}|$ is decreasing in $|\omega|$ (see Fig. B.4(d)). For smaller $|\mathbf{k}|$, it is decreasing in $|\omega|$ only for $|\omega|>\omega_{\max}>0$ (see Figures B.4(a), B.4(b), B.4(c)). Using this observation, (B.25) and (B.26) lead to the weaker condition

$$|\mathbf{k}|<\sqrt{2m_{\mathrm{F}}\left(\mu_{\mathrm{F}}-|\Sigma_{\mathrm{F}}\left(\mathbf{k},\omega_{\max}\left(\mathbf{k}\right)\right)|\right)}\ \text{ if } |\mathbf{k}|<k_{\mu_{\mathrm{F}}} \tag{B.27}$$

$$|\mathbf{k}|>\sqrt{2m_{\mathrm{F}}\left(\mu_{\mathrm{F}}+|\Sigma_{\mathrm{F}}\left(\mathbf{k},\omega_{\max}\left(\mathbf{k}\right)\right)|\right)}\ \text{ if } |\mathbf{k}|>k_{\mu_{\mathrm{F}}}. \tag{B.28}$$

We define k_{gs1} and k_{gs2} as the solutions to the equations

$$|\mathbf{k}|-\sqrt{2m_{\mathrm{F}}\left(\mu_{\mathrm{F}}\mp|\Sigma_{\mathrm{F}}\left(\mathbf{k},\omega_{\max}\left(\mathbf{k}\right)\right)|\right)}=0$$

respectively, and $\omega_{\mathrm{gs1}}\equiv\omega_{\max}(k_{\mathrm{gs1}})$, $\omega_{\mathrm{gs2}}\equiv\omega_{\max}(k_{\mathrm{gs2}})$.

By taking the trace $(2\pi)^{-3}\int \mathrm{d}\mathbf{P}\int \mathrm{d}\Omega\ (\ldots)\mathrm{e}^{i\omega 0^+}$ of the Green's function G_{F} and expanding the latter as a geometric series where possible, one reaches the following equation for the fermion density:

$$\begin{aligned}n_{\mathrm{F}}=&\int_{\mathbb{R}^+\setminus[k_{\mathrm{gs1}},k_{\mathrm{gs2}}]}\frac{\mathrm{d}k}{2\pi}\,k\int\frac{\mathrm{d}\omega}{2\pi}\,G^0_{\mathrm{F}}(\mathbf{k},\omega)\left(1+G^0_{\mathrm{F}}(\mathbf{k},\omega)\Sigma_{\mathrm{F}}(\mathbf{k},\omega)+G^0_{\mathrm{F}}(\mathbf{k},\omega)^2\Sigma_{\mathrm{F}}(\mathbf{k},\omega)^2\right)\mathrm{e}^{i\omega 0^+}\\&+\int_{k_{\mathrm{gs1}}}^{k_{\mathrm{gs2}}}\frac{\mathrm{d}k}{2\pi}\,k\int\frac{\mathrm{d}\omega}{2\pi}\,G^0_{\mathrm{F}}(\mathbf{k},\omega)\frac{1}{1-G^0_{\mathrm{F}}(\mathbf{k},\omega)\Sigma_{\mathrm{F}}(\mathbf{k},\omega)}\mathrm{e}^{i\omega 0^+}+\ \text{higher orders.}\end{aligned} \tag{B.29}$$

Since $k_{\mathrm{gs1}}<k_{\mu_{\mathrm{F}}}$ and $k_{\mathrm{gs2}}>k_{\mu_{\mathrm{F}}}$, the first line yields

$$\begin{aligned}&\int_{\mathbb{R}^+\setminus[k_{\mathrm{gs1}},k_{\mathrm{gs2}}]}\frac{\mathrm{d}k}{2\pi}\,k\int\frac{\mathrm{d}\omega}{2\pi}\,G^0_{\mathrm{F}}(\mathbf{k},\omega)\left(1+G^0_{\mathrm{F}}(\mathbf{k},\omega)\Sigma_{\mathrm{F}}(\mathbf{k},\omega)+G^0_{\mathrm{F}}(\mathbf{k},\omega)^2\Sigma_{\mathrm{F}}(\mathbf{k},\omega)^2\right)\mathrm{e}^{i\omega 0^+}\\&=\frac{k^2_{\mathrm{gs1}}}{4\pi}+\int_{\mathbb{R}^+\setminus[k_{\mathrm{gs1}},k_{\mathrm{gs2}}]}\frac{\mathrm{d}k}{2\pi}\,k\int\frac{\mathrm{d}\omega}{2\pi}\,G^0_{\mathrm{F}}(\mathbf{k},\omega)^2\Sigma^{(2)}_{\mathrm{F}}(\mathbf{k},\omega)+\ \text{higher orders.}\end{aligned} \tag{B.30}$$

Here, we have expanded the fermion self-energy as discussed for (B.22). Moreover, by definition

of k_{gs1}

$$k_{\mathrm{gs1}}^2 = 2m_{\mathrm{F}} \left(\mu_{\mathrm{F}} - |\Sigma_{\mathrm{F}} \left(k_{\mathrm{gs1}}, \omega_{\mathrm{gs1}}\right)|\right). \tag{B.31}$$

Plugging these expressions inside the equation for the fermion density and isolating μ_{F}, we obtain the following self-consistent equation for the fermion chemical potential, valid up to orders higher than $\mathrm{O}(1/g^2)$:

$$\mu_{\mathrm{F}} = E_{\mathrm{F}} - \left(\frac{2\pi}{m_{\mathrm{F}}} I_1 - |\Sigma_{\mathrm{F}} \left(k_{\mathrm{gs1}}, \omega_{\mathrm{gs1}}\right)|\right) - \frac{2\pi}{m_{\mathrm{F}}} I_2, \tag{B.32}$$

where we have defined

$$I_1 \equiv \int_{k_{\mathrm{gs1}}}^{k_{\mathrm{gs2}}} \frac{\mathrm{d}k}{2\pi}\, k \int \frac{\mathrm{d}\omega}{2\pi}\, G_{\mathrm{F}}^0(\mathbf{k}, \omega) \frac{1}{1 - G_{\mathrm{F}}^0(\mathbf{k}, \omega)\Sigma_{\mathrm{F}}(\mathbf{k}, \omega)} \mathrm{e}^{i\omega 0^+} \tag{B.33}$$

$$I_2 \equiv \int_{\mathbb{R}^+ \setminus [k_{\mathrm{gs1}}, k_{\mathrm{gs2}}]} \frac{\mathrm{d}k}{2\pi}\, k \int \frac{\mathrm{d}\omega}{2\pi}\, G_{\mathrm{F}}^0(\mathbf{k}, \omega)^2 \Sigma_{\mathrm{F}}^{(2)}(\mathbf{k}, \omega). \tag{B.34}$$

Note that the Fermi step momentum $\widetilde{k}_{\mathrm{F}} > k_{\mathrm{gs1}}$, as can be seen by comparing their approximations at the first order in $1/g$; furthermore, we observe that $\widetilde{k}_{\mathrm{F}} \leq k_{\mathrm{gs2}}$. Indeed,

$$|\Sigma_{\mathrm{F}} \left(k_{\mathrm{gs2}}, \omega_{\mathrm{gs2}}\right)| \geq \left|\Sigma_{\mathrm{F}} \left(k_{\mathrm{gs2}}, 0^+\right)\right| = \left|\Sigma_{\mathrm{F}} \left(\widetilde{k}_{\mathrm{F}}, 0^+\right)\right|, \tag{B.35}$$

where the last equality holds up to orders higher than $\mathrm{O}(1/g^2)$; therefore,

$$k_{\mathrm{gs2}} = \sqrt{2m_{\mathrm{F}} \left(\mu_{\mathrm{F}} + |\Sigma_{\mathrm{F}} \left(k_{\mathrm{gs2}}, \omega_{\mathrm{gs2}}\right)|\right)} \geq \sqrt{2m_{\mathrm{F}} \left(\mu_{\mathrm{F}} + \left|\Sigma_{\mathrm{F}} \left(\widetilde{k}_{\mathrm{F}}, 0^+\right)\right|\right)} = \widetilde{k}_{\mathrm{F}}. \tag{B.36}$$

This shows that the momentum interval of I_1, $[k_{\mathrm{gs1}}, k_{\mathrm{gs2}}]$, contains the Fermi step momentum $\widetilde{k}_{\mathrm{F}}$. Consequently, the frequency integral in I_1 yields

$$\int \frac{\mathrm{d}\omega}{2\pi} \frac{1}{i\omega - k^2/(2m_{\mathrm{F}}) + \mu_{\mathrm{F}} - \Sigma_{\mathrm{F}}(k, \omega)} \mathrm{e}^{i\omega 0^+} = \Theta\left(\widetilde{k}_{\mathrm{F}} - k\right) + \mathrm{O}\left(\frac{1}{g^2}\right). \tag{B.37}$$

This result is justified as follows: a correction of order $1/g$ could only come from the first order $\Sigma_{\mathrm{F}}^{(1)}$ of $\Sigma_{\mathrm{F}}(k, \omega)$; such a correction is however not present, since $\Sigma_{\mathrm{F}}^{(1)}$ is constant in (k, ω) and inserting it in the integral yields

$$\int \frac{\mathrm{d}\omega}{2\pi} \frac{1}{i\omega - k^2/(2m_{\mathrm{F}}) + \mu_{\mathrm{F}} - \Sigma_{\mathrm{F}}^{(1)}} \mathrm{e}^{i\omega 0^+} = \Theta\left(\sqrt{2m_{\mathrm{F}}(\mu_{\mathrm{F}} - \Sigma_{\mathrm{F}}^{(1)})} - k\right), \tag{B.38}$$

a step of unit height.

(B.37) is all we need to know to derive an estimate of μ_{F} at $\mathrm{O}(1/g^2)$, since the interval $[k_{\mathrm{gs1}}, k_{\mathrm{gs2}}]$

has width of order $1/g$. Plugging (B.37) inside I_1 we get, up to orders higher than $\mathrm{O}(1/g^2)$,

$$I_1 = -\frac{m_{\mathrm{F}}}{2\pi}\left(\Sigma_{\mathrm{F}}\left(\widetilde{k}_{\mathrm{F}}, 0^+\right) - \left|\Sigma_{\mathrm{F}}\left(k_{\mathrm{gs1}}, \omega_{\mathrm{gs1}}\right)\right|\right). \tag{B.39}$$

Let us now move to the evaluation of I_2, which reads

$$I_2 = \int' \frac{\mathrm{d}\mathbf{k}}{(2\pi)^2}\int \frac{\mathrm{d}\omega}{2\pi}\, \mathrm{e}^{i\omega 0^+}\left(\frac{1}{i\omega - \xi^{\mathrm{F}}_{\mathbf{k}}}\right)^2\Bigg(n_{\mathrm{B}}\Gamma^{(2)}(\mathbf{k},\omega) \tag{B.40}$$

$$- \int \frac{\mathrm{d}\mathbf{P}}{(2\pi)^2}\int \frac{\mathrm{d}\Omega}{2\pi}\, \Gamma^{(2)}(\mathbf{P},\Omega)\frac{1}{i(\Omega-\omega) - \xi^{\mathrm{B}}_{\mathbf{P}-\mathbf{k}}}\mathrm{e}^{i\Omega 0^+} \tag{B.41}$$

$$- n_{\mathrm{B}}\big(\Gamma^{(1)}\big)^2 \int \frac{\mathrm{d}\mathbf{P}}{(2\pi)^2}\int \frac{\mathrm{d}\Omega}{2\pi}\, \frac{1}{i\Omega - \xi^{\mathrm{F}}_{\mathbf{P}}}\frac{1}{i(\Omega-\omega) - \xi^{\mathrm{B}}_{\mathbf{P}-\mathbf{k}}}\mathrm{e}^{i\Omega 0^+}\Bigg), \tag{B.42}$$

where, in Γ and in the Green's functions, the fermion chemical potential is set to E_{F} and the boson one to 0^-. The notation $\int' \mathrm{d}\mathbf{k}\,(\ldots)$ indicates that the integration over $|\mathbf{k}|$ is performed on $\mathbb{R}^+ \setminus A_{k_{\mathrm{F}}}$, where $A_{k_{\mathrm{F}}}$ is an interval of infinitesimal width centered at k_{F}. These approximations for the chemical potentials and for the integration domain are justified by the fact that I_2 is already of order $1/g^2$; therefore, higher-order corrections in μ_{F}, μ_{B}, k_{gs1} and k_{gs2} would contribute only at orders higher than $1/g^2$.

The frequency integral of (B.40),

$$\int \frac{\mathrm{d}\omega}{2\pi}\left(\frac{1}{i\omega - \xi^{\mathrm{F}}_{\mathbf{k}}}\right)^2 \Gamma^{(2)}(\mathbf{k},\omega)\mathrm{e}^{i\omega 0^+}, \tag{B.43}$$

receives a contribution only from the frequency dependent term of (3.51), since the integral of the counter-term vanishes as the residue at its only pole $\omega = -i\xi^{\mathrm{F}}_{\mathbf{k}}$ is zero.[3] Hence, we shall compute

$$\begin{aligned}\int \frac{\mathrm{d}\omega}{2\pi}\left(\frac{1}{i\omega - \xi^{\mathrm{F}}_{\mathbf{k}}}\right)^2 \frac{\Theta(-\xi^{\mathrm{F}}_{\mathbf{k}-\mathbf{q}}) - 1}{\xi^{\mathrm{F}}_{\mathbf{k}-\mathbf{q}} + \xi^{\mathrm{B}}_{\mathbf{q}} - i\omega}\mathrm{e}^{i\omega 0^+} \\ = \Theta(\xi^{\mathrm{F}}_{\mathbf{k}-\mathbf{q}})\int \frac{\mathrm{d}\omega}{2\pi}\left(\frac{1}{i\omega - \xi^{\mathrm{F}}_{\mathbf{k}}}\right)^2 \frac{\Theta(\xi^{\mathrm{F}}_{\mathbf{k}-\mathbf{q}} + \xi^{\mathrm{B}}_{\mathbf{q}})}{i\omega - \xi^{\mathrm{F}}_{\mathbf{k}-\mathbf{q}} - \xi^{\mathrm{B}}_{\mathbf{q}}}\mathrm{e}^{i\omega 0^+},\end{aligned} \tag{B.44}$$

where we introduced the redundant $\Theta(\xi^{\mathrm{F}}_{\mathbf{k}-\mathbf{q}}+\xi^{\mathrm{B}}_{\mathbf{q}})$ to highlight the fact that we get a contribution only if the pole $\omega = -i(\xi^{\mathrm{F}}_{\mathbf{k}-\mathbf{q}} + \xi^{\mathrm{B}}_{\mathbf{q}})$ lies on the negative imaginary axis since $\Theta(\xi^{\mathrm{F}}_{\mathbf{k}-\mathbf{q}})\Theta(-\xi^{\mathrm{F}}_{\mathbf{k}-\mathbf{q}} - \xi^{\mathrm{B}}_{\mathbf{q}}) = 0$. By closing the contour in the upper half-plane, encircling only the pole $\omega = -i\xi^{\mathrm{F}}_{\mathbf{k}}$ when it lies on the

[3] Notice the importance of k_{F} not belonging to the integration domain.

positive imaginary axis:

$$\begin{aligned}\int \frac{\mathrm{d}\omega}{2\pi}\left(\frac{1}{i\omega-\xi^{\mathrm{F}}_{\mathbf{k}}}\right)^2 \frac{\Theta(-\xi^{\mathrm{F}}_{\mathbf{k}-\mathbf{q}})-1}{\xi^{\mathrm{F}}_{\mathbf{k}-\mathbf{q}}+\xi^{\mathrm{B}}_{\mathbf{q}}-i\omega}\mathrm{e}^{i\omega 0^+}&\\ = i\Theta(|\mathbf{k}-\mathbf{q}|-k_{\mathrm{F}})\Theta\left(k_{\mathrm{F}}-|\mathbf{k}|\right)\mathrm{Res}\left(\left(\frac{1}{i\omega-\xi^{\mathrm{F}}_{\mathbf{k}}}\right)^2\frac{1}{i\omega-\xi^{\mathrm{F}}_{\mathbf{k}-\mathbf{q}}-\xi^{\mathrm{B}}_{\mathbf{q}}},\omega=-i\xi^{\mathrm{F}}_{\mathbf{k}}\right)&\\ = -\Theta(|\mathbf{k}-\mathbf{q}|-k_{\mathrm{F}})\Theta\left(k_{\mathrm{F}}-|\mathbf{k}|\right)\left(\frac{1}{\xi^{\mathrm{F}}_{\mathbf{k}}-\xi^{\mathrm{F}}_{\mathbf{k}-\mathbf{q}}-\xi^{\mathrm{B}}_{\mathbf{q}}}\right)^2.&\end{aligned} \tag{B.45}$$

The contribution to I_2 stemming from (B.40) is thus the double momentum integral

$$I_2^{[\mathrm{I}]}\equiv -\frac{1}{g^2}\frac{n_{\mathrm{B}}\pi^2}{m_{\mathrm{r}}^2}\int\frac{\mathrm{d}\mathbf{k}}{(2\pi)^2}\int\frac{\mathrm{d}\mathbf{q}}{(2\pi)^2}\,\Theta(|\mathbf{k}-\mathbf{q}|-k_{\mathrm{F}})\Theta\left(k_{\mathrm{F}}-|\mathbf{k}|\right)\left(\frac{1}{\xi^{\mathrm{F}}_{\mathbf{k}}-\xi^{\mathrm{F}}_{\mathbf{k}-\mathbf{q}}-\xi^{\mathrm{B}}_{\mathbf{q}}}\right)^2, \tag{B.46}$$

where we have dropped the prime on $\int \mathrm{d}\mathbf{k}\,(\ldots)$ due to the factor $\Theta\left(k_{\mathrm{F}}-|\mathbf{k}|\right)$, which prevents the integration from crossing $k=k_{\mathrm{F}}$.

The term from (B.41) vanishes since the integral over Ω is zero. The integral over Ω of (B.42) instead reads

$$\int\frac{\mathrm{d}\Omega}{2\pi}\,\frac{1}{i\Omega-\xi^{\mathrm{F}}_{\mathbf{P}}}\frac{1}{i(\Omega-\omega)-\xi^{\mathrm{B}}_{\mathbf{P}-\mathbf{k}}}\mathrm{e}^{i\Omega 0^+}=\Theta(-\xi^{\mathrm{F}}_{\mathbf{P}})\frac{1}{\xi^{\mathrm{F}}_{\mathbf{P}}-\xi^{\mathrm{B}}_{\mathbf{P}-\mathbf{k}}-i\omega} \tag{B.47}$$

and the integral over ω is therefore

$$\begin{aligned}\int\frac{\mathrm{d}\omega}{2\pi}\left(\frac{1}{i\omega-\xi^{\mathrm{F}}_{\mathbf{k}}}\right)^2\frac{\Theta(-\xi^{\mathrm{F}}_{\mathbf{P}})}{\xi^{\mathrm{F}}_{\mathbf{P}}-\xi^{\mathrm{B}}_{\mathbf{P}-\mathbf{k}}-i\omega}&\\ = -i\Theta(-\xi^{\mathrm{F}}_{\mathbf{P}})\Theta\left(\xi^{\mathrm{F}}_{\mathbf{k}}\right)\mathrm{Res}\left(\left(\frac{1}{i\omega-\xi^{\mathrm{F}}_{\mathbf{k}}}\right)^2\frac{1}{\xi^{\mathrm{F}}_{\mathbf{P}}-\xi^{\mathrm{B}}_{\mathbf{P}-\mathbf{k}}-i\omega},\omega=-i\xi^{\mathrm{F}}_{\mathbf{k}}\right)&\end{aligned} \tag{B.48}$$

since the other pole $\omega=-i(\xi^{\mathrm{F}}_{\mathbf{P}}-\xi^{\mathrm{B}}_{\mathbf{P}-\mathbf{k}})$ lies on the positive imaginary axis. Computing the residue yields

$$\begin{aligned}\int\frac{\mathrm{d}\omega}{2\pi}\left(\frac{1}{i\omega-\xi^{\mathrm{F}}_{\mathbf{k}}}\right)^2\frac{\Theta(-\xi^{\mathrm{F}}_{\mathbf{P}})}{\xi^{\mathrm{F}}_{\mathbf{P}}-\xi^{\mathrm{B}}_{\mathbf{P}-\mathbf{k}}-i\omega}&\\ = -\Theta(k_{\mathrm{F}}-|\mathbf{P}|)\Theta\left(|\mathbf{k}|-k_{\mathrm{F}}\right)\left(\frac{1}{\xi^{\mathrm{F}}_{\mathbf{P}}-\xi^{\mathrm{B}}_{\mathbf{P}-\mathbf{k}}-\xi^{\mathrm{F}}_{\mathbf{k}}}\right)^2.&\end{aligned} \tag{B.49}$$

The contribution to I_2 stemming from (B.42) is thus the double momentum integral

$$I_2^{[\mathrm{III}]}\equiv \frac{1}{g^2}\frac{n_{\mathrm{B}}\pi^2}{m_{\mathrm{r}}^2}\int\frac{\mathrm{d}\mathbf{k}}{(2\pi)^2}\int\frac{\mathrm{d}\mathbf{P}}{(2\pi)^2}\,\Theta(k_{\mathrm{F}}-|\mathbf{P}|)\Theta\left(|\mathbf{k}|-k_{\mathrm{F}}\right)\left(\frac{1}{\xi^{\mathrm{F}}_{\mathbf{P}}-\xi^{\mathrm{B}}_{\mathbf{P}-\mathbf{k}}-\xi^{\mathrm{F}}_{\mathbf{k}}}\right)^2, \tag{B.50}$$

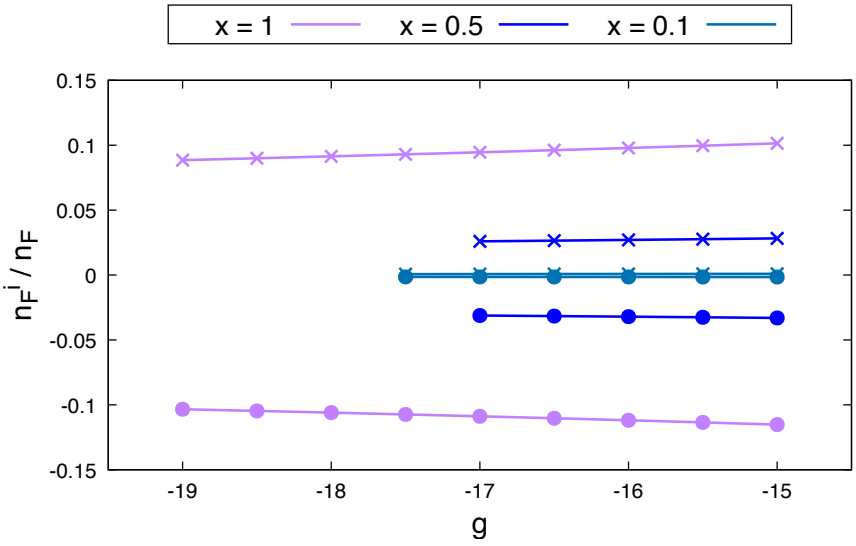

Figure B.5: The crosses represent $n_{\mathrm{F}}^1/n_{\mathrm{F}}$, while the circles $n_{\mathrm{F}}^2/n_{\mathrm{F}}$, for different values of the BF coupling g and the boson concentration x. The considered mass ratio is $\gamma_{\mathrm{m}} = 2$.

again dropping the prime on $\int \mathrm{d}\mathbf{k}\,(\ldots)$ due to the presence of $\Theta\left(|\mathbf{k}| - k_{\mathrm{F}}\right)$.

By performing the variable transformation $\mathbf{k} \mapsto \mathbf{P} - \mathbf{q}$, the above integral becomes

$$I_2^{[\mathrm{III}]} = \frac{1}{g^2}\frac{n_{\mathrm{B}}\pi^2}{m_{\mathrm{r}}^2}\int\frac{\mathrm{d}\mathbf{q}}{(2\pi)^2}\int\frac{\mathrm{d}\mathbf{P}}{(2\pi)^2}\,\Theta(k_{\mathrm{F}} - |\mathbf{P}|)\Theta\left(|\mathbf{P}-\mathbf{q}| - k_{\mathrm{F}}\right)\left(\frac{1}{\xi_{\mathbf{P}}^{\mathrm{F}} - \xi_{\mathbf{q}}^{\mathrm{B}} - \xi_{\mathbf{P}-\mathbf{q}}^{\mathrm{F}}}\right)^2, \tag{B.51}$$

which we recognize to be $-I_2^{[\mathrm{I}]}$. Therefore, when we sum the two contributions to obtain I_2, we realize that $I_2 = 0$ up to orders higher than $\mathrm{O}(1/g^2)$.

All in all, collecting the results (B.32), (B.39), (B.46) and (B.51), we find that up to orders higher than $1/g^2$

$$\mu_{\mathrm{F}} = E_{\mathrm{F}} + \Sigma_{\mathrm{F}}\left(\widetilde{k}_{\mathrm{F}}, 0^+\right). \tag{B.52}$$

Furthermore, since Σ_{F} depends on the (2+1)-momentum $(\mathbf{k}, \omega)$ only from the second order $\mathrm{O}(1/g^2)$ and since k_{F} and $\widetilde{k}_{\mathrm{F}}$ differ by an order $\mathrm{O}(1/g)$, within the second order approximation we find

$$\mu_{\mathrm{F}} = E_{\mathrm{F}} + \Sigma_{\mathrm{F}}(k_{\mathrm{F}}, 0^+). \tag{B.53}$$

Fig. B.5 displays the approximate cancellation of $|\Sigma_{\mathrm{F}}(k_{\mathrm{gs1}}, \omega_{\mathrm{gs1}})|$ that occurs when we insert (B.39) in (B.32), up to the second order in $1/g$. In particular, for $\gamma_{\mathrm{m}} = 2$ and several values for the boson

concentration x, we report the quantities

$$n_{\mathrm{F}}^{1} \equiv \left(\int_{\mathbb{R}^{+} \setminus [k_{\mathrm{gs}1}, k_{\mathrm{gs}2}]} \frac{\mathrm{d}k}{2\pi} \int \frac{\mathrm{d}\omega}{2\pi} \, k \, G_{\mathrm{F}}(k,\omega) \mathrm{e}^{i\omega 0^{+}} - \frac{m_{\mathrm{F}}}{2\pi} \left(\mu_{\mathrm{F}} + \Sigma_{\mathrm{F}}^{(1)} \right) \right) g^{2} \tag{B.54}$$

$$n_{\mathrm{F}}^{2} \equiv \left(\int_{k_{\mathrm{gs}1}}^{k_{\mathrm{gs}2}} \frac{\mathrm{d}k}{2\pi} \int \frac{\mathrm{d}\omega}{2\pi} \, k \, G_{\mathrm{F}}(k,\omega) \mathrm{e}^{i\omega 0^{+}} + \frac{m_{\mathrm{F}}}{2\pi} \left(\Sigma_{\mathrm{F}} \left(\widetilde{k}_{\mathrm{F}}, 0^{+} \right) + \Sigma_{\mathrm{F}}^{(1)} \right) \right) g^{2}. \tag{B.55}$$

The integrals are performed numerically by Gauss-Legendre integration, employing the approximations $k_{\mathrm{gs}1} \approx \sqrt{2m_{\mathrm{F}}(\mu_{\mathrm{F}} + \mu_{\mathrm{F}}^{(1)})}$ and $k_{\mathrm{gs}2} \approx \widetilde{k}_{\mathrm{F}}$. In agreement with our analytical calculation, Fig. B.5 shows that $n_{\mathrm{F}}^{1} \approx -n_{\mathrm{F}}^{2}$.

Appendix C

Numerical results with the mean-field shift of the fermion chemical potential

In this present appendix, we refer to the modified T-matrix approach featuring the mean-field shift of $\mu_{\rm F}$ as $mTMA$, while TMA indicates the ordinary T-matrix method. The analytical expressions and numerical results presented here do not include the contribution from the anomalous self-energy $\Sigma^{12}_{\rm BF}$.

C.1 Fully numerical implementation

In this section we discuss the Fortran program to compute $\mu_{\rm B}$, $\mu_{\rm F}$, n_0 at given couplings, mass ratio and concentration, in the case where $\mu_{\rm F}$ is shifted by $\Sigma^0_{\rm F}$ as discussed in Sec. 3.5.

The starting point is again the set of equations (3.43), (3.44), (3.45), and the logic of the algorithm to find a solution is substantially unchanged with respect to the case with no mean-field shift. The main differences are the following:

- Eqs. (3.44), (3.45) are solved for $\mu'_{\rm F}$ and n_0 instead of $\mu_{\rm F}$ and n_0;
- the addition-and-subtraction scheme discussed in Appendix A for the calculation of the self-energies is borrowed with no changes, upon the replacement of $\mu_{\rm F}$ with $\mu'_{\rm F}$ in the transition matrices and in the fermion propagator within the frequency convolutions;
- the addition-and-subtraction scheme to improve the convergence of the frequency integral that determines $n_{\rm F}(\mathbf{k})$ consists in adding and subtracting $G^0_{\rm F}(\mathbf{k},\omega) = 1/(i\omega - \mathbf{k}^2/(2m_{\rm F}) + \mu'_{\rm F} + \Sigma^0_{\rm F})$,

so that

$$G_{\rm F}(\mathbf{k}) - G^0_{\rm F}(\mathbf{k},\omega) = \frac{\Sigma_{\rm F}(\mathbf{k},\omega)}{(i\omega - \mathbf{k}^2/(2m_{\rm F}) + \mu'_{\rm F} + \Sigma^0_{\rm F} - \Sigma_{\rm F}(\mathbf{k},\omega))(i\omega - \mathbf{k}^2/(2m_{\rm F}) + \mu'_{\rm F} + \Sigma^0_{\rm F})} \tag{C.1}$$

and we recover in mTMA the same asymptotic behavior $1/(\omega^2 \ln \omega)$ we had for the integrand at large ω in the ordinary TMA;

- the large k forms (A.15) and (A.16) for the momentum distributions have to be modified by a suitable replacement of $\mu_{\rm F}$ with $\mu'_{\rm F}$, where needed. First of all, inside the T-matrix the fermion propagators contain the chemical potential $\mu'_{\rm F}$, both in (A.15) and in (A.16). Concerning the factor $F_s \equiv 1/(\mathbf{k}^2/(2m_{\rm r}) - \mu_{\rm B} - \mu_{\rm F})^2$ (with $s = $ F or B) in front of the integral, it is necessary to distinguish between the fermionic and the bosonic case. In the fermion momentum distribution, the dependence of $F_{\rm F}$ on $\mu_{\rm F}$ comes from the external propagator in Dyson's equation. Therefore, in the modified theory it is maintained as the "real" fermion chemical potential $\mu_{\rm F} = \mu'_{\rm F} + \Sigma^0_{\rm F}$. In the boson momentum distribution, on the other hand, the dependence of $F_{\rm B}$ on $\mu_{\rm F}$ comes from the internal propagator in the convolution integral for the boson self-energy. Hence, in this case it must be replaced by $\mu'_{\rm F}$. All in all, within mTMA the appropriate limiting forms for the momentum distributions are

$$n^{(k\gg k_{\rm F})}_{\rm F}(\mathbf{k}) = \frac{1}{(\mathbf{k}^2/(2m_{\rm r}) - \mu_{\rm B} - \mu'_{\rm F} - \Sigma^0_{\rm F})^2} \int \frac{{\rm d}\mathbf{P}}{(2\pi)^2} \int \frac{{\rm d}\Omega}{2\pi}\, T(\mathbf{P},\Omega) {\rm e}^{i\Omega 0^+} \tag{C.2}$$

$$n^{(k\gg k_{\rm F})}_{\rm B}(\mathbf{k}) = \frac{1}{(\mathbf{k}^2/(2m_{\rm r}) - \mu_{\rm B} - \mu'_{\rm F})^2} \int \frac{{\rm d}\mathbf{P}}{(2\pi)^2} \int \frac{{\rm d}\Omega}{2\pi}\, T(\mathbf{P},\Omega) {\rm e}^{i\Omega 0^+} + \frac{\left(\Sigma^{\rm BB}_{12}\right)^2}{4(\mathbf{k}^2/(2m_{\rm B}) - \mu_{\rm B})^2}. \tag{C.3}$$

Fig. C.1 presents the plots of the boson chemical potential $\mu_{\rm B}$, the fermion chemical potentials $\mu_{\rm F}$ and $\mu'_{\rm F}$, and the condensate fraction $n_0/n_{\rm B}$ from weak to strong coupling, in the density- and mass-balanced case $x = 1$, $\gamma_{\rm m} = 1$. The insets report the comparison with the weak-coupling formulae derived in Secs. 3.4 and 3.5 (in absence of the anomalous term $\Sigma^{12}_{\rm BF}$):

$$\mu^{\rm TMA}_{\rm B} = E_{\rm F}\, \frac{1}{2} \frac{\gamma_{\rm m}+1}{\gamma_{\rm m}\, g} \left(1 + \frac{1}{2g}\left(\frac{\gamma_{\rm m} \ln\left(\gamma_{\rm m}^2\right)}{\gamma_{\rm m}-1} - \ln\left((\gamma_{\rm m}+1)^2\right) - 1\right)\right) \tag{C.4}$$

$$\mu^{\rm mTMA}_{\rm B} = E_{\rm F}\, \frac{1}{2} \frac{\gamma_{\rm m}+1}{\gamma_{\rm m}\, g} \left(1 + \frac{1}{2g}\left(-x\,\frac{\gamma_{\rm m}+1}{\gamma_{\rm m}} + \frac{\gamma_{\rm m} \ln\left(\gamma_{\rm m}^2\right)}{\gamma_{\rm m}-1} - \ln\left((\gamma_{\rm m}+1)^2\right) - 1\right)\right) \tag{C.5}$$

$$\mu^{\rm TMA}_{\rm F} = \mu^{\rm mTMA}_{\rm F} = E_{\rm F} + E_{\rm F}\, \frac{x}{2} \frac{\gamma_{\rm m}+1}{\gamma_{\rm m}\, g} \left(1 + \frac{1}{2g}\left(\ln\left(\frac{\gamma_{\rm m}}{(1+\gamma_{\rm m})^2}\right) + \frac{\gamma_{\rm m}+1}{\gamma_{\rm m}-1} \ln \gamma_{\rm m}\right)\right). \tag{C.6}$$

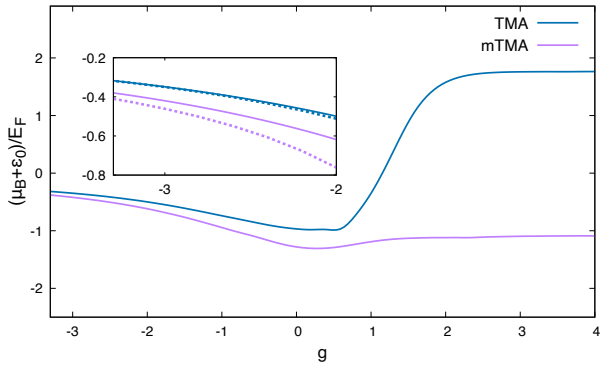

(a)

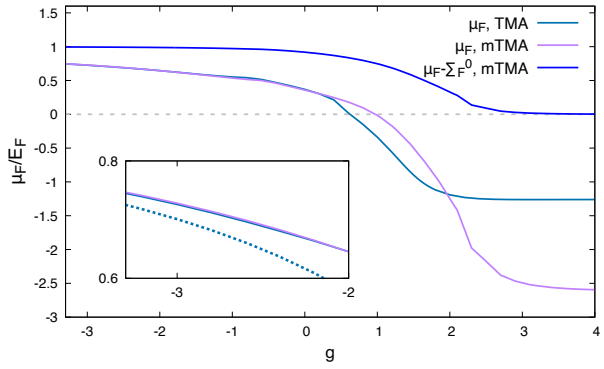

(b)

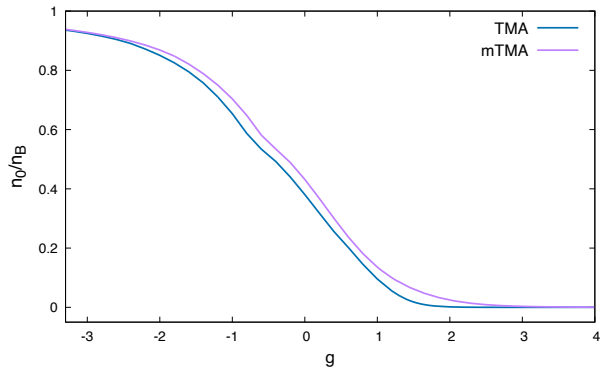

(c)

Figure C.1: Plots for $\mu_{\rm B}$, $\mu_{\rm F}$, n_0 as functions of the BF coupling g, implementing the mean-field shift $\mu_{\rm F} \mapsto \mu'_{\rm F} = \mu_{\rm F} - \Sigma^0_{\rm F}$ inside the self-energies (mTMA), compared with the analogous quantities computed within the ordinary T-matrix approach (TMA). Results are for $x = 1$, $\gamma_{\rm m} = 1$. (a): boson chemical potential $\mu_{\rm B}$ (shifted by the binding energy ε_0), in units of $E_{\rm F}$, as a function of the BF coupling g. Inset: comparison between $\mu_{\rm B} + \varepsilon_0$ and the weak-coupling predictions (C.4) and (C.5) (dotted lines). (b): corresponding fermion chemical potentials $\mu_{\rm F}$ and $\mu'_{\rm F}$ in units of $E_{\rm F}$. Inset: comparison between $\mu_{\rm F}$ and the weak-coupling prediction (C.6) (dotted lines). (c): corresponding boson condensate fraction.

In Fig. C.2 we report the fermion momentum distribution $n_{\mathrm{F}}(\mathbf{k})$ for $x = 1$, $\gamma_{\mathrm{m}} = 1$, and different values of the BF coupling g, both within TMA and mTMA. Within TMA, as discussed in [56] and as it can be seen in the inset of Fig. C.2, the position of the Fermi step $\widetilde{k}_{\mathrm{F}}$ in the strong-coupling limit decreases only slightly from the non-interacting value k_{F}, although its height becomes (vanishingly) small. For mTMA, on the other hand, the strong-coupling profile of $n_{\mathrm{F}}(\mathbf{k})$ is quite different: the height of the step remains finite, while $\widetilde{k}_{\mathrm{F}}$ tends to vanish. This can be seen in the main panel of Fig. C.2 and, correspondingly, from μ'_{F} reported in Fig. C.1, since within mTMA $\widetilde{k}_{\mathrm{F}} = \sqrt{2m_{\mathrm{F}}\mu'_{\mathrm{F}}}$. In this context, mTMA yields a prediction that is more physically sensible than TMA, since the disappearance of the Fermi sphere of atomic fermions should be accompanied by a decrease in the Fermi step momentum. This is expected if the following extension of the Luttinger theorem from Fermi liquids to a Bose-Fermi mixture with a condensate [103] holds: the sum of the volumes of the Fermi spheres of dressed atomic fermions and molecules does not depend on interactions, i.e. $k_{\mathrm{F}}^2 = \widetilde{k}_{\mathrm{F}}^2 + P_{\mathrm{CF}}^2$, with P_{CF} being the step momentum of the momentum distribution of the interacting fermions.

In [56], the authors discuss the violation of this version of the Luttinger theorem within the ordinary T-matrix approach TMA. One of the identified causes is precisely the absence of self-consistency in the fermion Green's functions. Therefore, it would be interesting to study in detail whether the partial self-consistency in mTMA is sufficient to satisfy the Luttinger theorem in the above form. We postpone this analysis to future work, as it requires a systematic study of the fermion momentum distribution at lower boson concentrations, as well as of the momentum distribution of composite fermions.

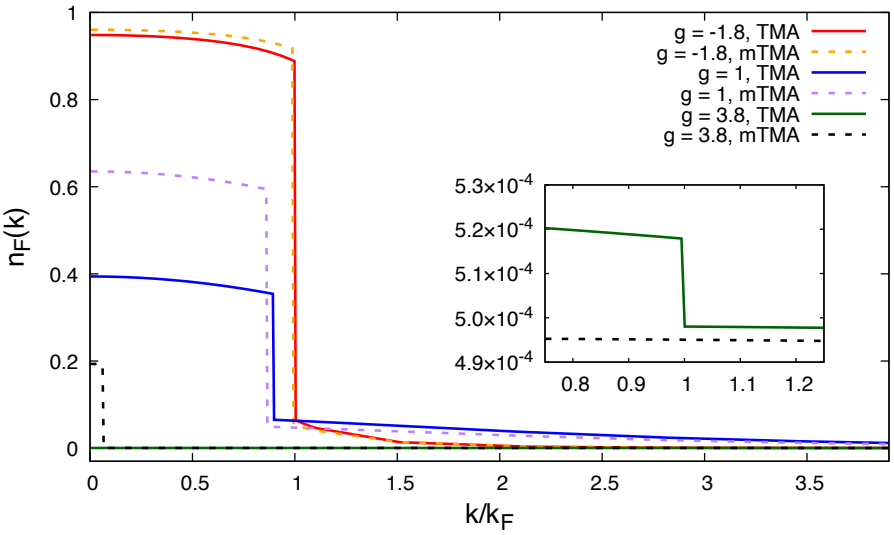

Figure C.2: Fermion momentum distribution $n_{\mathrm{F}}(\mathbf{k})$ as a function of k/k_{F}, for various BF couplings, at boson concentration $x = 1$, mass ratio $\gamma_{\mathrm{m}} = 1$, and BB repulsion $\eta = 0$. Inset: zoom on the Fermi step within TMA for the strong coupling $g = 3.8$.

C.2 Strong-coupling expressions

In this section, we present the fundamental equations for mTMA in the strong-coupling regime,[1] derived in analogy with the ordinary TMA in Sec. 3.6:

- dressed composite fermion Green's function, weights and dispersions

$$G_{\mathrm{CF}}(\mathbf{P},\Omega)^{-1} = i\Omega - \widetilde{\xi}_{\mathbf{P}}^{\mathrm{CF}'} - \frac{\Delta_0^2}{i\Omega - \widetilde{\xi}_{\mathbf{P}}^{\mathrm{F}'}} \tag{C.7}$$

$$E_{\mathbf{P}}^{\pm} = \frac{\widetilde{\xi}_{\mathbf{P}}^{\mathrm{CF}'} + \xi_{\mathbf{P}}^{\mathrm{F}'} \pm \sqrt{\left(\widetilde{\xi}_{\mathbf{P}}^{\mathrm{CF}'} - \xi_{\mathbf{P}}^{\mathrm{F}'}\right)^2 + 4\Delta_0^2}}{2} \tag{C.8}$$

$$u_{\mathbf{P}}^2 = \frac{1}{2}\left(1 + \frac{\widetilde{\xi}_{\mathbf{P}}^{\mathrm{CF}'} - \xi_{\mathbf{P}}^{\mathrm{F}'}}{\sqrt{\left(\widetilde{\xi}_{\mathbf{P}}^{\mathrm{CF}'} - \xi_{\mathbf{P}}^{\mathrm{F}'}\right)^2 + 4\Delta_0^2}}\right) \tag{C.9}$$

$$v_{\mathbf{P}}^2 = 1 - u_{\mathbf{P}}^2, \tag{C.10}$$

with

$$\widetilde{\mu}'_{\mathrm{CF}} \equiv \mu_{\mathrm{B}} + \mu'_{\mathrm{F}} + \varepsilon_0 - \frac{m_{\mathrm{F}}\,\mu'_{\mathrm{F}}}{m_{\mathrm{r}}}\Theta(\mu'_{\mathrm{F}}) \tag{C.11}$$

$$\widetilde{\xi}_{\mathbf{P}}^{\mathrm{CF}'} = \frac{\mathbf{P}^2}{2M} - \widetilde{\mu}'_{\mathrm{CF}} \tag{C.12}$$

$$\widetilde{\xi}_{\mathbf{P}}^{\mathrm{F}'} = \frac{\mathbf{P}^2}{2m_{\mathrm{F}}} - \mu'_{\mathrm{F}}; \tag{C.13}$$

- composite fermion density

$$\frac{n_{\mathrm{CF}}}{n_{\mathrm{F}}} = \frac{1}{4E_{\mathrm{F}}}\Bigg(\widetilde{\mu}'_{\mathrm{CF}}(1+\gamma_{\mathrm{m}}) + \mu'_{\mathrm{F}} + \mathcal{K} - 2\frac{1+\gamma_{\mathrm{m}}}{\gamma_{\mathrm{m}}}\Bigg(\sqrt{4\Delta_0^2 + (\widetilde{\mu}'_{\mathrm{CF}} - \mu'_{\mathrm{F}})^2} - \sqrt{\left(4\Delta_0^2 + \frac{1}{4(1+\gamma_{\mathrm{m}})^2}\mathcal{J}^2\right)}\Bigg)\Bigg), \tag{C.14}$$

with

$$\mathcal{K} \equiv \sqrt{4\Delta_0^2(1+\gamma_{\mathrm{m}}) + \left(\widetilde{\mu}'_{\mathrm{CF}}(1+\gamma_{\mathrm{m}}) - \mu'_{\mathrm{F}}\right)^2} \tag{C.15}$$

$$\mathcal{J} \equiv \widetilde{\mu}'_{\mathrm{CF}}(\gamma_{\mathrm{m}}^2 + 3\gamma_{\mathrm{m}} + 2) - \mu'_{\mathrm{F}}(2+\gamma_{\mathrm{m}}) + \gamma_{\mathrm{m}}\mathcal{K}; \tag{C.16}$$

[1] The expressions listed in this appendix have been tested for $(x,\gamma_{\mathrm{m}}) \in \{0.1, 0.5, 1\} \times \{0.5, 2\}$ and $(x,\gamma_{\mathrm{m}}) \in (0,1] \times \{1\}$.

- boson chemical potential

$$\mu_{\mathrm{B}} = -\varepsilon_0 \left(\frac{1+\gamma_{\mathrm{m}}}{\gamma_{\mathrm{m}}}\right)^2 \left(\ln\left(2(1+\gamma_{\mathrm{m}})\right) + \ln\left(\mu'_{\mathrm{F}} - \widetilde{\mu}'_{\mathrm{CF}} + \sqrt{4\Delta_0^2 + \left(\widetilde{\mu}'_{\mathrm{CF}} - \mu'_{\mathrm{F}}\right)^2}\right) - \ln\left(2\sqrt{4\Delta_0^2(1+\gamma_{\mathrm{m}})^2 + \frac{1}{4}\mathcal{J}^2} - \mathcal{J}\right)\right); \tag{C.17}$$

- mean-field shift of μ_{F}

$$\Sigma_{\mathrm{F}}^0 = \frac{\Delta_0^2}{-\mu'_{\mathrm{F}}/(2M) + \widetilde{\mu}'_{\mathrm{CF}}} - \frac{\Delta_{\mathrm{CF}}^2}{\mu'_{\mathrm{F}}/(2m_{\mathrm{B}}) - \mu_{\mathrm{B}}}; \tag{C.18}$$

- fermion Green's function

$$G_{\mathrm{F}}(\mathbf{k},\omega)^{-1} = i\omega - \frac{\mathbf{k}^2}{2m_{\mathrm{F}}} + \mu'_{\mathrm{F}} + \Sigma_{\mathrm{F}}^0 - \frac{\Delta_0^2}{i\omega - \widetilde{\xi}_{\mathbf{P}}^{\mathrm{CF}\prime}} - \frac{\Delta_{\mathrm{CF}}^2}{i\omega + \xi_{\mathbf{k}}^{\mathrm{B}}}. \tag{C.19}$$

Eqs. C.14, C.17 and C.19, together with $n_{\mathrm{F}} = (2\pi)^{-3}\int \mathrm{d}\mathbf{k} \int \mathrm{d}\omega\ G_{\mathrm{F}}(\mathbf{k},\omega)\mathrm{e}^{i\omega 0^+}$ that determines the fermion density, form a system of three equations for the unknowns μ_{F}, μ_{B}, and n_0. Assuming $n_{\mathrm{B}} - n_0 \sim n_{\mathrm{CF}}$ and denoting $z = i\Omega$, such system reads

$$\mu_{\mathrm{B}} = -\varepsilon_0 \left(\frac{1+\gamma_{\mathrm{m}}}{\gamma_{\mathrm{m}}}\right)^2 \left(\ln\left(2(1+\gamma_{\mathrm{m}})\right) + \ln\left(\mu'_{\mathrm{F}} - \widetilde{\mu}'_{\mathrm{CF}} + \sqrt{4\Delta_0^2 + \left(\widetilde{\mu}'_{\mathrm{CF}} - \mu'_{\mathrm{F}}\right)^2}\right) - \ln\left(2\sqrt{4\Delta_0^2(1+\gamma_{\mathrm{m}})^2 + \frac{1}{4}\mathcal{J}^2} - \mathcal{J}\right)\right) \tag{C.20}$$

$$n_{\mathrm{B}} = n_0 + \frac{n_{\mathrm{F}}}{4E_{\mathrm{F}}}\left(\widetilde{\mu}'_{\mathrm{CF}}(1+\gamma_{\mathrm{m}}) + \mu'_{\mathrm{F}} + \mathcal{K} - 2\frac{1+\gamma_{\mathrm{m}}}{\gamma_{\mathrm{m}}}\left(\sqrt{4\Delta_0^2 + \left(\widetilde{\mu}'_{\mathrm{CF}} - \mu'_{\mathrm{F}}\right)^2} - \sqrt{\left(4\Delta_0^2 + \frac{1}{4(1+\gamma_{\mathrm{m}})^2}\mathcal{J}^2\right)}\right)\right) \tag{C.21}$$

$$n_{\mathrm{F}} = \int \frac{\mathrm{d}\mathbf{k}}{(2\pi)^2}\left(\sum_{z_i \in \{G_{\mathrm{F}}(z,\mathbf{k})^{-1}=0\}} \lim_{z\to z_i}(z - z_i)\, G_{\mathrm{F}}(z,\mathbf{k})^{-1}\,\Theta(-z_i)\right). \tag{C.22}$$

As in the TMA case discussed in Sec. 3.6, these equations can be solved using a standard root-finding algorithm. No particular care is required in the evaluation of the momentum integral in Eq. (C.22). All numerical calculations are performed using Wolfram Mathematica.

With these formulae at hand, we can further justify the asymptotic behavior in the strong-coupling limit of the curves in Fig C.1.

In Fig. C.3 we report Δ_0^2 as a function of the boson concentration, comparing it with the same quantity evaluated in the TMA framework. Note that, within the mTMA formalism, the square of the hybridization energy scale $\Delta_0^2 = 2\pi\varepsilon_0 n_0/m_{\mathrm{r}}$ is non-vanishing in the strong-coupling limit if $x \approx 1$. This feature is not found in the ordinary TMA, where $\Delta_0^2 \approx 0$ at matched densities.

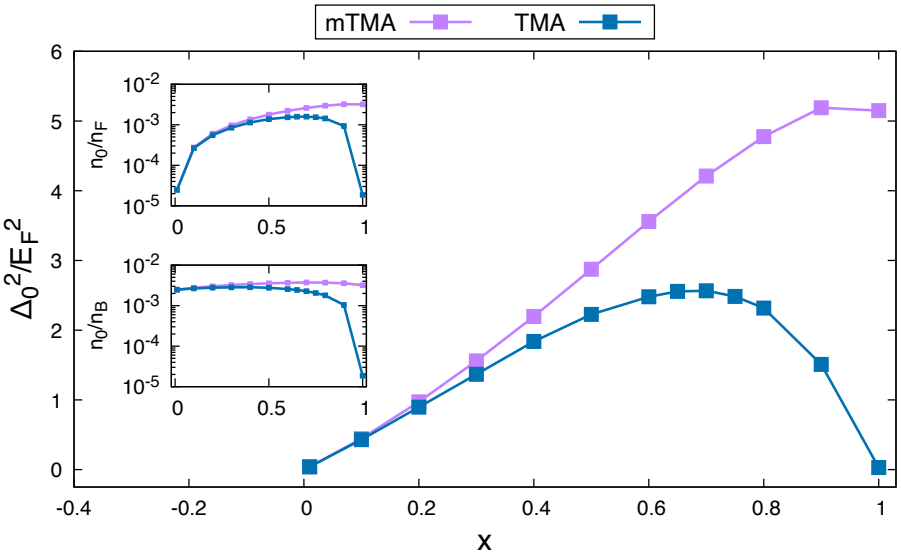

Figure C.3: Square of the hybridization energy Δ_0^2, in units of E_F^2, as a function of the boson concentration x, for strong BF attraction $g = 3$, BB repulsion $\eta = 0$, and mass ratio $\gamma_\mathrm{m} = 1$. Results are depicted for both TMA and mTMA. Insets: condensate density n_0 in units of n_F (top) and condensate fraction n_0/n_B (bottom).

Since, within mTMA and at sufficiently large boson concentration (namely $x \gtrsim 0.2$), Δ_0^2 is a non-zero constant of the order of E_F^2, both terms in Eq. (C.18) contribute to Σ_F^0. In the density- and mass-balanced case, Σ_F^0 can be approximated as

$$\Sigma_\mathrm{F}^0 \approx \frac{\Delta_0^2}{\mu_\mathrm{B} + \varepsilon_0} - 2E_\mathrm{F}\frac{\varepsilon_0}{\mu_\mathrm{B}}, \tag{C.23}$$

with the two contributions being of the same order. This follows since $\mu_\mathrm{B} + \varepsilon_0 = \mathrm{O}(E_\mathrm{F})$ in the denominator of the first term, while $\varepsilon_0/\mu_\mathrm{B} = \mathrm{O}(1)$ in the second term. Σ_F^0 provides the dominant contribution to $\mu_\mathrm{F} = \mu_\mathrm{F}' + \Sigma_\mathrm{F}^0$, resulting, at large g, in the limiting negative value of μ_F visible in Fig. C.1(b).

Appendix D

Additional figures

In this appendix, we present further plots supporting the numerical study of Chap. 4.

D.1 Figures for the boson momentum distributions, for $n_B < n_F$

In this section, figures for the the boson momentum distributions of a density- and mass-imbalanced mixture are reported. We consider the boson concentration to be $x < 1$, specifically $x = 0.5$ (Fig. D.1) and $x = 0.1$ (Fig. D.2), and different values for the mass ratio γ_m, proximate to those in Tab. 1.1. We do not include the anomalous self-energy Σ^{12}_{BF} in the calculations, nor do we treat the interaction between bosons (setting $\eta = 0$) or the mean-field shift of the chemical potential $\mu_F \mapsto \mu_F - \Sigma^0_F$.

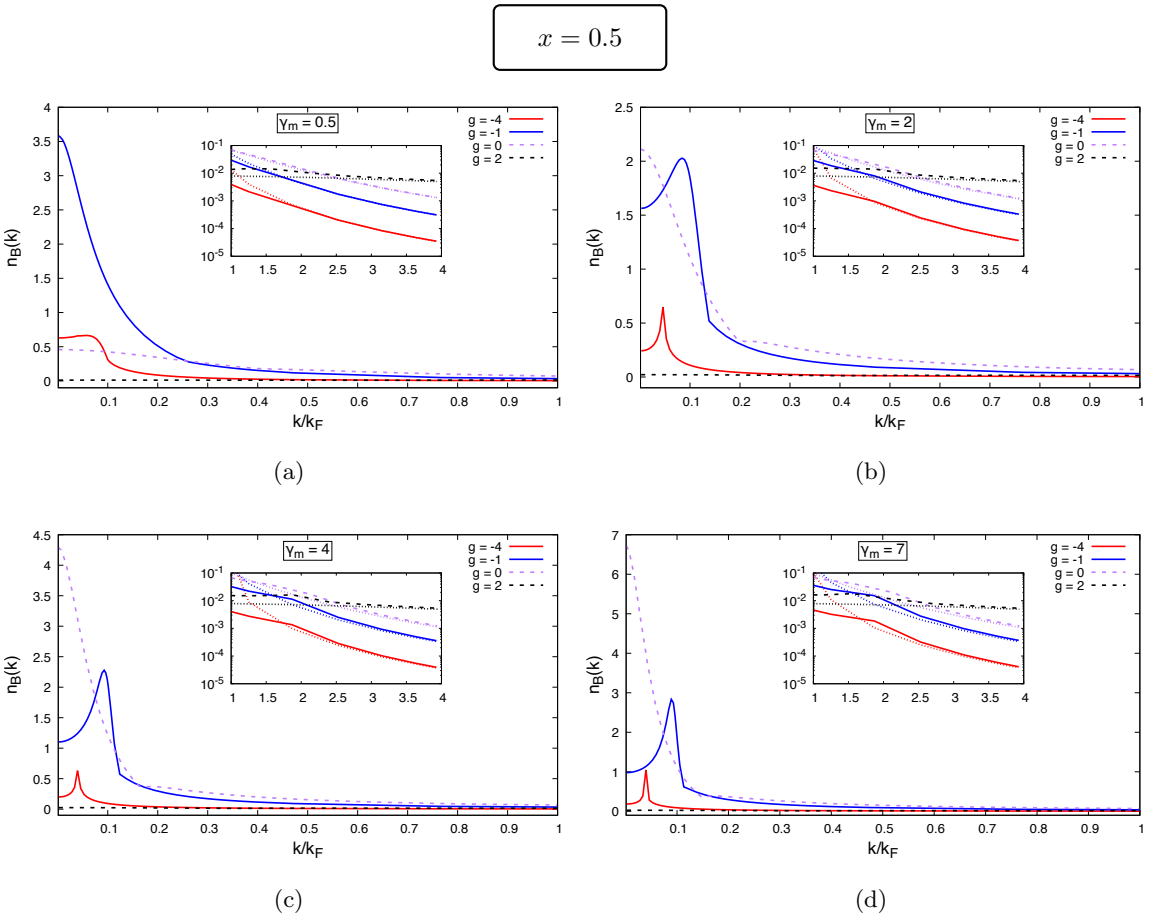

Figure D.1: Boson momentum distribution $n_B(\mathbf{k})$ as a function of k/k_F, for different values of the BF coupling g, and boson concentration $x = 0.51$. Different values of the mass ratio $\gamma_m = m_B/m_F$ are reported: (a) $\gamma_m = 0.5$ (b) $\gamma_m = 2$ (c) $\gamma_m = 4$ (d) $\gamma_m = 7$. Inset: comparison between numerical results and large momentum behavior described by equation (A.16) (dotted lines).

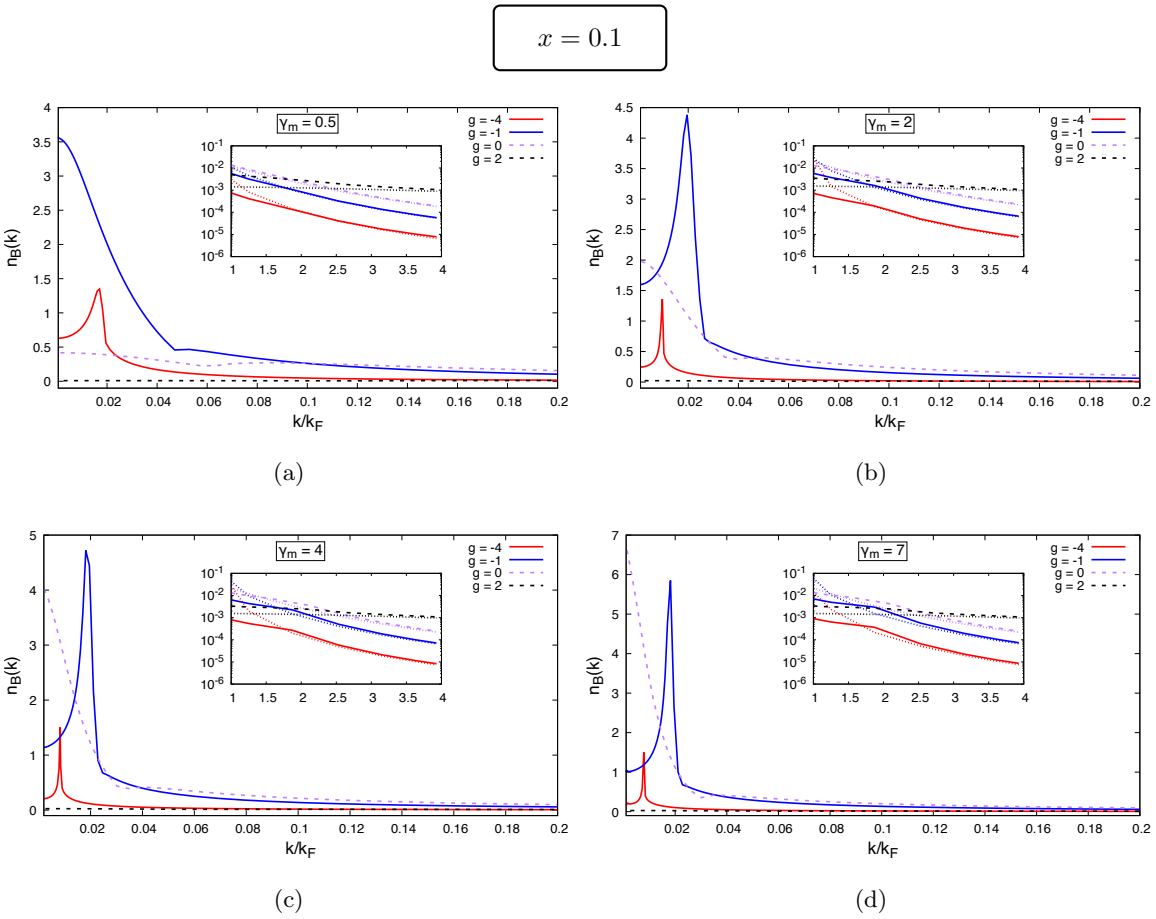

Figure D.2: Boson momentum distribution $n_{\mathrm{B}}(\mathbf{k})$ as a function of k/k_{F}, for different values of the BF coupling g, and boson concentration $x = 0.1$. Different values of the mass ratio $\gamma_{\mathrm{m}} = m_{\mathrm{B}}/m_{\mathrm{F}}$ are reported: (a) $\gamma_{\mathrm{m}} = 0.1$ (b) $\gamma_{\mathrm{m}} = 2$ (c) $\gamma_{\mathrm{m}} = 4$ (d) $\gamma_{\mathrm{m}} = 7$. Inset: comparison between numerical results and large momentum behavior described by equation (A.16) (dotted lines).

D.2 Figures for the chemical potentials, the condensate fraction and Tan's contact parameter for $n_{\mathrm{B}} < n_{\mathrm{F}}$

In this section, figures for the the boson and fermion chemical potentials μ_{F} and μ_{B}, the condensate density n_0 and Tan's contact C_{BF} of a density- and mass-imbalanced mixture are reported. We consider the boson concentration to be $x < 1$, specifically $x = 0.5$ (Fig. D.3), $x = 0.175$ (Fig. D.4) and $x = 0.1$ (Fig. D.5), and different values for the mass ratio γ_{m}, proximate to those in Tab. 1.1. We do not include the anomalous self-energy $\Sigma^{12}_{\mathrm{BF}}$ in the calculations, nor do we treat the interaction between bosons (setting $\eta = 0$) or the mean-field shift of the chemical potential $\mu_{\mathrm{F}} \mapsto \mu_{\mathrm{F}} - \Sigma^{0}_{\mathrm{F}}$.

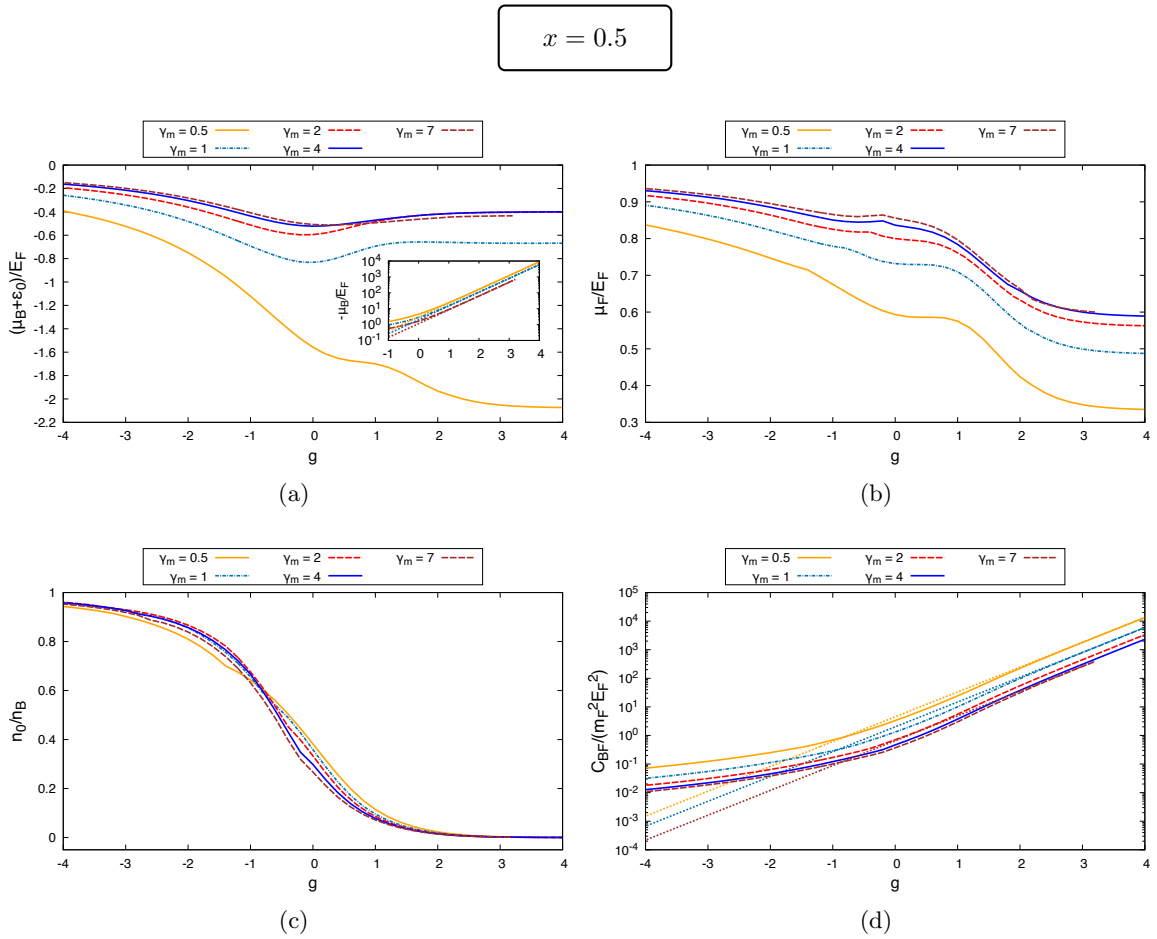

Figure D.3: (a): boson chemical potential $\mu_{\rm B}$ (shifted by the binding energy ε_0), in units of $E_{\rm F}$, as a function of the BF coupling g, for different values of the mass ratio $\gamma_{\rm m}$, for the boson concentration $x = 0.5$. Inset: comparison between $-\mu_{\rm B}$ and the binding energy ε_0 (dotted lines, reported for clarity only for $\gamma_{\rm m} = 0.5$, $\gamma_{\rm m} = 1$ and $\gamma_{\rm m} = 7$). (b): corresponding fermion chemical potential $\mu_{\rm F}$ in units of $E_{\rm F}$. (c): corresponding boson condensate fraction. (d): corresponding dimensionless Tan's contact constant $C_{\rm BF}/(m_{\rm F}^2 E_{\rm F}^2)$. Dotted lines: quantity $\left(x\,\varepsilon_0\,(\gamma_{\rm m}+1)/\gamma_{\rm m}\right)/E_{\rm F}$, reported for clarity only for $\gamma_{\rm m} = 0.5$, $\gamma_{\rm m} = 1$, $\gamma_{\rm m} = 7$.

$x = 0.175$

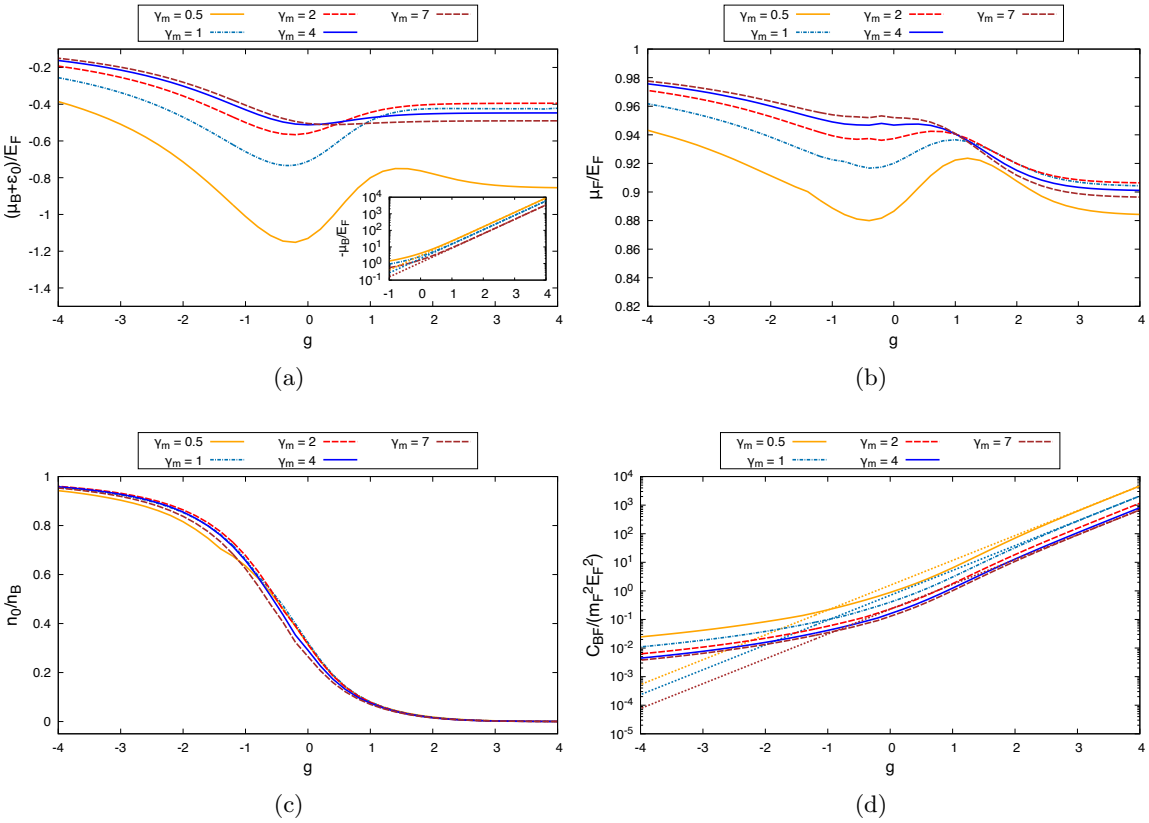

Figure D.4: (a): boson chemical potential $\mu_{\rm B}$ (shifted by the binding energy ε_0), in units of $E_{\rm F}$, as a function of the BF coupling g, for different values of the mass ratio $\gamma_{\rm m}$, for the boson concentration $x = 0.175$. Inset: comparison between $-\mu_{\rm B}$ and the binding energy ε_0 (dotted lines, reported for clarity only for $\gamma_{\rm m} = 0.5$, $\gamma_{\rm m} = 1$ and $\gamma_{\rm m} = 7$). (b): corresponding fermion chemical potential $\mu_{\rm F}$ in units of $E_{\rm F}$. (c): corresponding boson condensate fraction. (d): corresponding dimensionless Tan's contact constant $C_{\rm BF}/(m_{\rm F}^2 E_{\rm F}^2)$. Dotted lines: quantity $\left(x\,\varepsilon_0\,(\gamma_{\rm m}+1)/\gamma_{\rm m}\right)/E_{\rm F}$, reported for clarity only for $\gamma_{\rm m} = 0.5$, $\gamma_{\rm m} = 1$, $\gamma_{\rm m} = 7$.

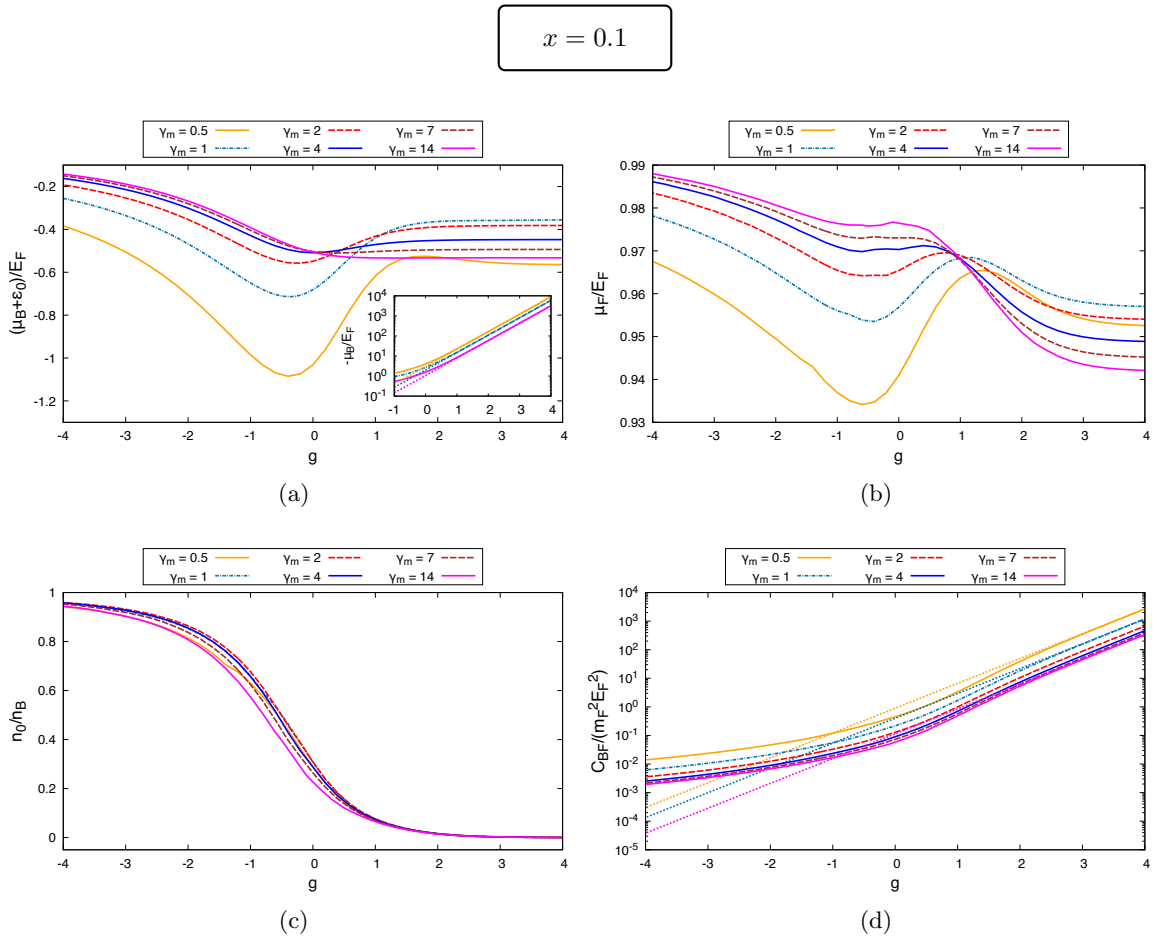

Figure D.5: (a): boson chemical potential μ_B (shifted by the binding energy ε_0), in units of E_F, as a function of the BF coupling g, for different values of the mass ratio γ_m, for the boson concentration $x = 0.1$. Inset: comparison between $-\mu_B$ and the binding energy ε_0 (dotted lines, reported for clarity only for $\gamma_m = 0.5$, $\gamma_m = 1$ and $\gamma_m = 14$). (b): corresponding fermion chemical potential μ_F in units of E_F. (c): corresponding boson condensate fraction. (d): corresponding dimensionless Tan's contact constant $C_{BF}/(m_F^2 E_F^2)$. Dotted lines: quantity $(x\,\varepsilon_0\,(\gamma_m + 1)/\gamma_m)\,/E_F$, reported for clarity only for $\gamma_m = 0.5$, $\gamma_m = 1$, $\gamma_m = 14$.

Fig. D.6 reports a plot for the "relative difference" $|\mu_B + \varepsilon_0|/\varepsilon_0$, for the usual values of γ_m and the boson concentrations $x = 0.1$, $x = 0.5$ and $x = 1$.

Finally, Fig D.7 reports a zoom on the condensate density at strong-BF attraction $g = 3$, as a function of γ_m and for the boson concentrations $x = 0.1$, $x = 0.175$, $x = 0.5$ and $x = 1$.

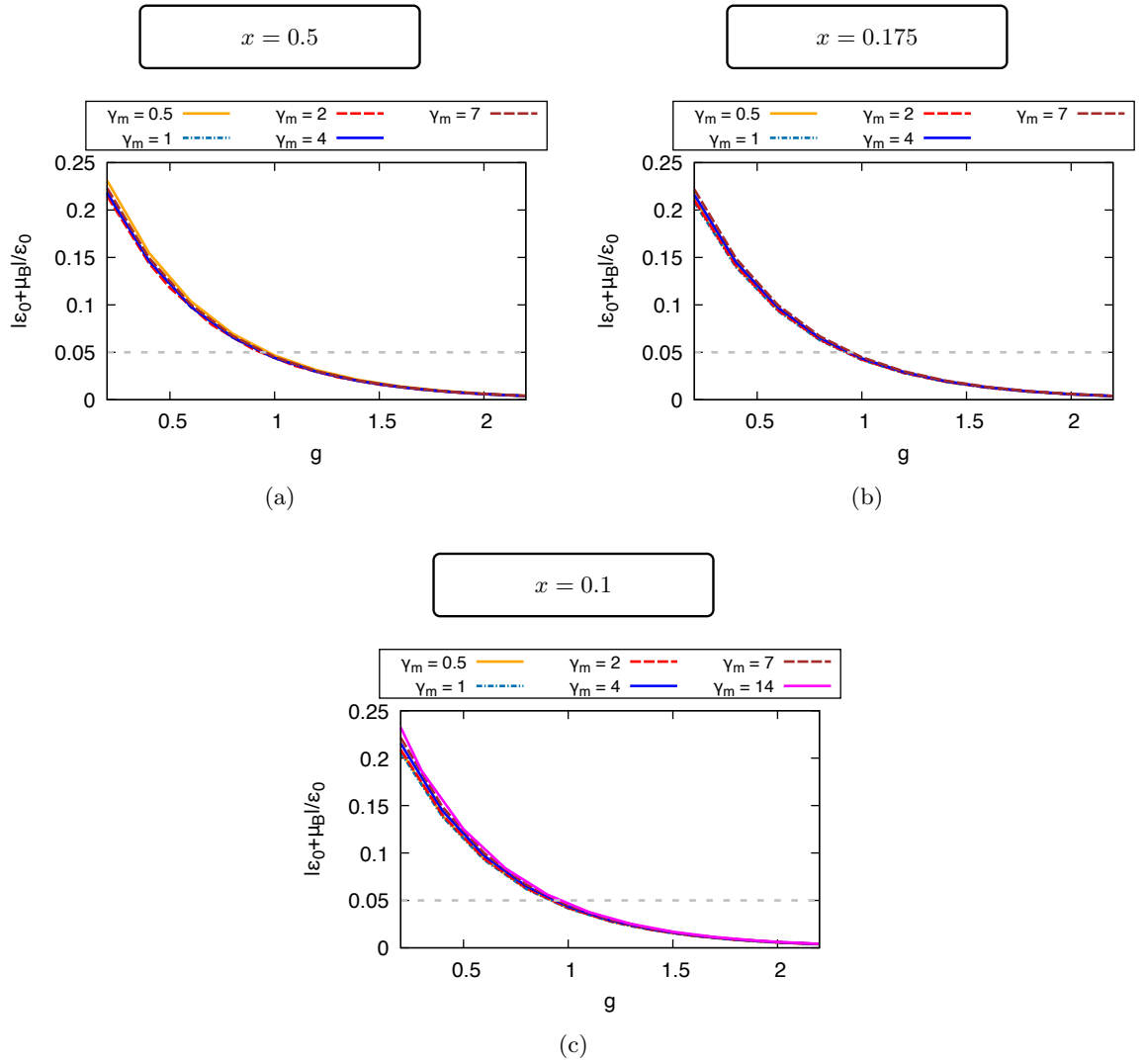

Figure D.6: Relative difference $|\mu_B + \varepsilon_0|/\varepsilon_0$ compared to 0.05 (dashed gray line), as a function of g for: (a) $x = 0.5$, (b) $x = 0.175$ and (c) $x = 0.1$.

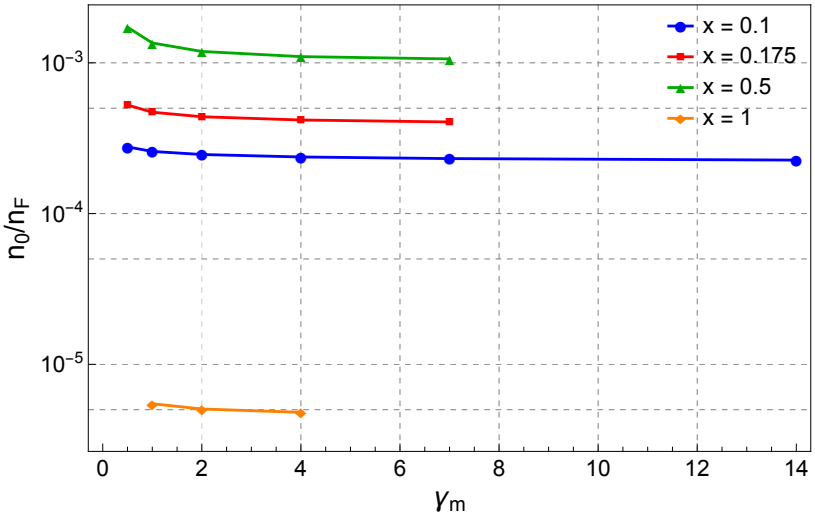

Figure D.7: Condensate density n_0 (in units of n_F) as a function of the mass ratio γ_m, for strong BF attraction $g = 3$, BB repulsion $\eta = 0$, and several different boson concentrations x.

D.3 Figures for the chemical potentials in the weak-coupling limit, for $n_B < n_F$

In this section, figures for the the boson and fermion chemical potentials μ_F and μ_B in the weak-coupling regime are reported. We consider the boson concentration to be $x < 1$, specifically $x = 0.5$, $x = 0.175$ (Fig. D.4) and $x = 0.1$, and different values for the mass ratio γ_m, proximate to those in Tab. 1.1. We do not include the anomalous self-energy Σ^{12}_{BF} in the calculations, nor do we treat the interaction between bosons (setting $\eta = 0$) or the mean-field shift of the chemical potential $\mu_F \mapsto \mu_F - \Sigma^0_F$.

Fig. D.8 reports the fermion chemical potential in the weak-coupling regime $-4 \leq g \leq 2$, while Fig. D.9 in the "extreme" weak coupling regime $g \leq -15$. Fig. D.10 the boson chemical potential in the weak-coupling regime $-4 \leq g \leq 2$.

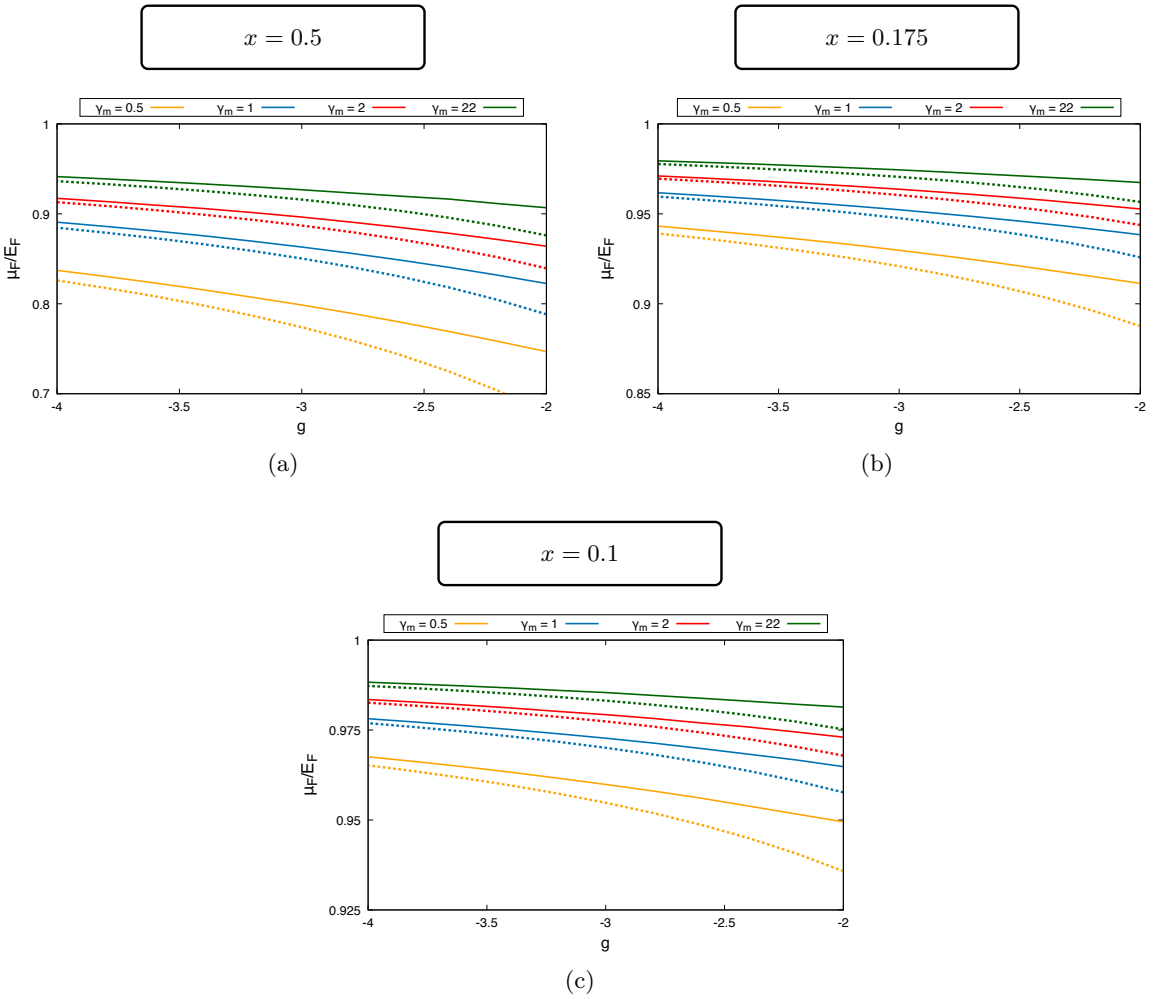

Figure D.8: Fermion chemical potential μ_F, in units of E_F, as a function of the BF coupling g, for several different values of the boson concentration and the mass ratio. The dotted lines represent the weak-coupling result (4.3).

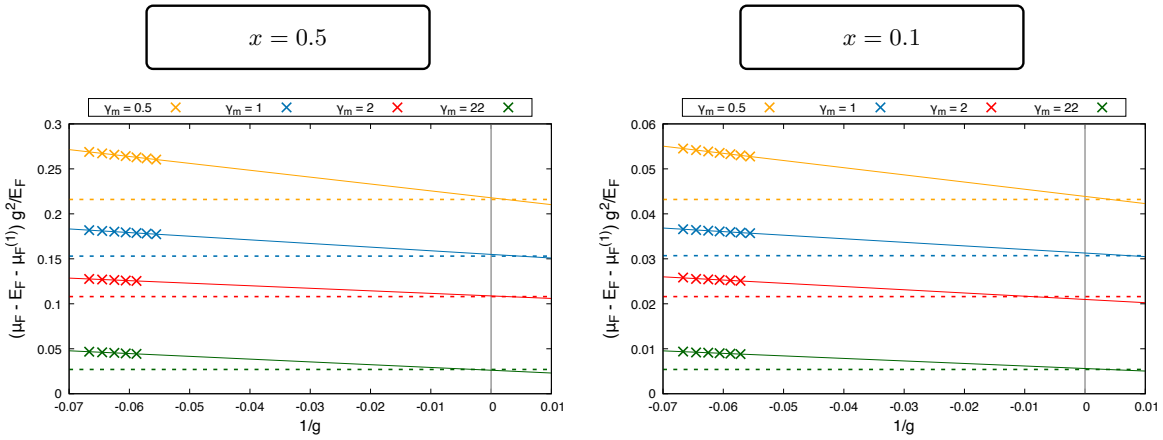

(a)

$\gamma_{\rm m}$	$\mu_{\rm F}^{(2)} g^2/E_{\rm F}$	A	B
0.5	0.216	0.218	−0.765
1	0.153	0.155	−0.404
2	0.108	0.109	−0.283
22	0.027	0.026	−0.309

(b)

$\gamma_{\rm m}$	$\mu_{\rm F}^{(2)} g^2/E_{\rm F}$	A	B
0.5	0.043	0.044	−0.160
1	0.031	0.031	−0.079
2	0.022	0.021	−0.072
22	0.005	0.006	−0.056

Figure D.9: Crosses: $(\mu_{\rm F} - E_{\rm F} - \mu_{\rm F}^{(1)})g^2/E_{\rm F}$ as a function of $1/g$. Full lines: fit to the model $f(g) = A + B/g$. Dashed lines: expected asymptotic value $\mu_{\rm F}^{(2)} g^2$ of the fitting curve in the limit $1/g \to 0^-$. Tables: outcomes of the fit procedure; the second column is useful for comparing A with the coupling independent, perturbative result $\mu_{\rm F}^{(2)} g^2$ in (4.3).

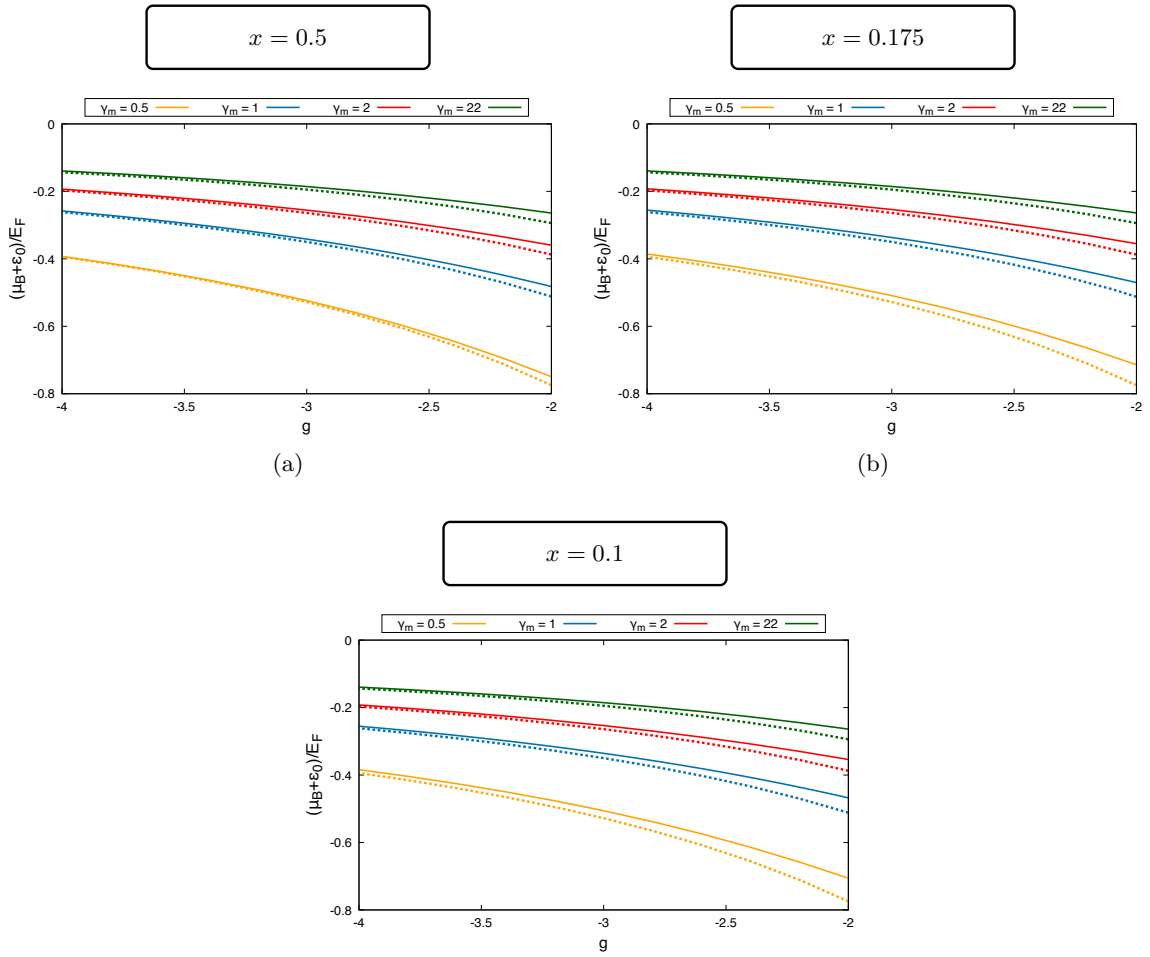

Figure D.10: Boson chemical potential μ_B (shifted by the binding energy ε_0), in units of E_F, as a function of the BF coupling g, for several different values of the boson concentration and the mass ratio. The dotted lines represent the weak-coupling result (4.4) (shifted by the binding energy ε_0).

Bibliography

[1] S. N. Bose. "Planck's law and light quantum hypothesis". In: *Z. Phys.* 26 (1924), pp. 178–181. DOI: 10.1007/BF01327326.

[2] Albert Einstein. "Quantentheorie des einatomigen idealen Gases". In: *Sitzungsberichte der Preussischen Akademie der Wissenschaften* (1924), pp. 261–267.

[3] Albert Einstein. "Quantentheorie des einatomigen idealen Gases. Zweite Abhandlung". In: *Sitzungsberichte der Preussischen Akademie der Wissenschaften* (1925), pp. 3–14.

[4] Enrico Fermi. "Sulla quantizzazione del gas perfetto monoatomico". In: *Rendiconti Lincei* 3 (1926), pp. 145–149.

[5] Paul A. M. Dirac. "On the Theory of Quantum Mechanics". In: *Proceedings of the Royal Society of London A* 112 (1926), pp. 661–677. DOI: 10.1098/rspa.1926.0133.

[6] S. Chu et al. "Three-Dimensional Viscous Confinement and Cooling of Atoms by Resonance Radiation Pressure". In: *Physical Review Letters* 55 (1985), pp. 48–51. DOI: 10.1103/PhysRevLett.55.48.

[7] J. Dalibard and C. Cohen-Tannoudji. "Laser cooling below the Doppler limit by polarization gradients: simple theoretical models". In: *Journal of the Optical Society of America B* 6 (1989), pp. 2023–2045. DOI: 10.1364/JOSAB.6.002023.

[8] M. H. Anderson et al. "Observation of Bose-Einstein Condensation in a Dilute Atomic Vapor". In: *Science* 269 (1995), pp. 198–201. DOI: 10.1126/science.269.5221.198.

[9] K. B. Davis et al. "Bose-Einstein Condensation in a Gas of Sodium Atoms". In: *Physical Review Letters* 75 (1995), pp. 3969–3973. DOI: 10.1103/PhysRevLett.75.3969.

[10] B. DeMarco and D. S. Jin. "Onset of Fermi Degeneracy in a Trapped Atomic Gas". In: *Science* 285 (1999), pp. 1703–1706. DOI: 10.1126/science.285.5434.1703.

[11] A. G. Truscott et al. "Observation of Fermi Pressure in a Gas of Trapped Atoms". In: *Science* 291 (2001), pp. 2570–2572. DOI: 10.1126/science.1059318.

[12] A. Trautmann et al. "Dipolar Quantum Mixtures of Erbium and Dysprosium Atoms". In: *Phys. Rev. Lett.* 121 (21 Nov. 2018), p. 213601. DOI: 10.1103/PhysRevLett.121.213601. URL: https://link.aps.org/doi/10.1103/PhysRevLett.121.213601.

[13] Yu-Ping Wu et al. "A quantum degenerate Bose–Fermi mixture of ^{41}K and ^{6}Li". In: *J. Phys. B At. Mol. Opt. Phys.* 50.9 (Apr. 2017), p. 094001. DOI: 10.1088/1361-6455/aa658b. URL: https://dx.doi.org/10.1088/1361-6455/aa658b.

[14] Zhu-Xiong Ye et al. "Double-degenerate Bose-Fermi mixture of strontium and lithium". In: *Phys. Rev. A* 102 (3 Sept. 2020), p. 033307. DOI: 10.1103/PhysRevA.102.033307. URL: https://link.aps.org/doi/10.1103/PhysRevA.102.033307.

[15] V. D. Vaidya et al. "Degenerate Bose-Fermi mixtures of rubidium and ytterbium". In: *Phys. Rev. A* 92 (4 Oct. 2015), p. 043604. DOI: 10.1103/PhysRevA.92.043604. URL: https://link.aps.org/doi/10.1103/PhysRevA.92.043604.

[16] D. S. Petrov and G. V. Shlyapnikov. "Interatomic collisions in a tightly confined Bose gas". In: *Phys. Rev. A* 64 (1 June 2001), p. 012706. DOI: 10.1103/PhysRevA.64.012706. URL: https://link.aps.org/doi/10.1103/PhysRevA.64.012706.

[17] Jesper Levinsen and Meera M. Parish. "Strongly Interacting Two-Dimensional Fermi Gases". In: *Annual Review of Cold Atoms and Molecules*. World Scientific, Mar. 2015, pp. 1–75. DOI: 10.1142/9789814667746_0001. URL: http://dx.doi.org/10.1142/9789814667746_0001.

[18] Elmar Haller et al. "Confinement-Induced Resonances in Low-Dimensional Quantum Systems". In: *Phys. Rev. Lett.* 104 (15 Apr. 2010), p. 153203. DOI: 10.1103/PhysRevLett.104.153203. URL: https://link.aps.org/doi/10.1103/PhysRevLett.104.153203.

[19] Rianne S. Lous et al. "Probing the Interface of a Phase-Separated State in a Repulsive Bose-Fermi Mixture". In: *Phys. Rev. Lett.* 120 (24 June 2018), p. 243403. DOI: 10.1103/PhysRevLett.120.243403. URL: https://link.aps.org/doi/10.1103/PhysRevLett.120.243403.

[20] Isabella Fritsche et al. "Stability and breakdown of Fermi polarons in a strongly interacting Fermi-Bose mixture". In: *Phys. Rev. A* 103 (5 May 2021), p. 053314. DOI: 10.1103/PhysRevA.103.053314. URL: https://link.aps.org/doi/10.1103/PhysRevA.103.053314.

[21] Ming-Guang Hu et al. "Bose Polarons in the Strongly Interacting Regime". In: *Phys. Rev. Lett.* 117 (5 July 2016), p. 055301. DOI: 10.1103/PhysRevLett.117.055301. URL: https://link.aps.org/doi/10.1103/PhysRevLett.117.055301.

[22] Richard Schmidt et al. "Universal many-body response of heavy impurities coupled to a Fermi sea: a review of recent progress". In: *Reports on Progress in Physics* 81.2 (Jan. 2018), p. 024401. DOI: 10.1088/1361-6633/aa9593. URL: https://dx.doi.org/10.1088/1361-6633/aa9593.

[23] Zoe Z. Yan et al. "Bose polarons near quantum criticality". In: *Science* 368.6487 (2020), pp. 190–194. DOI: 10.1126/science.aax5850. URL: https://www.science.org/doi/abs/10.1126/science.aax5850.

[24] Francesco Scazza et al. "Repulsive Fermi and Bose Polarons in Quantum Gases". In: *Atoms* 10.2 (2022), p. 55. ISSN: 2218-2004. DOI: 10.3390/atoms10020055. URL: https://www.mdpi.com/2218-2004/10/2/55.

[25] Pietro Massignan, Matteo Zaccanti, and Georg M Bruun. "Polarons, dressed molecules and itinerant ferromagnetism in ultracold Fermi gases". In: *Reports on Progress in Physics* 77.3 (Feb. 2014), p. 034401. DOI: 10.1088/0034-4885/77/3/034401. URL: https://dx.doi.org/10.1088/0034-4885/77/3/034401.

[26] I. Ferrier-Barbut et al. "A mixture of Bose and Fermi superfluids". In: *Science* 345.6200 (2014), pp. 1035–1038. DOI: 10.1126/science.1255380. URL: https://www.science.org/doi/abs/10.1126/science.1255380.

[27] Richard Roy et al. "Two-Element Mixture of Bose and Fermi Superfluids". In: *Phys. Rev. Lett.* 118 (5 Feb. 2017), p. 055301. DOI: 10.1103/PhysRevLett.118.055301. URL: https://link.aps.org/doi/10.1103/PhysRevLett.118.055301.

[28] Yu-Ping Wu et al. "Coupled dipole oscillations of a mass-imbalanced Bose-Fermi superfluid mixture". In: *Phys. Rev. B* 97 (2 Jan. 2018), p. 020506. DOI: 10.1103/PhysRevB.97.020506. URL: https://link.aps.org/doi/10.1103/PhysRevB.97.020506.

[29] Marion Delehaye et al. "Critical Velocity and Dissipation of an Ultracold Bose-Fermi Counterflow". In: *Phys. Rev. Lett.* 115 (26 Dec. 2015), p. 265303. DOI: 10.1103/PhysRevLett.115.265303. URL: https://link.aps.org/doi/10.1103/PhysRevLett.115.265303.

[30] Krutik Patel et al. "Sound Propagation in a Bose-Fermi Mixture: From Weak to Strong Interactions". In: *Phys. Rev. Lett.* 131 (8 Aug. 2023), p. 083003. DOI: 10.1103/PhysRevLett.131.083003. URL: https://link.aps.org/doi/10.1103/PhysRevLett.131.083003.

[31] Zoe Z. Yan et al. "Collective flow of fermionic impurities immersed in a Bose–Einstein condensate". In: *Nature Physics* 20.9 (2024), pp. 1395–1400. DOI: 10.1038/s41567-024-02541-w.

[32] Hagai Edri et al. "Observation of Spin-Spin Fermion-Mediated Interactions between Ultracold Bosons". In: *Phys. Rev. Lett.* 124 (16 Apr. 2020), p. 163401. DOI: 10.1103/PhysRevLett.124.163401. URL: https://link.aps.org/doi/10.1103/PhysRevLett.124.163401.

[33] Xin Shen et al. "Strongly Interacting Bose-Fermi Mixtures: Mediated Interaction, Phase Diagram, and Sound Propagation". In: *Phys. Rev. Lett.* 132 (3 Jan. 2024), p. 033401. DOI: 10.1103/PhysRevLett.132.033401. URL: https://link.aps.org/doi/10.1103/PhysRevLett.132.033401.

[34] Cosetta Baroni et al. "Mediated interactions between Fermi polarons and the role of impurity quantum statistics". In: *Nature Physics* 20.1 (Jan. 2024), pp. 68–73. DOI: 10.1038/s41567-023-02248-4. URL: https://doi.org/10.1038/s41567-023-02248-4.

[35] K.-K. Ni et al. "A High Phase-Space-Density Gas of Polar Molecules". In: *Science* 322.5899 (2008). *The work reports the observation of the transition from losely bound Feshbach molecules to tightly bound ground-state molecules*, pp. 231–235. DOI: 10.1126/science.1163861. URL: https://www.science.org/doi/abs/10.1126/science.1163861.

[36] Ruth S. Bloom et al. "Tests of Universal Three-Body Physics in an Ultracold Bose-Fermi Mixture". In: *Phys. Rev. Lett.* 111 (10 Sept. 2013), p. 105301. DOI: 10.1103/PhysRevLett.111.105301. URL: https://link.aps.org/doi/10.1103/PhysRevLett.111.105301.

[37] Cheng-Hsun Wu et al. "Ultracold Fermionic Feshbach Molecules of ^{23}Na ^{40}K". In: *Phys. Rev. Lett.* 109 (8 Aug. 2012), p. 085301. DOI: 10.1103/PhysRevLett.109.085301. URL: https://link.aps.org/doi/10.1103/PhysRevLett.109.085301.

[38] Myoung-Sun Heo et al. "Formation of ultracold fermionic NaLi Feshbach molecules". In: *Phys. Rev. A* 86 (2 Aug. 2012), p. 021602. DOI: 10.1103/PhysRevA.86.021602. URL: https://link.aps.org/doi/10.1103/PhysRevA.86.021602.

[39] Luigi De Marco et al. "A degenerate Fermi gas of polar molecules". In: *Science* 363.6429 (2019), pp. 853–856. DOI: 10.1126/science.aau7230. URL: https://www.science.org/doi/abs/10.1126/science.aau7230.

[40] Andreas Schindewolf et al. "Evaporation of microwave-shielded polar molecules to quantum degeneracy". In: *Nature* 607.7920 (July 2022), pp. 677–681. ISSN: 1476-4687. DOI: 10.1038/s41586-022-04900-0. URL: https://doi.org/10.1038/s41586-022-04900-0.

[41] Marcel Duda et al. "Transition from a polaronic condensate to a degenerate Fermi gas of heteronuclear molecules". In: *Nature Physics* 19 (2023), p. 720. DOI: 10.1038/s41567-023-01948-1. URL: https://doi.org/10.1038/s41567-023-01948-1.

[42] Tyler D. Cumby et al. "Feshbach-molecule formation in a Bose-Fermi mixture". In: *Phys. Rev. A* 87 (1 Jan. 2013), p. 012703. DOI: 10.1103/PhysRevA.87.012703. URL: https://link.aps.org/doi/10.1103/PhysRevA.87.012703.

[43] B. J. DeSalvo et al. "Observation of fermion-mediated interactions between bosonic atoms". In: *Nature* 568 (7750 2019), p. 61. DOI: 10.1038/s41586-019-1055-0. URL: https://doi.org/10.1038/s41586-019-1055-0.

[44] Alexander Y. Chuang et al. "Observation of a Halo Trimer in an Ultracold Bose-Fermi Mixture". In: *Physical Review X* 15 (June 2025), p. 021098. DOI: 10.1103/PhysRevX.15.021098. eprint: 2411.04820.

[45] Gang Wang et al. "Colloquium: Excitons in atomically thin transition metal dichalcogenides". In: *Rev. Mod. Phys.* 90 (2 Apr. 2018), p. 021001. DOI: 10.1103/RevModPhys.90.021001. URL: https://link.aps.org/doi/10.1103/RevModPhys.90.021001.

[46] Ido Schwartz et al. "Electrically tunable Feshbach resonances in twisted bilayer semiconductors". In: *Science* 374.6565 (2021), pp. 336–340. DOI: 10.1126/science.abj3831.

[47] Luis A. Jauregui et al. "Electrical control of interlayer exciton dynamics in atomically thin heterostructures". In: *Science* 366.6467 (2019), pp. 870–875. DOI: 10.1126/science.aaw4194.

[48] Christian Fey et al. "Theory of exciton-electron scattering in atomically thin semiconductors". In: *Phys. Rev. B* 101 (19 May 2020), p. 195417. DOI: 10.1103/PhysRevB.101.195417. URL: https://link.aps.org/doi/10.1103/PhysRevB.101.195417.

[49] Clemens Kuhlenkamp et al. "Tunable Feshbach Resonances and Their Spectral Signatures in Bilayer Semiconductors". In: *Phys. Rev. Lett.* 129 (3 July 2022), p. 037401. DOI: 10.1103/PhysRevLett.129.037401. URL: https://link.aps.org/doi/10.1103/PhysRevLett.129.037401.

[50] Kin Fai Mak et al. "Atomically Thin MoS_2: A New Direct-Gap Semiconductor". In: *Phys. Rev. Lett.* 105 (13 Sept. 2010), p. 136805. DOI: 10.1103/PhysRevLett.105.136805. URL: https://link.aps.org/doi/10.1103/PhysRevLett.105.136805.

[51] Meinrad Sidler et al. "Fermi polaron-polaritons in charge-tunable atomically thin semiconductors". In: *Nature Physics* 13.3 (2017), pp. 255–261. DOI: 10.1038/nphys3949. URL: https://doi.org/10.1038/nphys3949.

[52] Miguel A. Bastarrachea-Magnani, Arturo Camacho-Guardian, and Georg M. Bruun. "Attractive and Repulsive Exciton-Polariton Interactions Mediated by an Electron Gas". In: *Phys. Rev. Lett.* 126 (12 Mar. 2021), p. 127405. DOI: 10.1103/PhysRevLett.126.127405. URL: https://link.aps.org/doi/10.1103/PhysRevLett.126.127405.

[53] Haifeng Kang et al. "Exciton polaritons in emergent two-dimensional semiconductors". In: *ACS nano* 17.24 (2023), pp. 24449–24467. DOI: 10.1021/acsnano.3c07993. URL: https://doi.org/10.1021/acsnano.3c07993.

[54] Zeng-Qiang Yu, Shizhong Zhang, and Hui Zhai. "Stability condition of a strongly interacting boson-fermion mixture across an interspecies Feshbach resonance". In: *Phys. Rev. A* 83 (4 Apr. 2011), p. 041603. DOI: 10.1103/PhysRevA.83.041603. URL: https://link.aps.org/doi/10.1103/PhysRevA.83.041603.

[55] Christian Gualerzi, Leonardo Pisani, and Pierbiagio Pieri. "Mechanical stability of resonant Bose-Fermi mixtures". In: *SciPost Physics* 19.2 (Aug. 2025). ISSN: 2542-4653. DOI: 10.21468/scipostphys.19.2.039. URL: http://dx.doi.org/10.21468/SciPostPhys.19.2.039.

[56] Leonardo Pisani et al. "Boson-fermion pairing and condensation in two-dimensional Bose-Fermi mixtures". In: *SciPost Physics* 18 (2025), p. 076. DOI: 10.21468/SciPostPhys.18.3.076. eprint: 2405.05029.

[57] Xin Shen et al. "Strongly Interacting Bose-Fermi Mixtures: Mediated Interaction, Phase Diagram, and Sound Propagation". In: *Phys. Rev. Lett.* 132 (3 Jan. 2024), p. 033401. DOI: 10.1103/PhysRevLett.132.033401. URL: https://link.aps.org/doi/10.1103/PhysRevLett.132.033401.

[58] Cheng Chin et al. "Feshbach resonances in ultracold gases". In: *Rev. Mod. Phys.* 82 (2 Apr. 2010), pp. 1225–1286. DOI: 10.1103/RevModPhys.82.1225. URL: https://link.aps.org/doi/10.1103/RevModPhys.82.1225.

[59] Jee Woo Park et al. "Quantum degenerate Bose-Fermi mixture of chemically different atomic species with widely tunable interactions". In: *Phys. Rev. A* 85 (5 May 2012), p. 051602. DOI: 10.1103/PhysRevA.85.051602. URL: https://link.aps.org/doi/10.1103/PhysRevA.85.051602.

[60] T. L. Nicholson et al. "Optical Feshbach resonances: Field-dressed theory and comparison with experiments". In: *Phys. Rev. A* 92 (2 Aug. 2015), p. 022709. DOI: 10.1103/PhysRevA.92.022709. URL: https://link.aps.org/doi/10.1103/PhysRevA.92.022709.

[61] C. J. Pethick and H. Smith. *Bose–Einstein Condensation in Dilute Gases*. 2nd ed. Cambridge University Press, 2008.

[62] Stefano Simonucci, Pierbiagio Pieri, and Giancarlo Strinati. "Broad vs. narrow Fano-Feshbach resonances in the BCS-BEC crossover with trapped Fermi atoms". In: *Europhysics Letters (epl)* 69 (Mar. 2005), pp. 713–718. DOI: 10.1209/epl/i2004-10412-2.

[63] J. Bardeen, L. N. Cooper, and J. R. Schrieffer. "Theory of Superconductivity". In: *Phys. Rev.* 108 (5 Dec. 1957), pp. 1175–1204. DOI: 10.1103/PhysRev.108.1175. URL: https://link.aps.org/doi/10.1103/PhysRev.108.1175.

[64] Q CHEN et al. "BCS–BEC crossover: From high temperature superconductors to ultracold superfluids". In: *Physics Reports* 412.1 (June 2005), pp. 1–88. ISSN: 0370-1573. DOI: 10.1016/j.physrep.2005.02.005. URL: http://dx.doi.org/10.1016/j.physrep.2005.02.005.

[65] R. Haussmann et al. "Thermodynamics of the BCS-BEC crossover". In: *Physical Review A* 75.2 (Feb. 2007). ISSN: 1094-1622. DOI: 10.1103/physreva.75.023610. URL: http://dx.doi.org/10.1103/PhysRevA.75.023610.

[66] "Making, probing and understanding ultracold fermi gases". In: *La Rivista del Nuovo Cimento* 31.506 (July 2008), pp. 247–422. ISSN: 0393697X, 0393697X. DOI: 10.1393/ncr/i2008-10033-1. URL: https://doi.org/10.1393/ncr/i2008-10033-1.

[67] Stefano Giorgini, Lev P. Pitaevskii, and Sandro Stringari. "Theory of ultracold atomic Fermi gases". In: *Rev. Mod. Phys.* 80 (4 Oct. 2008), pp. 1215–1274. DOI: 10.1103/RevModPhys.80.1215. URL: https://link.aps.org/doi/10.1103/RevModPhys.80.1215.

[68] Mohit Randeria and Edward Taylor. "Crossover from Bardeen-Cooper-Schrieffer to Bose-Einstein Condensation and the Unitary Fermi Gas". In: *Annual Review of Condensed Matter Physics* 5.1 (Mar. 2014), pp. 209–232. ISSN: 1947-5462. DOI: 10.1146/annurev-conmatphys-031113-133829. URL: http://dx.doi.org/10.1146/annurev-conmatphys-031113-133829.

[69] Mohit Randeria and Edward Taylor. "Crossover from Bardeen-Cooper-Schrieffer to Bose-Einstein Condensation and the Unitary Fermi Gas". In: *Annual Review of Condensed Matter Physics* 5.Volume 5, 2014 (2014), pp. 209–232. ISSN: 1947-5462. DOI: https://doi.org/10.1146/annurev-conmatphys-031113-133829. URL: https://www.annualreviews.org/content/journals/10.1146/annurev-conmatphys-031113-133829.

[70] Giancarlo Calvanese Strinati et al. "The BCS–BEC crossover: From ultra-cold Fermi gases to nuclear systems". In: *Phys. Rept.* 738 (2018), pp. 1–76. DOI: 10.1016/j.physrep.2018.02.004. arXiv: 1802.05997 [cond-mat.quant-gas].

[71] C. A. Regal, M. Greiner, and D. S. Jin. "Observation of Resonance Condensation of Fermionic Atom Pairs". In: *Phys. Rev. Lett.* 92 (4 Jan. 2004), p. 040403. DOI: 10.1103/PhysRevLett.92.040403. URL: https://link.aps.org/doi/10.1103/PhysRevLett.92.040403.

[72] J. Kinast et al. "Evidence for Superfluidity in a Resonantly Interacting Fermi Gas". In: *Phys. Rev. Lett.* 92 (15 Apr. 2004), p. 150402. DOI: 10.1103/PhysRevLett.92.150402. URL: https://link.aps.org/doi/10.1103/PhysRevLett.92.150402.

[73] T. Bourdel et al. "Experimental Study of the BEC-BCS Crossover Region in Lithium 6". In: *Phys. Rev. Lett.* 93 (5 July 2004), p. 050401. DOI: 10.1103/PhysRevLett.93.050401. URL: https://link.aps.org/doi/10.1103/PhysRevLett.93.050401.

[74] C. Chin et al. "Observation of the Pairing Gap in a Strongly Interacting Fermi Gas". In: *Science* 305.5687 (Aug. 2004), pp. 1128–1130. ISSN: 1095-9203. DOI: 10.1126/science.1100818. URL: http://dx.doi.org/10.1126/science.1100818.

[75] G. B. Partridge et al. "Molecular Probe of Pairing in the BEC-BCS Crossover". In: *Phys. Rev. Lett.* 95 (2 July 2005), p. 020404. DOI: 10.1103/PhysRevLett.95.020404. URL: https://link.aps.org/doi/10.1103/PhysRevLett.95.020404.

[76] Wikipedia contributors. *Magneto-optical trap — Wikipedia, The Free Encyclopedia. [Online; accessed 2-March-2026]*. 2026. URL: https://en.wikipedia.org/wiki/Magneto-optical_trap.

[77] Wikipedia contributors. *Laser cooling — Wikipedia, The Free Encyclopedia. [Online; accessed 2-March-2026]*. 2026. URL: https://en.wikipedia.org/wiki/Laser_cooling.

[78] Wikipedia contributors. *Evaporative cooling (atomic physics) — Wikipedia, The Free Encyclopedia. [Online; accessed 2-March-2026]*. 2026. URL: https://en.wikipedia.org/wiki/Evaporative_cooling_(atomic_physics).

[79] Wikipedia contributors. *Sympathetic cooling — Wikipedia, The Free Encyclopedia. [Online; accessed 2-March-2026]*. 2026. URL: https://en.wikipedia.org/wiki/Sympathetic_cooling.

[80] Bo Huang et al. "Breathing mode of a Bose-Einstein condensate repulsively interacting with a fermionic reservoir". In: *Phys. Rev. A* 99 (4 Apr. 2019), p. 041602. DOI: 10.1103/PhysRevA.99.041602. URL: https://link.aps.org/doi/10.1103/PhysRevA.99.041602.

[81] Mohammad Mansoob Khan, ed. *Chalcogenide-Based Nanomaterials as Photocatalysts*. Micro and Nano Technologies. Amsterdam: Elsevier, 2021. ISBN: 9780128204986. DOI: 10.1016/B978-0-12-820498-6.00001-9. URL: https://www.sciencedirect.com/book/9780128204986.

[82] Andres Castellanos-Gomez et al. "Deterministic transfer of two-dimensional materials by all-dry viscoelastic stamping". In: *2D Materials* 1.1 (2014), p. 011002. DOI: 10.1088/2053-1583/1/1/011002.

[83] Hui Deng, Hartmut Haug, and Yoshihisa Yamamoto. "Exciton-polariton Bose-Einstein condensation". In: *Rev. Mod. Phys.* 82 (2 May 2010), pp. 1489–1537. DOI: 10.1103/RevModPhys.82.1489. URL: https://link.aps.org/doi/10.1103/RevModPhys.82.1489.

[84] Alexey Chernikov et al. "Exciton Binding Energy and Nonhydrogenic Rydberg Series in Monolayer WS_2". In: *Phys. Rev. Lett.* 113 (7 Aug. 2014), p. 076802. DOI: 10.1103/PhysRevLett.113.076802. URL: https://link.aps.org/doi/10.1103/PhysRevLett.113.076802.

[85] L. V. Keldysh and A. N. Kozlov. "Collective Properties of Excitons in Semiconductors". In: *Soviet Journal of Experimental and Theoretical Physics* 27 (Sept. 1968), p. 521.

[86] Michael M. Fogler, Leonid V. Butov, and Kostya S. Novoselov. "High-temperature superfluidity with indirect excitons in van der Waals heterostructures". In: *Nature Communications* 5 (July 2014), p. 4555. DOI: 10.1038/ncomms5555.

[87] Marco Manca et al. "Enabling valley selective exciton scattering in monolayer WSe_2 through upconversion". In: *Nature Communications* 8 (Apr. 2017), p. 14927. DOI: 10.1038/ncomms14927.

[88] R. A. Suris. "Correlation Between Trion and Hole in Fermi Distribution in Process of Trion Photo-Excitation in Doped QWs". In: *Optical Properties of 2D Systems with Interacting Electrons*. Ed. by Wolfgang J. Ossau and Robert Suris. Vol. 119. NATO Science Series II: Mathematics, Physics and Chemistry. Dordrecht: Springer, 2003. ISBN: 978-1-4020-1548-9. DOI: 10.1007/978-94-010-0078-9_9.

[89] Meinrad Sidler et al. "Fermi polaron-polaritons in charge-tunable atomically thin semiconductors". In: *Nature Physics* 13 (2017), pp. 255–261. DOI: 10.1038/nphys3949.

[90] Dmitry K. Efimkin and Allan H. MacDonald. "Many-body theory of trion absorption features in two-dimensional semiconductors". In: *Phys. Rev. B* 95 (3 Jan. 2017), p. 035417. DOI: 10.1103/PhysRevB.95.035417. URL: https://link.aps.org/doi/10.1103/PhysRevB.95.035417.

[91] Alexander L. Fetter and John Dirk Walecka. *Quantum Theory of Many-Particle Systems*. New York: McGraw-Hill, 1971. URL: https://api.semanticscholar.org/CorpusID:5661190.

[92] J. M. Luttinger and J. C. Ward. "Ground-State Energy of a Many-Fermion System. II". In: *Phys. Rev.* 118 (5 June 1960), pp. 1417–1427. DOI: 10.1103/PhysRev.118.1417. URL: https://link.aps.org/doi/10.1103/PhysRev.118.1417.

[93] Beliaev, S. T. "Energy-spectrum of a non-ideal Bose Gas". In: *Soviet Physics JETP* 34(7).2 (1958).

[94] N. M. Hugenholtz and D. Pines. "Ground-State Energy and Excitation Spectrum of a System of Interacting Bosons". In: *Phys. Rev.* 116 (3 Nov. 1959), pp. 489–506. DOI: 10.1103/PhysRev.116.489. URL: https://link.aps.org/doi/10.1103/PhysRev.116.489.

[95] P.C Hohenberg and P.C Martin. "Microscopic theory of superfluid helium". In: *Annals of Physics* 34.2 (1965), pp. 291–359. ISSN: 0003-4916. DOI: https://doi.org/10.1016/0003-4916(65)90280-0. URL: https://www.sciencedirect.com/science/article/pii/0003491665902800.

[96] H. Stoof, K. Gubbels, and D. Dickerscheid. *Ultracold Quantum Fields*. Vol. 2009. Jan. 2009. ISBN: 978-1-4020-8762-2. DOI: 10.1007/978-1-4020-8763-9.

[97] P. G. Averbuch. "Zero energy divergence of scattering cross sections in two dimensions". In: *Journal of Physics A: Mathematical and General, Volume 19, Issue 12, pp. 2325-2335 (1986).* (Aug. 1986). DOI: 10.1088/0305-4470/19/12/018.

[98] H.-W. Hammer and Dean Lee. "Causality and the effective range expansion". In: *Annals of Physics* 325.10 (2010), pp. 2212–2233. ISSN: 0003-4916. DOI: https://doi.org/10.1016/j.aop.2010.06.006. URL: https://www.sciencedirect.com/science/article/pii/S0003491610001211.

[99] Jacopo D'Alberto et al. "Quantum Monte Carlo and perturbative study of two-dimensional Bose-Fermi mixtures". In: *Phys. Rev. A* 109 (5 May 2024), p. 053302. DOI: 10.1103/PhysRevA.109.053302. URL: https://link.aps.org/doi/10.1103/PhysRevA.109.053302.

[100] M. Schick. "Two-Dimensional System of Hard-Core Bosons". In: *Phys. Rev. A* 3 (3 Mar. 1971), pp. 1067–1073. DOI: 10.1103/PhysRevA.3.1067. URL: https://link.aps.org/doi/10.1103/PhysRevA.3.1067.

[101] V. N. Popov. *Functional integrals and collective excitations*. Cambridge University Press, Cambridge, 1987.

[102] Pierbiagio Pieri and Giancarlo Calvanese Strinati. "Luttinger theorem and imbalanced Fermi systems". In: *Eur. Phys. Jour. B* 90.68 (2017), pp. 1–6. DOI: 10.1140/epjb/e2017-80071-2. URL: https://doi.org/10.1140/epjb/e2017-80071-2.

[103] Stephen Powell, Subir Sachdev, and Hans Peter Büchler. "Depletion of the Bose-Einstein condensate in Bose-Fermi mixtures". In: *Phys. Rev. B* 72 (2 July 2005), p. 024534. DOI: 10.1103/PhysRevB.72.024534. URL: https://link.aps.org/doi/10.1103/PhysRevB.72.024534.

[104] Cardarelli Lorenzo. "Ground state properties of dilute Bose-Fermi mixtures in two and three dimensions". Master's thesis. Camerino, Italy: Università di Camerino, 2013/2014.

[105] A. Perali et al. "Pseudogap and spectral function from superconducting fluctuations to the bosonic limit". In: *Phys. Rev. B* 66 (2 July 2002), p. 024510. DOI: 10.1103/PhysRevB.66.024510. URL: https://link.aps.org/doi/10.1103/PhysRevB.66.024510.

[106] P. Pieri, L. Pisani, and G. C. Strinati. "Comparison between a diagrammatic theory for the BCS-BEC crossover and quantum Monte Carlo results". In: *Phys. Rev. B* 72 (1 July 2005), p. 012506. DOI: 10.1103/PhysRevB.72.012506. URL: https://link.aps.org/doi/10.1103/PhysRevB.72.012506.

[107] Digvijay Kharga et al. “Single-Particle Excitations and Effects of Hetero-Pairing Fluctuations in a Bose–Fermi Mixture with a Feshbach Resonance”. In: *Journal of the Physical Society of Japan* 86.8 (2017), p. 084301. DOI: 10.7566/JPSJ.86.084301. URL: https://doi.org/10.7566/JPSJ.86.084301.

[108] Koki Manabe, Daisuke Inotani, and Yoji Ohashi. “Single-particle properties of a strongly interacting Bose-Fermi mixture with mass and population imbalance”. In: *Phys. Rev. A* 100 (6 Dec. 2019), p. 063609. DOI: 10.1103/PhysRevA.100.063609. URL: https://link.aps.org/doi/10.1103/PhysRevA.100.063609.

[109] Andrea Guidini. “Superconductivity and Superfluidity in Multicomponent Systems”. PhD thesis. Camerino, Italy: Università di Camerino, 2016.

[110] A. Guidini et al. “Condensed phase of Bose-Fermi mixtures with a pairing interaction”. In: *Phys. Rev. A* 91 (2015), p. 023603. DOI: 10.1103/PhysRevA.91.023603.

[111] Meera M. Parish. “Polaron-molecule transitions in a two-dimensional Fermi gas”. In: *Phys. Rev. A* 83 (5 May 2011), p. 051603. DOI: 10.1103/PhysRevA.83.051603. URL: https://link.aps.org/doi/10.1103/PhysRevA.83.051603.

[112] Jonas Vlietinck, Jan Ryckebusch, and Kris Van Houcke. “Diagrammatic Monte Carlo study of the Fermi polaron in two dimensions”. In: *Phys. Rev. B* 89 (8 Feb. 2014), p. 085119. DOI: 10.1103/PhysRevB.89.085119. URL: https://link.aps.org/doi/10.1103/PhysRevB.89.085119.